Current Awareness Bulletin

of

SCHOLARLY ARTICLES PUBLISHED BY

Faculty, Students and Alumni

~ February 2013 ~

DELHI TECHNOLOGICAL UNIVERSITY CENTRAL LIBRARY
(formerly Delhi College of Engineering, Bawana Road, DELHI)

PREFACE

This is the Second Current Awareness Bulletin Service started by Delhi Technological University Library for the year 2013. The aim of the bulletin is to compile, preserve and disseminate information published by the Faculty, Students and Alumni for mutual benefits. The bulletin also aims to propagate the intellectual contribution of DTU as a whole to the academia. It contains information resources available in the internet in the form of articles, reports, presentation published in international journals, websites, etc. by the faculty and students of Delhi Technological University in the field of science and technology. The publication of Faculty and Students, which are not covered in this bulletin, may be because of the reason that the full text either was not accessible or could not be searched by the search engine used by the library for this purpose. To make the bulletin more comprehensive, the learned faculty and Students may provide their uncovered publication to the library either through email or in CD, etc.

This issue contains the information published during February 2013. The arrangement of the contents is alphabetical wise starting from A-Z. The Full text of the article, which is either subscribed by the University or available in the web, is provided in this Bulletin.

CONTENTS

12. Temperature Dependent Analysis of Thermoelectric Module using Matlab/SIMULINK by *Aarti Kane* ***, @Vishal Verma*** and ***@Bhim Singh.***

13. Interconnection Issues for Distributed Resources in a Smart Distribution System by ***# Mini S Thomas*** and *Parveen Poon Terang*.

14. Investigations of Model Order Reduction Techniques for Large Scale Linear Systems by *Chandan Kumar*, ***# S.K.Jha*** and ***# Prerna Gaur***.

15. Load Compensation with DSTATCOM and BESS by ***@Alka Singh, @Suman Bhowmick*** and ***@Kapil Shukla***.

16. Master-Slave Current Control DOs in a Microgrid for Transient Decoupling with Mains by ***@Vishal Verma*** and ***@Girish Gowd Talapur***.

17. Microstrip Antenna for WLAN Application Using Probe Feed by ***@Amit Kumar*** and ****Prof.P.R.Chadha***.

18. Mitigation of Induction Generator Effect Due to SSR with STATCOM in Synchronous Generator by ***@S. T.Nagarajan*** and ***@Narendra Kumar***.

19. Performance Evaluation of BLDC Motor with Conventional PI and Fuzzy Speed Controller by ****Madhusudan Singh*** and ****Archna Garg***.

20. Study of Potential Energy Term in VMINS model by *Pallavi Bhatt, Hardik P. Trivedi, Lalit K. Gupta, Anil Kumar*, ***@Than Singh Saini***, *Krishna Chandra* and *Jai Prakash Gupta*.

21. Temperature Dependent Analysis of Thermoelectric Module using Matlab/SIMULINK by *Aarti Kane* ***, @Vishal Verma*** *and* ***@Bhim Singh***.

***** **Faculty**
@ **Students/Research Scholars**
# **Alumn**

A Comparative Study of Damping Subsynchronous Resonance Using SSSC and STATCOM

Nisha Kamboj
Electrical Department
Delhi Technological University
nisha.kamboj1@gnail.com

Narendra Kumar
Electrical Department
Delhi Technological University
dnk_1963@yahoo.com

Ajendra Singh
Electrical Department
Delhi Technological University
ajendrasingh25@yahoo.co

***Abstract*—Application of series capacitor in long transmission line is a cost effective method to increase power transfer. But presence of series capacitor has sometimes been limited because of the concern for subsynchronous resonance phenomenon in transmission line. SSR is basically an electrical power system condition where the electrical network exchanges energy with the turbine generator at one or more of the natural frequencies of the combined system below the synchronous frequency of the system. Presence of SSR torque causes oscillation which causes shaft fatigue and possible damage or failure of shaft. Long transmission line needs series or shunt compensation for power flow control as well as for mitigating the SSR phenomenon. An idea of this paper is to damp SSR by adding static synchronous series compensator (SSSC, Series device) or Static compensator (STATCOM, Shunt device). This paper shows that damping characteristics obtained by SSSC is better than STATCOM for damping SSR phenomenon. The results are obtained by modelling a lineralized system in MATLAB and study is performed on the system adapted from the IEEE first bench mark model for Eigen value analysis.**

***Keywords*—static compensator (STATCOM); subsynchronous resonance (SSR); Static synchronous series compensator (SSSC); modelling; IEEE first benchmark model; eigenvalue analysis**

I. INTRODUCTION

It is a very challenging task for power system engineer to efficiently utilize the existing transmission facilities in a secure manner because of continuous increase of demand of electrical energy and constraint on right of way for transmission lines has caused the power system to operate in stressed condition. Subsynchronous resonance is more concerned for turbine generator connected to series compensated transmission line. This stressed condition can cause fatigue and damage of shaft and become very costly.

The concept of Flexible AC Transmission Systems (FACTS) which is originated by Hingorani [1] can overcome the bottlenecks of AC power transmission. In addition to power flow control and voltage regulation, FACTS controllers are also used for transient stability improvement and mitigating SSR phenomenon. A problem of interest in the power industry in which FACTS controllers could play a major role is the mitigation of Subsynchronous Resonance (SSR) oscillations. SSR is a dynamic phenomenon in the power system which has certain special characteristics. Various papers on modelling and improvement of this scheme have also been given [2, 3].

The idea to control SSR phenomenon by introducing SSSC was introduced in [4, 5] which is a series FACTS device. An idea to suppress SSR by adding STATCOM was introduced in [6, 7].

The main emphasis of this paper is to test the effectiveness of SSSC and STATCOM for damping SSR in a series compensated system and compare their results. This paper also shows that damping characteristics obtained by using SSSC are better than STATCOM. The IEEE First Benchmark Models [8] for subsynchronous studies is used to conduct eigenvalue analyses and time domain simulations.

II. SYSTEM DESCRIPTION

A. Synchronous Machine Model

We have use Model 1.1 (Field circuit with one equivalent damper on q-axis) published By IEEE task force, of synchronous machine for modelling.

The electrical dynamic equations of the synchronous machine are presented below [9]:

1) Stator Equation:

$$v_q = -\frac{1}{\omega_B}\frac{d\Psi_q}{dt} - (1+S_m)\Psi_d - R_a i_q \quad (1)$$

$$v_d = -\frac{1}{\omega_B}\frac{d\Psi_d}{dt} - (1+S_m)\Psi_q - R_a i_d \quad (2)$$

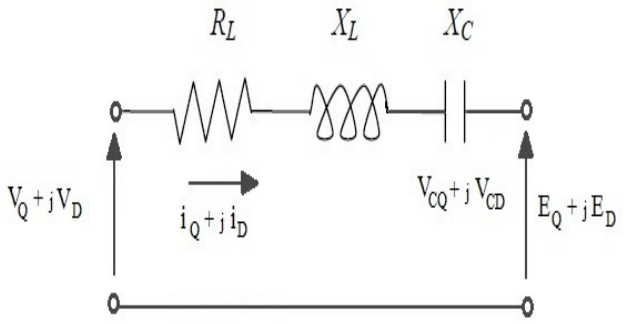

Fig.1 A series capacitor compensated network model

978-1-4673-0934-9/12/$31.00 ©2012 IEEE

2) Rotor Equations:

$$\frac{dE_d'}{dt} = \frac{1}{T_{qo}'}\left[-E_d' - (x_q - x_q')i_q\right] \quad (3)$$

$$\frac{dE_q'}{dt} = \frac{1}{T_{do}'}\left[-E_q' + (x_d - x_d')i_d + E_{fd}\right] \quad (4)$$

B. Network Model:

Fig.1. shows that a series capacitor-compensated transmission line may be represented by the RLC circuit [9]

$$\dot{\Delta x}_N = [A_N]\Delta x_N + [B_{N1}]\Delta y_G \quad (5)$$

$$\Delta u_G = \frac{X_L}{W}\Delta \dot{y}_G + [F1]\Delta y_G + [F_{S1}]\Delta x_{n1} + \Delta e1 \quad (6)$$

III. System Modelling for Eigenvalue Analysis

We shall now demonstrate the damping effects of SSSC and STATCOM through eigenvalue analysis. To do this, we have to develop a linear model of the overall system. The linearized models for the generator and shaft system for IEEE first benchmark are well documented. Here we use approach given in [10]

The linearized state equations are given by

$$\dot{\Delta x}_G = [A_G]\Delta x_G + [B_{G1}]\Delta u_g + [B_{G2}]E_{fd} \quad (7)$$

$$\Delta y_G = [C_G]\Delta x_G$$

A. Combined Generator and Shaft System Model

The state vector Δx_G, input vector Δu_g and output vector Δy_G are given by

$$\left[\Delta x_m\right]^t = \left[\delta_{GEN} \quad S_{EXC} \quad T_{GE} \quad S_{GEN} \quad T_{LBG} \quad S_{LPB} \quad T_{LAB} \quad S_{LPA} \quad T_{ILA} \quad S_{IP} \quad T_{HI} \quad S_{HP}\right]$$

$$\left[\Delta x_e\right]^t = \left[\Delta\Psi_d \quad \Delta\Psi_q \quad \Delta E_d' \quad \Delta E_q'\right]$$

$$\left[\Delta y_G\right]^t = \left[\Delta i_D \quad \Delta i_Q\right]$$

B. Modelling the Transmission line

The differential equations for the circuit elements, after applying Park's transformation, can be expressed in the d-q reference frame as following

The voltage across the capacitor [11]:

$$\begin{bmatrix}\dot{\Delta V}_{CD}\\ \dot{\Delta V}_{CQ}\end{bmatrix} = \begin{bmatrix}0 & -\omega_B\\ \omega_B & 0\end{bmatrix}\begin{bmatrix}\Delta V_{CD}\\ \Delta V_{CQ}\end{bmatrix} + \begin{bmatrix}\omega_B X_C & 0\\ 0 & \omega_B X_C\end{bmatrix}\begin{bmatrix}\Delta i_D\\ \Delta i_Q\end{bmatrix} \quad (8)$$

The above equations can be represented in state space model as:

$$\dot{\Delta x}_N = [A_N]\Delta x_N + [B_{N1}]\Delta u_{N1} + [B_{N2}]\Delta u_{N2} \quad (9)$$

where state vector Δx_N and Input vector Δu_{N1} are

$$\left[\Delta x_N\right]^t = \left[\Delta V_{CD} \quad \Delta V_{CQ}\right]$$

$$\left[\Delta U_{N1}\right] = \begin{bmatrix}\Delta i_D\\ \Delta i_Q\end{bmatrix}$$

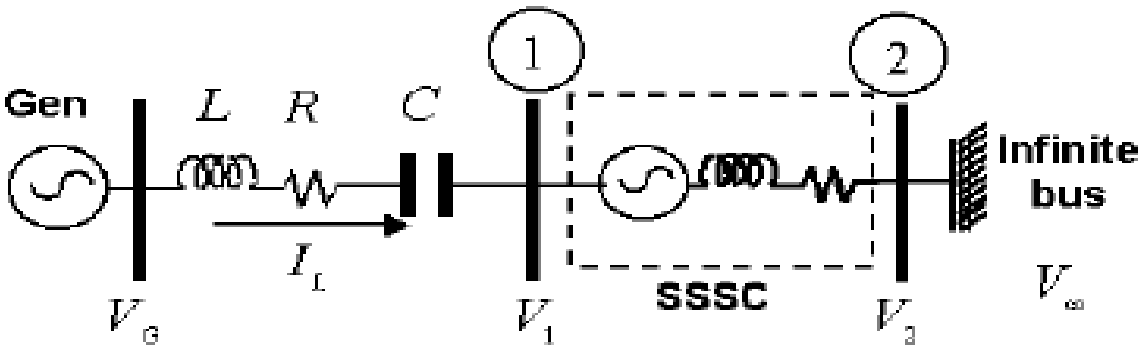

Fig.2 SSSC connected to first benchmark model

C. Modelling SSSC unit

Here Fig. 2. shows the SSSC connected to transmission line for Eigenvalue analysis. Eigenvalue studies and time domain simulations conducted on the IEEE first benchmark model show the damping benefits on SSR of SSSC coupled to transmission line. Addition of SSSC in a series compensated power system provides superior performance characteristics and application flexibility not achievable by conventional series capacitor. The voltage source nature of the SSSC can stabilize the unstable torsional modes of a fixed capacitor compensated transmission system as it increase the damping of the torsional and network modes. The presence of series capacitor increase the synchronising power coefficient .it also improve the small signal stability of power system reduction of MVAR rating of SSSC is an added advantage of the combination. High values of capacitive reactance can cause torsional interaction. An auxiliary controller that modulated the output of the PI controller can stabilize the torsional torsional modes. Thus, with the combination of SSSC and damping controller, the amount of fixed compensation can be increased without endangering the system stability.

Normalized per unit equations of the SSSC in DQ frame are [4, 5].

$$\frac{d}{dt}\begin{bmatrix} i_{ld} \\ i_{lq} \\ v_{dc} \end{bmatrix} = \begin{bmatrix} -\frac{WR_R}{X_R} & -W & -\rho_1 Sin\theta_f \\ W & -\frac{WR_R}{X_R} & -\rho_1 Cos\theta_f \\ \rho_2 Sin\theta_f & \rho_2 Cos\theta_f & -\frac{WX_{DC}}{R_{DC}} \end{bmatrix} \begin{bmatrix} i_{ld} \\ i_{lq} \\ v_{dc} \end{bmatrix} + \begin{bmatrix} \frac{W}{X_R} & 0 & 0 \\ 0 & \frac{W}{X_R} & 0 \\ 0 & 0 & 1 \end{bmatrix} \begin{bmatrix} v_{TD} \\ v_{TQ} \\ 0 \end{bmatrix} \tag{10}$$

where $X_R = WL_R$, $X_{DC} = \frac{1}{WC_{DC}}$, $\rho 1 = \sqrt{3}W / X_R$

$$\rho 2 = \sqrt{3}WX_{DC}$$

Linearizing SSSC equations can be written as

$$\Delta \dot{x}_{N2} = [AN2]\Delta x_{N2} + [BN2]\Delta Y_G + [B_C]\Delta\theta_F \tag{11}$$

$$\Delta v_1 = -\frac{X_R}{W}\Delta \dot{Y}_G + [F2]\Delta Y_G + [F_{S2}]\Delta X_{N2} + [F_C]\Delta\theta_F + \Delta e_2 \tag{12}$$

where

$$\Delta X_{N2} = \Delta V_{dc}$$

$$\Delta e_2^T = \begin{bmatrix} \Delta V_{\alpha D} & \Delta V_{\alpha Q} \end{bmatrix}$$

$$\begin{bmatrix} A_{N2} \end{bmatrix} = -wX_{dc} / R_{dc}$$

$$\begin{bmatrix} B_{N2} \end{bmatrix} = \sqrt{3}wX_{dc}\begin{bmatrix} Sin\theta_{f0} & Cos\theta_{f0} \end{bmatrix}$$

$$[B_C] = \sqrt{3}wX_{dc}\left(i_{D0}Cos\theta_{f0} - i_{D0}Sin\theta_{f0}\right)$$

$$F_2 = \begin{bmatrix} R_R & X_R \\ -X_R & R_R \end{bmatrix}$$

$$[F_{S2}]^T = \begin{bmatrix} \sqrt{3}Sin\theta_{f0} & \sqrt{3}Cos\theta_{f0} \end{bmatrix}$$

$$[F_c] = \sqrt{3}v_{dc0}\left(Cos\theta_{f0} - Sin\theta_{f0}\right)$$

$$\Delta \dot{x}_n = [A_N]\Delta x_N + [B_N]\Delta y_G + [B_c]\Delta\theta_f$$

$$\Delta u_G = \frac{X}{w}\Delta \dot{y}_G + [F_S]\Delta x_N + [F]\Delta y_G + [F_c]\Delta e_2 \tag{13}$$

Equation (13) is obtained by combining (5), (6), (11) and (12), so overall network equation is given by (13).

D. Modelling STATCOM unit

The STATCOM is modelled [6,7] in detail when switching function are approximated by their fundamental frequency components neglecting harmonics, STATCOM can be modelled by transforming the three phase voltage and current to DQ variables using Kron's transformation[12].

$$V_S = \sqrt{v_{SQ}^2 + v_{SD}^2} \tag{14}$$

$$\frac{di_{sa}}{dt} = -\frac{W_B}{X_S}\left[R_S i_{sa} + v^i{}_{sa} - v_{sa}\right] \tag{15}$$

$$\frac{di_{sb}}{dt} = -\frac{W_B}{X_S}\left[R_S i_{sb} + v^i{}_{sb} - v_{sb}\right] \tag{16}$$

$$\frac{di_{sc}}{dt} = -\frac{W_B}{X_S}\left[R_S i_{sc} + v^i{}_{sc} - v_{sc}\right] \tag{17}$$

$$\frac{di_{sd}}{dt} = -\frac{R_S W_B}{X_S} i_{sd} - W_0 i_{sq} + \frac{W_B}{X_S}\left[v_{sd} - v^i{}_{sd}\right] \tag{18}$$

$$\frac{di_{sq}}{dt} = -\frac{R_S W_B}{X_S} i_{sq} + W_0 i_{sd} + \frac{W_B}{X_S}\left[v_{sq} - v^i{}_{sq}\right] \tag{19}$$

$$\frac{dv_{dc}}{dt} = -\frac{W_B i_{dc}}{b_c} - \frac{W_B v_{dc}}{b_c R_B} \tag{20}$$

$$v^i{}_{sd} = Kv_{dc}Sin(\alpha + \theta_s) \tag{21}$$

$$v^i{}_{sq} = Kv_{dc}Cos(\alpha + \theta_s) \tag{22}$$

where $K = \frac{2\sqrt{6}}{\pi}$, $\theta_s = Tan^{-1}\frac{v_{sd}}{v_{sq}}$, $V_S = \sqrt{v_{SQ}^2 + v_{SD}^2}$

E. Combined System Model Including SSSC only

Combined system model is given by [4-5]

$$\dot{X} = Ax + Bu$$

where $x^t = \left[\triangle x_G \quad \triangle x_N\right]$, and $u = \triangle\theta_f$

$$A = \begin{bmatrix} \left\{A_G + B_G H\left(FC_G + \dfrac{X_T C_G A_G}{w_B}\right)\right\} & B_G H F_S \\ B_N C_G & A_N \end{bmatrix} \quad (23)$$

$$B^T = \begin{bmatrix} B_G H F_C & B_C \end{bmatrix}$$

$$\text{and } H = \left\{I - \frac{X_L}{w_B}[C_G][B_G]\right\}^{-1}$$

F. Combined System Model Including STATCOM only

$$\triangle X_{SC} = \left[A_{SC}\right]\triangle X_{SC} + \left[B^i_{Sc}\right]\begin{bmatrix}\triangle i_{SD} \\ \triangle i_{SQ}\end{bmatrix} + \left[B^V_{SE}\right]\triangle U_{SE} \quad (24)$$

$$\left[A_{SE}\right] = \begin{bmatrix} -\dfrac{R_S W_B}{X_S} & -W_0 & -\dfrac{W_B K Sin(\alpha+\theta_s)}{X_S} \\ W_0 & -\dfrac{R_S W_B}{X_S} & -\dfrac{W_B K Cos(\alpha+\theta_s)}{X_S} \\ \dfrac{W_B K Sin(\alpha+\theta_s)}{b_c} & \dfrac{W_B K Cos(\alpha+\theta_s)}{b_c} & -\dfrac{W_B}{b_c R_p} \end{bmatrix} \quad (25)$$

$$\left[B^V_{SE}\right] = \begin{bmatrix} \dfrac{W_B}{X_S}\left[1 - \dfrac{K v_{dc} Cos(\alpha+\theta_s) vsq}{Vs^2}\right] & \dfrac{W_B K v_{dc} Cos(\alpha+\theta_s) v_{SD}}{X_S Vs^2} \\ \dfrac{W_B K v_{dc} Sin(\alpha+\theta_s) v_{SQ}}{X_S Vs^2} & \dfrac{W_B}{X_S}\left[1 - \dfrac{K v_{dc} Sin(\alpha+\theta_s) v_{SD}}{Vs^2}\right] \\ -\dfrac{W_B K_{c1} vsq}{b_c Vs^2} & \dfrac{W_B K_{c1} v_{SD}}{b_c Vs^2} \end{bmatrix} \quad (26)$$

$$\theta_s = tan^{-1}\frac{v_{sd}}{v_{sq}}$$

$$\text{And } cl = -i_{sD} Cos(\alpha+\theta_s) + i_{sQ} Sin(\alpha+\theta_s)$$

TABLE I. EIGEN VALUE ANALYSIS USING DIFFERENT CASES

S.No.	Without SSSC P=0.7 ,P.F.=0.9, Xc=0.35	With SSSC Only P=0.7 ,P.F.=0.9 Xc=0.1	With STATCOM P=0.7 ,PF=0.9, Xc=0.55	Comments
1	-1.4621 + j10.264 -1.4621 – j10.264	-0.4000 + j8.40 -0.4000 – j8.40	-0.0326 + j17.21 -0.0326 - j17.21	Torsional Mode #0
2	0.022651+ j99.626 0.022651– j99.626	-0.1500 + j99.13 -0.1500 – j99.13	-0.0013 + j99.41 -0.0013 – j99.41	Torsional Mode #1
3	0.026317 + j127.14 0.026317 – j127.14	-0.6600 + j127.02 -0.6600 – j127.02	-0.00001+ j127.1 -0.00001– j127.1	Torsional Mode #2
4	0.041363+ j160.35 0.041363 – j160.35	-0.6600 + j160.63 -0.6600 – j160.63	-0.0002 + j160.8 -0.0002 – j160.8	Torsional Mode #3
5	0.0024116 + j202.86 0.0024116 – j202.86	-0.0300 + j203.04 -0.0300– j203.04	-0.0003 + j203.3 -0.0003 – j203.3	Torsional Mode #4
6	-2.9973e-007 + j298.18 -2.9973e-007 - j298.18	-0.1800 + j298.18 -0.1800 – j298.18	-0.0000 + j298.2 -0.0000 – j298.2	Torsional Mode #5
7	-3.3952 + j141.24 -3.39752– j141.24	-3.9400+ j250.13 -3.9000– j250.13	-0.09333 + j276.4 -0.09333–j276.4	Network Mode #1
8	-4.4198 + j612.42 -4.4198 – j612.42	-4.3400 + j502.79 -4.3400 – j502.79	0.0262 + j641.7 0.0262 – j641.7	Network Mode #2
9	-0.95897	-0.0001	-0.0004	
10	-1.2155	-3.3333	-0.0008	
11		-0.0328	-0.0000+j98.7 -0.0000-j98.7	

IV. CASE STUDIES

The system considered is the IEEE first benchmark model for SSR analysis [12]. The FBS system is simulated with the help of MATLAB. The Network parameter are based on generator base of 892.4 MVA are given in [2,3] .The Synchronous M/C data are given in [12].The shaft inertia and spring constant are given in [12]. There are six inertias corresponding to six rotors, which are four turbines, one generator and one rotating exciter. A steady-state operating point is chosen in which the machine operates with a power factor of 0.9 while delivering a power of 0.7 p.u. Self-damping of 0.1 is added to the shaft. No mutual damping is assumed.

For SSSC [4] we assume X_C=0.1, X_L=0.7, X_d =1.79 and for STATCOM [6] X_C =0.55, X_S=0.15, bc=0.2984; R_p=299.66. Table I shows eigenvalues of system with and without SSSC and STATCOM. As we can see that on adding SSSC and STATCOM, the system Eigen values have negative real parts.

This indicates that system has reached in stable configuration.

V. TIME DOMAIN ANALYSIS

A digital computer simulation study, using a liberalized system model, has been carried out to demonstrate the effectiveness of the proposed controllers. The MATLAB SIMULINK model was used to obtain time domain simulation under large disturbances. The SSSC is coupled to HP and electrical connected to System. The STATCOM is connected in the network. The SIMULINK model is run for 10 seconds and various shaft torques and power angle delta response were obtained. Fig.3 (a, d, g, j, m, p) shows the response obtained without SSSC. Fig.3 (b, e, h, k, n, q) the same responses when SSSC is connected to the system. Fig. 3 (c, f, i, l, o, r) shows the responses when STATCOM connected to the system. We see that SSR is effectively damped out by using SSSC which is a series device.

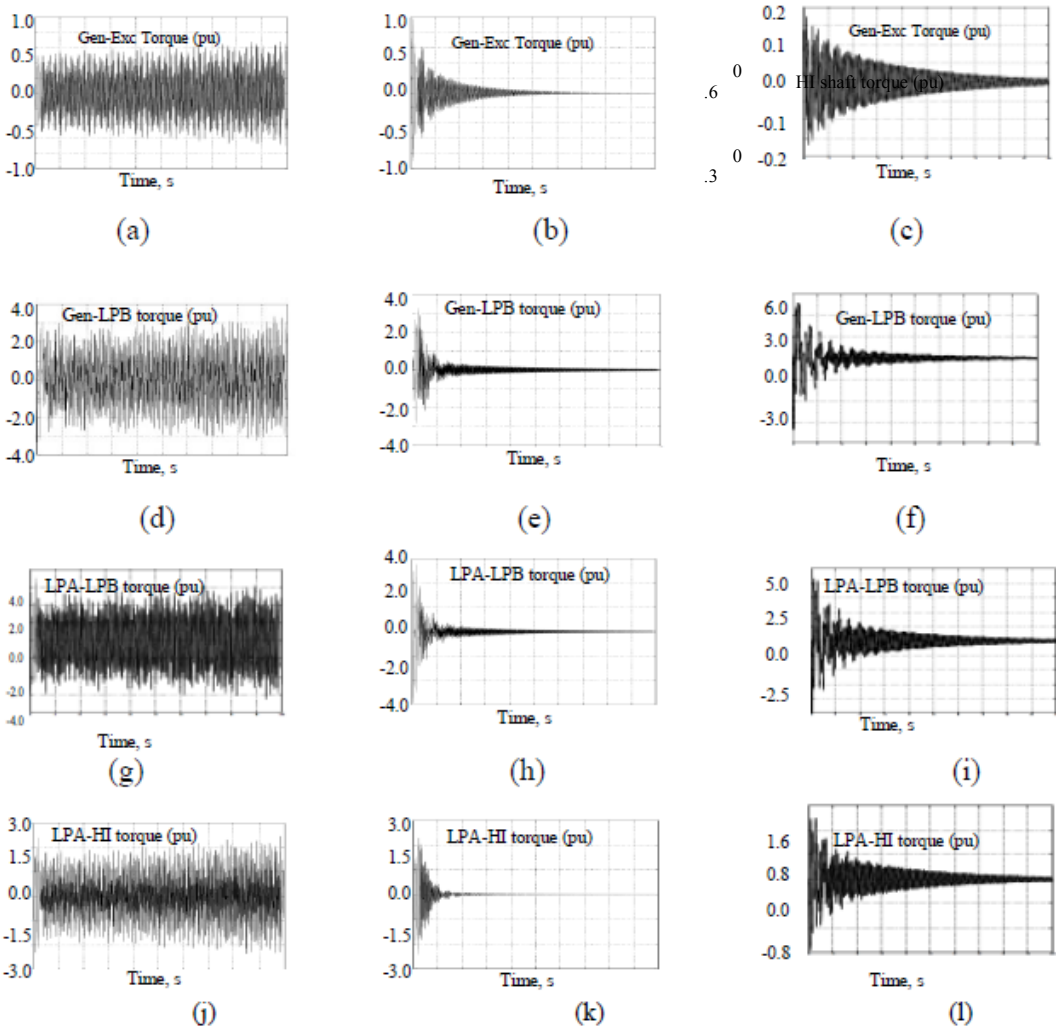

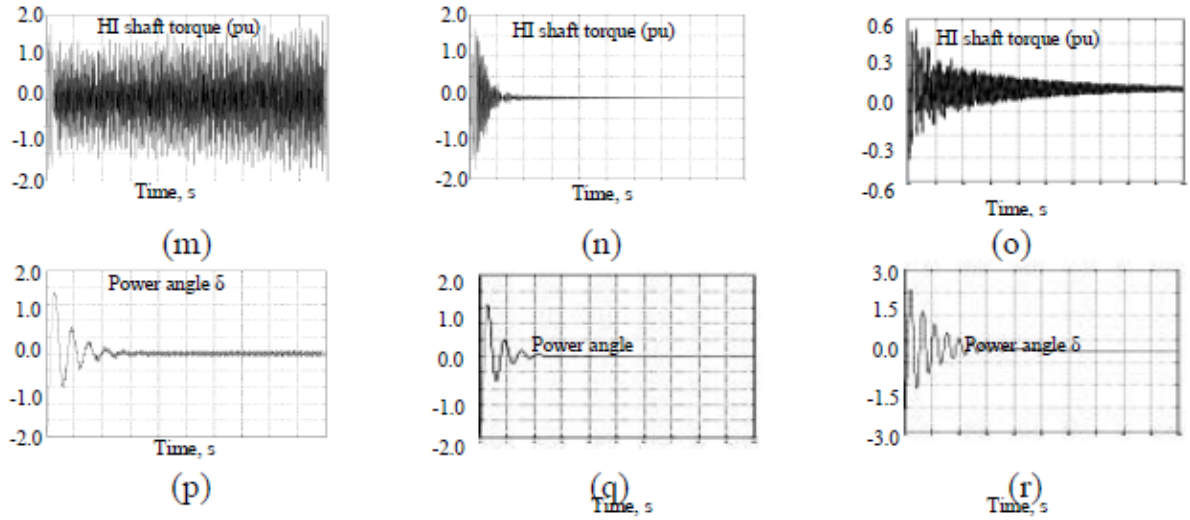

Fig.3 Generator exciter torque oscillations with fixed capacitor, (b) Generator exciter torque oscillations with SSSC, (c) Generator exciter torque oscillations with STATCOM, (d) Generator LPB shaft torque oscillations with fixed capacitor, (e) Generator LPB shaft torque oscillations with SSSC, (f) Generator LPB shaft torque oscillations with STATCOM, (g) LPA-LPB shaft torque oscillations with fixed capacitor, (h) LPA-LPB shaft torque oscillations with SSSC, (i) LPA-LPB shaft torque oscillations with STATCOM (j) LPA-HI shaft torque oscillations with fixed capacitor, (k) LPA-HI shaft torque oscillations with SSSC (l) LPA-HI shaft torque oscillations with STATCOM, (m) HI shaft torque oscillations with fixed capacitor, (n) HI shaft torque oscillations with SSSC (o) HI shaft torque oscillations with STATCOM, (p) Power angle oscillations with fixed capacitor, (q) Power angle oscillations with SSSC, (r) Power angle oscillation with STATCOM

VI. CONCLUSIONS

Eigenvalue studies and time domain simulations conducted on the IEEE First Benchmark Models show the damping benefits on SSR of SSSC and STATCOM the major findings of the study are as follows.

- SSR phenomenon going to increase with the increase in shunt capacitance in transmission line.
- As SSSC can exchange both active and reactive power so it makes possible to control reactive and resistive line drops and maintain a effective x/r ratio for series compensation.
- Reduction in MVAR rating of SSSC is an added advantage for suppressing SSR.
- SSSC is a series FACTS device, which could be used to completely replace traditional series capacitor with even more flexibility of series compensation.
- By including STATCOM in series compensated transmission line we do not change the SSR characteristics of network significantly.
- STATCOM can control the line reactive power and by adding an auxiliary speed controller in STATCOM we can control SSR also effectively. This paper provides comparative study of damping SSR by using FACTS Devices SSSC and STATCOM which is series and shunt device respectively.
- SSSC a series FACTS device is more effective in damping SSR in comparison the STATCOM which is a shunt FACTS device.

REFERENCES

[1] N. G. Hingorani, and L. Gyugyi, "Understanding FACTS: concepts and technology of flexible AC transmission systems," New York, IEEE Press, 2000.

[2] B. K. Perkins and M. R. Iravani, "Dynamic modeling of a TCSC with application to SSR analysis," IEEE Trans. Power Syst., vol. 12, no. 4,pp. 1619–1625, Nov. 1997.

[3] X. Zhao and C. Chen, "Damping subsynchronous resonance using an improved NGH SSR damping scheme," in Proc. IEEE Power Eng. Soc. Summer Meeting, Jul. 1999, vol. 2, pp. 780–7.

[4] G. N. Pilani ,Arindam Ghosh, and Avinash Joshi "Torsinal interaction studies on power system compensated by SSSC and fixed capacitor," IEEE Trans.on Power delivery., vol. 18, no. 3,july 2003.

[5] L. S. Kumar and A. Ghosh ,"Modelling and control design of a static synchronous series compensator," IEEE Trans. Power Delivery., vol. 14,pp.1448-1453,Oct. 1999.

[6] K.V. Patil, J. Senthil, J. Jiang and R.M. Mathur, "Application of STATCOM for Damping Torsional Oscillations in Series Compensated AC Systems," IEEE Transactions on Energy Conversion, vol. 13, No. 3, September 1998, pp. 237-243.

[7] K. R. Padiyar and Nagesh Prabhu, "Design and Performance Evalution of Subsynchronous Damping Controller with STATCOM," IEEE Trans. On Power Delivery, vol.21, No.3, July 2006.

[8] IEEE Subsynchronous Resonance Task Force, "First benchmark model for Computer simulation of subsynchronous resonance," IEEE Trans. Power App. Syst., vol. PAS-96, no. 5, pp. 1565–1572, Sep. 1977.

[9] K. R. Padiyar, "Power System Dynamics stability and control," BS Publication, second Edition, 2008.

[10] S. Purushothaman, "Eliminating Subsynchronous oscillations with an Induction Machine Damping Unit (IMDU)," IEEE Trans. On Power System, vol. 26, No. 1,Feb. 2011

A Generalized Neural Simulator for Computing Different Parameters of Circular/Triangular Microstrip Antennas Simultaneously

Taimoor Khan and Asok De
Department of Electronics and Communication Engineering
Delhi Technological University (Formerly Delhi College of Engineering)
Delhi-110042, India, E-mail: ktaimoor@gmail.com

***Abstract*— Computation of different parameters using a generalized hardware/software approach leads to save time and resources. Keeping this concept in mind authors are proposed a generalized neural simulator for computing two parameters each of circular patch (i.e. resonance frequency and radius) and triangular patch (i.e. resonance frequency and side-length) microstrip antennas simultaneously. For the purpose nine different training algorithms are used and Levenberg-Marquardt (LM) backpropagation is proved to be the fastest converging training algorithm and producing the results with least error. The results thus obtained by this simulator are in conventionality and very good in agreement with their measured counterparts.**

***Keyword*—** *Computing parameters; different microstrip patches; generalized simulator and RBF neural simulator.*

I. INTRODUCTION

The most popular conventional models used to solve the real electromagnetic (EM) problems, are the transmission line model [1], cavity model [2], and full wave model [3]. Basically three stages are involved in solving typical EM problems using conventional models. Firstly the problem is formulated by writing-up a set of system equations to be solved. Then in the second stage, geometry is created which describes the problem and the necessary discretization of the problem domain into smaller elements and the system of equations using the method of choice is solved in the third stage. There are various situations like optimization of problem geometry for optimum outputs, where repetitive computation of EM field is required. A minor change in the problem geometry would require a different discretization which itself is a time consuming exercise. Further all these techniques have their own strong and weak points and require elaborate mathematics in applying on EM problems.

In the last one decade, the artificial neural networks (ANNs) have acquired tremendous utilization in the design and optimization of RF/Microwave Circuits [4-7] and especially in analyzing and designing the microstrip antennas [8-20]. It is so because the neuro-models (NMs) are computationally much more efficient than EM models and require lesser time to model a circuit. The training of NM is done off-line using few patterns generated through measurement, simulation and/or analytical model suitable for a problem. Once the NM is trained for a specified error it will return the results for every infinitesimal change in the input patterns within a fraction of a second. The neural models [8, 9, 10, 15, 16, and 17] have been used for calculating the single parameter i.e. the resonance frequency of the microstrip antennas. Again the models [18, 19, and 20] have been utilized for calculating the single parameter i.e. the physical dimension of the microstrip patch antennas. Turker et al [11] have calculated two parameters i.e. the resonance frequency and physical dimensions of the same rectangular patch microstrip antennas whereas Guney and Sarikaya [12-13] and Guney et al [14] have calculated the resonance frequency of different patches. In the literature [8-20] no one has utilized the capability of neural networks in computing more than two parameters of different microstrip patch antennas simultaneously. In this paper authors have proposed a generalized radial basis function neural simulator (GRBFNS) for computing the resonance frequency and radius of circular patch microstrip antennas (CPMSA) and the resonance frequency and side-length of equilateral triangular patch microstip antennas (ETMSA) simultaneously. Although the neural models can be trained for the measured results, simulated results and/or calculated results but to understand the novelty of the proposed work initially it has been decided to utilize the available measured results [21-29] as training and testing patterns. Once it is tested and validated successfully, it can be generalized on measured patterns, simulated patterns and/or calculated patterns.

II. PROPOSED GENERALIZED NEURAL APPROACH

The generalized neural approach for computing four different parameters is based on radial basis function neural network

9978-1-4673-3115-9/12/$31.00 ©2012 IEEE

(RBFNN). A RBF neural network consists of three layers feed-forward neural network with entirely different roles. The first layer i.e. input layer is made-up of source nodes which connect the network to the outside environment. The second layer i.e. the hidden layer uses a multivariate Gaussian non-linear transformation as an activation function. The third layer i.e. the output layer is linear, supplying the response of the network. During training process, an RBFNN model is developed by learning from the available patterns. The aim of training process is to minimize the error between target output and actual output of the RBFNN model. As far as training is concerned, the RBFNN is much faster than the multi-layered perceptron neural network (MLPNN). It is so because the training process in RBFNN has two stages and both the stages are made more efficient by using appropriate learning algorithms. That is the reason of using RBFNN instead of MLPNN. Once the model is trained for a specified mean square error (MSE), then it will return the results for every infinitesimal change in the applied input patterns within a fraction of a second. There are three main steps in applying neural networks for the instant calculation of desired parameter (resonance frequency, radius or side-length) of desired patch (circular or equilateral triangular). In the first step training and testing patterns are generated and the structural configuration of hidden layers and the neurons in each hidden layer is selected for training in the second step. And finally, training algorithm is applied on RBFNN model in the third step. The details of the steps involved are being discussed in the subsequent sections below.

A. Generation of Training and Testing Patterns

A microstrip antenna, in its simplest configuration, consists of a radiating conductive patch (circular or equilateral triangular patch) on one side of a dielectric substrate (of relative permittivity, 'ε_r', and of thickness, 'h',) having a ground plane on the other side. The side-view of the proposed antenna is shown in Fig. 1(a) whereas Fig. 1(b) shows the two radiating patches used on the top of the substrate in Fig. 1(a). The radius of CPMSA and the side-length of ETMSA are represented by 'r_c' and 'L_e' respectively as shown in Fig. 1(b).

It is clear from the literature [21-29] that the resonance frequency of a microstrip patch antenna is the function of physical dimension(s) of patch, relative permittivity, 'ε_r' and thickness , 'h' of the substrate and mode of propagation represented by integer 'm' and 'n'. Here physical dimension corresponds to the radius 'r_c' in case of CPMSA or side-length 'L_e' in case of ETMSA. Now if the resonance frequency, thickness of the substrate, relative permittivity, and mode of propagation are given, then the physical dimension(s) can also be easily calculated. Keeping this concept in mind, total 70 patterns (20 each for resonance frequency and radius of CPMSA and 15 each for resonance frequency and side-length of ETMSA) have been arranged from the open literature [21-27] and [28-29] respectively. These patterns are used in training and testing of the proposed neural model. Although the proposed approach can be applied on simulated, measured and/or calculated patterns. But for making it convenient it has been decided firstly to apply on available patterns [21-29] only.

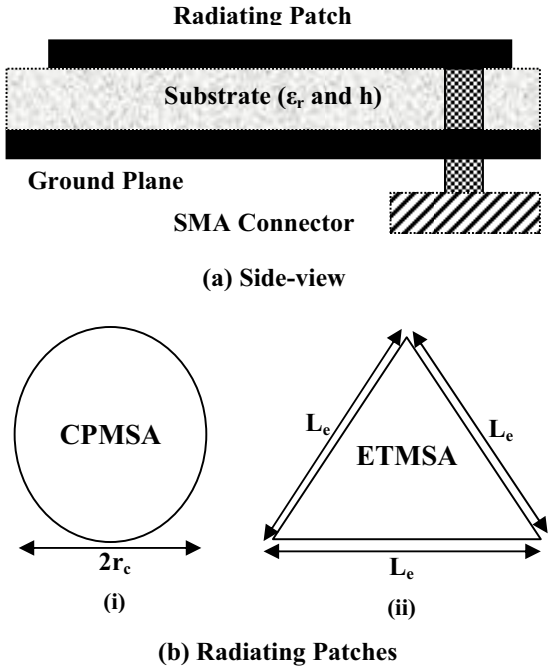

Fig. 1: Geometry of Proposed Microstrip Antenna

B. Proposed Structure and Training Algorithms

From the literature [21-29] it is concluded that the calculated parameter is the function of five input parameters each for analysis of CPMSA, design of CPMSA, analysis of ETMSA, and design of ETMSA. To distinguish these four different cases, an arbitrary parameter (say x_1) is included in 5-dimensional input pattern where x_1 = 1, 2, 3 and 4 corresponds to the analysis of CPMSA, design of CPMSA, analysis of ETMSA and design of ETMSA. Thus the total inputs become six each for analysis and design of CPMSA and ETMSA. This is shown in Table 1.

For calculating these four parameters simultaneously a generalized radial basis function neural simulator (GRBFNS) is suggested as shown in Fig. 2. In the training process of RBFNN firstly the RBF centers and width are determined and then the weights are estimated [30].

The center function is Gaussian function:

$$h_i(X) = \exp\left[\frac{\|X - c_i\|^2}{2\sigma_i^2}\right] \qquad (1)$$

Where i = 1, 2, 3……..k……..N. X denotes n dimensional input vector $X = (x_1, x_2, \ldots\ldots x_n)$. c_i denotes RBF center, σ_i^2 denotes width and $h_i(X)$ denotes output of i^{th} neuron.

Now the output is

$$y[x(k)] = \sum_{i=1}^{N} w_i h_i(k) + b \qquad (2)$$

Where w_i represents weight of i^{th} neuron and b is the bias term.

TABLE 1: INPUT-OUTPUT CODING FOR GRBFNN

CASE I: CPMSA ANALYSIS (x_1=1) Total patterns=20		
Patch Parameters	**Inputs**	**Output (f_{cn})**
Radius (cm)	x_2	Resonance Frequency of CPMSA (GHz)
Dielectric Thickness (cm)	x_3	
Dielectric Constant (ε_r)	x_4	
Mode of Propagation (m)	x_5	
Mode of Propagation (n)	x_6	
CASE II: CPMSA DESIGN (x_1=2) Total patterns=20		
Patch Parameters	**Inputs**	**Output (r_{cn})**
Resonance Frequency (GHz)	x_2	Radius of CPMSA (cm)
Dielectric Thickness (cm)	x_3	
Dielectric Constant (ε_r)	x_4	
Mode of Propagation (m)	x_5	
Mode of Propagation (n)	x_6	
CASE III: ETMSA ANALYSIS (x_1=3) Total patterns=15		
Patch Parameters	**Inputs**	**Output (f_{cn})**
Side-Length (cm)	x_2	Resonance Frequency of ETMSA (GHz)
Dielectric Thickness (cm)	x_3	
Dielectric Constant (ε_r)	x_4	
Mode of Propagation (m)	x_5	
Mode of Propagation (n)	x_6	
CASE III: ETMSA DESIGN (x_1=4) Total patterns=15		
Patch Parameters	**Inputs**	**Output (L_{cn})**
Resonance Frequency (GHz)	x_2	Side-length of ETMSA(cm)
Dielectric Thickness (cm)	x_3	
Dielectric Constant (ε_r)	x_4	
Mode of Propagation (m)	x_5	
Mode of Propagation (n)	x_6	

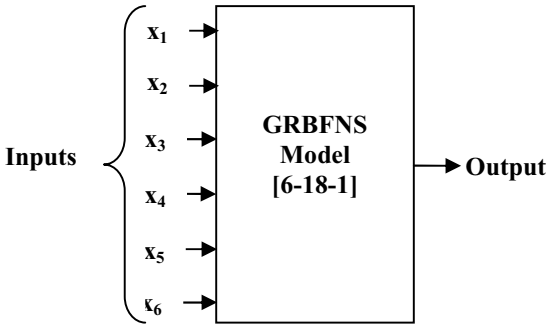

Fig. 2: Generalized RBF Neural Simulator

Selecting the structural configuration of hidden layers and the neurons in each hidden layer is the prime requirement before applying training on the RBF neural network. By using trial and error method a single hidden layer with eighteen neurons is optimized. For training the RBF neural network a number of algorithms such as BFGS (Broyden–Fletcher–Goldfarb–Shanno) quasi-Newton backpropagation, Bayesian regulation backpropagation, scaled conjugate gradient backpropagation, Powell-Beale conjugate gradient backpropagation, conjugate gradient backpropagation with Fletcher-Peeves, one step secant backpropagation, and Levenberg-Marquardt backpropagation, are used [31-33]. In this work the Levenberg-Marquardt (LM) backpropagation [33] is proved to be the fastest converging training algorithm and producing the results with least error. All initial synaptic weights and bias values are selected randomly and rounded-off between -1.0 and +1.0. The mean square error (MSE), learning rate, momentum coefficient and spread value is taken as: 5×10^{-7}, 0.1, 0.5 and 0.5, respectively and epochs required for getting a MSE of 5×10^{-7} is only 112. After getting training successfully, one can predict the response for any desired case (CPMSA Analysis, CPMSA Design, ETMSA Analysis or ETMSA Design) by applying any arbitrary set of corresponding input parameters within a fraction of a second without having knowledge of microstrip antennas and/or neural network. Thus the trained RBFNN model becomes just like to a calculating device for CPMSA Analysis, CPMSA Design, ETMSA Analysis or ETMSA Design asking for corresponding 5-dimensional input pattern.

III. CALCULATED RESULTS AND COMPARISONS

The proposed neural model is trained by nine different training algorithms [31-33] but only Levenberg-Marquardt (LM) backpropagation [33] is proved to be the fastest converging training algorithm and producing the results with least error as can be seen from Table II. The resonance frequency and radius of CPMSA and resonance frequency and side-length of ETMSA calculated during training and testing of the proposed model are given in Table III and Table IV respectively.

A comparison between present results and previous results [12], [13], [14], [15], [16], [17], and [20] is given in Table V. Table V shows that in the models [12], [13], [14], [15], and [16] the training and testing error for CPMSA analysis is calculated as 91.00 MHz, 117.00 MHz 462.00 MHz, 692.15 MHz and 16.00 MHz respectively whereas in the present model it is only 14.70 MHz. In the designing of CPMSA the present model is having error (training and testing) as 0.00045 cm whereas there was no model for designing the CPMSA using neural network in the literature [8-20]. For ETMSA analysis the models [12], [13], [14] and [17] are having error (training and testing) as 27.00 MHz, 28.00 MHz, 272.00MHz and 23.00 MHz respectively whereas in the present method it is only 1.400 MHz. In the

designing of ETMSA the error in testing patterns of the present method is only 0.00040 cm whereas in the model [20] it is 0.0213cm.

TABLE II: TRAINING ALGORITHM VS. ERROR

Training Algorithm	**ERROR IN**		**Iteration Required**
	Case-I: CPMSA Analysis	**Case-II: CPMSA Design**	
Trainlm	**0.00073(GHz)**	**0.00017 (cm)**	**112**
Trainbfg	0.73029(GHz)	6.58400(cm)	33376
Trainbr	0.12298(GHz)	1.02320(cm)	3900
Trainscg	0.61253(GHz)	4.10110(cm)	31481
Traincgb	0.00880(GHz)	129.000(cm)	1372
Traincgf	0.01020(GHz)	98.0000(cm)	1451
Traincgp	0.00990(GHz)	139.000(cm)	34301
Trainoss	0.07990(GHz)	803.000(cm)	25501
Traingdm	0.04380(GHz)	486.000(cm)	94201
Training Algorithm	**Case-III: ETMSA Analysis**	**Case-IV: ETMSA Design**	**Iteration Required**
Trainlm	**0.00009**(GHz)	**0.00008**(cm)	**112**
Trainbfg	0.01003(GHz)	0.57588(cm)	33376
Trainbr	0.00246(GHz)	0.03060(cm)	3900
Trainscg	0.05799(GHz)	0.44433(cm)	31481
Traincgb	8.70000(GHz)	23.0000(cm)	1372
Traincgf	12.3000(GHz)	19.0000(cm)	1451
Traincgp	13.8000(GHz)	62.0000(cm)	34301
Trainoss	187.800(GHz)	115.000(cm)	25501
Traingdm	51.2000(GHz)	489.000(cm)	94201

IV. CONCLUSIONS

A simple, accurate generalized approach based on RBF neural networks has been discussed for CPMSA analysis, CPMSA design, ETMSA analysis and ETMSA design simultaneously. The proposed methodology have been utilized for calculating four different parameters of two different microstrip whereas the previously reported neural models [8, 12, 13, 14, 15, 16, 17 and 20] have been used for calculating only one parameter.

Thus the strength of the proposed model is as summarized here. Firstly, the model is having only one hidden layer of 18 neurons which means the structural configuration of the proposed model is smaller to the structural configuration of [8-20]. Secondly, the model is capable of designing the CPMSA as there is no model for neural design of CPMSA in the literature [8-20]. Thirdly, a common model is calculating four different parameters with more encouraging results simultaneously.

TABLE III: ERRORS IN CPMSA ANALYSIS AND DESIGN

f_{cn}(GHz)	r_{cn}(cm)	f_c~f_{cn}(GHz)	r_c~r_{cn}(cm)
Training and Testing Results			
0.83660	6.80030	0.00160	0.00030
0.82630◄	**6.79950◄**	0.00270	0.00050
0.81550	6.80000	0.00050	0.00000
1.12780	5.00020	0.00020	0.00020
1.44290	3.79980	0.00010	0.00020
1.09890	4.84990	0.00010	0.00010
1.57010	3.49310	0.00010	0.00010
4.07010	1.27010	0.00010	0.00010
1.51010	3.49290	0.00010	0.00010
0.82500	4.95040	0.00000	0.00040
1.03000	3.97500	0.00000	0.00000
1.36010◄	**2.99020◄**	0.00010	0.00020
2.00320	2.00000	0.00020	0.00000
3.75010	1.04010	0.00010	0.00010
4.94500	0.77000	0.00000	0.00000
4.42660	1.14950	0.00160	0.00050
4.72010	1.07040	0.00290	0.00040
5.22660◄	**0.95980◄**	0.00260	0.00020
6.63450	0.73990	0.00050	0.00010
6.07280	0.82000	0.00120	0.00000
Avg. Absolute Error ➔		**0.00073**	**0.00017**
◄ represents testing patterns			

Table IV: ERRORS IN ETMSA ANALYSIS AND DESIGN

f_{en}(GHz)	L_{en} cm)	f_e~f_{en}(GHz)	L_e~L_{en}(cm)
Training and Testing Results			
1.51890◄	**4.0999◄**	0.00010	0.00010
2.63690	4.1000	0.00010	0.00000
2.99500	4.0999	0.00000	0.00010
3.97300	4.1000	0.00000	0.00000
4.43900	4.0999	0.00000	0.00010
1.48900◄	**8.7000◄**	0.00000	0.00000
2.59620	8.6999	0.00020	0.00010
2.96890	8.7001	0.00010	0.00010
3.96780	8.7000	0.00020	0.00000
4.44280	8.7000	0.00020	0.00000
1.28000	10.0000	0.00000	0.00000
2.24180	9.9998	0.00020	0.00020
2.55010	10.0001	0.00010	0.00010
3.40000	10.0001	0.00000	0.00010
3.82380◄	**9.9997◄**	0.00020	0.00030
Avg. Absolute Error ➔		**0.00009**	**0.00008**
◄ represents testing patterns			

TABLE V: COMPARISON OF ERRORS IN PRESENT METHOD AND PREVIOUS METHODS

Case-I: CPMSA Analysis		**Case-III: ETMSA Analysis**	
Method	**Error**	**Method**	**Error**
Ref. [12]	91.00 MHz♦	Ref. [12]	27.00 MHz♦
Ref. [13]	117.00 MHz♦	Ref. [13]	28.00 MHz♦
Ref. [14]	462.00 MHz♦	Ref. [14]	272.00 MHz♦
Ref. [15]	692.15 MHz♦	Ref. [17]	23.00 MHz♦
Ref. [16]	16.00 MHz♦	**PM**	**1.40 MHz♦**
PM	**14.70 MHz**	**Case-IV: ETMSA Design**	
Case-II: CPMSA Design		Ref. [20]	0.02130 cm Δ
PM	**0.00045 cm**	**PM**	**0.00040 cm Δ**
PM represents present method. ♦-represents Total Error and **Δ**-represents Testing Error only			

REFERENCES

[1] R.F. Munson, "Conformal microstrip antennas and microstrip phased arrays", IEEE Trans. on Antennas and Propagation, Vol 22, pp. 74-78. 1974.

[2] Y.T. Lo, D. Solomon and W.F. Richards, "Theory and experiment on microstrip antennas", IEEE AP-S Symposium Japan, pp 53-55, 1993.

[3] K.R. Carver and E.L. Coffey, "Theoretical investigation of the microstrip antennas", Tech. Rept. PT-00929, Physical Science Laboratory New Maxico State University, Las Cruces New Mexico, 1979.

[4] Q. J. Zhang and K. C. Gupta, "Neural Networks for RF and Microwave Design", Artech House Publishers, 2000.

[5] P. M. Watson and K. C. Gupta, "Design and optimization of CPW circuits using EM ANN models for CPW components", IEEE Trans on Microw Theory and Tech, Vol 45(12), pp.2515-2523, 1997.

[6] P.M. Watson and K.C. Gupta, "EM-ANN models for microstrip vias and interconnects in multilayer circuits", IEEE Trans Microw Theory Tech Vol 44, pp. 2495-2503, 1996.

[7] P.M. Watson, K.C. Gupta, and R.L. Mahajan, "Development of knowledge based artificial neural network models for microwave components", IEEE Int Microwave Dig Vol 1, pp. 9-12, 1998.

[8] D. Karaboga, K. Guney, S. Sagiroglu, and M. Erler, "Neural computation of resonant frequency of electrically thin and thick rectangular microstrip antennas", IEEE Proc.- Microwave Antenna Propag, Vol 146(2), pp. 155-159, 1999.

[9] Vandana Vikas Thakare and Pramod Singhal, "Microstrip Antenna Design using Artificial Neural Networks", Int J RF and Microw CAE, Vol 20, pp. 76-86, 2010.

[10] V.V. Thakare and P.K. Singhal, Bandwidth Analysis by Introducing Slots in Microstrip Antenna Design using ANN, Progress In Electromagnetics Research M, Vol 9, pp.107-122, 2009.

[11] Turker, Nurhan, Gunes, Filiz and Yildirim, Tulay, "Artificial neural design of microstrip antennas", Turk J Elec. Engin, Vol 14(3), 2006.

[12] K. Guney and N. Sarikaya, "A hybrid method based on combining artificial neural network and fuzzy interference system for simultaneous computation of resonant frequencies of rectangular, circular, and triangular microstrip antennas", IEEE Trans. on Antenna and Propag., Vol 55(3), 2007.

[13] K. Guney and N. Sarikaya, "Concurrent neuro-fuzzy systems for resonant frequency computation of rectangular, circular, and triangular microstrip antennas", Progress In Electromagnetics Research, Vol 84, pp. 253-277, 2008.

[14] Guney Karim, Sagiroglu Seref and Erler Mehmet, "Generalized neural method to determine resonant frequencies of various microstrip antennas", International Journal of RF and Microw Computer Aided Engineering, Vol. 12, pp. 131-139, 2002.

[15] A. Qucher, R. Aksas, and H. Baudrand, "Artificial neural network for computing the resonant frequency of circular patch antennas", Microw and Optical Technol Lett, Vol. 4, pp. 564-566, 2005.

[16] Sagiroglu Seref, Guney Karim and Erler Mehmet, "Resonant frequency calculation for circular microstrip antennas using artificial neural networks", International Journal of RF, Microw and CAE, Vol 8, 1998.

[17] S. Sagiroglu and K. Guney, "Calculation of Resonant Frequency for an Equilateral Triangular Microstrip Antenna With the use of Artificial Neural Networks", Microw and Opt. Technol. Lett. Vol 14(2), pp. 89-93, 1997.

[18] R.K. Mishra and A. Patnaik, "Neural network-based CAD model for the design of square-patch antennas", IEEE Trans on Antennas and Propag, Vol 46(12), pp. 1890-1891, 1998.

[19] Rabindra K. Mishra and Amalendu Patnaik, "Designing rectangular patch antenna using the neurospectral method", IEEE Trans on Antennas and Propag, Vol 51(8), 2003.

[20] R. Gopalakrishnan and N. Gunasekaran, "Design of equilateral triangular microstrip antenna using artificial neural networks", IEEE International Workshop on Antenna Technology: Small Antennas and Metamaterials, 2005.

[21] J. S. Dahele and K. F. Lee "Effect of substrate thickness on the performance of a circular-disk microstrip antenna", IEEE Trans Antenna and Propagat, Vol 31(2), pp.358-364, 1983.

[22] J. S. Dahele and K.F. Lee, "Theory and experiment on microstrip antennas with air-gaps", IEE Proc, Vol 132(7), pp 455-460, 1985.

[23] K.R. Carver, "Practical analytical techniques for the microstrip antenna", Proc. Workshop on Printed Circuit Antennas, New Mexico State University, pp. 7.1-7.20, 1979.

[24] K. Antoszkiewicz, and L. Shafai, Impedance characteristics of circular microstrip patches, IEEE Trans Antenna and Propag, 38(6), 1990, 942-946.

[25] J. Q. Howell, "Microstrip antennas", IEEE Trans Antenna and Propagat, 23, 1975, 90-93.

[26] T. Itoh and R. Mittra, "Analysis of a microstrip disk resonator", Arch Electron Ubertrugungs, Vol 27(11), pp.456-458, 1973.

[27] F. Abboud, J.P. Damiano and A. Papiernik, "New determination of resonant frequency of circular disc microstrip antenna: application to thick substrate", Electron Lett, Vol 24(1), pp.1104-1106, 1988.

[28] W. Chen, K.F. Lee and J.S. Dahele, "Theoretical and experimental studies of the resonant frequencies of the equilateral triangular microstrip antenna", IEEE Trans on Antennas & Propag, Vol 40(10), pp.1253-1256, 1992.

[29] J.S. Dahele and K.F. Lee, "On the resonant frequencies of the triangular patch antenna", IEEE Trans on Antenna & Propag, Vol 35(1), pp.100-101, 1987.

[30] P.D. Wasserman," Advanced Methods in Neural Computing", New York: Van Nostrand Reinhold, pp. 155–61 and pp. 35-55, 1993.

[31] P. E. Gill, W. Murray, and M. H. Wright, "Practical Optimization", New York: Academic Press, 1981.

[32] L. E. Scales, "Introduction to Non-Linear Optimization", New York: Springer-Verlag, 1985.

[33] M.T. Hagan and M. Menhaj, "Training feed forward networks with the Marquardt algorithms", IEEE Trans. on Neural Networks, Vol 5, pp. 989-993, 1994.

A Novel Multifunction Modified CFOA based Inverse Filter

Kamini Garg
Electrical Engineering department
Delhi Technological University
kamini.garg.23@gmail.com

Ram Bhagat
Assistant Professor
Electrical Engineering department
Delhi Technological University

Bhavnesh Jaint
Assistant Professor
Electrical Engineering department
Delhi Technological University

***Abstract*—Inverse filter has been a topic of great interest and research. A novel multifunction inverse bi-quad configuration based on modified current feedback operational amplifiers (MCFOAs) and a minimum number of grounded passive elements are presented in this paper. To show the flexibility of the proposed MCFOA inverse Lowpass, inverse Bandpass and inverse Highpass filter functions employing MCFOA are reported. All the passive elements in the proposed scheme are grounded to benefit easier electronic tunability. The layout of the proposed MCFOA is also given. The workability of the proposed inverse filters is demonstrated by PSPICE simulations.**

Keywords—inverse active filters, modified current-feedback operational amplifier (MCFOA), analogue signal processing.

I. INTRODUCTION

In communication, control and instrumentation systems an electrical signal may get altered by many linear or nonlinear transformation caused by the signal processors or transmission system. To recover these distortions of the signal, A system is required that has inverse transfer characteristics of the original system. An inverse filter can correct these distortions because it has frequency response, which is the reciprocal of the frequency response of the system that caused the, distortion. There are several schemes for performing inverse digital filtering in digital signal processing, but for realising continuous-time analogue inverse filters there are very few methods/circuits. In [1], a general procedure is presented for obtaining the inverse transfer function for linear dynamic systems and the inverse transfer characteristic for non-linear resistive circuits. In [2], a technique for transforming current-mode, four terminal floating nullor (FTFN) based inverse filter from the voltage-mode filter is given. The realisation procedure utilises network theory concepts related to nullors and RC: CR (capacitor-resistor) dual transformation. Due to the use of dual transformation, this approach can only be applied to planar circuit. By the use of ad joint transformation, another easier procedure for deriving current-mode FTFN-based inverse filter from the voltage-mode filter is presented and it is applicable to nonplanar circuits [3].

All the above procedure in [1-3] can be utilised for obtaining single-input single-output inverse filters. In [4] and [5] various inverse current-mode and voltage-mode filters are proposed, respectively. But, each circuit presented in [4, 5] have one inverse filter function.

This paper is organized as follows. A CMOS implementation of the MCFOA and its terminal resistance calculations are given in Section II and as application, A circuit for realizing a novel multifunction inverse filter based on MCFOAs and minimum number of grounded passive elements using MCFOA's is proposed in Section III. Contrary to the previously reported circuits in [1-5], the above inverse filters uses a minimum number of active and passive components. For very large-scale integration (VLSI) implementation, a circuit having a minimum number of active and passive components is advantageous in perspective of area, power consumption, and cost. Various inverse filter functions can be realized by slight changes in the passive elements of the proposed scheme, to verify the performance of the presented scheme various PSPICE simulations are carried out.

II. MODIFIED CFOA (MCFOA)

Modified CFOA is a four terminal device characterized by the matrix equation:

$$\begin{bmatrix} I_Z \\ I_Y \\ V_X \\ V_W \end{bmatrix} = \begin{bmatrix} \alpha_1 & 0 & 0 & 0 \\ 0 & -\alpha_2 & 0 & 0 \\ 0 & 0 & \beta_1 & 0 \\ 0 & 0 & 0 & \beta_2 \end{bmatrix} \begin{bmatrix} I_X \\ I_W \\ V_Y \\ V_Z \end{bmatrix} \quad (1)$$

As we can conclude from (1), the MCFOA is different from the conventional current-feedback operational amplifier (CFOA) because the Y-terminal current of the MCFOA is not equal to zero as in the conventional CFOA but the W terminal current of the MCFOA is copied to the Y terminal in the opposite direction.

978-1-4673-0934-9/12/$31.00 ©2012 IEEE

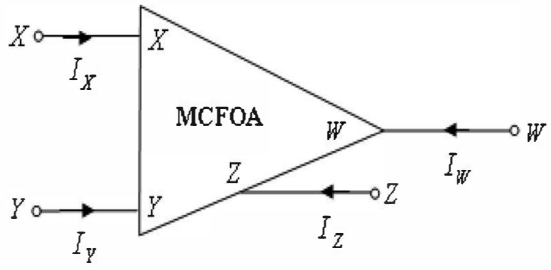

Fig.1. Symbolic representation of the MCFOA

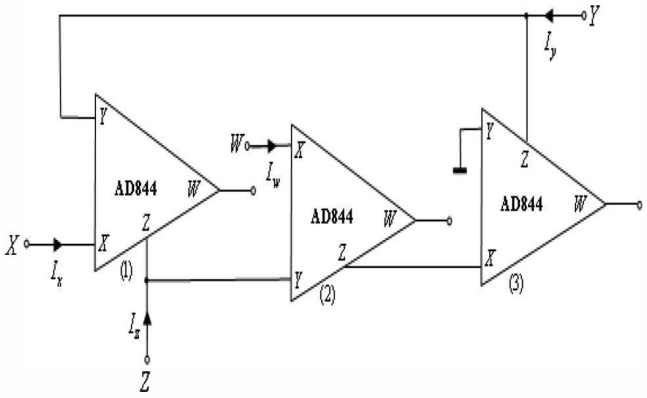

Fig.2. MCFOA construction using commercially available active devices

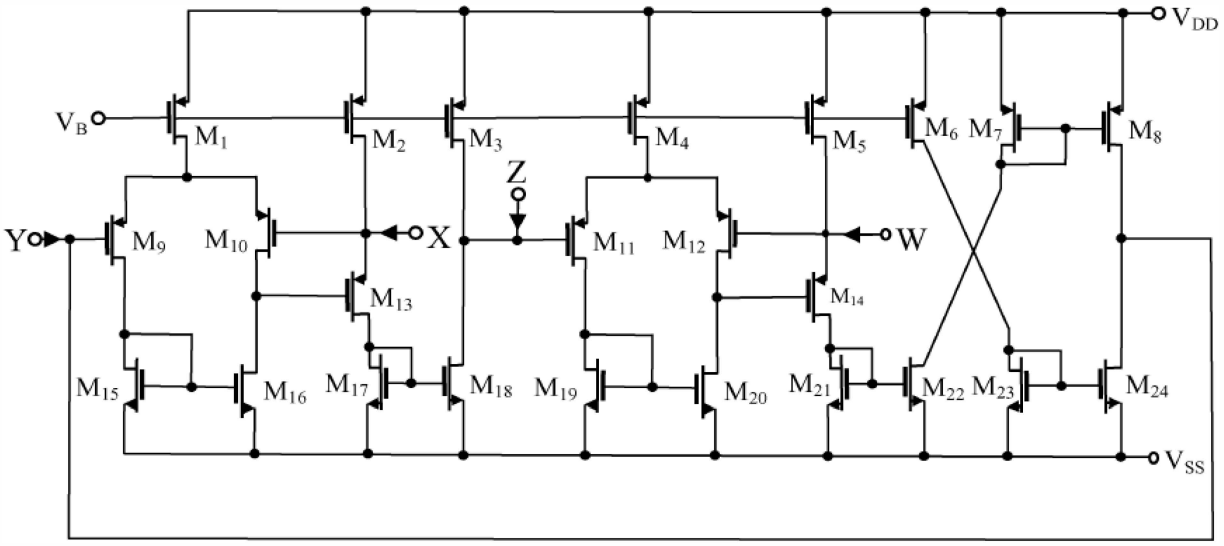

Fig.3. Developed CMOS structure for the MCFOA.

Fig.1. and Fig. 2. show the symbol and construction using commercially available active devices of modified CFOA (MCFOA) respectively.

CMOS realization of modified CFOA is shown in Fig.3. The output resistances of the transistors M_9, M_{10}, M_{19}, and M_{20} in the MCFOA of Fig.3 are assumed to be equal to r_0 and similarly, the output resistances of the transistors M_{11}, M_{12} , M_{19} , and M_{20} of the MCFOA are equal to r'_0 . Thus, the resistances seen at terminals Y, Z, X, and W are respectively calculated as

$$R_Y = \frac{r_{03}\, r_{024}}{r_{03} + r_{024}} \tag{2}$$

$$R_Z = \frac{r_{03}\, r_{018}}{r_{03} + r_{018}} \tag{3}$$

$$R_X = \left(\frac{r_{013} + \dfrac{r_{017}}{1 + g_{m17} r_{017}}}{1 + r_{013} g_{m13} \left(1 + \dfrac{r_0}{2} g_{m10}\right)} \right) \| r_{02} \tag{4}$$

$$\cong \frac{2}{g_{m13} g_{m10} r_0}$$

$$R_W = \left(\frac{r_{014} + \dfrac{r_{021}}{1 + g_{m21} r_{021}}}{1 + r_{014} g_{m14} \left(1 + \dfrac{r'_0}{2} g_{m12}\right)} \right) \| r_{05} \tag{5}$$

$$\cong \frac{2}{g_{m12} g_{m14} r'_0}$$

Here, r_{0i} and g_{mi} are the output resistance and transconductance of the ith CMOS transistor, respectively. From (2)–(5), it can be seen that, while the terminals Y and

Z have very high resistances, the terminals X and W exhibit low resistances due to the feedback loops composed of the transistors (M_{10}, M_{13}) and (M_{12}, M_{14}), respectively.

In this paper, we present new configurations for inverse Lowpass, inverse Bandpass and inverse Highpass configurations using Modified current feedback Operational amplifier (MCFOAs) and grounded passive elements.

III. PROPOSED INVERSE FILTERS EMPLOYING MCFOA (MODIFIED CFOA)

Various types of inverse filters have been devised, using MCFOA, in a variety of ways which exhibit a number of interesting features in respect of the total number of active and passive components involved, tenability properties of the resulting circuits and their input and output impedances. The advantages of MCFOAs are their constant bandwidths, independent closed-loop gains and high slew-rate capabilities.

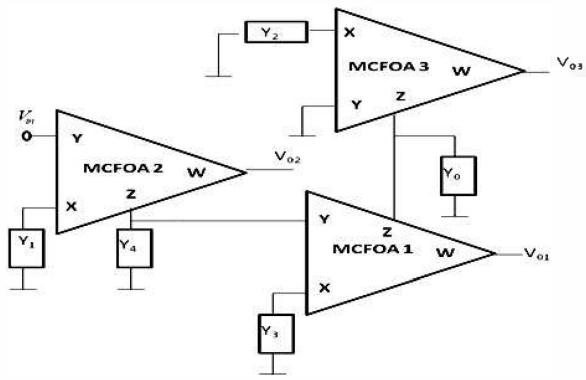

Fig.4. The proposed inverse filter scheme

The proposed circuit for the realisation of various inverse filters is shown in Fig. 4, the transfer functions can be expressed as:

$$\frac{V_{o_1}}{V_{in}} = \frac{V_{o_3}}{V_{in}} = \frac{\alpha_1\beta_2}{Y_0Y_4}(Y_2Y_4 + \alpha_1Y_1Y_3) \quad (6)$$

$$\frac{V_{o_2}}{V_{in}} = \frac{\alpha_1\beta_2Y_1}{Y_4} \quad (7)$$

If the admittances are $Y_0 = G_0$, $Y_1 = sC_1$, $Y_2 = SC_2 + G_2$, $Y_3 = sC_3$ and $Y_4 = G_4$, the inverse Lowpass filter and inverse integrator can be realized at Vo_1 and Vo_2, respectively. They are given by

$$\frac{V_{o_1}}{V_{in}} = \frac{V_{o_3}}{V_{in}} = \alpha_1\beta_2\left(\frac{\alpha_1S^2C_1C_3 + SC_2G_4 + G_2G_4}{G_0G_4}\right) \quad (8)$$

$$\frac{V_{o_2}}{V_{in}} = \frac{\alpha_1\beta_2SC_1}{G_4} \quad (9)$$

The coefficients of the S^2, S^1 and S^0 terms can be tuned by the values of C_1, C_2, G_2 and G_0 in the numerator and the denominator respectively. So the parameters, such as the corner angular frequency ω_o and quality factor Q of the inverse filter are tuneable by independent passive elements. In (2), if the admittances are $Y_0 = SC_0$, $Y_1 = SC_1$, $Y_2 = SC_2+G_2$, $Y_3 = SC_3$ and $Y_4 = G_4$, the functions of inverse bandpass filter and inverse integrator can be realized at V_{01} and V_{02}, respectively and given by

$$\frac{V_{o_1}}{V_{in}} = \alpha_1\beta_2\left(\frac{\alpha_1S^2C_1C_3 + SC_2G_4 + G_2G_4}{sG_0G_4}\right) \quad (10)$$

$$\frac{V_{o_2}}{V_{in}} = \frac{\alpha_1\beta_2SC_1}{G_4} \quad (11)$$

Similarly, if the admittances are$Y_0 = SC_0$, $Y_1 = G_1$, $Y_2 = SC_2+G_2$, $Y_3 = G_3$ and $Y_4 = SC_4$, the functions of inverse highpass filter and inverse differentiator can be realized at Vo_1 and Vo_2, respectively. They can be expressed by

$$\frac{V_{o_1}}{V_{in}} = \alpha_1\beta_2\left(\frac{S^2C_2C_4 + SC_4G_2 + \alpha_1G_1G_3}{S^2C_0C_4}\right) \quad (12)$$

$$\frac{V_{o_2}}{V_{in}} = \frac{\alpha_1\beta_2G_1}{SC_4} \quad (13)$$

The output of Vo_3 has the same function as Vo_1, it provides the additional output which makes the filter application more flexible.

TABLE I. ASPECT RATIO OF THE CMOS TRANSISTOR USED IN THE MCFOA

PMOS Transistors	$W_{(\mu m)}/L_{(\mu m)}$
M_1, M_4 and M_9, M_{10}, M_{11} and M_{12}	1.0/0.25
M_2, M_3, M_5, M_6, M_7 and M_8	2.0/0.25
M_{13} and M_{14}	4.0/0.25
NMOS Transistors	$W_{(\mu m)}/L_{(\mu m)}$
M_{15}, M_{16}, M_{17}, M_{18}, M_{19}, M_{20}, M_{21}, M_{22}, M_{23} and M_{24}	0.5/0.25

IV. SIMULATION RESULT

Simulations for the MCFOA of Fig. 3 based on 0.25 um TSMC CMOS technology with power supply voltages $V_{DD} = -V_{SS} = 1.25V$ and $V_B = .8V$ are performed. The dimensions of the MOS transistors used in the proposed MCFOA are given in Table I. To verify the effectiveness of the proposed scheme, circuit simulations of the presented multifunction inverse filters have been carried out.

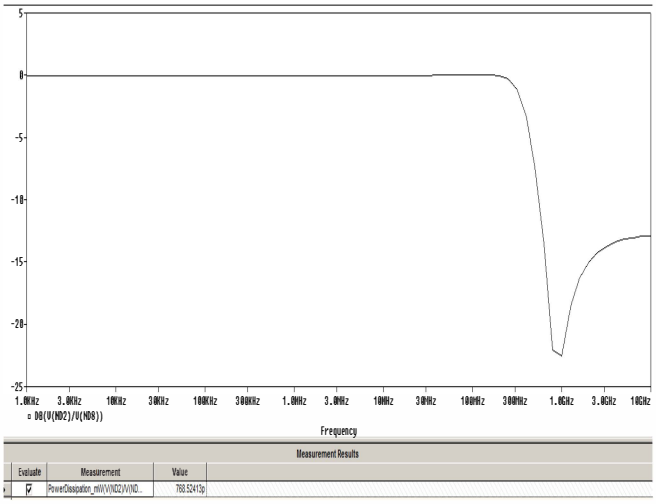

(a)

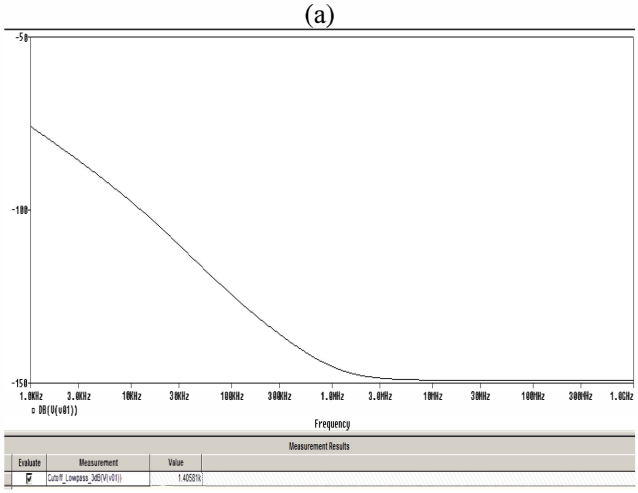

(b)

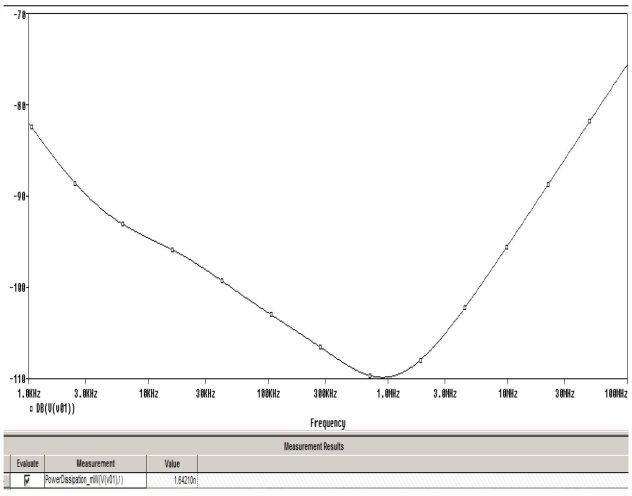

(c)

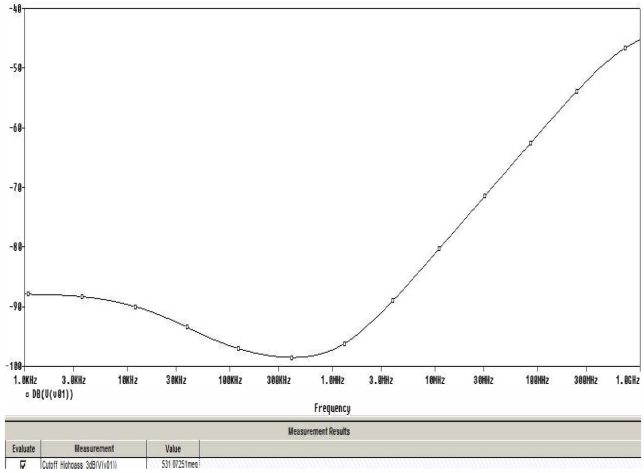

(d)

Fig. 5. (a) Variation of the voltage gains of the MCFOA against frequency
(b) Frequency response of inverse Highpass filter using Modified CFOA
(c) Frequency response of inverse Bandpass filter using Modified CFOA
(d) Frequency response of inverse Lowpass filter using Modified CFOA

In the simulation, the values of all resistors and all capacitors are 40kΩ and 1nF, respectively. It is found that the workability of all the inverse biquids is in good agreement with our theoretical prediction. The typical frequency responses of inverse Lowpass, inverse Bandpass and inverse Highpass are shown in Figure 5.

V. CONCLUSION

A modified current-feedback operational amplifier (MCFOA), which is a CMOS active device, has been proposed. Using the proposed MCFOA and grounded-passive elements a novel voltage mode multifunction scheme for inverse filter realisation has been presented. Various inverse filter functions have been realized by slight modification in the passive elements of the proposed scheme. It offers more convenient realizations for inverse filter functions. The proposed circuit thus adds new configurations to the existing work of inverse analog filters known earlier.

REFERENCES

[1] A. Leuciuc, “Using Nullors for Realisation of Inverse TransferFunctions and Characteristics,” *Electronics Let-ters*, Vol. 33, No. 11, 1997, pp. 949-951. doi:10.1049 /el:19970637.

[2] B. Chipipop and W. Surakampontorn, “Realisation of Current-Mode FTFN-Based Inverse Filter,” *Electronics Letters*, Vol. 35, No. 9, 1999, pp. 690-692. doi:10.10 49/el:19990495.

[3] H. Y. Wang and C. T. Lee, “Using Nullors for Realisa-tion of Current-Mode FTFN-Based Inverse Filters,” *Electronics Letters*, Vol. 35, No. 22, 1999, pp. 1889-1890. doi:10.1049/el:19991336.

[4] M. T. Abuelma’atti, “Identification of Cascadable Cur-rent-Mode Filters and Inverse-Filters Using Single FTFN,” *Frequenz*, Vol. 54, No. 11, 2000, pp. 284-289.

[5] S. S. Gupta, D. R. Bhaskar, R. Senani and A. K. Singh, “Inverse Active Filters Employing CFOAs,” *Electrical Engineering*, Vol. 91, No. 1, 2009, pp. 23-26. doi:10.10 07/s00202-009-0112-3.

[6] Erkan Yuce (2008) "A Modified CFOA and its application to simulated inductor, capacitor multipliers and analog filters" *IEEE TRANSACTIONS O, Vol. 55, NO. 1, February 2008.*

[7] S. S. Gupta, D. R. Bhaskar, Raj Senani, A. K. Singh "Inverse active filters employing CFOAs" *Electr Eng (2009) 91:23–26 DOI 10.1007/s00202-009-0112-3.*

“ACTION WILL BE TAKEN”: DELHI TRAFFIC POLICE@FB

Sidharth Chhabra
School of Information
University of Michigan
sidc@umich.edu

Joyojeet Pal
School of Information
University of Michigan
joyojeet@umich.edu

Dhruv Goel
Delhi Technological University
dhruv.goel92@gmail.com

ABSTRACT
We examine the use of social networking by the Delhi Traffic Police and find that open online exchanges represent a new communicative paradigm in eGovernance. By showing patterns in citizen comments and bureaucrat responses, we argue that the Delhi Police case is an instructive example for the evolution of eGovernance in various parts of the developing world where the legacy means of communication between official channels and the general public are strained by complex and inaccessible red tape.

Categories and Subject Descriptors
Developing Regions

General Terms
Human Factors

Keywords
Facebook, Police, Social Networking, Traffic, eGovernance

1. INTRODUCTION
The evolution of bureaucracy with the expansion of social media and eGovernance has been a significant part of discussions in the ICTD world. Negative perceptions of the interface with state agencies has traditionally been a major concern in citizens’ interaction with government and many agencies have started developing online presences with a view to changing that. Traffic Police in various cities of India have initiated facebook pages which have over time become active grievance redressal mechanisms for the citizenry.

Such outward facing state service sites build on the fundamental idea of transparency and participatory mechanisms, which have been studied and confirmed as having important positive outcomes by scholarship on good governance [1]. Putnam has shown variance in governance related to social networks, specifically that networks can pressurize public institutions to perform.

While several studies have shown the use of social media as a potentially beneficial tool for openness and transparency in developing world [3], the importance of the longevity of such projects and the legacy of discursive exchange with the government is particularly important. In many parts of the developing world, there is thus this added element of a deeply negative perception of the state and the lack of institutional history of direct communication with the government. In this paper, we discuss the evolution of Delhi Traffic Police's Official page and the impact of its responsiveness on the participation.

DEV '13, January 11-12, 2013 Bangalore India

2. BACKGROUND
India is a house to world’s largest bureaucracy. The government employs 18.7 million people at the state and central level.[1] Indian bureaucracy has been frequently criticized for red-tapism and lack of transparency. From among the agencies, the police in India have been found by studies to be perceived as highly corrupt [4]. In part to deal with a common perception of the police as citizen-unfriendly, the Traffic Police in many cities and states have adopted social media (specifically Facebook) to interact with the citizens, serve as a public relations tool and provide general information.[2]Some key statistics for four metropolitan cities are presented in Table 1. Delhi leads the lot with more likes than the sum of other three cities. We chose to analyse data from Delhi, primarily because of its usage. While we do not go into the reasons of that, these could be factors such as the relative high use of road traffic in commuting in Delhi, compared to cities like Mumbai and Kolkata which rely more on suburban rail services.

3. SOCIAL MEDIA PRESENCE
Delhi Traffic Police was the one of the first public institutions in India to start an official Facebook page. It began as an experiment for announcements, but it quickly picked up a significant following. Within a month, it had more than 5000 ‘likes’ and in what was a more unplanned development, people had started posting their grievances on their page. Interestingly, rather than ignore this, the administratos started at first redirecting people to other sources, but as the grievances and comments grew, they started responding directly to each comment(Fig 1).

This is a relatively new paradigm for state agencies in India, because the sense of largely unsupervised, unstructured content on a forum technically ‘owned’ by the government is very usual. This was a new world for a government organization in India. Not only did the actual channel of communication change, even the content of communications evolved.

In Fig 1, use of word “ATTN” to address a user indicates a fairly traditional and bureaucratic mode of communication. But with time we find that the ‘voice’ changed significantly (Fig 2) as they started using ‘@’ and instead of replying individually to every complaint; they updated their status with action reports for multiple complaints together.

Table 1. Statistics for Facebook pages of different cities

Traffic Police	Created on	Likes
Delhi	04/30/2010	138,974
Chennai	07/18/2010	34,345
Kolkata	09/09/2010	23,423
Bangalore	04/10/2011	46,481

[1] www.wakeupcall.org/administration_in_india /world_class_governance.php downloaded on 15 October 2012.

[2] http://lighthouseinsights.in/a-list-of-10-indian-city-traffic-police-on-facebook.html downloaded on 15 October 2012.

Figure 1. Initial style of response by admin.

Figure 2. Later response of admin; subdued and cumulative.

Most strikingly, the site has become a location for conversations that would otherwise likely be censored. For instance, a user posted a video with Chief Minister of Delhi without the seat belt and asked the traffic police to take action. Rather than block this or ignore the posting, the traffic police administrator had to reply to the thread and assure the people that action will be taken. Irrespective of whether action was taken, it implied that the police were not entirely mute spectators to politicians being above the law and served as an interesting instance of communicative democracy (Fig 3). The page is used now for multiple purposes, namely, notifying about traffic obstructions, advising traffic routes, applauding heroic acts by policemen, educating people about violations and traffic rules and redressing the grievances.

4. ANALYSIS & RESULTS

Using Facebook Graph API, we collected the posts created between 1st and 30th September, 2012 from Delhi Traffic Police's Facebook Page. Authors of the posts were segregated into two categories, namely, people and administrator. Posts by administrator are displayed prominently on the page whereas posts by people are visible in an expandable panel. On average, people and page administrator posted 91.57 (1068.94) and 4.43 (9.21) posts in a day respectively. Each posts by administrator received 146.16 comments and 29.62 likes on average whereas each posts by people received 0.62 comments and 1.32 likes on average.

Assuming people mostly posted complaints, we observed how people respond to actions (comment) by administrator on the posts by people. We compared the number of likes and number of comments on the posts commented and not commented by administrator (Table2). A two-sided t-test confirms that difference was statistically significant for both number of comments and likes; $t(2744) = -6.95$, $p < 0.001$ for likes and $t(2744) = 2.05$, $p = 0.03$ for comments. The most common reply by administrator was "*Thanks, Action will be taken*".

To probe further, we counted number of comments after the admin has replied. We found 73.8% (1082 out of 1466) of the posts answered by administrator did not have any comment after the reply. Thus, posts which were not answered by administrator have more number of comments and likes and most posts answered by administrator are not discussed further.

Figure 3. A user posted a video showing that Chief Minister violated traffic rules. Within ten hours, the administrator responded.

5. DISCUSSION & FUTURE WORK

That the Facebook site did not start as an explicit grievance redressal system makes the evolution of the site particularly important. The changing pattern of posts from citizens based of officials' response is an important indicator of how the grievance mechanism is operationalized. Posts containing administrator's reply receive less comments and likes than others, and on an analysis of this, we found that an administrator's response to a query stopped discussion. Thus citizens saw the police response to a post as a culmination - evidence of their successful call to action. The police likewise felt the need to respond to a post as a means of confirming their commitment to the grievance system.

The second evolution was that of the verbal discourse on the posts – while the police notes at first began very rooted in the language of bureaucratic officialdom in India, but we see the eventual movement of the posts to more of a social-networking savvy use of language. This is an important issue for future projects since it emphasizes the way technology itself can change practices, a key issue that ICTD scholars have been grappling with for the last decade. While we cannot predict what the Delhi Police actually does with any of the complaints, the Facebook site has become an important element for public relations and for citizens' means of having their voice heard.

6. REFERENCES

[1] Ackerman, John. "Co-Governance for Accountability: Beyond 'Exit' and 'Voice'." *World Development* 32, no. 3 (March 2004): 447–463.

[2] Putnam, Robert D., Robert Leonardi, and Raffaella Y. Nanetti. *Making Democracy Work: Civic Traditions in Modern Italy*. Princeton University Press, 1994.

[3] Bertot, John C., Paul T. Jaeger, and Justin M. Grimes. "Using ICTs to Create a Culture of Transparency: E-government and Social Media as Openness and Anti-corruption Tools for Societies." *Government Information Quarterly* 27, no. 3 (July 2010): 264–271.

[4] Bhattacharyya, Sambit, and Raghbendra Jha. Economic Growth, Law and Corruption: Evidence from India. ASARC Working Paper. Australian National University, Australia South Asia Research Centre, 2009. http://ideas.repec.org/p/pas/asarcc/2009-15.html.

Table 2. Statistics for feeds created in September '12

For every post	Has Admin Reply	No Admin Reply
Mean # comments	0.405 (0.48)	1.243 (7.42)
Max. # comments	7	41
Mean # likes	0.3718 (1.02)	0.9257 (7.21)
Max. # likes	10	46

An Analytical Study of Jet Cross-Section in Proton-Proton Interactions

Hardik P. Trivedi[1], Pallavi Bhatt[1], Anil Kumar[2*], Lalit K. Gupta[3], Jai Prakash Gupta[4], Krishna Chandra[5], Than Singh Saini[6] and Archna Kansal[7]

[1]*Department of Physics, Mewar University, Chittorgarh (Rajasthan) INDIA*
[2]*Deptartment of Physics, Vivekananda College of Technology and Management, Aligarh (UP) – 202 002, INDIA*
[3]*Department of Physics, Krishna Engineering College, Ghaziabad, INDIA*
[4]*Department of Physics, D. S. College, Aligarh (UP) - 202 001, INDIA*
[5]*Department of Physics, Goldfield institute of Technology & Management, Faridabad-, INDIA*
[6]*Department of Physics, Delhi Technological University, Delhi-42 INDIA*
[7]*Department of Physics, ITM, Gwalior (MP) INDIA*
** email: akguptaphysics@gmail.com*

Introduction

The concept of jets of a pair of jets of approximately equal and opposite large transverse momenta, produced by some dynamical mechanism[1]. The jets than fragment into the syatem of hadrons and thus multiparticle production takes place. This is the consequence of the character of the strong interaction between quarks and gluons.

The data from [2] and FERMILAB [3] indicate that the jets, observed in large p_T hadron-hadron collisions, similar to those processes, initiated by leptons(i.e. e^+e^-, ep and υp processes) fragment or cascade into a collection of hadrons, moving roughly, in the direction of the original quarks [4]. At higher energies, it was expected that jets, produced in hadronic collisions, would be distinctive, since the transverse momentum of the scattered parton, would be large enough to make jet.

In the present work, an attempt is made to discuss the mechanism of jet production in ptoton-proton interactions and also to calculate the jet production cross-section in different sub processes [5].

Jet Cross-Section

The jet production in hadronic collisions is interpreted in the frame work of the parton model [6] as hard scattering among the constituents of the incident hadrons since the initial state contains quarks, antiquarks and gluons, there are several elementary sub processes that can contribute to jet production. For each sub process the scattering cross-section calculated to first order in the strong running coupling constant α_s, is given by the following expression [7].

$$\frac{d\sigma}{dcos\theta} = \frac{\pi\alpha_s^2}{2s}|M|^2 \qquad \text{---------- (1)}$$

where θ is the scattering angle, s is the square of centre of mass energy of the two partons, $|M|^2$ is expressed by different expressions, depending upon the various sub processes [8] and $\pi = 3.14$. These sub processes are given in the table 1. In QCD, the running coupling constant α_s, is calculated from the relation $C = 4\ \alpha_s /3\pi$ [9] where C is a energy dependent parameter. It may also related to α, as $\alpha_s = (1- \alpha)$, where α is well known fine structure constant [10]. In the case of proton-proton interactions, since the proton consists of quarks and gluons only, the possible sub processes are only four viz. qq'→ qq', qq→ qq, qg→ qg and gg→ gg. The jet cross-section is calculated, in this work, for these sub processes, using equation (1).

Tables and Figure

Table 1: Formulae and Magnitudes of various sub processes.

Sub Processes	$\|M\|^2$	$\|M\|^2$ at $\theta=90^0$
qq'→ qq' $q\bar{q} \rightarrow q\bar{q}$	$\frac{4}{9}\left(\frac{s^2+u^2}{t^2}\right)$	2.22
qq→ qq	$\frac{4}{9}\left(\frac{s^2+u^2}{t^2}+\frac{s^2+t^2}{u^2}\right)-\frac{8}{27}\frac{s^2}{ut}$	3.26
$q\bar{q} \rightarrow q'\bar{q}'$	$\frac{4}{9}\left(\frac{t^2+u^2}{s^2}\right)$	0.22
$q\bar{q} \rightarrow q\bar{q}$	$\frac{4}{9}\left(\frac{s^2+u^2}{t^2}+\frac{t^2+u^2}{s^2}\right)-\frac{8}{27}\frac{u^2}{st}$	2.59
$q\bar{q} \rightarrow gg$	$\frac{32}{27}\frac{u^2+t^2}{ut}-\frac{8}{3}\frac{u^2+t^2}{s^2}$	1.04
$gg \rightarrow q\bar{q}$	$\frac{1}{6}\frac{u^2+t^2}{ut}-\frac{3}{8}\frac{u^2+t^2}{s^2}$	0.15
qg→ qg	$-\frac{4}{9}\frac{u^2+s^2}{us}+\frac{u^2+s^2}{t^2}$	6.11
gg→ gg	$\frac{9}{2}\left(3-\frac{ut}{s^2}-\frac{us}{t^2}-\frac{st}{u^2}\right)$	30.38

In the table-1, here s represents the square of centre of mass energy of interacting partons. The parameters u and t are related to s as,
$u = s(1+\cos\theta)/2$ and $t = -s(1-\cos\theta)/2$

Table 2: Jet cross-section at different centre of mass energies for the different sub processes, used in the case of proton-proton interactions.

$\sqrt{s}$ (Gev.)	α_s	$\left(\frac{d\sigma}{d\theta}\right)_{qq'}$	$\left(\frac{d\sigma}{d\theta}\right)_{qq}$	$\left(\frac{d\sigma}{d\theta}\right)_{qg}$	$\left(\frac{d\sigma}{d\theta}\right)_{gg}$
1	0.42	0.614	0.902	1.692	8.413
2	0.40	0.139	0.204	0.383	1.907
3	0.37	0.053	0.077	0.145	0.725
4	0.37	0.029	0.043	0.082	0.408
4.95	0.35	0.017	0.025	0.047	0.238
10.25	0.32	0.003	0.004	0.009	0.046
11.7	0.30	0.002	0.003	0.006	0.031
13.5	0.25	0.001	0.001	0.003	0.016
25	0.18	--	--	--	0.002
33.95	0.16	--	--	--	0.001

Fig. 1 Variation of jet cross-section in the case of proton-proton interactions as a centre of mass energy. The curves represent the present work for the different sub processes.

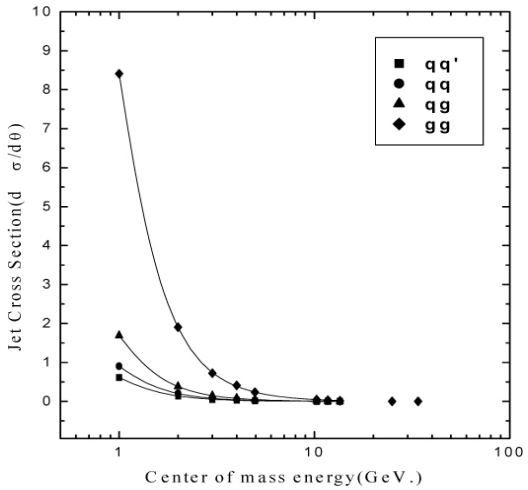

Result and Discussions

The results of the present work are presented in table-2 and the variation of jet cross-section, in different sub processes, with centre of mass energy is plotted in the Figure-1. The range of centre of mass energy is considered from 1 Gev. to 33.95 Gev. In all sub processes, the values of jet cross-section decreases on increasing the centre of mass energy. In the three sub process viz. qq'→ qq', qq→ qq, qg→ qg, the gets are found to appear up to only 13.5 Gev. But in the case of gg→ gg jets may found to be appearing up to 33.95 Gev.

Since the value of $|M|^2$ for gg→ gg is largest (i.e. 30.38), the jet cross-section for this sub process is expected to be dominated which is found to be consistent with our present work. Also found to be consistent with our present work. Also the running coupling constant α_s decreases on increasing the centre of mass energy, and hence the probability of jet production decreases with increase in centre of mass energy.

References

[1] P. V. Landshoff, etal; Nucl. Phys. B 87 (1975) 176
[2] J. Garvey, Rep. Prog. Phys. 50 (1987) 1311
[3] The DELPHI Collaboration CERN-PPE/90-117(Aug. 1990)
[4] M. L. Mangano, etal; Ann. Rev. Nul. Part. Sci. 55 (2005) 555
[5] A. S. Carroll, etal; Phys. Lett. 80B (1979) 319
[6] L. Dilella, etal; Ann. Rev. Nul. Part. Sci. 35 (1985) 107
[7] M. Shyam, etal; Phys. Lett. B 164 (1985) 189
[8] F. Wilczeck, Ann. Rev. Nul. Part. Sci. 32 (1982) 177
[9] K. J. Eskola, etal; Phys. Lett. B 489 (2000) 329
[10] C. Y. Wong, Nucl. Phys. A 700 (2002) 509

An Induction Machine Damping Unit for Damping SSR in a series compensated Power System

Prakash Chittora
Electrical Department
Delhi Technological University
Delhi, India
prakashchittora@gmail.com

Narendra Kumar
Electrical Department
Delhi Technological University
Delhi, India
Dnk_1963@yahoo.com

***Abstract*—The main focus of this paper is to analyse IMDU characteristics to damp subsynchronous resonance. IMDU is coupled to T-G shaft. The advantage of using IMDU to damp SSR is that we need no other controller. The IEEE First Benchmark Model for subsynchronous studies is used to study eigenvalue analysis and time domain simulations. The time domain simulation study under large disturbances condition is carried out with IMDU located at the HP turbine end of T-G shaft. The coupling coefficient between IMDU and masses were varied, and its effects on SSR mitigation and transient stability were observed. The scheme enhances the system performance considerably and torsional oscillations are damped out at all levels of series compensation**

***Keywords*—Induction machine damping unit (IMDU); subsynchronous resonance (SSR); damping oscillations; modelling; IEEE first benchmark model; eigenvalue analysis.**

I. INTRODUCTION

Series compensation of a transmission line gives rise to the problem of subsynchronous resonance (SSR) in the system which has two distinctive effects, namely the induction generator effect and torsional interactions effect. Because of torsional oscillations the shaft of the T-G set may break with disastrous consequences. Subsynchronous resonance is a phenomenon associated with the energy exchanged between the turbine-generator mechanical and electrical systems. A number of mechanical masses of the turbine-generator shaft (e.g. turbine stages and generator) oscillate at some frequencies known as torsional oscillations which are characterized by their mechanical properties like spring constants and mass inertia. The frequencies of these oscillations range from 10 to 55 Hz for 60 Hz system [17].

The oscillation of the generator rotor at a subsynchronous frequency 'f_m' results in voltages induced in the armature having components of:

- Sub-synchronous frequency (f_0 - f_m).
- Super-synchronous frequency (f_0 - f_m).

Damping SSR oscillations has been a topic of great interest and research. Early strategies suggested dissipating the energy during resonance in resistor banks [2]. Countermeasures utilizing TCSC, NGH schemes [3]–[5], phase shifters [6], excitation controllers, and static VAR compensators [7] have been extensively researched through the years. Numerous modelling techniques and improvements on these schemes have also been given [8], [9]. The use of stored magnetic energy has been published in [10]–[12].

The concept of the induction machine damping unit (IMDU) as a countermeasure to SSR was devised in [13] and extended in [14]. IEEE second benchmark model [23] for subsynchronous resonance was used in [15] to analyse the damping properties of an induction machine damping unit (IMDU) coupled to the shaft of a turbo-generator set. These papers stated the possibility of damping SSR using an IMDU in conjunction with additional control for static VAR systems. A system similar to the IEEE First Benchmark Model (FBM) [16] was utilized in these papers, while assuming negligible mass for the IMDU. In this paper, we use an IMDU to Eliminate SSR.

An IMDU is a special high-power, low energy induction machine, with small rotor resistance and leakage reactance values, designed to operate close to synchronous speed. It is mechanically coupled to the turbo-generator (T-G) shaft and electrically connected to the generator bus. The main contributions of this report include: putting forward the possibility of damping SSR with only an IMDU (no controllers needed) coupled to the shaft of the T-G, and corresponding IMDU parameters.

The IEEE First Benchmark Models for subsynchronous studies is used to conduct eigenvalue analyses and time domain simulations. Time domain simulation studies were conducted with the IMDU at the shaft HP end. Simulations to study large transients were conducted. The coupling coefficient between masses was varied, and its effects on SSR mitigation and transient stability were observed. The best location providing maximum damping is next to the HP turbine at the end of the shaft.

II. BASIC CONCEPT OF OSCILLATIONS DAMPING USING IMDU

The property of an induction machine to act either as a generator or motor is utilized to absorb mechanical power if there is excess and to release it when there is a deficiency.

978-1-4673-0934-9/12/$31.00 ©2012 IEEE

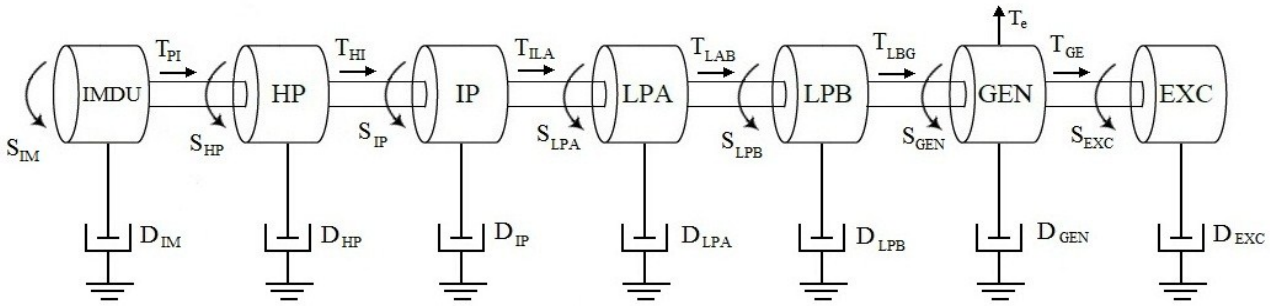

Fig.1. IMDU under speed operation

High pressure (HP) and other turbines produce torque in the direction of rotation (forward direction) and the generator produces the electromagnetic torque in the opposite direction. If an induction machine is connected to the HP turbine on its right side as shown in Fig.1 and if the speed of the machine exceeds the synchronous speed (mechanical input is greater than electrical output of generator) the machine acts as an induction generator. Torque produced by it is in the reverse direction. It can be visualized that this torque will tend to reduce the twist angle (δ), hence it reduces the amplitude of torsional oscillation. Alternatively, it can be said that it increases the damping of the system.

If the speed of the shaft is less than the synchronous speed, the induction machine will act as a motor and it produces a torque in the forward direction. In this operation, it supports the turbine torque and helps to restore the speed. So in any case it tries to oppose the change in the synchronous speed of the shaft. It can be said that it reduces the oscillations in the rotating mass around the nominal speed, or that the damping of the system is increased.

III. System Description

A. Synchronous Machine Model

We will use Model 1.1(22) (Field circuit with one equivalent damper on q-axis) published By IEEE task force, of synchronous machine for modelling.

The electrical dynamic equations of the synchronous machine (model 1.1) are developed by writing equations of the coupled circuits and presented below [18,21]:

1) Stator Equation:

$$v_q = -\frac{1}{\omega_B}\frac{d\Psi_q}{dt} - (1+S_m)\Psi_d - R_a i_q \tag{1}$$

$$v_d = -\frac{1}{\omega_B}\frac{d\Psi_d}{dt} - (1+S_m)\Psi_q - R_a i_d \tag{2}$$

2) Rotor Equations:

$$\frac{dE_d'}{dt} = \frac{1}{T_{qo}'}\left[-E_d' - (x_q - x_q')i_q\right] \tag{3}$$

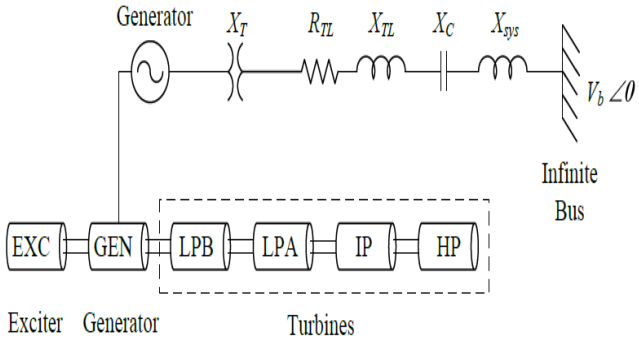

Fig.2. System under study

$$\frac{dE_q'}{dt} = \frac{1}{T_{do}'}\left[-E_q' + (x_d - x_d')i_d + E_{fd}\right] \tag{4}$$

B. Network Model

Fig.2. shows that a series capacitor-compensated transmission line may be represented by the RLC circuit [18]

IV. System Modelling for Eigenvalue Analysis

IEEE FBM model is used to study damping characteristics of IMDU. The eigenvalue analysis is performed by developing a linear model of the system. The state space model for the generator and shaft system for IEEE FBM model are illustrated below [18].

A. Combined Generator and Shaft System Model

The linearized state equations are given by:

$$\Delta\dot{x}_G = [A_G]\Delta x_G + [B_{G1}]\Delta u_g + [B_{G2}]E_{fd} \tag{5}$$

$$\Delta y_G = [C_G]\Delta x_G \tag{6}$$

Where the state vector Δx_G, input vector Δu_g and output vector Δy_G are given by

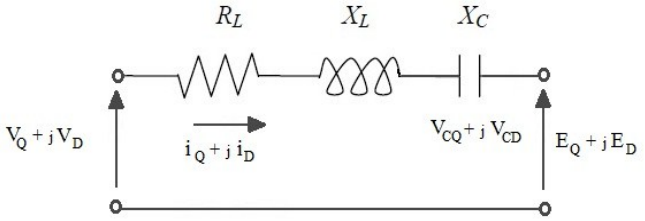

Fig.3. A series capacitor compensated transmission line

$$\left[\Delta x_G\right]^t = \left[\Delta x_e \quad \Delta x_m\right]$$

$$\left[\Delta u_g\right]^t = \left[\Delta v_D \quad \Delta v_Q\right]$$

$$\left[\Delta x_m\right]^t = \left[\delta_{GEN} \quad S_{EXC} \quad T_{GE} \quad S_{GEN} \quad T_{LBG} \quad S_{LPB} \quad T_{LAB} \quad S_{LPA} \quad T_{ILA} \quad S_{IP} \quad T_{HI} \quad S_{HP}\right]$$

$$\left[\Delta x_e\right]^t = \left[\Delta\Psi_d \quad \Delta\Psi_q \quad \Delta E_d' \quad \Delta E_q'\right]$$

$$\left[\Delta y_G\right]^t = \left[\Delta i_D \quad \Delta i_Q\right]$$

B. *Modelling the Transmission Line*

The differential equations for the circuit elements, after applying Park's transformation, can be expressed in the d-q reference frame as following.

The voltage across the capacitor [18]:

$$\begin{bmatrix}\dot{\Delta V}_{CD}\\ \dot{\Delta V}_{CQ}\end{bmatrix} = \begin{bmatrix}0 & -\omega_B\\ \omega_B & 0\end{bmatrix}\begin{bmatrix}\Delta Vc_D\\ \Delta Vc_Q\end{bmatrix} + \begin{bmatrix}\omega_B X_C & 0\\ 0 & \omega_B X_C\end{bmatrix}\begin{bmatrix}\Delta i_D\\ \Delta i_Q\end{bmatrix} \tag{7}$$

The above equations can be represented in state space model as:

$$\dot{\Delta x}_N = \left[A_N\right]\Delta x_N + \left[B_{N1}\right]\Delta u_{N1} + \left[B_{N2}\right]\Delta u_{N2} \tag{8}$$

Where state vector Δx_N and Input vector Δu_{N1} are

$$\left[\Delta x_N\right]^t = \left[\dot{\Delta V}_{CD} \quad \Delta V_{CQ}\right]$$

$$\left[\Delta U_{N1}\right] = \begin{bmatrix}\Delta i_D\\ \Delta i_Q\end{bmatrix}$$

C. *Modelling the Induction Machine Damping Unit*

For the eigenvalue analysis, the torque-speed characteristics of an induction machine, with small rotor resistance, to be used as IMDU can be considered linear between synchronous speed and the critical slip (maximum torque) when operated at constant terminal voltage and frequency. Therefore, the torque of the damping unit can be modelled as being proportional to speed deviation, (deviation from synchronous speed). The slope of the torque-speed characteristic found as [15]:

$$k = \left|\frac{\Delta T_{IM}}{\Delta\omega_{IM}}\right|$$

The field exciter dynamics is not modelled and the excitation is held constant at 1 pu. The time constant of the mechanical system is very large when compared to the electrical system, and hence, the speed governor dynamics are not included, keeping the input power to the turbines constant. Variables torque produced in the different shaft section, which are functions of the difference of the slip at the ends of the shaft. The differential equations governing the IMDU model are as follows [15] :

$$\dot{T}_{PI} = K_{IM}\left(S_{IM} - S_{HP}\right) \tag{9}$$

$$\dot{S}_{IM} = -\frac{D_{IM} - k}{2H_{IM}} S_{IM} - \frac{T_{PI}}{2H_{IM}} \tag{10}$$

D. *Combined System Model*

On combining generator, network and IMDU equations (5), (6), (8), (9), (10) The final system equations are

$$\dot{\Delta x}_{TI} = \left[A_{TI}\right]\Delta x_{TI} + \left[B_{T1}\right]\Delta E_{fd} + \left[B_{T2}\right]\Delta u_{N2} \tag{11}$$

Where

$$\left[\Delta x_{TI}\right]^t = \left[\Delta x_{GI} \quad \Delta x_N\right]$$

$$\left[A_{TI}\right] = \begin{bmatrix}\left[A_{GI}\right] + \left[B_{G1}HF_1\right] & \left[B_{G1}H\right]\\ \left[B_{N1}C_G\right] & \left[A_N\right]\end{bmatrix}$$

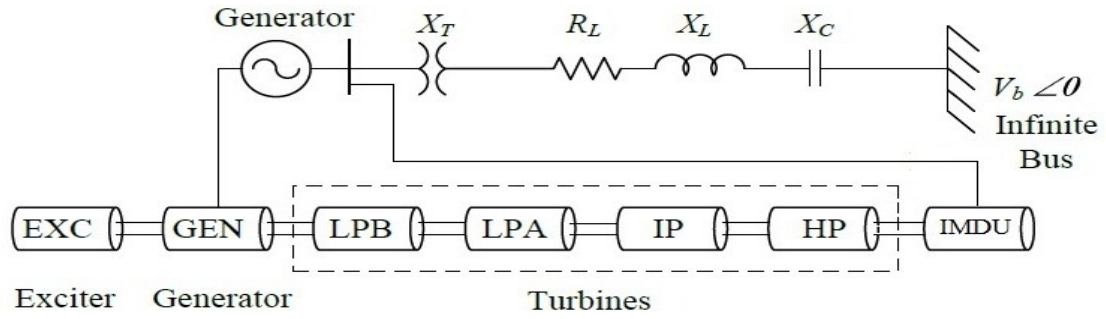

Fig 4. IMDU connected to the system

TABLE I EIGEN VALUES OF SYSTEM WITH AND WITHOUT IMDU

S.No.	Without IMDU P=0.7 ,P.F.=0.9, Xc=0.35	With IMDU P=0.7 ,P.F.=0.9 Xc=0.35	Comments
1	-0.46505 + j10.128 -0.46505 – j10.128	-0.88054 + j10.081 -0.88054 – j10.081	Torsional Mode #0
2	0.043375 + j99.574 0.043375 – j99.574	-2.33 + j96.698 -2.33 – j96.698	Torsional Mode #1
3	0.028616 + j127.13 0.028616 – j127.13	-0.59096 + j126.27 -0.59096 – j126.27	Torsional Mode #2
4	0.03606 + j160.34 0.03606 – j160.34	-5.0673 + j147.1 -5.0673 – j147.1	Torsional Mode #3
5	0.001427 + j202.85 0.001427 – j202.85	-0.27956 + j201.61 -0.27956 – j201.61	Torsional Mode #4
6	-2.879e-07 + j298.18 -2.879e-07 - j298.18	-2.1094 + j286.73 -2.1094 – j286.73	Torsional Mode #5
7	-3.3979 + j141.26 -3.3979 – j141.26	-2.7704 + j142.04 -2.7704 - j142.04	Network Mode #1
8	-4.4197 + j612.42 -4.4197 – j612.42	-4.4197 + j612.42 -4.4197 - j612.42	Network Mode #2
9	-0.083245	-0.082673	
10	-4.0937	-4.0916	
11		-23.67 + j737.19 -23.67 – j737.19	IMDU

V. SYSTEM STUDIES

The system considered is the IEEE first benchmark model for SSR analysis [16]. The FBM system is simulated with the help of MATLAB. The generator base is of 892.4 MVA. The network parameter are given in Appendix 1 and the Synchronous M/C data are given in Appendix 1. There are six inertia corresponding to six rotors, four for turbines, one for generator and one for rotating exciter. A steady-state operating point is chosen in which the machine operates with a power factor of 0.9 while delivering a power of 0.7 p.u. Self-damping of 0.1 is added to the shaft. No mutual damping is assumed. Constant field voltage is also assumed. Infinite bus voltage is 481.33 kV.

Table I shows eigen values of system with and without IMDU. As we can see that on adding IMDU , the system eigenvalues have real negative parts. This indicates that system has reached in stable configuration. The IMDU is connected to HP end of shaft.

VI. TIME DOMAIN ANALYSIS

A digital computer simulation study, using a linearized system model, has been carried out to demonstrate the effectiveness of the proposed controller without any auxiliary signals under large disturbance conditions. The MATLAB SIMULINK model was used to obtain time domain simulation.

The generator is assumed to be operated at 0.7 pu load(P_G=0.7). The infinite bus voltage is assumed to be 1.0 pu. The AVR is neglected in the study. The nominal value of series compensation is assumed to be 70% (X_C=0.35 pu). Self Damping is assumed to 0.1. The IMDU is coupled to HP and electrical connected to System. The SIMULINK model is run for 10 seconds and various shaft torques and power angle delta response were obtained. Note that the initial response (for about 2 s) with and without IMDU is similar. Therefore, the IMDU can remain electrically disconnected in steady state and be switched on when a torsional interaction problem is detected. Fig.5. (a,c,e,g,i,k) shows the response obtained without IMDU and fig.5. (b,d,f,h,j,l) shows the same responses when IMDU is connected to the system. We see that SSR is effectively damped out by using IMDU. .

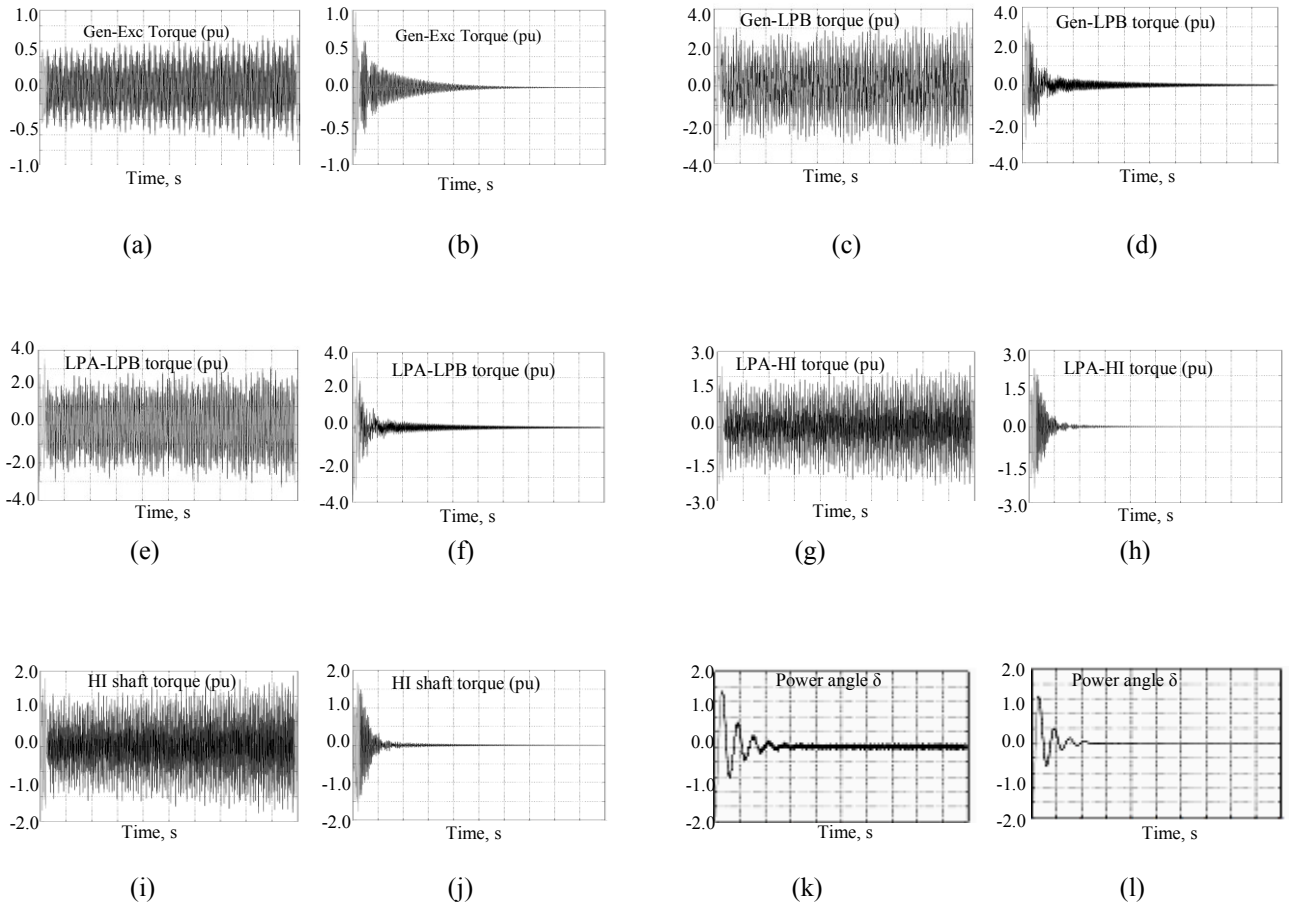

Fig.5. (a) Generator exciter torque oscillations without IMDU, (b) Generator exciter torque oscillations with IMDU (c) Generator LPB shaft torque oscillations without IMDU, (d) Generator LPB shaft torque oscillations with IMDU (e) LPA-LPB shaft torque oscillations without IMDU, (f) LPA-LPB shaft torque oscillations with IMDU (g) LPA-HI shaft torque oscillations without IMDU, (h) LPA-HI shaft torque oscillations with IMDU (i) HI shaft torque oscillations without IMDU, (j) HI shaft torque oscillations with IMDU (k) Power angle oscillations without IMDU, (l) Power angle oscillations with IMDU

VII. CONCLUSIONS

Eigenvalue studies and time domain simulations conducted on the IEEE First Benchmark Models show the damping benefits on IMDU to damp SSR. The IMDU is a small size high power and low energy induction machine. The major conclusions are as follows.

a. IMDU located at the turbine end of the T-G shaft can damp SSR oscillations without the aid of any other controller.

b. The IMDU can damp SSR over the entire range of power transfer conditions.

c. The IMDU redues the torsional stresses on the shaft sections during large transients.

d. The initial response (2 sec) with and without IMDU is same, therefore IMDU can be switched on only after a disturbance exciting torsional interaction is detected.

e. An IMDU of K (slope of torque speed characteristics value between 3 to 5 can effectively damp SSR.

f. To use IMDU damping the whole generator is need to be replaced. Therefore this method to damp SSR can be used only for new installations

So IMDU is a very powerful technique to damp SSR and we can do exhaustive analysis for practical installations.

REFERENCES

[1] IEEE Subsynchronous ResonanceWorking Group, "Terms, definitions and symbols for subsynchronous oscillations," *IEEE Trans. Power App. Syst.*, vol. PAS-104, no. 6,pp. 1326–1334, Jun. 1985.

[2] O. Wasynczuk, "Damping shaft torsional oscillations using a dynamically controlled resistor bank," *IEEE Trans. Power App. Syst.*, vol. PAS-100, no. 7, pp. 3340–3349, Jul. 1981.

[3] E. Gustafson, A. Aberg, and K. J. Astrom, "Subsynchronous resonance. A controller for active damping," in *Proc. 4th IEEE Conf. Control Applications*, Sep. 1995, pp. 389–394.

[4] N. Kakimoto and A. Phongphanphanee, "Subsynchronous resonance damping Control of thyristor-controlled series capacitor," *IEEE Power Eng. Rev.*, vol. 22, no. 9, p. 63,Sep. 2002.

[5] H. Sugimoto, M. Goto, W. Kai, Y. Yokomizu, and T. Matsumura, "Comparative studies of subsynchronous resonance damping schemes," in *Proc. Int. Conf. Power System Technology*, Oct. 2002,vol. 3, pp. 1472–1476.

[6] M. R. Iravani and R. M. Mathur, "Damping subsynchronous oscillations in power systems using a static phase-shifter," *IEEE Trans. Power Syst.*, vol. 1, no. 2, pp. 76–82, May 1986.
[7] L.Wang and Y. Y. Hsu, "Damping of subsynchronous resonance using excitation controllers and static VAr compensations: A comparative study," *IEEE Trans. Energy Convers.*, vol. 3, no. 1, pp. 6–13, Mar. 1988.
[8] B. K. Perkins and M. R. Iravani, "Dynamic modeling of a TCSC with application to SSR analysis," *IEEE Trans. Power Syst.*, vol. 12, no. 4,pp. 1619–1625, Nov. 1997.
[9] X. Zhao and C. Chen, "Damping subsynchronous resonance using an improved NGH SSR damping scheme," in *Proc. IEEE Power Eng. Soc. Summer Meeting*, Jul. 1999, vol. 2, pp. 780–785.
[10] W. Li, L. Shin-Muh, and H. Ching-Lien, "Damping subsynchronous resonance Using superconducting magnetic energy storage unit," *IEEE Trans. Energy Convers.*, vol. 9, no. 4, pp. 770–777, Dec. 1994.
[11] A. H. M. A. Rahim, A. M. Mohammad, and M. R. Khan, "Control of subsynchronous resonant modes in a series compensated system through superconducting magnetic energy storage units," *IEEE Trans. Energy Convers.*, vol. 11, no. 1, pp. 175–180, Mar. 1996.
[12] O. Wasynczuk, "Damping subsynchronous resonance using energy storage," *IEEE Trans. Power App. Syst.*, vol. PAS-101, no. 4, pp. 905–914, Apr. 1982.
[13] S. K. Gupta, A. K. Gupta, and N. Kumar, "Damping subsynchronous resonance in power systems," *Proc. Inst. Elect. Eng., Gen., Transm.,Distrib.*, vol. 149, no. 6, pp. 679–688, Nov. 2002.
[14] K. Narendra, "Damping SSR in a series compensated power system," in *Proc. IEEE Power India Conf.*, 2006, p. 7.
[15] S. Purushothaman, "Eliminating Subsynchronous oscillations with an Induction Machine Damping Unit(IMDU)" IEEE Trans. On Power System, vol. 26, No. 1,Feb. 2011.
[16] IEEE Subsynchronous Resonance Task Force, "First benchmark model for Computer simulation of subsynchronous resonance," *IEEE Trans. Power App. Syst.*, vol. PAS-96, no. 5, pp. 1565–1572, Sep. 1977.
[17] D. Walker, C. Bowler, R. Jackson, and D. Hodges, "Results of subsynchronous resonance test at Mohave," *IEEE Transactions on Power Apparatus and Systems*, vol. 94, no. 5, pp. 1878–1889, 1975.
[18] K. R. Padiyar, Power System Dynamics stability and control, BS Publication, second Edition,2008.
[19] G. Pillai, A. Ghosh, and A. Joshi, "Torsional interaction studies on a power system compensated by SSSC and fixed capacitor," *IEEE Transactions on Power Delivery*, vol. 18, no. 3, pp. 988–993, 2003.
[20] A. A. Edris, "Subsynchronous resonance countermeasure using phase imbalance," *IEEE Transactions on Power Systems*, vol. 8, no. 4, pp. 1438–1447, 1993.
[21] P. Kundur, Power system stability and control, New York: McGraw-Hill, 1994.
[22] IEEE Task Force,"Current usage and suggested practices in power system stability Simulations for synchronous machines", IEEE Trans. On Energy Conversion, Vol. EC-1,No.1, 1986, pp. 77-93
[23] IEEE Subsynchronous Resonance Working Group, "Second benchmark model for computer simulation of subsynchronous resonance," *IEEE Trans. Power App. Syst.*, vol. PAS-104, no. 5, pp. 1057–1066, May 1985.

APPENDIX 1

Generator data:

Electrical Parameters (in pu, base: 892.4MVA, 500 kV)

Parameter	Positive Sequence	Zero Sequence
R_L	0.02	0.50
X_T	0.14	0.14
X_L	0.50	1.56
X_{SYS}	0.06	0.06
X_C	0.35	0.35

Synchronous machine parameters, (in pu, base: 892.4MVA, 26 kV)

Reactance	Value, p.u.	Time Constant	Value, *second*
x_d	1.790	T_{do}'	4.300
x_d'	0.169	T_{do}''	0.032
x_d''	0.135	T_{qo}'	0.850
x_q	1.710	T_{qo}''	0.050
x_q'	0.228		
x_q''	0.200		

Mechanical Parameters:

Mass	Shaft	Inertia M (Seconds)	Spring constant *K* (p.u./rad)
EXC		0.0342165	
	GEN-EXC		2.822
GEN		0.868495	
	LPB-GEN		70.858
LPB		0.884215	
	LPA-LPB		52.038
LPA		0.858670	
	IP-LPA		34.929
IP		0.155589	
	HP-IP		19.303
HP		0.092897	
	IMDU-HP		70.8
IMDU		0.034248645	

Analyzing Software Effort Estimation using k means Clustered Regression Approach

Geeta Nagpal
Associate Professor
Dept. of Computer Science and Engg.
National Institute of Technology, Jalandhar
sikkag@gmail.com

Moin Uddin
Professor
Pro Vice Chancellor
Delhi Technological University
Delhi
prof_moin@yahoo.com

Arvinder Kaur
Associate Professor
University School of Information Technology, Indraprastha University
Delhi
arvinderkaurtakkar@yahoo.com

ABSTRACT
Software estimation is an area where more assurances have been broken than in any other area of software development. Numerous studies attempting new and reliable software effort estimation techniques have been proposed but no consensus as to which techniques are the most appropriate has been reached so far. Due to the intangible nature of "software", effort estimation with a high level of accuracy remains a dream for developers. It is unlikely to expect very accurate estimates of development effort because of the inherent uncertainty in software projects and the complex and dynamic interaction of factors that impact software development. Heterogeneity exists in software engineering datasets because data is obtained from diverse sources. This can be reduced by defining certain relationships between the data values by classifying them into different clusters. This study focuses on how the combination of clustering and regression techniques can reduce the potential problem in effectiveness of predictive efficiency due to heterogeneity of the data. Using a clustered approach creates subsets of data having a degree of homogeneity that enhances prediction accuracy. It was also observed in this study that ridge regression performs better than other regression techniques. Another key finding is that by selecting a subset of highly predictive attributes using Grey relational analysis a significant improvement in prediction can be achieved.

Categories and Subject Descriptors
D.2.9 [**Software Engineering**]: *Management---Cost Estimation*
K.6.3 *Software Management---Software Development*

General Terms
Management, Measurement, Performance

Keywords
Software estimation, Clustering, Grey relational analysis, *k* means clustering

1. INTRODUCTION
Software project planning and estimation are the most important confront for software developers and researchers. They encompass estimating the size of the software product to be produced, estimating the effort required, developing initial project schedules, and ultimately, estimating on the whole cost of the project. Software developers and researchers are using different techniques and are more concerned about accurately predicting the effort of the software product being developed. Commonly used algorithmic models for software cost estimation include Boehm's COCOMO [1], Albrecht's Function Point Analysis [2], and Putnam's SLIM [3]. These models require cost drivers to estimate the effort of the project. In recent years, a number of soft computing and computationally intelligent techniques have been proposed to handle the unpredictability and inherent uncertainty contributed by cost drivers' judgment and environment complexity of the projects. They include artificial neural network, genetic algorithm, support vector regression, genetic programming, neuro-fuzzy inference system and case base reasoning. These techniques use historical datasets of completed projects as training data and predict the values for new project's effort based on the previous training. Though a significant improvement has been achieved using these soft computing techniques in the cost, still they have limitations due to the heterogeneity of the datasets.

Soft computing techniques estimate accurately if there is a relationship between the tuples of the dataset. Due to the heterogeneity that exists among software projects, these techniques cannot estimate optimally. The heterogeneity of data can be reduced by clustering the data into similar groups. The goal of clustering is to create the groups of data that have similar characteristics. The clustering divides the data set X into *k* disjoint subsets that have some dissimilarity between them.

A clustered regression approach is used to generate more efficient estimation sub models. In this study, *k* means clustering is used for clustering the datasets. This algorithm uses Euclidean distance as the similarity measure, which considers all attributes to have equal impact. The result obtained showed that clustering could decrease the effect of irrelevant projects on the accuracy of estimations. After clustering the datasets, GRA is applied to find a subset of highly predictive attributes. Later, cluster specific regression models for the four publicly available data sets are generated. Empirical results have shown that regression when applied on clustered data gives outstanding results, indicating that the methodology has great potential to be used for software effort estimation. The results are subjected to statistical testing using the Wilcoxon signed rank test and the Mann Whitney U Test.

The rest of the paper is organized as follows. Section 2 reviews some related works on clustering algorithms and GRG as a similarity measure for feature selection. Section 3 introduces the modeling techniques. Further in Section 4, we present the proposed methodology. Section 5 gives description of the evaluation criteria. Section 6 describes the data sets and experimental results that demonstrate the use of the proposed clustered regression approach to software effort estimation. The conclusion is made in Section 7.

2. REVIEW OF LITERATURE
A number of data clustering techniques have been developed to find optimal subsets of data from existing datasets [4,5,6]. The main aim of clustering is to partition an unlabeled data set into subsets according to some similarity measure. This is called unsupervised classification. Clustering algorithms can be categorized into two main families: input clustering and input-output clustering [7]. In input clustering algorithms all attributes are considered as independent. Hard *c*-means [8] and fuzzy *c*-means [9] algorithms fall into this category. In the case of input-output clustering each multi-attribute data point is considered as a vector of independent attribute with some corresponding dependent value. Let $S = \{(x_1,y_1), (x_2,y_2) , \ldots (x_n, y_n)\}$ be a set of unlabelled input-output data pairs. Each independent input vector $x_i = [x_{1i}, x_{2i}, \ldots x_{ki}]$ has a corresponding dependent value y_i. Research work has been done to motivate this category of classification [10,11].

DOI: 10.1145/2413038.2413045 http://doi.acm.org/10.1145/2413038.2413045

Kung and Su [12] developed an effective approach to establish affine Takagi-Sugeno (T-S) fuzzy model for a nonlinear system from its input – output data. Chunheng, Cui and Wang [13] proposed FCM-SLNMM clustering algorithm, consisting of two stages. The FCM algorithm was applied in the first stage and supervised learning normal mixture model was applied in the second stage. Clustering results of the first stage are used as training data. Experiments on the real world data from the UCI repository showed that the supervised learning normal mixture model can improve the performance of the FCM algorithm sharply. Lin and Tsai [14] proposed a hierarchical grey clustering approach in which the similarity measure was a globalized modified grey relational grade instead of traditional distances. Chang and Yeh [15] generalized the concept of grey relational analysis in order to develop a technique for analyzing the similarity between given patterns. They also proposed a clustering algorithm to find cluster centers of a given dataset.

In this study, Grey Relational Analysis (GRA) has been applied for feature subset selection. GRA is a technique of Grey System Theory (GST) which utilizes the concept of absolute point-to-point distance between features [29]. GST was first established by Deng [18,19,20]. It draws out valuable information by generating and developing the partially known information. So far, GST has been applied in different areas of image processing [23], mobile communication [24], machine vision inspection [25], decision making [26], stock price prediction [27] and system control [28]. The success of GST motivated us to investigate its application in software effort estimation.

3. TECHNIQUES

3.1 Clustering Techniques

The data available for software cost estimation is inherently non linear and hence the accurate estimation of effort is difficult. Efficient estimation can be achieved if the non linearity can be treated by tracing relationships among data values. In this study, we try to reduce the heterogeneity in the software datasets by applying k means clustering approach. *k* means is a centroid-based clustering algorithm. It divides the dataset into *k* disjoint subsets that have some dissimilarity between them. It is more efficient and more scalable, with a complexity of *O* (*NKM*), where *K* is the number of clusters and *M* is the number of batch iterations.

Clustering using *k* Means Algorithm

k means algorithm assigns centers to represent the clustering of *N* points ($k < N$). The points are iteratively adjusted, so that each of the *N* points is assigned to one of the k clusters, and each of the *k* clusters is the mean of its assigned points. This procedure moves objects around from cluster to cluster with the goal of minimizing within-cluster variance and maximizing between-cluster variance. Suppose that there are n features $x_1, x_2, ..., x_n$, and they have to be divided into *k* compact clusters, $k < n$. Let m_i be the mean of cluster *i.* A minimum-distance classifier is used to separate them. That is, we can say that *x* is in cluster *i* if $|| x - m_i ||$ is the minimum of all k distances. Euclidean distances are computed from cluster means on each dimension. The algorithm for *k* Means clustering is given below:

1. Make preliminary estimate for means $m_1, m_2, ..., m_k$ for all *k* clusters.
2. Until there are no changes in any mean
   - Use the estimated means to classify samples into clusters
   - For i from 1 to k
     - Replace m_i with the mean of all samples for cluster i
   - end_for

   end_until

3.2 Grey System Theory (GST)

GST works on unascertained systems with partially known and partially unknown information. Systems with completely unknown information are *black* systems. Systems with complete information available are called *white* systems. The term ***"Grey"*** lies between "*Black"* and "*White*" and it indicates that the information is partially available. Various aspects of the GST are Grey generation, Grey modeling, Grey decision, Grey prediction, Grey relational analysis and Grey control.

3.2.1 Grey Relational Analysis

GRA is comparatively a novel technique in software estimations. It is used for analyzing relationships that exists between two series. The magnetism of GRA to software effort estimation shoots from its flexibility to model complex nonlinear relationship between effort and cost drivers [15].Basic concepts of GRA are explained below:

3.2.1.1 Factor space

Let $p(X)$ be a theme characterized by a factor set X, and Q be an influence relation, $\{p(X); Q\}$ is a factor space. The factor space $\{p(X); Q\}$ have the following properties:

- Existence of key factors,
- Number of factors is limited and countable,
- Factor independence,
- Factor expansibility.

3.2.1.2 Comparable series

Suppose $x_i = \{x_i(1), x_i(2) \ldots x_i(m)\}$, where $i = 0, 1, 2, \ldots, n \in N$; $m \in N$, is a data series. This series is said to be comparable if and only if following conditions are met:

Dimensionless: Factors must be processed so that they are non dimensional, irrespective of their units and scales.

Scaling: The factor values $x_i(k)$, (k=1,2,3…..,m) of different series x_i , (i=1,2,3,….,n) must be at the same level.

Polarized: The factor value of $x_i(k)$ of different series x_i (i=1,2,3,….,n) are described in the same direction.

3.2.1.3 Grey relational space

If all series in a factor space $\{p(X); Q\}$ are comparable, the factor space is a grey relational space which is denoted as $\{p(X); \Gamma\}$. In a grey relational space $\{p(X); \Gamma\}$, X is a collection of data series x_i ($i = 0, 1. \ldots n$), in which $x_i = \{x_i(1), x_i(2), \ldots, x_i(k)\}$, is the series; $k = 1, 2, \ldots, m$, are factors. Γ, is the Grey Relational Map set and based on geometrical mathematics, has four properties: Normality, Symmetry, Entirety, and Proximity.

Normality	$0 \le \Gamma(x_i(k), x_j(k)) \le 1, \forall i, \forall j, \forall k,$ $\Gamma(x_i, x_j) = 1 \Leftrightarrow x_i \equiv x_j$, $\Gamma(x_i, x_j) = 0 \Leftrightarrow x_i \cap x_j \in \phi.$
Symmetry	$\forall x_i, \forall x_j \in X,$ $\Gamma(x_i, x_j) = \Gamma(x_j, x_i) \Leftrightarrow X = \{x_i, x_j\}.$
Entirety	$\forall x_i, \forall x_j \in X = \{x\sigma \mid \sigma = 0, 1, \ldots, n\}, n \ge 2,$ $\Gamma(x_i, x_j)$ often $\neq \Gamma(x_j, x_i).$
Proximity	$\Gamma(x_i(k), x_j(k))$ increases as $\Delta(k) = \lvert x_i(k) - x_j(k) \rvert$ decrease for $\forall k \in \{1, 2, \ldots, m\}$.

3.2.2 Grey Relational Grade by Deng's Method for Feature Selection

GRA is used to quantify the influence of various factors and the relationship among data series that is a collection of measurements [15].The three main steps involved in the process are:

3.2.2.1 Data Processing

Data Processing reduces the randomization and increases the regularity of data. It tries to eliminate irregularities related with different measurement units and normalizes the raw data [15]. The raw data can be transformed into dimensionless forms by various methods like average value processing, initial value processing, upper bound effectiveness or lower bound effectiveness etc. The method adopted depends upon the nature of data. For upper bound effectiveness, the transformed value $x_i^*(k)$ of $x_i(k)$ is calculated by:

DOI: 10.1145/2413038.2413045 http://doi.acm.org/10.1145/2413038.2413045

$$x_i^*(k) = \frac{x_i(k) - min_i x_i(k)}{max_i x_i(k) - min_i x_i(k)}, \quad (1)$$

where $i=1,2,\ldots,m$, $k=1,2,\ldots,n$, $x_i(k)$ is the value of the k_{th} attribute in the i_{th} series; $x_i^*(k)$ is the normalized value of the k_{th} attribute in the i_{th} series; $max_i x_i(k)$ and $min_i x_i(k)$ are the maximum and minimum of the k_{th} attribute in all series.

3.2.2.2 Grey Relational Coefficient

GRA uses the grey relational coefficient γ to describe the trend relationship between an objective series and a reference series at a given point in a system. If x_0 is the reference series and $x_1, x_2 \ldots x_n \epsilon X$ are objective series, then the grey relational coefficient $\gamma(x_0(k), x_i(k))$ as per Deng [19,20] is given by

$$\gamma(x_0(k), x_i(k)) = \frac{\Delta_{min} + \zeta \Delta_{max}}{\Delta_{0,i}(k) + \zeta \Delta_{max}} \quad \text{where,} \quad (2)$$

$\Delta_{0,i}(k) = |x_0(k) - x_i(k)|$ is the difference of the absolute value between $x_0(k)$ and $x_i(k)$;

$\Delta_{min} = min_j min_k |x_0(k) - x_j(k)|$ is the smallest value of $\Delta_{0,j} \forall j \in \{1, 2, \ldots, n\}$;

$\Delta_{max} = max_j max_k |x_0(k) - x_j(k)|$ is the largest value of $\Delta_{0,j} \forall j \in \{1, 2, \ldots, n\}$;

and ζ is the distinguishing coefficient, $\zeta \in (0, 1)$. The ζ value will change the extent of $\gamma(x_0(k), x_i(k))$. It should be selected in order to justify the system need [15]. In this study, the value of ζ has been taken as 0.5 as suggested by Deng [16].

3.2.2.3 Grey Relational Grade

Grey Relational Grade (GRG) is used to find overall similarity degree between reference feature x_o and comparative feature x_i. When the value of GRG approaches 1, the two features are "more closely similar". When GRG approaches a value 0, the two features are "more dissimilar". The GRG $\Gamma(x_0, x_i)$ between an objective series x_i and the reference series x_0 was defined by[19,20] as :

$$\Gamma(x_0, x_i) = \frac{1}{n} \sum_{k=1}^{n} \gamma(x_0(k), x_i(k)) \quad (3)$$

3.3 Regression Techniques

As discussed earlier, a large number of techniques have been applied to the field of software effort estimation. The aim of this study is to assess which regression techniques perform best to estimate software effort. The following techniques are considered:

- Ordinary Least Square Regression
- Ridge Regression
- Forward Stepwise Regression
- Backward Stepwise Regression
- Multiple Adaptive regression Splines

These regression techniques are applied to four publicly available datasets: Desharnais dataset, Finnish dataset, Albrecht dataset and Maxwell dataset [22].

3.3.1 Ordinary Least Square Regression

It is the most popular and widely applied technique for software cost estimation. According to the principle of least squares, the `best fitting' line is the line which minimizes the deviations of the observed data away from the line. This type of regression is also referred to as multiple linear regression and is given by:

$$y_i = \beta_0 + \beta_1 x_{i,1} + \beta_2 x_{i,2} + \ldots\ldots \beta_k x_{i,k} + \varepsilon_i \quad (4)$$

where, Y_i is a dependent variable whereas, $x_1, x_2, \ldots\ldots x_k$ are k independent variables. β_o is the y intercept, β_1 , β_2 are slopes of y that are estimated by regression, ε_i is the error term. The corresponding prediction equation is given as:

$$\hat{y}_i = \hat{\beta}_0 + \hat{\beta}_1 x_{i,1} + \hat{\beta}_2 x_{i,2} + \ldots\ldots\ldots \hat{\beta}_k x_{i,k} \quad (5)$$

In this equation, $\hat{\beta}_0$, $\hat{\beta}_1, \ldots . \hat{\beta}_k$ are least square coefficients and $\hat{y}_i$ is the estimated response for i^{th} term. The least square method tries to minimize $\sum {e_i}^2$.

3.3.2 Ridge Regression

Ridge regression is an alternative regression technique that tries to address potential problems with OLS that arise due to highly correlated attributes. In regression, the objective is to "explain" the variation in one or more "response variables", by associating this variation with proportional variation in one or more "explanatory variables", but the problem arises when the explanatory variables vary in similar ways, reducing their collective power of explanation. The phenomenon is known as ***near collinearity***. As different variables are correlated the covariance matrix $X'X$ will be nearly singular and as a result estimates will be unstable. A small variation in error will have large impact on $\hat{\beta}$. Ridge regression reduces the sensitivity by adding a number δ to elements on the diagonal of the matrix to be inverted. δ is called the ridge parameter and it yields the following estimator of β.

$$\hat{\beta}_\delta = (X'X + \delta I_n)^{-1}(X'e), \quad (6)$$

where, I_n represents the identity matrix of rank n.

3.3.3 Forward Stepwise Regression

The purpose of stepwise regression is to generate regression model in which the detection of most predictive variables is carried out. It is carried out by a series of F tests. The method evaluates independent variables at each step by adding or deleting them from the model based on user-specified criteria. In the first step, each independent variable is evaluated individually and the variable that has the largest F value greater than or equal to the F to enter value, is entered into the regression equation. In the subsequent steps, when a variable is added to the model based on the F value, the method also examines variables included in the model based on F to remove criteria, and if any variable is found it is removed.

3.3.4 Backward Stepwise Regression

The backward stepwise elimination procedure is basically a series of tests for significance of independent variables. The process starts with the maximum model. It eliminates the variable with the highest p - value for the test of significance of the variable, conditioned on the p - value being bigger than some pre-determined level (say, 0.05). In the next step, it fits the reduced model after having removed the variable from the maximum model, and also removes from the reduced model the variable with the highest p-value for the test of significance of that variable (if p>=0.05) and so on. The process ends when no more variables can be removed from the model at significance level 5%.

3.3.5 Multiple Adaptive Regression Splines(MARS)

MARS (Multivariate Adaptive Regression Splines) focuses on the development and deployment of accurate and easy-to-understand regression models. MARS model is a regression model which automatically generates non-linearities and interactions between variables. MARS has shown evidences of very high-performance results in forecasting electricity requirement for power-generating companies, relating customer satisfaction scores to the engineering specifications of products, and presence/absence modeling in geographical information systems(GIS). MARS fits the data to the following equation.

$$e_i = b_o + \sum_{k=1}^{K} b_k \prod_{i=1}^{L} h_l(x_i(j))$$

where, b_o and b_k are the intercept and slope respectively.
Parameters $h_i(x_i\ (j))$ are hinge functions. They take the form $max\ (0, x_i(j)-b)$ where, b is the knot. MARS is a multiple piece wise linear regression with multiple hinge functions.

4. Proposed Methodology

In order to reduce the heterogeneity that exists in the dataset, the initial focus is to partition dataset into subsets according to a similarity measure. In this study, a k means clustering approach that divides projects into similar groups is used. After Cluster formation, we apply GRA for feature subset selection on the selected cluster from each data set. By analyzing the influence of continuous values of various features on the of project effort, GST can help us gain the most predictive feature subset from a small dataset[15].Thus an optimal feature subset

from the database of projects is generated. After generating *k* best features, we apply regression techniques like OLS, Ridge Regression, Stepwise Regression and MAR Spline. The structural framework of the proposed methodology is shown in figure 3.
The steps involved are explained in detail.

Step 1: Select all the continuous attributes from the dataset.
Step 2: Clustering using *k* means algorithm
For generating better software estimates, four datasets are divided into clusters using *k* means clustering. The *k* means clustering finds clusters of data iteratively, by starting with an initial estimate of means of clusters and then updating centers so that data close to centers are grouped together. The clustering for Albrecht and Desharnais datasets using *k* means algorithm is shown in figure1 and figure 2 respectively. The summary of the cluster means and number of cases in each cluster with their percentage are given in Table 1 and Table 2 respectively. For each datasets two homogeneous clusters were obtained. Models for effort estimation are then formed separately for one cluster from each dataset.

Clusters for Albrecht data set:

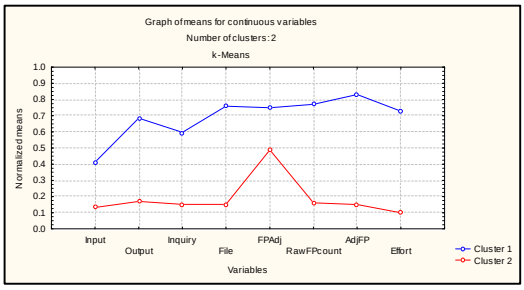

Figure 1. Clusters Albrecht data set

Table 1. Cluster Means (Albrecht dataset)

Cluster	1	2
Input	83.75000	31.55000
Output	106.5000	35.4000
Inquiry	44.75000	11.30000
File	46.25000	11.60000
FPAdj	1.087500	0.9700
RawFPcounts	1508.978	464.452
AdjFP	1614.75	454
Effort	76.72	10.90
Number of cases	4	20
%age	16.666	83.333

Cluster for Desharnais data set:

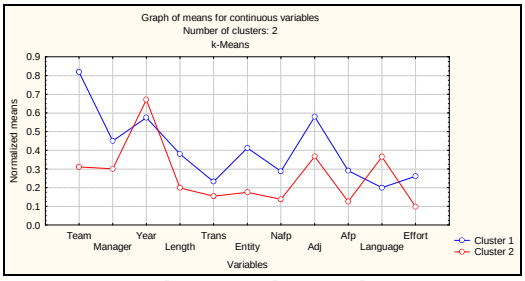

Figure 2. Clusters Desharnais data set

Table 2. Cluster Means (Desharnais dataset)

Cluster	1	2
Team	3.275000	1.243243
Manager	3.150000	2.108108
Year	85.45000	86.02703
Length	14.30000	7.94595
Trans	212.3750	144.5946
Entity	163.7000	73.8919
Nafp	376.0750	218.4865
Adj	32.27500	22.24324
Afp	368.3500	194.2973
Language	1.400000	1.729730
Effort	6658.750	2861.108
Cases	40	37
%age	51.94805	48.05195

The Euclidean distance is computed from the cluster means on each dimension.

Step 3: Feature Selection by GRA [15]

i. *Construction of data:* Columns in each cluster dataset are treated as series . The Effort series $x_e = \{e_1, e_2, e_3 ..... e_n\}$ is taken as the reference series and attribute columns are regarded as objective series.
ii. *Normalization:* Each data series is normalized in order to have the same degree of influence on the dependent variable "effort".
iii. *Generation of Grey Relational Grade:* Grey Relational grade is calculated for each series with respect to reference series according to equation 3.
iv. *Feature Selection :* To increase the efficiency of prediction accuracy of the *cluster,* features that have high implication on effort need to be identified. Features with higher value of GRG encompass the most favourable feature subset.

Algorithm for Feature Selection : For feature selection (e. g. Albrecht dataset) the Grey Relational Grade for each feature with respect to effort is generated. After finding similarity between the effort and each feature, it is necessary to retrieve the features that exhibit the largest similarity with the reference feature (Effort). These features are ranked in accordance to their GRGs. This procedure is called Grey Relation Rank (GRR). It ranks all features such as Input, Output, Inquiry, File, FPAdj, RawFPcounts, AdjFP and Effort. The GRG for features is shown in the Table 3. The Feature RawFPcounts and AdjFP have lowest GRG .

In the first step, the proposed feature selection method attempts to identify all the continuous features amongst set of all features and assess its fitness on the prediction accuracy in terms of Mean Magnitude of Relative Error (MMRE), Median MRE, Magnitude of Relative Error Relative to the Estimate (MMER) and Pred(25). In the second step, it deletes features with lowest GRG one at a time from the continuous set of features, and then re assesses its fitness on the prediction accuracy. The proposed feature selection method is described in the following steps:

Table 3. Grey Relational ranks of Albrecht datasets

Feature Number	Feature	Grey Relational Grade
8	Effort	*1.00000000*
4	File	*0.97193857*
3	Inquiry	*0.96244115*
5	FPAdj	*0.95735750*
2	Output	*0.92447003*
1	Input	*0.92335418*
7	AdjFP	*0.36955000*
6	RawFPcounts	*0.36513818*

Function Feature Selection

```
// calculate the Grey relational Grade (GRG) for each attribute
For  i = 1; i <= M; i++
     GRG(i) = GreyRelationalGrade(Data, i);
End_For
//arrange the GRG into decreasing order
Attribute_IDs = sort(GRG);
Optimal_Feature_Set = Attribute_IDs;
```

//Check the effect of attributes from the lowest GRG
For j = M; j >= 1; j- -
Remove AttributeIDs(j) from the ptimal_Feature_Set;
If Fitness (Optimal_Feature_Set) is poor then
Continue;
Else
Add Attribute_Ids(j) to the Optimal_Feature_Set;
Break;
End_For
Return Optimal_Feature_Set;

Step 4: Apply Regression Techniques on Clusters of data sets in order to estimate the effort.

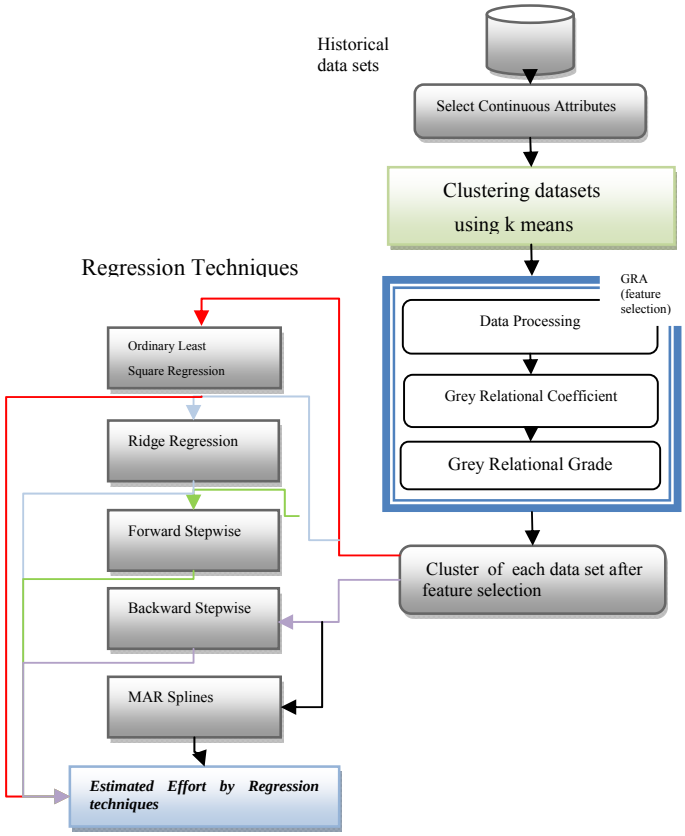

Figure 3. Structural framework

5. EVALUATION CRITERIA

For the purpose of validation and evaluation of the new methodology, the basic necessity is to measure how accurate the estimations are. Various approaches are used by researchers to measure the accuracy of effort prediction methods, such as MMRE, Median MMRE, MMER, adjusted R-squared or coefficient of determination and Pred(n). To measure the accuracy of the software estimation, we have used three most popularly used evaluation criteria in software engineering i.e MMRE, MdMRE and Pred(n).

5.1 Mean Magnitude of Relative Error (MMRE):

Relative error is the absolute error in the observations divided by its actual value. The Magnitude of Relative Error is the percentage of actual effort for the project and is given as

$$MRE = \frac{|actual_i - estimated_i|}{actual_i} \quad (8)$$

The MRE for each observation is aggregated over the total number of projects, N, to generate the Mean MRE (MMRE). MMRE is calculated as:

$$MMRE = \frac{1}{N}\sum_{x=1}^{N} MRE_x \quad (9)$$

MMRE favours models that underestimate, and it is extremely sensitive to small actuals.

5.2 Median MRE(MdMRE):

Median MRE is less sensitive to extreme values as compared to *MMRE* , so in case of large datasets we prefer using *MdMRE* as the estimation accuracy criteria. It is given by:

$$MdMRE = median(MRE_x) \quad (10)$$

A higher score for both *MMRE and MdMRE*, means worse prediction accuracy.

5.3 Pred (l):

It is used as an opposite measure to count the percentage of estimates that fall within less than *l* of actual values. The common used value for *Pred(l)* is 25% . $MRE_i <= l$ % .
A low score on *MRE*, *MMRE, MdMRE* whereas a high value on *Pred (l)* entails better accuracy.
MMRE is a measure of the spread (i.e. standard deviation) of the variable *x* where $x_i = E'_i / E_i$, and *Pred(l)* is a measure of how peaked the distribution of *x* is.

Thus, these accuracy statistics measure different properties of the distribution of *x*. This is why they may appear to give contradictory results when they are used to assess different prediction systems.

Boxplot of the absolute residuals ($|actual - estimate|$) has also been used as it provides good indication of the distribution of residuals and can explain summary statistics such as MMRE and Pred(25). The Boxplot is a five number summary. It includes the median as the central tendency of the distribution, the Inter Quartile Range (IQR) and the min–max values. It also shows outliers of the individual distribution. The length is the spread of the distribution. The box represents 50% of the observations in the distribution. A small box is a peaked distribution whereas; a long box is flattened distribution.

6. RESULTS AND DISCUSSIONS

6.1 Datasets

In order to evaluate and validate models based upon the proposed methodology, four well established datasets from the Promise repository [22] have been used. They are Desharnais, Finnish, Albrecht and Maxwell. The descriptive statistics of datasets are provided in Table 4. All datasets have a varied range of effort values. They have been treated individually as they have distinct features. Clusters from each dataset have also been treated separately. The prediction accuracy for all models with and without clustering are then compared.

Table 4. Descriptive Statistics of the data sets

	Desharnais	Finnish	Albrecht	Maxwell
Cases	77	38	24	62
Features	11	8	8	23
Effort Mean	4833.90	7678.28	21.8750	8223
Minimum(effort value)	546	460	0.50	583
Maximum (effort value)	23940	26670	105.20	63694
Effort Std. Dev.	4188.18	7135.27	28.4178	10499.90

6.2 Prediction Accuracy of the Proposed Methodology

The comparison between different research studies is difficult as each study adopts different empirical setup, preprocessing style, outlier treatment etc. This all leads to conflicting results. Secondly, each study varies with respect to number of datasets used for evaluating the techniques, the size of the dataset, evaluation and validation criteria involved. Hence, finding which modeling technique performs best on which data is tedious and conflicting. The modeling technique used should be reproducible on a larger number of datasets. In this study a comparison is made between the clustered regression approach using GRA for feature selection and regression only.

DOI: 10.1145/2413038.2413045 http://doi.acm.org/10.1145/2413038.2413045

6.2.1 Comparison over the Desharnais Data set

Results obtained suggest that applying regression techniques on clustered data produces more accurate models than applying regression on entire dataset. This is evident from results obtained shown in Table 5. The Pred(25) accuracy has improved from 35.06 % to 55 % using OLS regression whereas, the MMRE and MDMRE has fallen from 0.5 to 0.3 and from 0.31 to 0.22 respectively. Similar observations can be noticed from the Table 5 below for all other regression models also. Thus, heterogeneity has been reduced in datasets which in turn has improved the prediction accuracy.

Table 5. Prediction accuracy results (Desharnais data set)

	OLS	Ridge Regression	Forward Stepwise	Backward Stepwise	MAR Splines
Desharnais					
MMRE	0.5	**0.47**	0.5	0.5	0.51
MdMRE	0.31	**0.3**	0.31	0.31	0.32
Pred(25)	35.06	**41.56**	37.66	37.66	35.06
Desharnais(Cluster_1)					
MMRE	**0.3**	0.34	0.32	0.32	0.3
MdMRE	**0.22**	0.27	0.25	0.25	0.25
Pred(25)	**55**	45	45	45	47.5

The Boxplot of absolute residuals provide good indication of the distribution of residuals and can help better understand the mean magnitude of relative error and Pred (25).

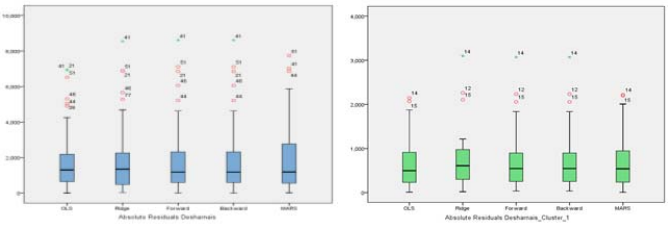

Figure 4. Boxplot of Absolute Residuals for Desharnais

The Boxplot of absolute residuals is shown in figure 4 . It suggests that:

- Medians for all regression techniques applied on Desharnais _Cluster are more close to zero, as it is evident from values on the Y-axis, indicating that estimates are closer to the minimum value.
- The median and range of absolute residuals is also small, especially in case of ridge regression, indicating accurate predictions. Medians are more skewed to the minimum value indicating that predictions are good.
- Outliers are few and less extreme in the case of the Desharnais_Cluster as compared to the Desharnais dataset.

WILCOXON Signed Rank Test:

Step 1: Hypotheses

H_0: μ (*Before*) = μ(*After*) ; H_a: μ(*Before*) >μ (*After*)

(Residual Median = Hypothetical Median (test value)

Step 2: Significance Level : α= 0.05

Step 3: Rejection Region: Reject the null hypothesis if p-value <= 0.05.

Step 4: Test Statistic: Wilcoxon signed rank test.

Step 5: Decision

The p-value in all cases is greater 0.05 as shown in Table 6. Thus, we accept the null hypothesis. Consequently, we conclude that residuals obtained by using both approaches were not significantly different from the test value zero. As a result, the proposed methods can be used for software effort estimation.

TABLE 6: WILCOXON SIGNED RANK TEST Test Statistics[c]

	DESHARNAIS		DESHARNAIS_CLUSTER_1	
	Desharnais Z	Asymp. Sig. (2-tailed)	Desharnais_Cluster_1 Z	Asymp. Sig. (2-tailed)
OLS-Actual	-.419[a]	.675	-.536[a]	.592
Ridge - Actual	-.551[a]	.582	-.415[a]	.678
Forward - Actual	-.449[a]	.653	-.460[a]	.645
Backward - Actual	-.449[a]	.653	-.460[a]	.645
MARS – Actual	-.566[a]	.571	-.143[a]	.886

The Statistical test was performed using SPSS 19 for windows. Results of Mann Whitney U Test are provided in Table 7. Predictions obtained using the clustered approach presented statistically significant estimations over regression on entire data set.

Table 7 : Results Mann-Whitney U Test

Desharnais vs. Desharnais_Cluster_1		**Mann-Whitney test**
1	OLS Regression	-4.167
2	Ridge Regression	-3.344
3	Forward Stepwise	-3.664
4	Backward Stepwise	-3.664
5	MAR Splines	-3.658

6.2.2 Comparison over the Finnish data set:

For the Finnish dataset, some significant results (as shown in Table 8.) were obtained on the clustered data. The Pred(25)accuracy improved from 36.84 % to 100 % using Ordinary least square regression whereas, the MMRE and MDMRE has fallen from 0.75 to 0.05 and from 0.36 to 0.04 respectively. Similar observations can be notified from the Table 8 for all other regression models. Thus, a significant improvement has been brought in by using clustered approach.

Table 8. Prediction accuracy results(Finnish data set)

	OLS	Ridge Regression	Forward Stepwise	Backward Stepwise	MAR Splines
Finnish					
MMRE	0.75	0.71	1.01	0.76	**0.08**
MdMRE	0.36	0.32	0.43	0.42	**0.07**
Pred(25)	36.84	36.84	36.84	36.84	**97.37**
Finnish(Cluster_I)					
MMRE	0.05	**0.05**	0.06	0.06	0.06
MdMRE	0.04	**0.03**	0.06	0.05	0.05
Pred(25)	100	**100**	100	100	100

Boxplot of absolute residuals for Finnish dataset and Finnish_cluster is shown in Figure 5. It suggests that:

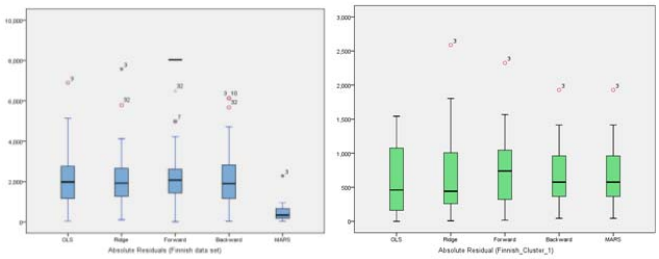

Figure 5. Boxplot of Absolute Residuals for Finnish

- Medians for all regression techniques applied on Finnish _Cluster are very close to zero, as it is clear from values on the Y-axis. This indicates that estimates are closer to the minimum value.
- The median is also small, especially in the case of Ridge regression, indicating more accurate prediction.
- Outliers are less extreme in case of Finnish_Cluster

One sample Wilcoxon signed rank test has been applied in order to investigate the significance of results by setting level of confidence to 0.05. From the results obtained, shown in Table 9, we can conclude that no significant difference exists between the residual median and hypothetical median.

TABLE 9 : WILCOXON SIGNED RANK TEST Test Statistics[c]

	FINNISH		FINNISH_CLUSTER_1	
	Finnish Z	Asymp. Sig. (2-tailed)	Finnish_Cluster_1 Z	Asymp. Sig. (2-tailed)
OLS-Actual	-.268[a]	.788	-.114[a]	.910
Ridge - Actual	-.355[a]	.722	-.672[a]	.501
Forward - Actual	-.268[a]	.788	-.207[a]	.836
Backward - Actual	-.152[a]	.879	-.103[a]	.918
MARS – Actual	-.558[a]	.577	-.103[a]	.918

Unsurprisingly, predictions based on clustered regression model presented statistically significant accurate estimations, measured using absolute residuals, confirmed by the results of Boxplot of absolute residuals and verified using Mann Whitney U test(Table 10.).

Table 10. Results Mann-Whitney U Test

Finnish vs. Finnish_Cluster_1		Mann-Whitney test
1	OLS Regression	-4.054
2	Ridge Regression	-3.637
3	Forward Stepwise	-4.187
4	Backward Stepwise	-3.808
5	MAR Splines	-2.538

6.2.3 Comparison over the Albrecht data set:

Results obtained using the proposed clustered regression approach produced more accurate models. This is evident from the Pred(25) accuracy that improved from 37.5 % to 45.45 % using OLS regression whereas, the MMRE and MDMRE has fallen from 0.9 to 0.79 and from 0.43 to 0.27 respectively. Similar observations can be notified for all other regression models also (Table11). Thus, an improvement has been brought in by using clustered approach. The heterogeneity has been reduced in datasets which in turn has improved the prediction accuracy.

Table 11. Prediction accuracy results(Albrecht data set)

	OLS	Ridge Regression	Forward Stepwise	Backward Stepwise	MAR Splines
Albrecht					
MMRE	0.9	0.91	**0.86**	1	1.23
MdMRE	0.43	0.52	**0.5**	0.49	0.6
Pred(25)	37.5	37.5	**41.67**	37.5	29.17
Albrecht(Cluster_I)					
MMRE	**0.79**	0.91	0.83	0.83	0.81
MdMRE	**0.27**	0.34	0.26	0.26	0.28
Pred(25)	**45.45**	40	50	50	35

The boxplot of absolute residuals for the Albrecht dataset and Albrecht_Cluster suggest that:

- Medians for all regression techniques applied on Albrecht_Cluster are very close to zero, as it is clear from values on the Y-axis. This indicates that the estimates are closer to the minimum value.
- Outliers are less extreme in the case of Finnish_Cluster (except MAR Splines).

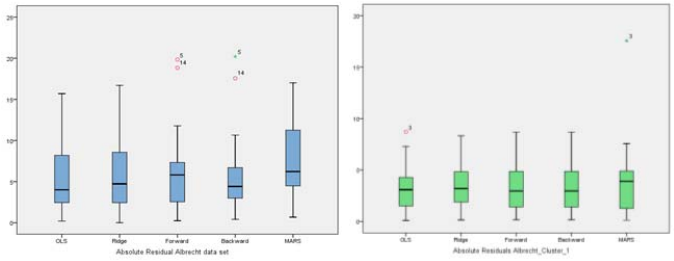

Figure 6. Boxplot of Absolute Residuals for Albrecht

Results of Wilcoxon signed rank conclude that no significant difference exists between the residual median and hypothetical median, thus indicating good predictions (Table 12.)

TABLE 12. WILCOXON SIGNED RANK TEST Test Statistics[c]

	ALBRECHT		ALBRECHT_CLUSTER_1	
	Albrecht Z	Asymp. Sig. (2-tailed)	Albrecht_Cluster_1 Z	Asymp. Sig. (2-tailed)
OLS-Actual	-.029[a]	.977	-.075[a]	.940
Ridge - Actual	-.057[a]	.954	-.131[b]	.896
Forward - Actual	-.057[a]	.954	-.112[a]	.911
Backward - Actual	-.086[b]	.932	-.112[a]	.911
MARS – Actual	-.029[b]	.977	-.560[b]	.575

Table 13. Results Mann-Whitney U Test

Albrecht vs. Albrecht_Cluster_1		Mann-Whitney test
1	OLS Regression	-1.791
2	Ridge Regression	-1.744
3	Forward Stepwise	-2.121
4	Backward Stepwise	-1.909
5	MAR Splines	-1.791

Residuals obtained using the clustered regression approach for Albrecht dataset are smaller than those obtained using entire data set, indicating

that estimates based on clustered model provided better accuracy . Results obtained using Mann Whitney U test are shown in Table 13.They confirm no significant difference between the two approaches. This may be because of the small size of the dataset. The dataset comprised of 24 projects. It was divided into two clusters one with 20 projects and other with 4 projects. Clustered regression approach was applied on the cluster with 20 projects.

6.2.4 Comparison over the Maxwell Dataset:

Results obtained using the proposed clustered regression approach produced more accurate models for Maxwell dataset also. This is evident from the Pred(25) accuracy that improved from 38.71 % to 58.33 % using OLS regression whereas, the MMRE and MDMRE has fallen from 0.59 to 0.25 and from 0.38 to 0.19 respectively. For Ridge regression also, the Pred(25) accuracy increased from 43.55% to 61.11% which is a significant improvement. The MMRE and MdMRE has gone low from 0.54 to 0.30 and 0.3 to 0.16 respectively. Similar observations can be notified from the Table14 below for all other regression models also. Thus, a significant improvement has been brought in by using clustered approach. The heterogeneity has been reduced in datasets which in turn has improved the prediction accuracy.

Table 14. Prediction accuracy results (Maxwell data set)

	OLS	Ridge Regression	Forward Stepwise	Backward Stepwise	MAR Splines
Maxwell					
MMRE	0.59	**0.54**	0.53	0.59	0.7
MdMRE	0.38	**0.3**	0.32	0.33	0.46
Pred(25)	38.71	**43.55**	38.71	37.1	32.26
Maxwell(Cluster_1)					
MMRE	0.25	**0.30**	0.42	0.42	0.41
MdMRE	0.19	**0.16**	0.29	0.29	0.30
Pred(25)	58.33	**61.11**	44.44	44.44	36

Boxplots of absolute residuals for the Maxwell dataset and Maxwell_Cluster suggest that:

- Medians for all regression techniques applied on Maxwell _Cluster are more close to zero, as it is clear from the values on the Y-axis. This indicates that the estimates are closer to the minimum value.
- The median and range of absolute residuals is also small, especially in case of OLS, Ridge regression and MARS, indicating accurate predictions. The medians are more skewed to the minimum value indicating that predictions are good.
- Outliers are few and less extreme in case of Maxwell_Cluster as compared to Desharnais data set.

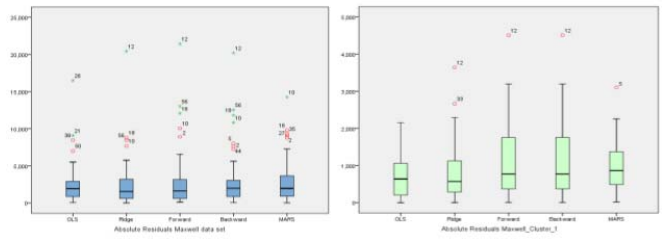

Figure 7. Boxplot of Absolute Residuals for Maxwell

Results of Wilcoxon signed rank test suggest that no significant difference exists between the residual median and hypothetical median. Results of Wilcoxon signed rank test are given in Table 15.

Concerning the statistical test based on Mann Whitney U, we found significant difference between clustered regression approach and regression approach. Results in Table 16 signify that predictions obtained using the clustered approach present statistically significant estimations over regression on entire data set.

TABLE 15. WILCOXON SIGNED RANK TEST Test Statistics[c]

	MAXWELL		MAXWELL_CLUSTER_1	
	Maxwell Z	Asymp. Sig. (2-tailed)	Maxwell_Cluster_1 Z	Asymp. Sig. (2-tailed)
OLS-Actual	-.249[a]	.803	-.303[a]	.762
Ridge - Actual	-.508[a]	.611	-.786[a]	.432
Forward - Actual	-.691[a]	.490	-.550[a]	.582
Backward - Actual	-.831[a]	.406	-.550[a]	.582
MARS – Actual	-.109[a]	.913	-.189[a]	.850

Table 16. Results Mann-Whitney U Test

Maxwell vs. Maxwell_Cluster_1		**Mann-Whitney test**
1	OLS Regression	-2.815
2	Ridge Regression	-2.690
3	Forward Stepwise	-2.793
4	Backward Stepwise	-2.565
5	MAR Splines	-2.632

7. CONCLUSION

This work resolves the heterogeneity problems that exist in datasets. In order to confirm the effectiveness of proposed work, four different data sets have been used with two different models for software estimation. Simulation results provide a comparison of clustered regression approach over regression only. Results confirm that the clustered regression approach performs appreciably better for software effort estimation. The results improved by using GRA for feature subset selection. Hence, the influence of features on output variables can be effectively worked out using GRA. The statistical test based on Mann Whitney U further confirmed that statistical significant difference exists between the proposed clustered-regression models and regression models. It is evident from results obtained using the test that there is difference if predictions are generated using the clustered regression approach for almost for all datasets.

Further, this work can be extended by using clustered approach with different soft computing techniques with different similarity measures for feature selection. Also, for enhanced efficiency in software estimation the techniques should be applied to large data sets with other clustering algorithms.

8. ACKNOWLEDGMENTS

Our thanks to Promise Repository for providing such useful data sets which are helpful in carrying out research work.

9. REFERENCES

Boehm B.“Software Engineering Economics Englewood Cliffs,” NJ, Prentice Hall (1981).

Albrecht A.J. and Gaffney J.R.(1983), “Software measurement, source lines of code, and development effort prediction: a software science validation,” *IEEE Transactions on Software Engineering*, Vol. 9,No. 6, pp. 639–648.

Putnam, Lawrence H. (1978) "A General Empirical Solution to the Macro Software Sizing and Estimating Problem". *IEEE Transactions on Software Engineering,* Vol.4, No. 4, pp. 345-361.

El-Zaghmouri, B. M. and Abu-Zanona, M. A. (2012) ‘Fuzzy C-Mean Clustering Algorithm Modification and Adaption for

Application' *World of Computer Science and Information Technology Journal*, ISSN: 2221-0741, Vol.2, No.1, pp.42-45.

Lin, C. T and Tsai, H. Y(2005) 'Hierarchical Clustering Analysis Based on Grey Relation grade', *Information and Management Sciences*, Vol. 16, No. 1, pp.95-105.

Wong, C.C and Chen, C.C(1998) 'Data clustering by grey relational analysis', *J. Grey Syst*, 10, (3), pp. 281 – 288.

Hu, Y.C, Chen, R. S, Hsu, Y. T and Tzebg, G. H(2002) 'Grey self-organizing feature maps', *Neuro computing*, Vol.48, No.(1–4), pp. 863 – 877.

Duda, R.O and Hart, P.E (1973) 'Pattern classification and scene analysis', *John Wiley &Sons*, Inc., New York.

Bezdek, J. C, Ehrlich, R. and Full, W. (1984) 'FCM: The Fuzzy c- Means Clustering Algorithm', *Computers & Geoscience* Vol. 10, No. 2-3, pp. 191-203.

Runkler, T.A. and Bezdek, J.C.(1999) 'Alternating cluster estimation: a new tool for clustering and function approximation', *IEEE Trans. Fuzzy Syst.* , Vol.7, No.4, pp. 377–393.

Pedrycz,W.(1996) 'Conditional fuzzy c-means', *Pattern Recogn. Lett.*,Vol.17,No.6, pp. 625–632.

Kung C. C and Su J. Y(2007) "Affine Takagi-Sugeno fuzzy modeling algorithm by Fuzzy c-regression models clustering with a novel cluster validity criterion", IET Control Theory Appl., pp. 1255–1265.

Wang, W., Wang, C., Cui, X. and Wang, A.(2008), 'A clustering algorithm combine the FCM algorithm with supervised learning normal mixture model', ICPR 2008: 1-4

Lin, C. T. and Tsai, H. Y. (2005) 'Hierarchical Clustering Analysis Based on Grey Relation grade', *Information and Management Sciences*, Vol. 16, No. 1, pp.95-105.

Chang, K. C. and Yeh, M. F.(2005) 'Grey Relational Based Analysis approach for data clustering', *IEEE Proc.-Vis. Image Signal Process*, Vol.152, No.2.

Song, Q., Shepperd M., Mair C.,(2005)"Using Grey Relational Analysis to Predict Software Effort with Small Data Sets". Proceedings of the 11th International Symposium on Software Metrics (METRICS'05), 35-45.

Azzeh, M., Neagu, D and Cowling, P. I.(2010) "Fuzzy grey relational analysis for software effort estimation", *Journal of Empirical Software Engineering* 15(1).

[doi:10.1007/s10664-009-9113-0]

Deng, J. L.(1982) "Control problems of grey system". *System and Control Letters*, Vol. 1, pp.288–94

Deng, J. (1989) "Introduction to Grey System theory", *The Journal of Grey System*,Vol.1 No.1pp.1-24

Deng, J. (1989) "Grey information space", *The Journal of Grey System* Vol.1No.1,pp. 103–117

MATLAB®Documentation, http://www.mathworks.com/help/techdoc/

PROMISE Repository of empirical software engineering data http://promisedata.org/ repository,

Jou, J. M , Chen, P. Y and Sun, J. M.(1999) "The grey prediction search algorithm for block motion estimation", *IEEE Transactions on Circuits and Systems for Video Technology*, Vol.9 No.6, pp.843–848

Su, S. L., Su, Y. C. and Huang, J. F. (2000),"Grey-based power control for DS-CDMA cellular mobile systems", *IEEE Transactions on Vehicular Technology*, Vol.49 No.6, pp.2081–2088

Jiang, B.C, Tasi, S. L and Wang, C. C.(2002) "Machine vision-based gray relational theory applied to IC marking inspection", *IEEE Transactions on Semiconductor Manufacturing*, Vol.15 No.4, pp.531–539

Luo, R. C, Chen, T. M and Su, K. L.(2001) "Target tracking using a hierarchical grey-fuzzy motion decision making method". *IEEE Transactions on Systems, Man and Cybernetics, Part A*, Vol.31 No.3, pp.179–186

Wang, Y. F. (2003) "On-demand forecasting of stock prices using a real-time predictor", *IEEE Transactions on Knowledge and Data Engineering*, Vol.15, No.4, pp.1033–1037

Huang, S. J, Huang, C. L.(2000) "Control of an inverted pendulum using grey prediction model". *IEEE Transactions on Industry Applications*, Vol.36, No.2, pp. 452–458.

Li, G, Ruhe, J, Emran, A. Al and Richter, M.M.(2007) "A flexible method for software effort estimation by analogy", *Empirical Software Engineering*, Vol.12, pp.65–106.

[doi:10.1007/s10664-006-7552-4]

Biogeography based Anticipatory Computing Framework for Intelligent Battle Field Planning

Lavika Goel[1], Daya Gupta[2]
[1,2] Department of Computer Engineering
Delhi Technological University (formerly Delhi College of Engineering), Delhi, India
goel_lavika@yahoo.co.in, dgupta@dce.ac.in

V.K. Panchal[3]
[3]Defense & Terrain Research Lab,
Defense & Research Development Organization (DRDO),
Metcalfe House, Delhi, India.
vkpans@ieee.org

Abstract— **It is possible to go and physically observe any situation under the area of our reach, but this is not so for the areas beyond our physical boundaries. For the purpose, a methodology inspired from nature is proposed using remote sensing inputs based on swarm intelligence for the anticipatory computation of the regions beyond our borders. The paper presents a nature inspired anticipatory computing framework for intelligent preparation of the battlefield. The algorithm predicts the most suitable destination for the enemy troops to position their forces, for which it uses the population based optimization technique i.e. Biogeography Based Optimization. The paper also introduces a new concept of efforts required in migration to a high HSI solution for optimization in BBO and hence also proposes an advanced optimization technique that was originally proposed by Dan Simon in December, 2008 [5]. Hence, the algorithm can be used to improve the Ant Colony Optimization (ACO) approach, since it lacks the ability to predict the destination and can only find a suitable path to the given destination, leading to coordination problems and target misidentification which can lead to severe casualties. The algorithm can be of major use for the commanders in the battlefield who have been using traditional decision making techniques of limited accuracy for predicting the destination.**

Keywords--battlefield; anticipatory computing; enemy base camps;biogeography based optimization; remote sensing.

I. INTRODUCTION

It is said that if you know about your enemy and about yourself, you will not be imperiled in a hundred battles; if you do not know about your enemies but do know yourself, you will win one and lose one; if you do not know about your enemies nor yourself, you will be imperiled in every single battle [1]. This quote along with the theory of biogeography proposed by Dan Simon in December, 2008 [5] was the driving force of this project. There are a few works available in this field of anticipatory computing for situation awareness, which we modify to suit our purpose of intelligent battlefield planning. Some of which are Disaster Situation Awareness [2], Terrorist Camps Detection [3] and Electronic Situation Awareness [4]. But as such no computing method is available for the prediction of enemy base station directly. The known available methods for the prediction of the enemy base camps are still the conventional methods employed by military which involve manual study of geography of the area and various other factors.

The prediction of enemy base camps was previously done through manual analysis by military personnels, we here use **Biogeography Based Optimization** (BBO) for determining the location of probable base stations of the enemy [6]. This paper is an implementation of an extended form of the first phase of the concept that we proposed earlier in the two-phase hybrid algorithm for predicting the deployment strategies of enemy troops in a military terrain application [6] and also extends the work done in [7].

Reason for the selection of this particular natural computing technique: The soft computing technique of swarm intelligence was preferred over other soft computing techniques because of its versatile and distributive nature. The BBO methodology of swarm intelligence was selected over other swarm intelligence methodologies like Ant Colony Optimization (ACO), Particle Swarm Optimization (PSO) and others because BBO allows many factors to be taken into consideration simultaneously. These factors are modeled as the SIVs in our proposed algorithm and contribute the habitat suitability index value (HSI) as detailed in sections II and III that follow.

The main aim of the work done in this paper is to enhance the decision capability which will enable the commanders in the battlefield to make better strategies to combat the actions of enemy. This all would be possible if we are able to determine the enemy's probable base stations thereby leading to intelligent battlefield planning. This paper introduces a methodology to determine the probable enemy base stations based on remote sensing data, using biogeography based optimization technique of swarm intelligence.

The work done in this paper aims at predicting the most probable enemy base station based on the geographic features of the area under consideration. Though geographic features are not the only source for determining the same, here we are only considering the remote sensing inputs that is, the satellite images of the area. The decisions over the suitability of a geographic feature for the probability of finding the enemy base station were taken on the basis of Expert Knowledge in Military domain. The methodology developed is tested on the regions of Alwar and Mussoorie.

Section II describes the biogeography based optimization, a swarm intelligence technique. Section III gives the terminology used in this paper with their respective meanings. Section IV elucidates on the functional architecture that was used for the proposed work. Section V provides the results of the experimental

978-1-4673-5116-4/12/$31.00 ©2012 IEEE

study conducted over the two regions. Finally section VI concludes the paper.

II. BIOGEOGRAPHY BASED OPTIMIZATION (BBO)

The soft computing technique to tackle the problem of predicting the enemy base station; selected in this project is Biogeography based optimization from the swarm intelligence techniques [6]. So going by the technique we consider the probable base stations as 'islands' [4]. These islands have a Habitat Suitability Index (HSI) determined on the basis of certain factors, here referred as Suitable Index Variables [4]. Following is the BBO Algorithm proposed by Dan Simon [5]:

1) Initialize the BBO parameters.
2) Initialize a random set of habitats, each habitat corresponding to a potential solution to the given problem.
3) For each habitat, map the HSI to the number of species, the immigration rate, and the emigration rate.
4) Probabilistically use immigration and emigration to modify each non-elite habitat, then recomputed each HSI.
5) For each habitat, update the probability of its species count using the (2). Then, mutate each non-elite habitat based on its probability, and recomputed each HSI.
6) Go to step (3) for the next iteration. This loop can be terminated after a predefined number of generations or after an acceptable problem solution has been found.

The algorithm proposed by Dan Simon [5] is used in its variant form to suit to the problem statement of this work.

III. TERMINOLOGY USED

A. Suitability Index Variables (SIVs)

In accordance with the problem statement and expert knowledge of military domain, the following are the Suitable Index Variables (SIV) taken into consideration for deciding the Habitat Suitability Index (HSI) for the base stations:

1. *Elevation of that area (C):* The more the elevation of that area is, more are the base stations on that area visible. Hence the enemy would like to have its base station located on such an area that is out of the line of sight of others.

2. *Evenness of the area (D):* The evenness of the area is important as a base station would not be possible on an uneven surface that has pits and peaks. There has to be certain evenness of surface in that area for the construction of a base station.

3. *Area covered under Slope (S)*: More is the vertical area covered; more is the probability of locating a base station there.

4. *Aspect (Direction/Angle) of area (A)*: More is the aspect vertically aligned towards enemy; more is the probability of having their base station there as it acts as a natural shield for them.

5. *Degree of urbanity (U)*: More the area under consideration is urban; less is the probability of having a base station there. As civilians are kept as away from military operations as possible.

6. *Degree of water (W)*: For a base station the degree of water of that area should be from low to medium, as little water could be of their help for their daily household work. But if it is in excess the probability of hiding their base station decreases.

7. *Degree of forest (F)*: The more is the degree of forest in that area, the more is the ease for them to situate their base station as that is the best location to maintain the anonymity of base station.

8. *Degree of barren land (B)*: The more is the barren land in the area, less are the chances of constructing a base station there as it would easily be detectable in satellite images.

9. *Degree of rocky land (R)*: Medium level of rocky land is the best for the construction of base station, but both the extremities are not suited for the construction of a base station.

B. Scales for SIVs

These SIVs were then determined for each area on a scale of one to five.

1) *Elevation of that area (C)*: The ranges were determined after calculating minimum, maximum, average, mode, median and mid of all DEM (Digital elevation model) values for the stretch of area taken under consideration.
2) *Evenness of the area (D)*: This was determined by considering the neighboring area of the small area taken into consideration at a time. If the neighboring area was of similar height than the area was considered even. The levels were decided by considering the percentage of area (around the area under consideration) that is even.
3) *Area covered under Slope (S)*: This was determined by scaling the area on the scale of four, depending on the percentage of area coming under the slope.
4) *Aspect (Direction/Angle) of area (A)*: This was determined by calculating the angle for each area and was then categorized into eight categories first that is zero to 45 degree first, 45 to 90 degrees second, 90 to 135 degrees third, 135 to 180 degrees fourth, 180 to 225 degrees fifth, 225 to 270 degrees sixth, 270 to 315 degrees seventh and 315 to 360 degrees eighth. Then using these categories we scale the aspect of an area on scale of five.
5) *Degree of urbanity (U)*: The area was scaled on a scale of one to five by determining if the area itself is urban or what percentage of the area around is urban.
6) *Degree of water (W):* The area was scaled on a scale of one to five by determining if the area itself is water or what percentage of the area around is water.
7) *Degree of forest (F):* The area was scaled on a scale of one to five by determining if the area itself is water or what percentage of the area around is forest.
8) *Degree of barren land (B):* The area was scaled on a scale of one to five by determining if the area itself is water or what percentage of the area around is barren land.

9) *Degree of rocky land (R):* The area was scaled on a scale of one to five by determining if the area itself is water or what percentage of the area around is rocky land.

C. Weights assigned to SIV : These SIVs are given weights from a scale of one to ten according to their importance in deciding the location of the base station. These weights are then utilized in determining the effort for migration from this base station to the ideal base station. This effort further helps in determining the selectivity factor of the base station.

D. Ideal Enemy Base Station: For Ideal Base Station the value of each SIV was taken, as per Expert Knowledge in Military Domain, on a scale of one to five.

E. Habitat Suitability Index: First HSI of the Ideal base station is calculated and then the HSI of all the other base stations are calculated using the following formula (the formula was generated by the interpretation of military data and the meaning of the Ideal base station in terms of its SIVs) [7]:

$$if\ A > 3$$
$$HSI = F + \left(\frac{C}{D}\right) + mod((6-R),4) + \left(\frac{A * S}{10}\right) - U - B - (W-2)$$
$$else$$
$$HSI = F + \left(\frac{C}{D}\right) + mod((6-R),4) - \left(\frac{A * S}{10}\right) - U - B - (W-2)$$

Where F, C, D, R, A, S, U, B and W are SIVs of the island whose HSI is being calculated.

F. Required Effort: We also define a variable called Effort which calculates the amount of effort required in migrating the SIV's during the computation for the selection of the most probable base station which enemy is likely to choose and in our case, this is the destination base station which the second phase of the algorithm takes as input. We calculate the effort for each base station.

$$Effort = \sum i\ (SIV_{ideal} - SIV_i) \times Weightage\ of\ SIV_i$$

where SIV_{ideal} is the ideal value of the i^{th} SIV and SIV_i is the actual value of the i^{th} SIV and i ranges from 1-13 (depending upon the no. of factors (SIVs) considered).

G. Ideal Base Station: We define the term Ideal Base station which is the base station which is the collection of ideal values of each SIV under consideration. The ideal SIV values are determined by a statistical data analysis and through the expert knowledge in the military domain. These values are then normalized so that they range on a scale of 1-5. The HSI calculated for this base station is also ideal and used for comparison in the algorithm.

H. Threshold HSI: is defined as the minimum HSI value which makes the input/candidate base station an eligible candidate for the further consideration in the algorithm for the choice of the destination base station. If the HSI value for the input base station is less than the threshold HSI, then the base station is rejected without proceeding further in the algorithm because this base station cannot be an enemy base station. The threshold HSI value was found to be one-third of the ideal base station's HSI value based on military inputs.

I. Selectivity Factor: We define the term Selectivity Factor which is the factor which determines the selectivity of the candidate base station to be chosen by the enemy as their base station. The base station which has the highest selectivity factor is most likely to be chosen by the enemy and hence at the end of the processing by our algorithm, this candidate base station will be the one which will be recommended by the system to be considered by the friendly troops as the enemy base station and the destination base station for the next phase of the algorithm to begin with. To calculate the selectivity factor, we subtract the threshold HSI value from the candidate base station's calculated HSI value and then divide it by the effort as below-

$$Selectivity\ Factor = (HSI_i - HSI_{Threshold}) / Effort$$

where 'i' ranges from 1 - 13.

J. Probable Enemy Base Station

The initial base station selection is based on the drainage pattern of the area under consideration. The drainage pattern helps in deciding the areas which would have higher denser canals (by canal it means a line in drainage map, by density of canal it means the number of the sub canals that join to form this canal), which actually implies the probability of finding the ground water at that place.

IV. BIOGEOGRAPHY BASED FUNCTIONAL ARCHITECTURE

This section presents the proposed algorithm for the biogeography based anticipatory computing framework. To solve the problem of finding the highly probable enemy base station through Bio-geographic based optimization the following functional architecture was modeled and used.

Input: Set of candidate base stations suitable for the enemy to position its forces and mount attack (derived based on the drainage pattern of the area under consideration).

Output: Best Feasible base station for the Enemy Troops as anticipated by the proposed algorithm.

A. Assumptions:

[1] Initially it is considered that there exists a Universal habitat consisting of all the candidate base stations.

[2] It has been assumed that the SIVs migrate between the Universal habitat, Feature habitat and the isolated habitat.
[3] All the candidate base stations are considered exactly once.
[4] At the completion of the algorithm we get a base station that is best suited as the destination base station.

B. Algorithm for predicting the location of enemy base station

(i) Get the set of suitable base stations for the enemy to position its forces.
No. of habitats = no. of candidate solutions to the problem.
(ii) Put the set of the above base stations in the Universal Habitat.
(iii) Consider an isolated habitat with zero SIVs. This habitat represents the state of no solution in the initial stage of the algorithm.
(iv) Define HSI, Smax, immigration rate (λ) and emigration rate (μ) for each of the base stations in the universal habitat.
(v) Construct a standard habitat which is analogous to the base station with ideal characteristics that are best suited for the enemy troops. This habitat is called the feature habitat and consists of the collection of Standard SIVs (or ideal SIVs) on the basis of historic and intelligence data obtained through a statistical survey of the area, the parameters (SIVs) of which were defined in section II before. The feature Habitat is used for comparison with the candidate base stations in the Universal Habitat.
(vi) Calculate the HSI of the feature habitat based on its SIVs and hence calculate the Ideal HSI value (SIV_{ideal}) .
(vii) Calculate the Threshold HSI value by taking one-third of the ideal HSI value (based on military inputs).
(viii) (a) Now calculate the HSI for the candidate base station based on its SIVs as given by the HSI formula derived in section II applying the corresponding HSI formula depending upon the value of 'A' where A is the Aspect (Direction/Angle) of the area under consideration. If A >3, then the first formula is applicable else the second one.

(b) Compare the HSI of the habitat (candidate base station) with the threshold HSI. The threshold HSI denotes that the candidate base stations of the Universal habitat can only be made feature habitat after migration if their HSI falls within this range i.e. it is greater than the threshold HSI).

(i) If the HSI is greater than the threshold HSI value, then find out the SIVs to be migrated and the effort required for migration using the weights assigned to those SIVs (on a scale of 1-5). Probabilistically use immigration and emigration to modify the non elite base station by immigrating the ideal SIVs of the feature habitat that match with the SIVs of the input base station of the universal habitat to the universal habitat & emigrating the SIVs of the input base station that do not match with the ideal SIVs of the feature habitat from the universal habitat to the isolated habitat. This is the effort required in the migration of SIVs to and from the universal habitat which can be calculated from the formula derived in section II.

(ii) If the HSI is less than the threshold, transfer the SIVs of this base station to isolated habitat. This base station will not be considered further and is removed from the Universal habitat.
(ix) Repeat the step (viii) for each of the candidate base stations in the Universal Habitat.
(x) Calculate the selectivity factor for the remaining base stations in the Universal Habitat using the formula derived in section II. These are the set of left over base stations, one among which will be the most likely enemy base station and the output of the first phase of the 2-phase recommender system algorithm.
(xi) Next, compare the selectivity factor of all the base stations. The base station with the highest selectivity factor is the most suitable base station for the enemy troops for their deployment and this will be the destination base station for the friendly troops to mount attack on.

The proposed algorithm can be summarized as below in figure 1.

Step 1. Input all the candidate base stations to be considered in the universal habitat. Also input the isolated habitat and the feature habitat.
Step 2. Calculate the HSI for each of the candidate base station using the corresponding HSI formula depending upon whether the value of A (Aspect/ Direction) >3 or not.
Step 3. Calculate the HSI of the feature habitat and the threshold HSI by taking $1/3^{rd}$ of the ideal HSI value
i.e. $1/3 \times \mathbf{HSI}_{\mathbf{ideal}}$
Step 4. Compare the HSI of the input base station with the ideal HSI.
Step 5. If the $HSI_{input} > HSI_{Threshold}$,
then
Find out the SIVs to be migrated and the effort required for migration using the weights assigned to those SIVs.
else
Transfer the SIVs of this base station to the isolated habitat i.e. remove this base station from the universal habitat.
Step 6. Repeat steps 2-5 for each of the candidate base stations in the Universal Habitat.
Step 7. Calculate the selectivity factor for each of the remaining base stations in the Universal Habitat.
Step 8. Compare the selectivity factor of all the base stations. The base station with the highest selectivity factor is the destination enemy base station.

Figure 1: Algorithm for Biogeography based anticipatory computation

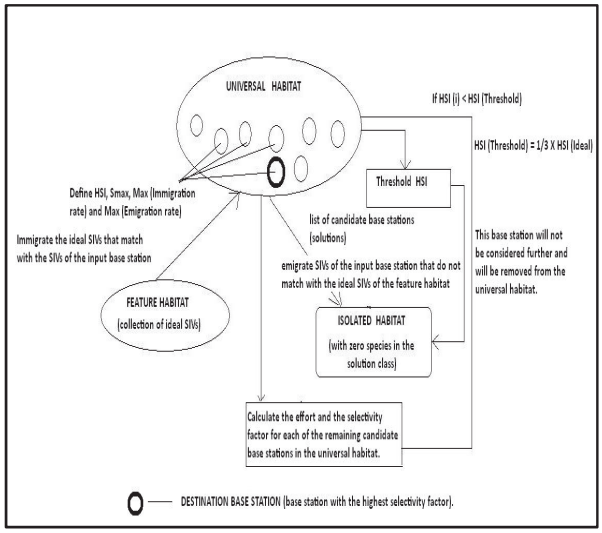

Figure 2: Biogeography based functional architecture.

The modified BBO Technique for selecting the best destination for the enemy base station is shown in figure 2.

V. EXPERIMENTAL STUDY

For the purpose of experiment Alwar region (India) and Mussoorie region (India) was selected as it has all the geographic features. The results obtained after applying the work proposed in this paper are as followed:

A. Alwar region in Rajasthan

HSI for the Ideal base station is taken as 13. We have considered 12 base stations and fed their SIV values which are given by the expert to our algorithm. From the table I, it can be seen that the HSI values of the base stations 2,3,4,6,7,8,10 and 12 are 3.066667, 1.65, 2.55, 2.65, 1.75, 3.25, 2.55 and 3.067 respectively which is less than the threshold HSI of 4.000000, hence these base stations are rejected and no further calculations are made for these base stations. The effort and selectivity factors are calculated for the remaining base stations. The selectivity factors for the base stations 1, 5, 9, 11 are 0.0357, 0.059, 0.0051, 0.1054. From these values, the normalized selectivity factor values are calculated with the highest selectivity factor value taken as one as shown in table I. The normalized selectivity factors are 0.3395, 0.5598, 0.0493 and 1.0000 respectively. Hence, the base stations are classified as in table II below.

B. Mussourie region in Himachal Pradesh

HSI for the Ideal base Station is taken as 13. We consider 12 base stations whose SIV values generated by the expert knowledge are taken as input to our algorithm. From the table III, it can be seen that the HSI values of the base stations 2 and 6 are 1.55 and -0.6 respectively which is less than the threshold HSI of 4.000000, hence these base stations are rejected and no further calculations are made for these base stations. The effort and selectivity factors are calculated for the remaining base stations. The selectivity factors for the base stations 1, 3, 4, 5, 7, 8, 9, 10, 11 and 12 are 0.021, 0.051, 0.034, 0.064, 0.03, 0.06, 0.0363, 0.0187, 0.0161 and 0.13 and the normalized values are 0.1623, 0.3962, 0.2657, 0.4946, 0.2339, 0.4615, 0.2792, 0.1439, 0.1241 and 1.0000. Hence, the base stations are classified as in table IV below.

TABLE I: HSI, EFFORT AND SELECTIVITY FACTOR CALCULATIONS FOR ALWAR

Base station 'n'	D	C	S	A	U	W	R	B	F	HSI	Effort	Selectivity Factor	Normalized Selectivity Factor
1	3	5	1	2	1	1	1	2	5	5.47	41	0.03578	0.3395
2	3	5	1	4	1	1	1	5	5	3.07	∞	0	0
3	4	5	2	3	1	1	5	1	1	1.65	∞	0	0
4	4	3	2	4	1	1	5	1	1	2.55	∞	0	0
5	3	5	1	4	1	1	1	3	5	5.07	18	0.0590	0.5598
6	4	5	1	4	1	1	5	1	1	2.65	∞	0	0
7	4	3	2	5	1	1	5	2	1	1.75	∞	0	0
8	4	5	2	5	1	1	5	1	1	3.25	∞	0	0
9	3	5	1	4	1	1	1	4	5	4.07	13	0.0052	0.0493
10	4	3	2	4	1	1	5	1	1	2.55	∞	0	0
11	2	5	1	4	1	1	1	1	5	7.90	37	0.1054	1.0000
12	3	5	1	4	1	1	5	1	1	3.07	∞	0	0

TABLE II: FINAL CATEGORIZATION OF THE PROBABLE ENEMY BASE STATIONS

Base station	Category
11	Most probable base station
1,5	Highly Probable base stations
9	Least probable base station

TABLE III: HSI, EFFORT AND SELECTIVITY FACTOR CALCULATIONS FOR MUSSOORIE

Base station 'n'	D	C	S	A	U	W	R	B	F	HSI	Effort	Selectivity Factor	Normalized Selectivity Factor
1	5	2	3	2	1	1	1	1	5	4.8	38	0.0211	0.1623
2	4	3	2	4	1	1	3	5	2	1.55	∞	0	0
3	1	3	3	2	1	1	1	1	5	7.4	66	0.0515	0.3962
4	2	3	2	3	1	1	1	1	5	5.9	55	0.03454	0.2657
5	5	5	1	2	1	1	1	1	5	5.8	28	0.0643	0.4946
6	5	2	2	5	1	1	1	5	2	-0.6	∞	0	0
7	5	3	2	1	1	1	1	1	5	5.4	46	0.0304	0.2339
8	5	2	2	4	1	1	2	1	5	5.2	20	0.06	0.4615
9	1	3	2	1	1	1	1	2	5	6.8	77	0.0363	0.2792
10	1	1	3	1	1	1	1	1	5	5.7	91	0.0187	0.1439
11	5	1	2	1	1	1	1	1	5	5	62	0.01613	0.1241
12	5	2	3	4	1	1	1	1	5	6.6	20	0.13	1.0000

TABLE IV: FINAL CATEGORIZATION OF THE PROBABLE ENEMY BASE STATIONS

Base station	Category
12	Most probable base station
3,5,8	Highly Probable base stations
1,4,7,9,10,11	Least probable base stations

VI. CONCLUSION AND FUTURE SCOPE

Based on the results of the proposed algorithm, the commanders in the war theatre will have an increased battlefield awareness since they can now anticipate the destined enemy base station. This will be of prime importance since in the modern warfare strategies, the ability of an army to position its troops at an effective geographical location (having predicted the location of the enemy base station), in the shortest possible time, will significantly gain a tactical advantage over the enemy and prove to be the deciding factor for winning. Thus the proposed system is very well suited for anticipating the next action of the enemy – to anticipate the enemy's deployment strategies and can replace the currently employed traditional decision making Techniques.

The methodology presented in the paper based on biogeography based optimization is applicable to both the direct satellite images as well as the google earth images. The results, as specified gives three categories the most likely, the highly likely and the less likely enemy's probable base stations. Couple of factors such as weapon capability and skills of the enemy are certain things which require human interpretation as it cannot be judged by the satellite images. Also the surprise factor contributes negatively to the comfort factor (HSI) in other words we can say these are inversely proportional to each other. This would further help in determining additional information aiding in better anticipation hence that could be of great help in designing of the war / battlefield strategies. This information could be:

- Enemy's camping areas.
- Our desirable targets, for e.g. enemy's resource areas, enemy's connectivity areas etc.
- Desirable routes for the enemy.
- Methodology or way to breach the enemy's region.

Also we can sample the above SIVs round the year to generate very precise and accurate results. This would also enable us to detect any changes if there are, hence giving us the capability of any kind of movement detection thereby enhancing the anticipatory capabilities.

REFERENCES

[1] Sun Tzu, "The Art of War, a chinese military treatise", Chapter 3, 6th century BC.

[2] Rajeev Kumar Jaiswal, Saumitra Mukherjee, Kumaran D. Raju, Rajesh Saxena, "Forest Fire Risk Zone Mapping from Satellite Imagery and GIS" , International Journal of Applied Earth Observation and Geoinformation, Elsevier Publications, vol. 4, pp. 1-10, 2002.

[3] Yasar Guneri Sahin and Tuncay Ercan , "Detection of Hidden Hostile/Terrorist Groups in Harsh Territories by Using Animals as Mobile Biological Sensors, Sensors 2008, vol. 8, pp. 4365-4383; DOI: 10.3390/s8074365, 2008.

[4] Patrick Chisan Hew, "The Generation of Situational Awareness within Autonomous Systems – A Near to Mid Term Study", Issues by Defence Systems Analysis Division Information Sciences Laboratory DSTO-GD-0467, DSTO Information Sciences Laboratory, 2006.

[5] Simon, D. , "Biogeography-based Optimization" in IEEE Transactions on Evolutionary Computation, vol. 12, No.6, IEEE Computer Society Press., pp. 702-713, 2008.

[6] Lavika Goel, V.K. Panchal, Daya Gupta, Rajiv Bhola, "Hybrid ACO-BBO Approach for predicting the Deployment Strategies of enemy troops in a military Terrain Application", in 4th International MultiConference on Intelligent Systems & Nanotechnology (IISN), 2010.

[7] Sakshi Arora, " Biogeography based Battlefield Situation Awareness", Master of Engineering (M.E.) Thesis submitted to Delhi College of Engineering (now Delhi Technological University), 2010.

Broadband over Power Lines Implementation Roadmap for a Smarter Grid: A case study for Indian Power Sector

Mini S. Thomas, *Senior Member, IEEE,* Vinay Kumar Chandna, *Senior Member, IEEE* and Seema Arora, *Student Member, IEEE*

***Abstract*—This paper makes an effort to present the major concerns with broadband over power lines technology and implementation roadmap for making the grid smarter. The paper also strives to emphasize upon the need to prepare ourselves for a timed roadmap for this technology which requires no new cabling or infrastructure, instead using the long established power grid provided by electrical companies. The authors have tried to gain attention of the readers, utilities, regulatories and all involved in power sector, IT sector and communication sector to look and analyse the potential of this technology for the future of smart grids. The objective of this paper is also to highlight on the technology in terms of its salient features, working, drawbacks, deployments and future challenges associated in the implementation plans. The suitability of BPL as a smart grid technology has been simulated and studied for an indoor feeder and the results are analyzed.**

Keywords*—*Roadmap; Broadband over power line; Smart grid; Demand Response.

I. INTRODUCTION

Power sector experts across the world have put forward the smart grid development plans to curb the ever-increasing pressures on resources and environment, and the rising need to solve the issues pertaining to distributed energy grid connections, while building a more secure, reliable, environment friendly and economical power system, many. The smart grid has the potential to revolutionise the transmission, distribution and conservation of energy. Smart grid implementation requires many new technologies, such as grid control technology, information technology and communication technology covering power generation, transmission, substations, power distribution, automation at all levels and information of all aspects of power systems. The smart grid promises to bring unprecedented opportunities for both utilities and consumers [1].

Mini S.Thomas is with the Faculty of Engg. & Tech., Jamia Millia Islamia, New Delhi., India 110025 (e-mail: mini@ieee.org).
V.K. Chandna is with the Department of Electrical Engineering, ITS College of Engg., Greater Noida, India 201306 (e-mail:vinaychandna@yahoo.co.in).
S.Arora is Research Scholar in the Department of Electrical Engineering, Jamia Millia Islamia, New Delhi., India 110025 (e-mail: aroraseema1@gmail.com).

Smart grids intend to improve transparency, safety, security, increase reliability as well as efficiency. Broadband over Power Lines (BPL) can be exploited as one of the key technologies for making the country electrically smarter and reliable in terms of flow of power and information. A compelling reason for using BPL is the recent impetus in modernizing the traditional power grids through information highway dedicated to the management of energy transmission and distribution or the smart grid. It has been understood and revealed through work carried out in the modernization of the aging grids that the smart grid needs to be supported by a heterogeneous set of networking technologies, as no single solution fits all scenarios. One of the competitors in communication network technologies is BPL which is hitting the competitive market of broad band internet services in international telecom environment. In addition, value added services like internet, voice, video applications etc. can also be provided by BPL. All the utilities need to work on is to overlay a communications network layer on the already existing electrical infrastructure. BPL typically uses the 1-30 MHz frequency range to deliver the digital data in comparison to the 50 Hz frequency which is used to transmit electrical power [2]. The paper presents an overview of the BPL business, role of BPL in smart grid BPL deployments across the world and an implementation roadmap for India. The paper also presents simulation results of the BPL under varying indoor wiring characteristics such as line lengths and number of cascaded sections in Section VI.

II. BPL BUSINESS

According to an analysis carried out by Anderson in 2010, the estimated installation cost of BPL is $1000 per home, but it offers the capability to reach any home with electrical service [3]. This ability enables BPL technology in becoming more popular amongst other competitor technologies. Also, the cost evaluations depict that BPL is comparatively less expensive than an internet network as the transmission system requires a smaller investment [4]. Fig.1 shows a typical architecture of a BPL system which is a cost-effective telecommunication medium over existing power line grids without laying new cables.

978-1-4673-0934-9/12/$31.00 ©2012 IEEE

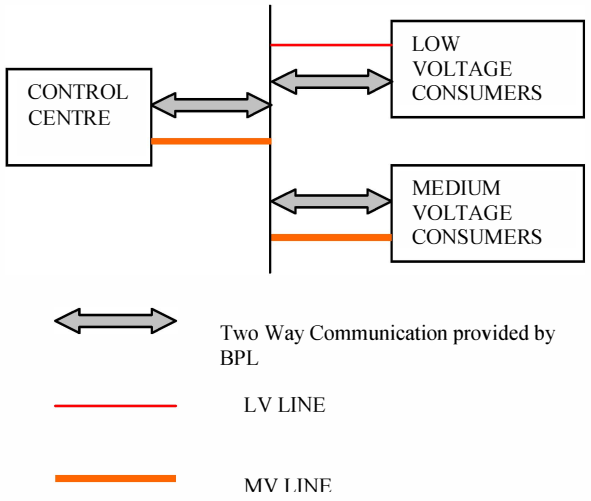

Fig.1. Typical Architecture of a BPL system.

Power and data overlaying in the same wires is nothing new as the phone companies have been powering telephones for last so many years with central office switch over the same wires that carry voice. The IEEE 802.3af PoE (power over Ethernet) standard has made it possible to provide more power across local area network wiring for voice over Internet Protocol phones and wireless access points. BPL is also similar, but with more technical and regulatory issues. The people who will succeed in the BPL business will not be from the public-utility services, but the telecommunication planners and those who operate the internet services. Consequently, the cost of installing all the equipment in homes, small offices, labs and in buildings, designated here as customer premises equipment (CPE), is a critical factor in the BPL business [2]. With the CPE cost continually and incrementally decreasing, there will soon be a point at which it will compete with other technologies, such as DSL or Wi-Fi Access Point.

BPL typically has limited bandwidth because the existing grid infrastructure was not designed to transfer digital data, but according to Schneider, speeds of 5Mbps are achievable in distances less than 1 kilometer [5]. As per Hrasnica et al [6], in the outdoor MV and LV supply networks, the data rates beyond 2 Mbps are provided by broadband over power lines and upto 12 Mbps in the in-home area. Those involved in manufacturing of BPL equipment have developed product prototypes providing data rates upto 40 Mbps. Although increased distances imply reduced speeds that BPL can achieve, but using additional devices can help solve this issue. The communications over power lines is specified in a European standard CENELEC EN 50065.

BPL technology can prove to be one of the key technologies in creating an automated distribution system since it is capable of providing two way flow of information i.e. from the customer end to the control centre or vice versa. This technology could allow utilities to effectively monitor and hence manage power, perform automated metering operations and to coordinate remotely the use of all distribution network components in a real time mode as a distribution engineering tool [7].

III. UBIQUITOUS ELECTRICAL INFRASTRUCTURE

High Voltage (HV), Medium Voltage (MV) and Low Voltage (LV) supply networks have been in use for internal data communication of electrical utilities and for realization of remote measuring and control tasks as well. Realization of BPL services can be used in a variety of ways on an electric utility distribution system [6].

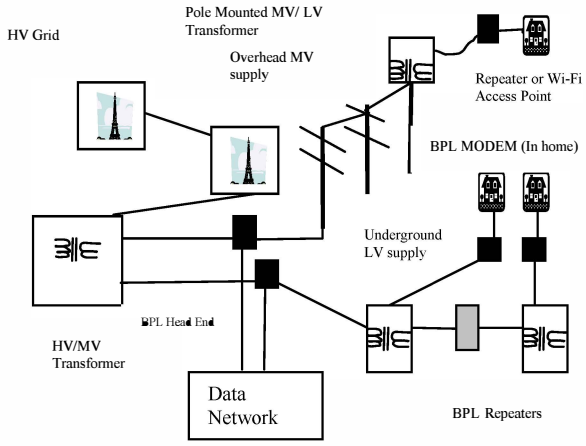

Fig.2. Electrical Infrastructure of a BPL system.

Fig.2 describes the electrical infrastructure of a smart distribution system. The three basic approaches to BPL implementation are End to End BPL systems, Hybrid BPL and Backhaul BPL systems. BPL transmits high frequency data signals to household/or business subscribers. Customers need to install a BPL modem that plugs into an ordinary electrical wall outlet to make use of BPL service, and pay a subscription fee similar to that paid for other types of such services. Fig.3 shows typical electrical infrastructure and BPL modem to be installed inside the customer premises.

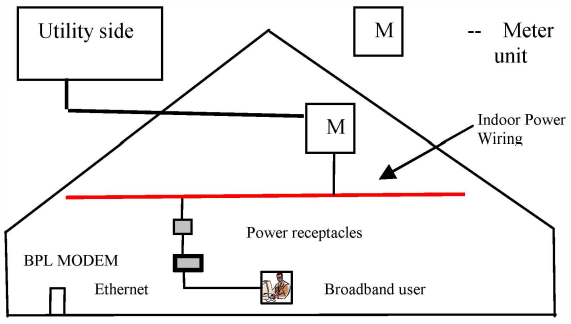

Fig.3. Electrical Infrastructure and BPL MODEM at Customer Premises.

IV. ROLE OF BPL IN SMART GRIDS

The world of BPL can be divided, based upon the network topology, into three main types: high-voltage (HV) BPL, medium-voltage (MV) BPL, and low-voltage (LV) BPL. Over the last few years, HVBPL and MVBPL have been oriented to teleprotection and telecontrol tasks, whereas LVBPL has attracted great expectations since its wideband capabilities have made this technology a suitable choice for last-mile access and in-home communications. Moreover, LV-BPL also includes a utility-oriented low-frequency and low-speed applications, such as automatic meter reading (AMR), load distribution, dynamic billing, and so on [8]. The role of BPL in Smart Grid is being discussed further.

A. Demand Response (DR) Management

Unidirectional by nature, the traditional Indian grids were designed to distribute power, not to manage a dynamic interconnected network of energy supply and demand. This inadequacy could possibly become hindrance to the country's progress. Infact, in India, the distribution network system is extraordinarily large and hence serious economical constraints exist in terms of heavy investments to be made for laying copper or installing satellite as a mode of final broadband transmission. Giving priority to BPL would be worthwhile, while addressing other pertinent issues. Since the consumers are having access to the electricity markets through the Internet that comes over the same wires that provide electricity to them, it gives advantages of easy market information access and real-time price signal determinations, all in an integrated system, which is necessary for an efficient and flexible Demand Response (DR) operation.

B. Extraordinarily Large Data Volume

The increased data volume being generated within the transmission and distribution network for monitoring and control has also led to the rising need for a fundamental driver technology for flow of two way data for the emergence of a smarter grid. The realization of Automated Metering Infrastructure (AMI), the integration of Renewable Energy Sources and other DER, and the new goals for improving distribution automation will produce drastic energy efficient changes in the power networks. With the increased emphasis on energy efficiency, the current electrical grid is in need of a robust communication network. The communication infrastructure may rely on three technologies: 4G wireless communications, fiber optics, and/or BPL to reliably transmit low latency data. The smart grid needs a communication system to handle two-way communication in order to share energy-related data amongst utilities and end-users [8 and 9].

Broadband over power lines may provide this service. The power lines are however not designed to carry information, rather they are meant to carry low frequency electrical signals. Thus the distances that can be covered, as well as the data rates that can be practically achieved are limited. To make transmission of signals over longer distances possible, it is necessary to apply a repeater technique as shown in fig. 4. Undoubtedly, the application of repeaters results in increased infrastructural and installation costs [4, 7, 8 and 9].

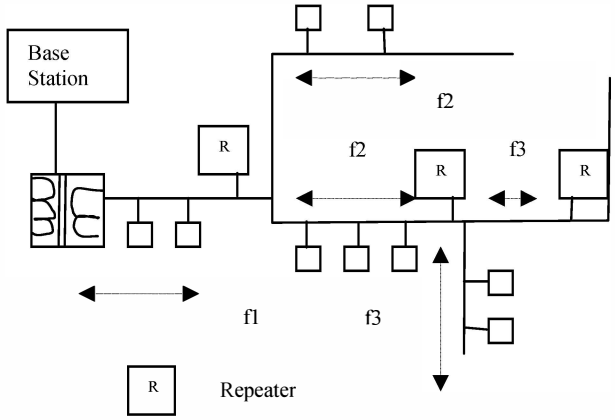

Fig.4. BPL Repeaters Technique

C. Other Advantages of BPL Deployments

- No regeneration of data;
- Utilizes the already Existing (Largest) Infrastructure in the world;
- Expediting the new resource integration;
- Helps in identifying potential opportunities and threats;
- Aids in finding rectifying solutions to such threats;
- Supporting high-level planning and control;
- Emphasizing understanding or close knowledge gaps;
- Providing support for decision making, resource allocation and risk management;
- No changes in household wiring;
- Broadband connection in every socket in the house.
- Plug and Play installation;
- Enables Alarm, Meter reading;
- Remote monitoring and management of household devices;
- Remote Maintenance, Automation;
- E-services (Web Hosting, Email, ASP);
- Ubiquitous service of audio/video data.

V. BPL DEPLOYMENTS

A number of experts in many countries including USA, Australia, Austria, China, Finland, Hong Kong, Hungary, Ireland, Italy, Korea, Japan, Netherlands, Poland, and Switzerland are currently studying BPL technology or have permitted equipment trials. The outcomes have shown mixed results. While some administrations decided to ban BPL systems, there are others who have allowed deployment under various conditions.

While there are plenty of trials ongoing in the U.S., Manassas is reported to be the first to deploy a city-wide BPL system. The positive results revealed for the city of Manassas where it has been estimated that $4.5 million over the life of the 10-year contract with Prospect Street Broadband can be generated, and thus the shift toward BPL hasn't seen many delays. The system is utilizing technology from Main.net, a BPL provider that offers related utility connectivity to 40 power utilities in more than 20 countries. Opponents to such systems argue that broadband over power-line sends wideband radio signals over poorly shielded wires not particularly designed with high-speed internet. The result is that these 2 to 80 MHz signals are broadcast into neighborhoods as if from antennas from every participating power-line, interfering with radio communications and polluting HF bands. The resulting noise, occasionally 10,000 times higher than acceptable levels in some world-wide trials, has in some cases been enough to disable 20-meter monobanders on high-rise buildings.

In India, IIIT Allahabad has undertaken a project in co-operation with Corinex Communications, Canada to implement a prototype of BPL for University campus and nearby villages. The objective of this research and development project is to develop BPL technology to suit Indian conditions so that the technology can be later deployed for large scale use. The technology will deliver multi-fold benefits to India when it connects villages throughout the country to the internet. The technology intends to provide access to multiple forms of communication including the World Wide Web and Voice over Internet Protocol (VoIP). This technology is being used successfully on IIIT-A Jhalwa campus with active support of partner Maple Leaf India. This will allow showcasing suitability of BPL technology for mass deployment opportunities across India.

The Ministry of Information Technology, Government of India also requested the power utilities to carry out BPL pilot projects jointly with educational institutions so as to analyze whether the technology is suitable in the country. Accordingly a pilot project was undertaken by CESC jointly with Bengal Engineering and Science University (BESU) to evaluate the technical suitability of providing broadband communication services through CESC's underground and overhead LV power lines as a last mile solution. In the pilot project, the equipment is capable of providing 200 Mbps speed at physical layer. It operates in the frequency range of 2 to 34 MHz. [10]. The current generation of BPL technologies has proven in electric utilities controlled circumstances and in field trials and small pilot programs. The key issue is whether BPL can and will perform acceptably in full scale commercial deployment. BPL equipment may cause interference with or be adversely affected by other uses of the spectrum. Without a large-scale commercial deployment, it is not possible to know what the radio interference issues will be with high penetrations in densely populated areas. BPL is a shared bandwidth technology. It may have too little bandwidth to provide acceptable speed to all subscribers in densely populated areas with a lot of subscribers. On sparsely populated rural feeders, many signal regenerators will have to operate reliably in series. A typical rural feeder that is 20 miles in length would require anywhere from 30 to 100 signal regenerators depending upon the feeder characteristics and the BPL vendor. There has been no lab or field experience with this degree of cascading. Further, outages of any one of the regenerators will intermit service to all downstream subscribers. None of the BPL vendors have completed a large scale commercial deployment. It remains to be seen whether any or all of the vendors will succeed in designing, producing and maintaining standards of equipment (acceptable quality, durability, affordability and ease of use) [8, 9 and 11]. The key advantages associated with the deployment of BPL are new source of revenue generation, enabling utilities to gather data and utilize utility infrastructure. There are disadvantages also in the technology usage which mainly include uncertainty in economic model, regulatory issues and inadequate roadmaps and technology readiness. The few vendors in the BPL field are depicted in Table I.

TABLE I

SERVICE AND VENDORS IN THE FIELD

Service	Vendors
Integrated BPL solution providers	Grindline Communications, Current Communications, IBEC (International Broadband Electric Comm. Inc.), Utility.net
BPL equipment suppliers	Ambient, Amperion, Corinex, Corridor System, Current Technologies, MainNet Communications
BPL IC chip makers	DS2, Intellon

VI. IMPLEMENTATION ROADMAP

The energy sector is now using technology roadmaps. The technology roadmaps for BPL is not available for energy people, vendors and regulatory bodies involved in development and deployment of BPL till the CPE, especially in a country like India which could be a potential sector for BPL market. The method of road-mapping consists of time usage in connection with business market, Product service, technology readiness and standards availability [4]. The good news for the people looking to invest in India's electrical and smart grid sector is that the government has already structured a plan to meet the challenges. By uniting the plans decided by Indian central government with the various states' governments, India has laid out an ambitious effort to modernize their grid over the next 10 years. The Ministry of Power, Indian Government, has laid six guiding principles for the implementation of Smart Grid in India.

1. The smart grid should be based on an Indian model and developed indigenously.
2. Focuses on power shortage problems.
3. Addresses theft prevention and loss reduction.
4. Provides power in rural areas.

5. Development of alternative sources of power.
6. It is affordable and enables sustainable production of power.

The key technological issues which act as impediments in governing power line networking to achieve high-speed communication and to the large scale deployment of BPL are interoperability, RFI related issues with other users of the spectrum, signal attenuation, signal boosting and repeater design. The time varying frequency response characteristics of the power channel, power line noise, power line network impedance are the other key issues in BPL as a key technology for smart grid plans. The telecommunication regulations for permitting communication outside the amplitude modulation frequency band, modems to modulate the carrier frequency of between 50 and 500 KHz using frequency shift keying or amplitude shift keying require constant tuning the use of Wi-Fi versus the low-voltage (LV) power line, and the development of IP-addressable electric meters, security issues in adoption of internet services and lack of coordination among communication service providers and power service also are responsible for delayed acceptance of BPL [11]. We have focused on two issues and the suitability of BPL as a smart grid technology has been simulated and studied for an indoor feeder and the results are analyzed.

A. Channel Modeling

BPL technology can offer a convenient and inexpensive medium for data transmission; however this technology still faces a difficult challenge: the channel modeling. Although efforts have been devoted to determine precise and universally agreed channel models for the power line as channel, there is not any widely accepted model [12, 13, 14 and 15].

B. Topology Dependence

The topology of the low voltage distribution network differs from place to place, depending on various factors viz. network location, subscriber density, characteristics of load, nature of stubs etc. It is very much necessary to know the consequences of these varying topologies on the performance of the indoor BPL system. The power line network differs in topology (radial/mesh/hybrid), structure, and physical properties from conventional media used for communicating digital data such as twisted pair, coaxial, or fiber-optic cables. Therefore BPL systems offer rather hostile properties [16 and 17]. The focus of the simulation is to achieve the transfer function of a radial indoor power line feeder using Scattering matrix method. An indoor feeder can be conveniently represented as an infinite series of cascaded identical two port sections, each representing an infinitely small section of transmission line. The two intrinsic line parameters which dominate the wave behavior along the power line are Zc and γ. They describe the transmission line behavior and are expressed as:

$$\gamma = \alpha + j\,\beta = \sqrt{((R + j\omega L)(G + j\omega C))} \quad (1)$$

$$Zc = \sqrt{((R + j\omega L) / (G + j\omega C))} \quad (2)$$

R, L, G and C are the distributed parameters per unit line length for two wire lines which are commonly used for indoor cabling in homes. The model is capable of determining the line characteristics under varying network topologies as they take in account the cable characteristics such as line lengths and number of cascaded sections. The results of simulation are given in Table II, Table III, Table IV and Table V.

TABLE II

SIMULATION RESULTS FOR CHANGING LINE LENGTHS OF INDOOR WIRING

Length	Signal Attenuation (dB)	Freq (MHz)	Phase Distortion (radians)	Freq (MHz)
15 m	0.069297	13.9968	0.092612	24.9865
30 m	11.386	13.9968	0.58413	24.9865

TABLE III

SIMULATION RESULTS FOR DIFFERENT CASCADED SECTIONS OF INDOOR WIRING (AT A FREQUENCY OF 5MHZ)

Number of Cascaded Sections	Length	Signal Attenuation (dB)	Phase Distortion (radians)
No section	15 m	1.5572	0.5346
Two Sections	7.5m each	0.26824	0.23293
Three Sections	5m each	8.6693	1.1855

TABLE IV

SIMULATION RESULTS FOR DIFFERENT CASCADED SECTIONS OF INDOOR WIRING (AT A FREQUENCY OF 16MHZ)

Number of Cascaded Sections	Length	Signal Attenuation (dB)	Phase Distortion (radians)
No section	15 m	1.1756	0.30328
Two Sections	7.5m each	0.13391	0.16383
Three Sections	5m each	36.787	1.473

The simulations are done in a frequency range of 0-30 MHz using MATLAB. The results (Table II) reveal that increased line lengths cause an increased attenuation in signal strength at a typical frequency of 13.9968 MHz. The phase distortion is also higher with increased line length as observed from Table II when the data is observed at a frequency of 24.9865 MHz. The similar results are observed at other frequencies as well. The results of cascaded sections are

tabulated in Table III, Table IV and Table V for frequencies of 5 MHz, 16 MHz and 22 MHz respectively. The attenuation and distortion in signals are section dependent and also change with frequency of signal.

TABLE V

SIMULATION RESULTS FOR DIFFERENT CASCADED SECTIONS OF INDOOR WIRING (AT A FREQUENCY OF 22MHZ)

Number of Cascaded Sections	Length	Signal Attenuation (dB)	Phase Distortion (radians)
No section	15 m	0.017417	0.0093
Two Sections	7.5m each	12.8699	1.1534
Three Sections	5m each	19.3498	1.4434

VII. CONCLUSION

The results of the simulation reveal that increased line lengths cause an increased attenuation in signal strength and phase distortion as well. The attenuation and distortion in signals are dependent on the number of sections and also change with frequency of signal. The results however strengthen the fact that at some selected frequencies the attenuation and distortion are very low and hence such frequencies can suitably be exploited for digital data transmission on existing power lines.

In a country like India where broadband penetration is extremely low and the costs of laying down copper cable or providing short haul satellite for furnishing broadband for its final leg of journey is very high, employing broadband over power lines holds a great promise. The issues related to modeling of channel, electromagnetic interference etc need to be addressed and resolved for successful implementation of the technology. The deployment of BPL service in semi rural areas that contain clusters of homes/ banks/gram udyog offices / entrepreneur units will provide the best opportunity for the initial deployment of BPL by the year 2013, because such areas are not served either by DSL or by cable modem providers. Later, BPL providers could expand service to more rural areas and by 2015 have an installed base of customers at rural level and sub urban level. It can also be used to assist utilities by adding smartness to the electric grids thereby improving efficiency in activities such as energy management, power outage notification and automated meter reading. Besides, low maintenance costs and lesser installation time make BPL a worth technology for increasing broad band penetration and making the grid smarter.

REFERENCES

[1] Kwon, B. (2009), "Broadband over Power Lines (BPL): Developments and Policy Issues", OECD Digital Economy Papers, No. 157, OECD Publishing.

[2] Tsiropoulos, G.I., Sarafi, A.M., Cottis, P.G., "Wireless-broadband over power lines networks: A promising broadband solution in rural areas", *PowerTech, 2009, IEEE Bucharest,* pp.1-6.

[3] Anderson, M., "WiMax for smart grids",*Spectrum, IEEE ,July 2010.*

[4] Choomon, Karnchana1; Leeprechanon, Nopporn1; Laosirihongthong, Tritos2, "A review of literature on technology roadmapping: a case study of Power Line Communication (PLC)", International Journal of Foresight and Innovation Policy, Vol. 5, No. 4, June 2009 , pp. 300-313(14).

[5] David Schneider, "Is This the Moment for Broadband Over Power Lines", IEEE Spectrum,July 2009.

[6] Hrasnica H., Haidine A. and Lehnert R. Broadband Power Line Communication Networks, 1st Edition: John Wiley, 2009.

[7] Ce Zheng and Mladen Kezunovic,"Integrated Solutions for Ubiquitous use of Electricity and Cyber Services", IEEE Power Symp., 2008, pp.1-7.

[8] Sood, V.K., Fischer, D., Eklund, J.M., Brown, T., "Developing a communication infrastructure for the Smart Grid", Electrical Power & Energy Conference (EPEC), 2009), pp.1-7.

[9] Aggarwal, A., Kunta, S., Verma, P.K., "A proposed communications infrastructure for the smart grid", IEEE Innovative Smart Grid Technologies (ISGT) Conf. 2010, pp.1-5.

[10] Pabitra Kumar Ray and Aveek Hazra,"Broadband Powerline Communication an Indian Experience, 2011IEEE International symposium on Power Line communications and its Applications, pp.364-369.

[11] http://www.tec.gov.in/studypaper/BPL

[12] D. Anastasiadou, T. Antonakopoulos, "Multipath characterization of Indoor power-line networks," *IEEE Trans. Power Delivery*, Vol. 20, Jan. 2005, pp.90-99.

[13] M. Zimmermann, K. Dostert, "A multipath model for the powerline channel," IEEE Trans. on Comm., Vol. 50, April 2002 pp. 553-539.

[14] H. Meng, S. Chen, Y. L. Guan, C. L. Law, P. L. So, E. Gunawan and T. T. Lie, " Modeling of Transfer Characteristics for the Broadband Power Line Communication Channel", IEEE Transactions on Power Delivery, Vol. 19, No. 3, July 2004, pp.1057-1064.

[15] T. Esmailian, F.R. Kschischang, and P.G. Gulak, "An in-building power line channel simulator," in Proc. 6th Int. Symp. Power-Line Communication and its Applications (ISPLC 2002), Athens, 2002.

[16] Seema Arora, Vinay Kumar Chandna and Mini S. Thomas, "Modeling of Broadband Indoor Power Line Channel for Various Network Topologies", IEEE Innovative Smart Grid Technologies Conf., India, 2011, pp. 229-235.

[17] Mathew N.O. Sadiku, Principles of Electromagnetics, Fourth Edition: Oxford University Press, 2010.

BIOGRAPHIES

Mini S. Thomas (M-88, SM-99), graduated from university of Kerala, completed her M. Tech from IIT Madras both with gold medals & Ph. D from IIT Delhi all in Electrical Engineering. She is presently working as Professor of Electrical Engineering at Jamia Millia islamia, New Delhi, Mini S Thomas received the prestigious 'Career Award for young teachers by Govt. of India for the year 1999. She has published 72 papers in International/National Journals & conferences. Her current research interests are in SCADA / EMS/DA systems and smart grid.

V. K. Chandna (M-08, SM-11) graduated from Nagpur University in 1994 in electronics & power, completed his M.E. from Walchand college of Engg. Sangli, Maharashtra and Ph.D. from Delhi College of Engineering. He is presently working as Head and Associate Professor in Electrical Engg. Department, ITS College of Engineering, Greater Noida. He has more than 20 papers in International Journal / Conferences of repute. His area of interest is Distributed Generation, Smart/ Microgrid, SCADA, operation, design and control.

Seema Arora (S-10) received her B.Tech (with Honors) in Electrical Engineering from PEC, Chandigarh, in 1995. She completed her M.E from M.D.University, Rohtak and is currently working as an Assistant Professor in the Department of Electrical and Electronics Engineering at GCET, Greater Noida. She is doing PhD from Jamia Millia Islamia, New Delhi and her research area is Broadband over Power Lines. Her research interests also include Smart Grids and Communication over Power Lines.

Evolutionary Algorithm based Combinational Circuit Design

Arun Rudra
Department of Electronics and Communication Engineering,
Delhi Technological University,
Delhi, India
arun.rudra01@gmail.com

Neeta Pandey
Department of Electronics and Communication Engineering,
Delhi Technological University,
Delhi, India
n66pandey@rediffmail.com

S. Indu
Department of Electronics and Communication Engineering,
Delhi Technological University,
Delhi, India
s.indu@rediffmail.com

***Abstract*—The hardware that allows autonomous reconfiguration to learn and adapt autonomously from the environment is called Evolvable hardware; employs evolutionary algorithms on PLDs so that the configuration may be changed without human intervention. The systems employed in dynamic operating conditions must be able to adapt to situation e.g. performance of the space system may vary due to sudden high radiation and self adaptation is needed to restore the performance as soon as possible. This paper, suggests a design method to evolve a Genetic algorithm (GA) based combinational logic circuit. The method is verified by designing an even parity generator circuit.**

Keywords—-Evolutionary algorithms; Evolvable hardware, genetic algorithm; Combinational logic circuit Verilog HDL; MATLAB.

I. INTRODUCTION

The evolutionary algorithms are based on biological evolution- reproduction, mutation, recombination and selection. The possible solutions to the optimization problem play the role of individuals in a population e.g. circuits in case of EHW. The circuits are assigned a fitness value which determines the efficiency with it satisfies the specifications. The evolution process generates new circuit configurations from the existing ones and determines their fitness [1] - [7]. The fitness may be determined by either extrinsic or intrinsic evolution. The former method simulates all the candidate circuits to see the fitness and the best solution set is implemented physically on reconfigurable device whereas the later one relies on testing all possible circuits on actual hardware. The process ultimately evolves the desired circuit.

The design of electronic circuits is generally a complex task requiring knowledge of large collections of domain-specific rules. This new approach is perhaps best expressed as a black-box view of the problem.

978-1-4673-0934-9/12/$31.00 ©2012 IEEE

In this view one regards the problem of implementing the circuit as being equivalent to designing a black-box with inputs and outputs with the property that on presentation of the original input signals the desired outputs are delivered. The basic feature of this technique is that the details inside the box are encoded into chromosomes and subjected to the usual processes of evolutionary algorithms. In this technique the fitness of a particular chromosome is measured purely as the degree to which the black-box outputs respond in the desired way.

Existing works on such arithmetic circuits like [2], [7] used an array of 2 input basic gates. Genetic Algorithm used for evolution in these circuits is capable of evolving 100% functional arithmetic circuits. The algorithm is able to re-discover conventionally optimum designs for the one-bit and two-bit adders, but more significantly is able to improve on the conventional designs for the two-bit multiplier. The analysis of the history of an evolving design up to complete functionality indicates that it is possible to gain insight into evolutionary process. The technique is based on evolving the functionality and connectivity of a rectangular array of logic cells and is modelled on the resources available on the Xilinx 6216 FPGA device [2]. Design of combinational circuits using 2x1 multiplexers has been carried out as described in [7]. In this method, multiplexors with 1- control line are used as basic design unit for synthesis of any logic function. It is similar to design with binary decision diagrams (BDD) which can be transformed in ordered binary decision diagrams OBDD. Minimising number of components using OBDD is difficult and hence not suitable for evolvable hardware design.

In this paper, we have proposed a method for designing the combinational logic circuits with 100% functionality. The rest of the paper is organized as follows. Sections 2 consider the main idea of the proposed method. Section 3 outlines GA operators, section 4 describes the chromosome encoding, Section 5 explains fitness evaluation process to evaluate the performance of evolved circuits. Simulation environment has been described in section 6. Section 7 summarizes the

experiment of proposed method on 3 bit even parity generator combinational circuit and shows the simulation results for target circuits. Finally, in section 8 the conclusion of this paper is presented.

II. PROBLEM DESCRIPTION

The aim of this paper is to propose a design method to evolve a combinational logic circuit with minimum components. Figure 1 shows universal logic modules of three variables as a black box with inputs, output and programmable control inputs. We all know that any combinational logic function of n variables can be implemented using 2^n-1 muxes of size 2x1 with 1 control input [3], [6], [7]. These muxes are to be arranged as "n" level programmable module using Verilog HDL. For example a 3 input programmable module of even parity generator is shown in Fig. 2. The control input Ctrl for any level is automatically selected in accordance with the chromosome encoding. We used 3 bits for selection of Ctrl so that we can have 8 different control input. The truth table for same is given in Table 1. These control inputs can be defined as inverted or non-inverted input signals or can be 0 or 1. The 3rd level of the multiplexers shown in Fig. 4 can have either a '0' or '1' connected to their inputs. The output of third level is defined as inputs of second level and so on. The 1st stage of the circuit has single multiplexer and its output becomes the module output.

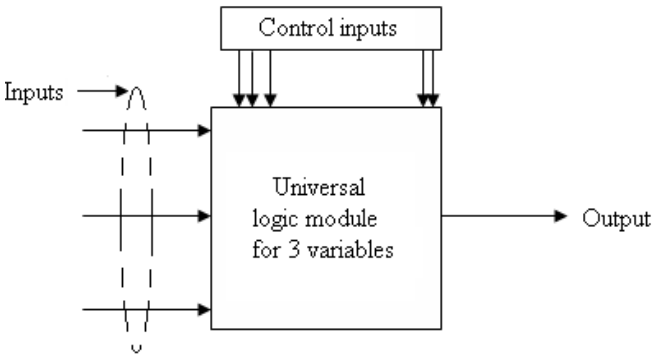

Figure 1. Universal logic module

III. GENETIC ALGORITHM

In this paper, genetic algorithm (GA) has been used to evolve the particular circuit. Genetic algorithm is a general search technique that can be applied to search problems where the solution can not be identified within a finite period of time [8]. In this approach, individuals have been defined in type of bit string. Genetic algorithm operators are defined as follows:

Selection: we have chosen the stochastic uniform a method for parent selection.

Crossover: a pair of parents produce child by using two point crossover.

Mutation: mutation is described as a random change of genes in the chromosome. The mutation method that has been used in this study is the Gaussian mutation.

In our experiments, population size has been defined as 100 and maximum number of generations is set to 20.

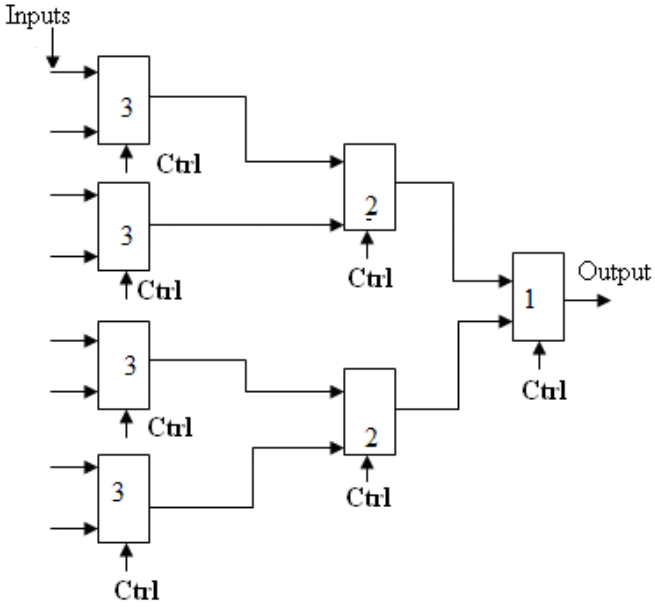

Figure.2 Universal Logic Module

IV. CHOMOSOME ENCODING

We present a 3 level logic module. The input for the module can be given as a chromosome consisting of a string of 29 bits. Bits from 0 to 7 decide what inputs to be fed to inputs of level 3 multiplexers, the inputs to the muxes can have a value of either a '0' or a '1' only. Bits from 8 to 19 decide what variable is to be fed as control inputs (Ctrl) to muxes at level 3, similarly the bits from 20 to 25 decide the control input for level 2 muxes and bits 26 to 28 decide control input for level 1 mux. GA optimizes the output by changing the chromosome bits using crossover and mutation.

V. FITNESS EVALUATION

A fitness function in GA measures goodness of every individual in population with respect to the problem under consideration. All possible combinations of the inputs i.e. 2^3=8 control inputs. Now the output of the circuit is compared with the desired output of the circuit. In the proposed method, we measure the fitness by comparing the Hamming distance between the desired output to the actual output of the circuit to a particular control input. For a fully functional circuit the Hamming distance will be 0.

$$f = \sum \left(abs(y_i - r_i) \right)$$

where y_i is the vector output received after simulation and r_i is the expected output vector, which is known.

TABLE I

Input	Control signal (Ctrl)
000	0
001	1
010	A
011	!A
100	B
101	!B
110	C
111	!C

VI. SIMULATION ENVIRONMENT

To demonstrate the functionality of the proposition, Modelsim is used as Verilog [9],[10] hardware programming language simulator and MATLAB [11] software is employed for GA implementation. Global Optimization toolbox in MATLAB software is used to run the evolutionary algorithm. In addition Simulator Link is also used to develop this software. It can access to Modelsim, open HDL code, run it for different inputs that are determined in MATLAB code and save outputs in the variables of MATLAB codes. Hence this toolbox is as a link between Modelsim and MATLAB. Fig. 3 shows block diagram of this process.

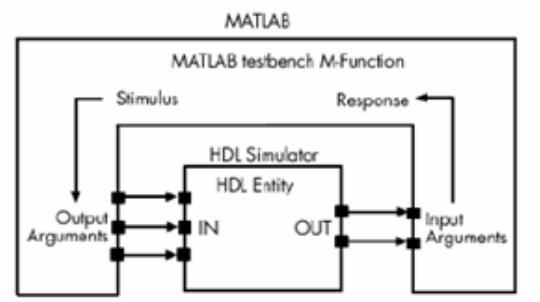

Figure 3

VII. EXPERIMENT AND RESULTS

In this section, the proposed method is utilized for the evolution of 3 bit even parity bit generator. The 3 bit even parity generator has an output as '1' if the number of 1s in the input is odd and an output '0' if the number of 1s in the input are even [12]. The truth table for the above combination circuit is given in Table II and the logic circuit diagram is given in Fig. 4.

TABLE II

Inputs			Outputs
A	B	C	F
0	0	0	0
0	0	1	1
0	1	0	1
0	1	1	0
1	0	0	1
1	0	1	0
1	1	0	0
1	1	1	1

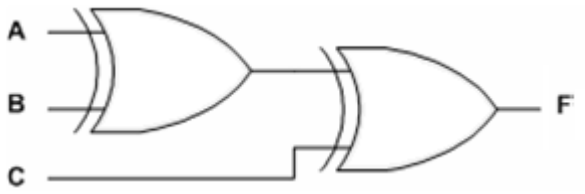

Figure 4. 3 bit even parity generator

Figure 5 shows the evolved circuit of a 3 bit even parity generator. The muxes labeled 3 have their control inputs as A, the muxes labeled 2 have B as their control input and mux labeled 1 has its control input as C. The inputs to muxes labeled 3 are {(0,1),(1,0),(1,0),(0,1)}. The parameters for the Genetic Algorithm are given in Table III.

TABLE III

Parameters	Value
Population Size	100
No. of Generations	20
Crossover Rate	0.8
Crossover Type	Two Point
Mutation Rate	Gaussian
Scaling	Rank
Elitism	2
Selection	Stochastic Uniform

The simulation results in Verilog testbench of the evolved circuit matched to those of a 3 bit even parity generator. Hence the circuit evolved using GA has been able replicate the behavior of the 3 bit even parity generator.

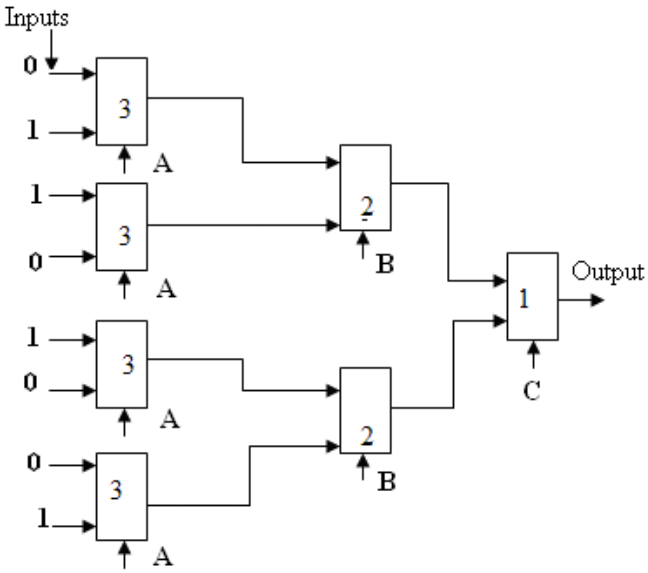

Figure. 5 Evolved Hardware

VIII. CONCLUSION

In this paper we have been able to demonstrate the fact that it is possible to use Evolutionary Algorithms such as Genetic Algorithm to evolve combinational circuit which meets our requirements and has 100% functionality. Next would now be to optimize the circuit and reduce the number of elements required to a bare minimum. Thus we would get a circuit which has 100% functionality and has minimum number of elements

REFERENCES

[1] Evolvable Hardware Series: Genetic and Evolutionary Computation Higuchi, Tetsuya; Yao, Xin (Eds.) Springer 2006

[2] J. F. Miller, P. Thomson, T. Fogarty, "Designing Electronic Circuits Using Evolutionary Algorithms. Arithmetic Circuits: A Case Study" Genetic Algorithms and Evolution Strategies in Engineering and Computer Science, D. Quagliarella, J. Periaux, C. Poloni, and G. Winter (eds.) Wiley, Chechester, UK, 1997, pp. 105-131.

[3] D. G. Whitehead, "Algorithm for Logic Circuit Synthesis by Using Multiplexers" Electronics Letters, vol. 13, pp. 355 – 356, 1997

[4] B.Ali and A.E.A.Almaini and T. Kalganova, "Evolutionary Algorithms and Their Use in the Design of Sequential Logic Circuits" Journal of Genetic Programming and Evolvable Machines, vol.5, pp. 11 – 29, 2004

[5] T. Kalganov, J. F. Miller and T. Fogarty, "Evolution of Digital Circuits with Variable Layout" Proceeding of the Genetic and Evolutionary Computation Conference, GECCO'99, Orlando, Florida, USA, 1999. vol. 2, pp. 1235

[6] S. S. Yau, C. K. Tang , Universal Logic Modules and their Application" IEEE Trans on Computers, vol. C-19, pp. 141 – 149, 1970

[7] A. H. Aguirre, B P Buckles, C. Coello-Coello, "Evolutionary Synthesis of Logic Functions using Multiplexers" delta.cs.cinvestav.mx/~ccoello/conferences/annie2000.pdf.gz

[8] D. Goldberg, Genetic Algorithm in Search, Optimization and Machine Learning, Pearson Education, 2009.

[9] M. D. Ciletti, "Advance Digital Design with Verilog HDL", PHI, 2003.

[10] J. Cavanagh "Verilog HDL Design and Modeling", CRC Press, 2007

[11] EDA Simulator Link User Guide, Mathworks

[12] M. M Mano, "Digital Design", 4th Edition, PHI, 2002.

Fuzzy Logic Based Control of STATCOM for Mitigation of SSR

S.T.Nagarajan
Electrical Engineering Department,
Delhi Technological University, Delhi, India.
email:selukka@yahoo.com

Narendra Kumar
Electrical Engineering Department,
Delhi Technological University, Delhi, India.
email:dnk_1963@yahoo.com

***Abstract*— Subsynchronous resonance is well known phenomenon in Series compensated transmission line. Flexible AC Transmission System (FACTS) devices can be used to enhance the performance of the transmission line and to mitigate SSR with auxiliary controllers. The use of STATCOM a FACTS device is increasing in the power system for enhancing power transfer capability and dynamic reactive power support in power system. In this paper a Fuzzy logic control method for STATCOM is proposed and applied for damping oscillations caused by SSR. The performance of the proposed controller has been tested on Second bench mark model for SSR studies. Time domain simulations have been carried out with MATLAB/SIMULINK. Significant improvement of damping of torsional oscillations has been achieved with the proposed fuzzy logic supplementary controller.**

Keywords—Subsynchronous Resonance; Fuzzy logic control; STATCOM; Torsional interaction

I. INTRODUCTION

Series compensation of the transmission line to improve the power transfer capability may lead to the phenomenon of Subsynchronous resonance (SSR). The first shaft failure due to SSR was experienced at Mohave Generating station in Southern Nevada [1]. To prevent turbine generator shaft form damages caused by SSR various devices and techniques have been proposed in literature [2]. Flexible AC transmission systems (FACTS) have been employed in modern power system due to its capability to work as VAR generation and absorption systems.

STATCOM a FACTS device is a second generation Static VAR Compensator (SVC) based on voltage sourced inverter and has better reactive power support even at low voltages. STATCOM uses a self commutating device like GTOs and can be designed as two level six-pulse bridge, three level twelve-pulse bridge, and forty eight pulse converter. The forty eight pulse converter has superior performance as the output current of the converter almost nears the sinusoidal form and the harmonic distortion is minimum compared to others [3]. Hence forty eight pulse converter is selected for this paper.

Supplementary signals like speed deviation, thevenin's voltage, hybrid Fuzyy/LQR method has been proposed for STATCOM in literature [4-5] for the suppression of oscillations due to SSR. Fuzzy logic controller (FLC) has inherent capabilities to overcome the system nonlinearities, as the exact knowledge of the system is not needed. Ali Ajami et al [5] have proposed a hybrid Fuzzy logic controller with LQR controller to a 3 level STATCOM.

In this paper a Mamdani type Double input Single output (DISO) Fuzzy controller has been proposed along with PI controller for forty- eight pulse converter STATCOM. The study system has been derived from the IEEE second bench mark model for SSR studies. A STATCOM along with Fuzzy auxiliary controller with speed deviation and terminal voltage deviation of generator, has been considered to be connected at the generator terminal for reactive power support and mitigation of SSR. Nonlinear time domain simulations have been carried out using MATLAB/SIMULINK.

II. SUBSYNCHRONOUS RESONANCE

The phenomenon of SSR can be explained as follows: When a line is Series compensated it results in excitation of SSR currents at electrical frequency

$$f_n = f_s \sqrt{\frac{X_c}{X_L}}$$

Where X_c= reactance of the series capacitor; X_L= reactance of the line including generator and transformer; and f_s= the nominal frequency of the power system. These currents result in rotor torques and currents at the complementary frequency:

$$f_e = f_S \pm f_n$$

These currents results in subsynchronous armature voltage components which may enhance subsynchronous armature currents to produce SSR.

SSR manifests in three forms [6].Self excitation, Torsional interaction and Transient SSR. In this paper only Transient SSR is analyzed. Transient SSR generally refers to transient torques on segments of the Turbine-Generator (T-G) shaft resulting from subsynchronous oscillating currents in the network caused by faults or switching operations. This occurs when the complement of the electrical network resonant frequency gets closely aligned with one of the torsional natural frequencies.

III. STUDY SYSTEM

Design of Fuzzy logic controller does not depend on the system model. This eliminates the need to linearise the power

978-1-4673-0934-9/12/$31.00 ©2012 IEEE

system model to tune the parameters of controller. The entire power system components are represented with their non linear equations/models for the IEEE second benchmark power system model for SSR studies shown in Fig.1. The system parameters for generator, turbine shaft and transmission line are taken form ref [7] given in Appendix.

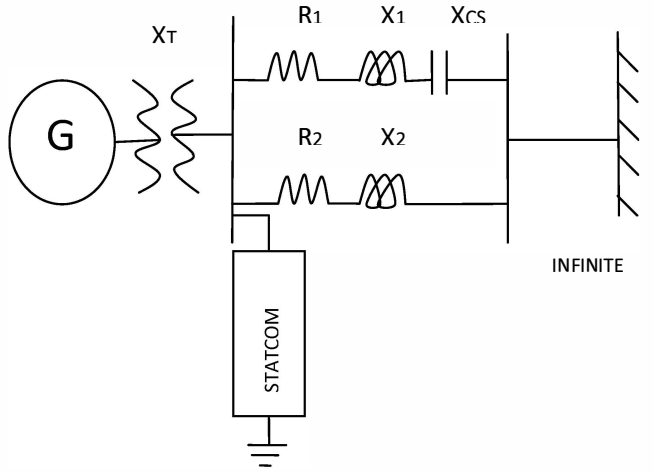

Fig. 1. System Model

A. Generator Model

The Generator was modeled by Park's equation one damper winding and field winding in direct axis and with two damper windings in quadrature axis [8]. The mechanical system was represented by a three mass spring damper system, a high pressure (HP) turbine, a low pressure turbine (LP) and the generator (GEN) as shown in Fig.2. The effect of Exciter mass is assumed to be negligible and hence not considered in this study.

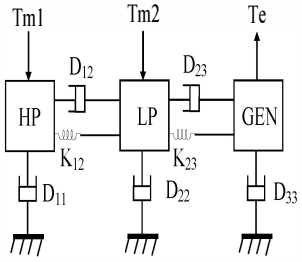

Fig. 2. Turbine generator shaft model

B. STATCOM Controller

The Controller for forty-eight pulse GTO based STATCOM is shown in Fig.3. The detailed explanation of STATCOM controller is given in reference [3]. The controller has inner current control loop and an outer voltage control loop. PI controller is considered for both the loops. V_r is the reference voltage and V_m is the measured voltage for the outer loop. I_{q_ref} and I_q is the quadrature axis reference and quadrature axis current for the inner loop.

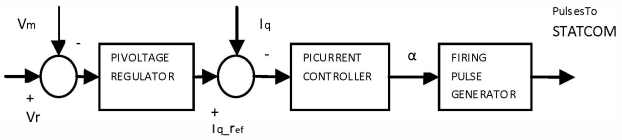

Fig. 3. STATCOM controller structure

C. Fuzzy logic controller

Fuzzy logic control essentially involves the derivation of a control law from heuristic and imprecise (fuzzy) rules. The configuration of the Fuzzy logic control system [9] that is employed for designing the Fuzzy supplementary controller is shown in Fig.4. The FLC contains four main components, the fuzzification interface (FUZZIFICATION), the knowledge base (FUZZY RULE BASE), the decision making logic (FUZZY INFERENCE ENGINE) and the defuzzification interface (DEFUZZIFICATION). A Mamdani type double input single output (DISO) FLC has been designed.

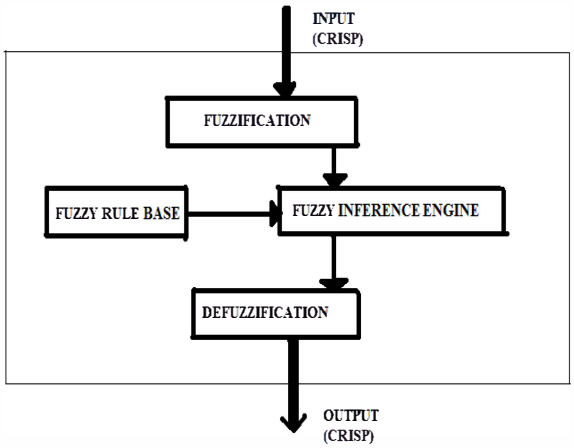

Fig. 4. Fuzzy logic control

The following steps are involved in the designing fuzzy logic controller.

1). Choose the inputs to FLC (INPUT-CRISP): The inputs to FLC used in this study are generator terminal voltage deviation (ΔV_t) and generator speed deviation($\Delta\omega$) which are given by

$$\Delta V_t(pu) = V_{ref} - V_t$$

$$\Delta\omega(pu) = \omega - \omega_0$$

Where

V_t= generator terminal voltage; V_{ref}=Reference voltage;

ω_o=synchronous speed of generator; ω= speed of generator;

2). Choose membership functions to represent the inputs and outputs in fuzzy set notation (FUZZIFICATION): Triangular membership functions were selected for this study as shown in

Fig.5 with five linguistic variables chosen as Large positive (LP), Small positive (SP), Very small (VS), Small negative (SN), Large Negative (LN) for both inputs and outputs. The values of the axes are given in Appendix.

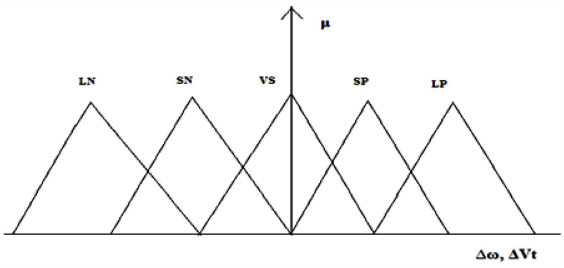

Fig. 5. Triangular member ship functions for speed deviation and voltage deviation

3). Develop fuzzy rules (FUZZY RULE BASE): A set of decision rules relating the inputs to the controller with the output are compiled and stored in the memory in the form of decision table. Twenty five rules for the present study are developed as follows.

Rule1: If $\Delta\omega$ is LN and ΔV_t is LN, then change in susceptance of SVS should be SN. The remaining twenty four rules are formed in the same way as shown in the Table I.

TABLE I. FUZZY RULE TABLE

$\Delta\omega\rightarrow$ $\Delta V_t\downarrow$	LN	SN	VS	SP	LP
LN	SN	SN	LN	LN	LN
SN	SN	SN	SN	LN	SN
VS	SP	SP	VS	SN	SN
SP	LP	SP	SP	SP	SP
LP	LP	LP	LP	SP	SP

4). Since there are N (five) membership functions for each input, there are N^2 (twenty five) possible combinations resulting in M (five) values for the decision variable u. All the possible combinations of inputs, called states, and the resulting control are arranged in a (N^2xM) fuzzy relationship matrix. The membership values for the output characterized by the M linguistic variables are then obtained from the intersection of N^2 values of membership function $\mu(x)$ with the corresponding values of each decision variables in the fuzzy relationship matrix.

5). Defuzzy to obtain crisp output (DEFUZZIFICATION): The output FLC is converted to crisp value by Centre or Gravity (COG) method in this study. The crisp value of FLC in COG is expressed as

$$Crispoutput(u) = \frac{\sum_{i=1}^{5} b_i \int \mu_{(i)}}{\sum_{i=1}^{5} \int \mu_{(i)}}$$

Where b_i is the centre of the membership function; $\mu_{(i)}$ is the membership of member i of output fuzzy set. The overall controller structure for STATCOM with FLC auxiliary controller is shown in Fig.6

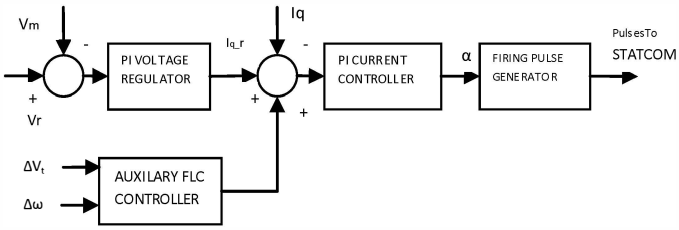

Fig. 6. STATCOM controller structure with auxiliary FLC controller.

IV. SIMULATION STUDY

A. *Case Study*

The system considered is a modified IEEE SBM [7] as shown in Fig.1 with STATCOM at the generator bus on high voltage side of transformer for reactive power support. The generator has ratings of 600MVA, 22kV and 60Hz and is connected to the infinite bus through a transformer of 22KV/ 500KV and two transmission lines one of which is series compensated with a value of 55% of that transmission line reactance. Load flow study was performed to keep the synchronous generator at no load at rated terminal voltage at 1.0pu and all the system variables were initialized.

B. *Analysis of study system*

As the generator shaft has been represented with three mass system, there shall exit two torsional modes, mode 1(LP-turbine mode) and mode 2(HP Turbine mode). The study has been performed for a compensation of 55% as the overall undamping of mode 2 is negligible compared to mode 1, which has maximum undamping at this level of compensation [7]. A damping of 0.4 rad/sec has been kept to make the unit steady state stable for this case. A Fast Fourier Transform (FFT) analysis has been performed on the generator speed signal to test the existence of this critical mode (mode 1) without STATCOM connected to the generator bus. The FFT scan result shown in Fig.7 reveals the presence of dominant 24.65 Hz mode (mode 1) in conformation. Also to test the study system for the presence of sub synchronous resonance condition, a frequency scan of the study system was performed without the STATCOM from generator terminals. The result of the frequency scan shown in Fig.8 reveals the presence of sub synchronous resonance condition in the system near 36 Hz for 55% compensation. The resulting

electromagnetic torque due to SSR oscillates at a frequency f_o-f_r (60-36=24Hz) which is near modal (mode1) frequency of the turbine generator shaft system leading to torque amplification.

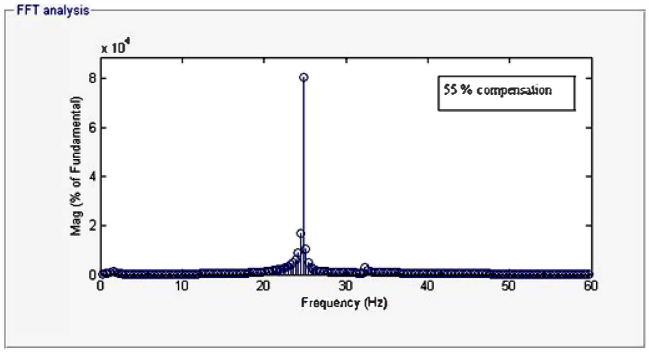

Fig. 7. FFT analysis of generator speed signal with 55%compenstion

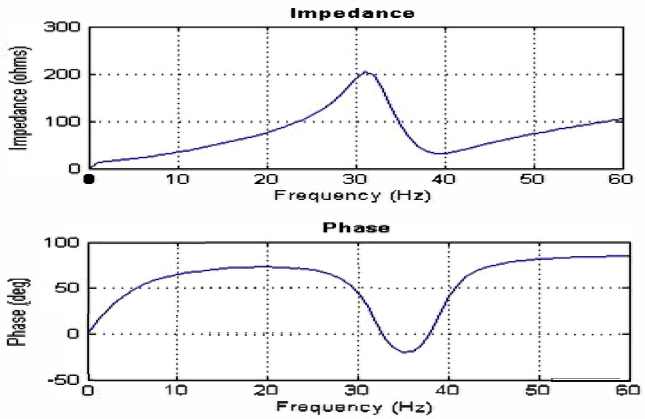

Fig. 8. Frequency response of the transmission network viewed from generator terminals with 55% compensation

C. *Transient analysis of study system*

The transient analysis of the study system was performed with three cases, without STATCOM, with STATCOM PI voltage controller, and with proposed supplementary FLC. For all the cases the load flow study was performed to initialize all system variables with no load on synchronous generator. A three phase fault is applied on the generator bus at time t=0.02s and removed after a duration of 0.017s on the high voltage side of the transformer. The influence of the proposed FLC has been studied through the following signals:

1. Generator speed deviation
2. Mechanical torque between shaft segments connecting generator (GEN) and (LP) turbine.
3. STATCOM reactive power.
4. Generator terminal voltage.

Case 1. Without STATCOM

The torsional oscillations in time domain with no load on generator (PG= 0 MW) is shown in Fig 9. It was observed that the rotor speed deviation, torsional oscillations and voltage at generator terminals are gradually increasing in magnitude and hence the system is unstable.

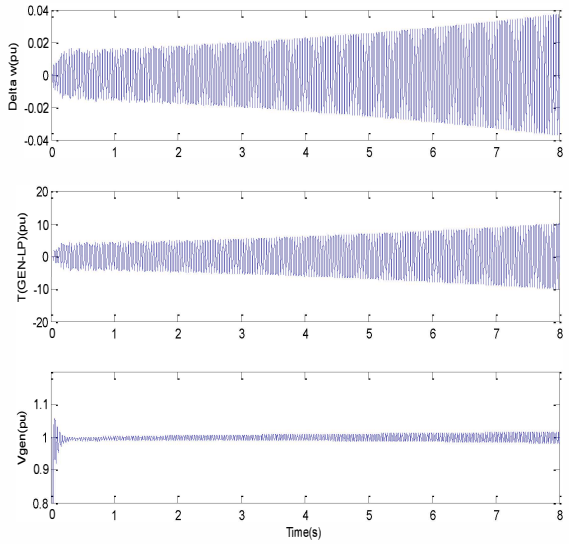

Fig. 9. Turbine-generator torque Oscillations without STATCOM

Case 2. With STACOM-PI voltage controller

STATCOM with a PI voltage controller was now connected to the generator bus on high voltage side of the transformer. The gain parameters for the controller were obtained by hit and trial method without the multi mass shaft system to get reasonable settling time. The value used has been given in Appendix.

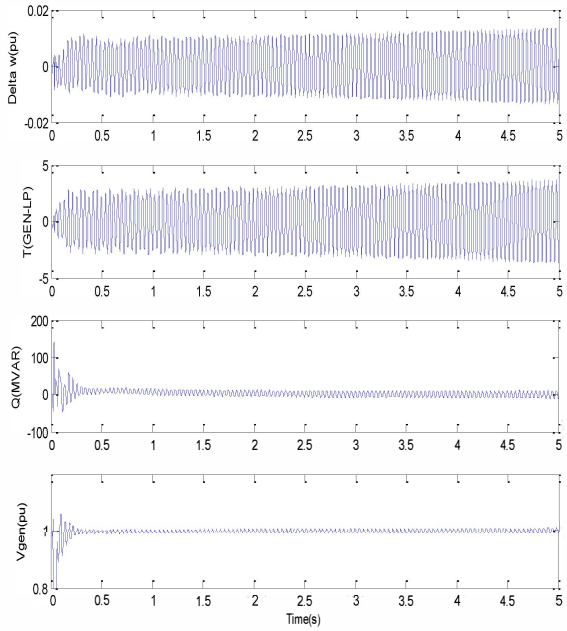

Fig. 10. Turbine-generator torque Oscillations with STATCOM

It can be observed from Fig.10 the torsional oscillations, rotor speed deviation and voltage at generator terminals are still gradually increasing in magnitude and the system is still unstable. Only PI voltage Controller of STATCOM is not able to suppress the torque amplification in the generator turbine shaft. This necessitates the demand for auxiliary control signals for the STATCOM to suppress torque amplification of generator turbine shaft.

Case 3. System with STACOM-PI Voltage regulator and supplementary FLC

The proposed supplementary FLC with membership values given in Appendix was applied to STATCOM and simulation was performed again.

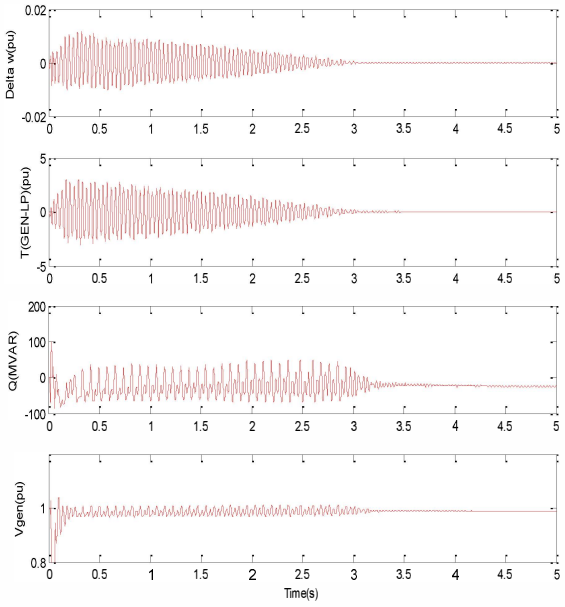

Fig. 11. Turbine-generator torque Oscillations with STATCOM and FLC

It can be observed from Fig.11that all SSR torsional oscillations are damped and the system becomes stable.

V. CONCLUSION

STATCOM is a widely used FACTS device for reactive power generation, voltage support and improving steady state stability of power system. In this paper a Fuzzy logic supplementary controller for STATCOM to damp Sub synchronous torsional oscillations has been presented for series compensated system. The Fuzzy logic controller has advantage over conventional controllers as the exact knowledge of the system is not required. With the proposed FLC supplementary control signal for STATCOM it has been shown through time domain simulations that torsional oscillations due to SSR can be successfully damped.

APPENDIX

Generator data:

Ratings: 600MVA, 22KV, 2P

Stability data:

X_l=0.14 pu R_a=0.0045 pu

X_d=1.65 pu X_q=1.59 pu

X'_d=0.25 pu X'_q=0.46 pu

X''_d=0.20 pu X''_q=0.20 pu

T'_{do}=4.5 s T'_{qo}=0.67 s

T''_{do}=0.040 s T''_{qo}=0.09 s

Torsional spring-mass system data

Mass	Shaft	Inertia H(s)	Damping (pu.T/rad)	Springconstant (pu/rad.)
HP		0.24894	0.05	
	HP-LP		0	42.702
LP		1.5498	0.3104	
	LP-GEN		0	83.47
GEN		0.8788	0.4	

Modal frequencies

Mode	ω_m (rad/s)	freq (Hz)	Damping factor	Xc
1	154.8	24.65	0.4	55%
2	203.4	32.39	0.04	35%

Transmission line data

500KV

Line with series capacitor:

R_1=0.0074pu, R_0=0.022pu, X_1=0.08pu, X_0=0.240pu

Line without series capacitor

R_1=0.0067pu, R_0=0.0186pu, X_1=0.0739pu, X_0=0.210pu

Transformer data:

600MVA, 60HZ, Δ/Y, 22KV/500KV, R_p=0.0006pu, R_S=0.0006 pu, X_P=0 pu, X_S=0.12pu

STATCOM data:

100 MVA, (100MVA Reactive TO 100 MVAR Capacitive)

PI Voltage Regulator Gains:

K_P=12, K_I=3000

PI Current Regulator Gains:

K_P=5, K_I=40

Fuzzy logic controller:

Input: Triangular membership function values

	LP	SP	VS	SN	LN
ΔV_t	0.3, 0.65, 1	0, 0.3, 0.6	-0.03, 0, 0.03	-0.6, -0.3, 0	-1, -0.65, -0.3
$\Delta\omega$	0.005, 0.0175, 0.03	0, 0.003, 0.006	-0.0005, 0, 0.0005	-0.006, -0.003, 0	-0.03, -0.0175, -0.005

Output: Triangular membership function values

	LP	SP	VS	SN	LN
OUTPUT	0.02, 0.11, 0.2	0, 0.035, 0.07	-0.004, 0, 0.004	-0.07, -0.035, 0	-0.2, 0.11, -0.02

REFERENCES

[1] P.M.Anderson, B.L.Agrewal and J.E Van Ness, *Subsysnchronous Resonance in Power System,* IEEE Press, New York, 1990.

[2] IEEE Working Committee Report, "Fourth Supplement to a Bibliography for the Study of Subsynchronous Resonance between Rotating Machines and Power Systems", *IEEE Trans. On Power Systems*, vol.12, no.3, 1997, pp.1276-1282.

[3] N.G. Hingorani and L. Gyugyi, *Understanding FACTS,* IEEE Press, 1996.

[4] K.R.Padiyar and Nagesh Prabhu, "Design and Performance Evaluation of Subsynchronous Damping Controller with STATCOM", *IEEE Trans on Power Delivery*, vol.21, no.3, 2006, pp.1398-1405.

[5] A.Ajami and N.Teheri, "A Hybrid Fuzzy/LQR Based Oscillation Damping Controller Using 3-level STATCOM", Proceedings of Second International Conference on Computer and Electrical Engineering, ICCEE, vol. 1, 2009, pp 348-352.

[6] IEEE Committee Report, "Reader's Guide to Subsynchronous Resonance", *IEEE Transactions on Power Systems,* vol. 7, no.1, 1992, pp. 152-157.

[7] IEEE SSR Working Group, "Second benchmark model for simulation of subsynchronous resonance", *IEEE Trans. On PAS*, vol. 104, no.5, 1985, pp. 1057-1066.

[8] Krause, P.C., *Analysis of Electric Machinery*, McGraw-Hill, 1986, Section 12.5.

[9] Zdenko Kovacic and Stjepan Bogdan, *Fuzzy Controller Design*, CRC Press, Taylor& Francis Group, New York, 2006.

Interconnection Issues for Distributed Resources in a Smart Distribution System

Mini S Thomas, Senior Member, *IEEE* and Parveen Poon Terang

***Abstract*- The purpose of this paper is to relate the issues which have an impact on the interconnection of distributed resources to the utility grid. Impact that can be clearly seen is with respect to the types of distributed resources and the power electronic (PE) devices used to interface them. A balance has to be maintained between the type of DER's and the interfaces in order to get the maximum benefit of incorporating Distributed Generation to the grid. Islanding methods which are the means for creating the microgrids and islanding detection methods are a critical feature. These, together with protection and reliability features have been discussed in the paper.**

Keywords- Distributed generation; distributed energy resource; islanding; interconnection; power systems; power electronic interface.

I. INTRODUCTION

Small, local electric energy generating units from various resources are classified as Distributed Resources (DR), Distributed Energy Resources (DER) and Distributed Generation (DG). There is no distinction between the sources of energy. Distributed Generation Systems have gained popularity in industries and utilities due to their various advantages. The numerous benefits include the following:

1) Better reliability
2) Improved power quality
3) Decrease of voltage sags
4) Emergency backup during utility outages
5) Potential utility capacity addition
6) Energy savings through peak shaving
7) Increased efficiency

DER's are directly connected to the distribution networks. These distribution networks then supply customers from different substations via routes that are categorized based on industrial, commercial and residential users who have various load demands. Outage time and system losses are reduced by using tie switches between feeders. The system operation efficiency and reliability is enhanced by a good two way communication to monitor and control equipment at the distribution substations and feeders.

Despite the benefits of distributed generation systems, a frequent question being asked is in relation to their interconnection. With significant advantages such as low fuel cost and no emissions, an increasing number of renewable resources or microsources such as solar panels, electric vehicles, fuel cells, stand-alone generators, wind generators, bio-fuel generators, and photovoltaic panels are being integrated into the grid; question arising is whether any compromise is being made with respect to reliability and power quality and to what extent. The nature of the alternative energy resources make the grid integration and reliability improvement difficult [1]. Microgrids have been proposed to overcome this drawback [2]. Microgrids are small scale, low/medium voltage electric power systems that house various distributed energy resources in a physically close location. The microgrids can be operated in two modes: grid connected and islanded. In the grid connected mode it acts like a generator from the grid point of view while in the islanded mode it is independent from the utility grid and energy generation, storage, load control, power quality control and regulation are implemented in the standalone system [3].

One of the points defining the major attributes of a Smart Grid given by the 2007 Energy Independence and Security Act (ESIA07) is development and integration of distributed energy resources, especially renewable sources [4][5]. [6] discusses the issue of optimizing network operation and use for accommodating DG integrating. With integration of renewable resources, customers have multiple choices to produce electricity for local usage as well as export to the grid making it essential for the smart grid to ensure safe and reliable connection.

II. ASPECTS AFFECTING INTERCONNECTION

A. Types of DER's

Distributed energy resources, or DER's, include distributed generation and energy storages. Typically ranging from 1kW to 10MW, they are located near the point of use. The concept of DER has existed for a long time; a natural way to connect power sources to the grid. When power systems were developed, neighboring systems were interconnected with transmission systems to increase the availability of the system. Off late it has again become common to connect power plants to the distribution system due to the fact that the size of many new plants makes the distribution grid the natural connection choice. These interconnections have been made as per the IEEE standards [7].

The distributed systems may be powered by renewable or fossil fuels. In-depth discussions on the details of DG technology for all types are given in [8] [9] and [11]. Some of the commonly used DER's are:

Mini S. Thomas is with the Faculty of Engg. And Technology, Jamia Millia Islamia, New Delhi -110025, India. (email : mini@ieee.org)
Parveen Poon Terang is a Research Scholar in the Department of Electrical Engg. Jamia Millia Islamia, New Delhi–110025, India (email : parveen_pt@yahoo.co.uk)

978-1-4673-0934-9/12/$31.00 ©2012 IEEE

1) Fuel Cells

Fuel cells work by the chemical reaction of combining hydrogen and oxygen to form electricity and water [10].They are static energy conversion devices and directly convert the chemical energy of fuel into DC electrical energy. This is further converted into ac using a suitable converter. The basic structure consists of two porous electrodes and an electrolyte layer in the middle. Depending on their electrolyte, several types of fuel cell are available such as phosphoric acid, molten carbonate, solid oxide and proton exchange membrane (PEM) [11]

2) Photovoltaic Systems

Photovoltaic (PV) effect is basically a process by virtue of which the solar energy is converted to electrical energy directly. Like fuel cells, the dc power is converted into ac power compatible with the electric power system.

3) Wind Systems

An indirect form of solar energy is wind energy. The wind results from the fact that the Earth's equatorial regions receive more solar radiation than the polar regions. This causes large-scale convection currents in the atmosphere. Wind Turbines convert the kinetic energy into electrical energy. Three basic wind turbine technologies are currently used for interconnecting with the electric power system i.e. induction machine, double fed induction generator and permanent magnet synchronous generator [11].

4) Microturbines

Microturbines are used to burn a variety of fuels like natural gas, gasoline, diesel methane, propane, alcohol, and naphtha. The speed of a microturbine is very high and electricity is produced at a very high frequency making it unsuitable to be connected directly to the grid [11].

5) Energy Storage Systems

Battery systems store energy in the form of electrical energy. Technologies used to store energy are classified according to the time, total energy and transient response required for their operation. The capacity of storage can be expressed in terms of needs i.e. energy density requirements. The highlight of using energy storage in Distributed Energy systems is that the performance is enhanced. [12] and [13] give a good description of battery types and technologies. The highlight of battery energy storage system is power quality enhancement. In the context of integration to the grid, the simplest way is a direct connection to the DC link of the grid side inverter [1].

6) Reciprocating Internal Combustion Engines

Reciprocating internal combustion engines (IC) convert chemical energy (or heat) into mechanical energy by burning fuel. The mechanical energy used to move pistons in turn spin the shaft and convert the mechanical energy to electrical energy via an electric generator. These engines can be either compression types or spark ignition types and the generator is usually induction or synchronous type. Interconnection to the power system is done directly.

7) Gas Turbines

Similar to IC engines, these gas turbines mix fossil fuels with air to give thermal energy. High temperature, high pressure air is used as the medium to transfer heat and air is allowed to expand in the turbine. This process converts heat energy into mechanical energy which rotates the shaft which in turn (connected to a series of gears) spins the synchronous generator.

B. Interconnection Interface

The interconnection to the grid for any type of DER is achieved with the help of induction generator, synchronous generator or power electronic devices.

1) Induction Generators

This is a rotating type of machine which converts mechanical power to electrical power. Two rotor designs are available: cage rotor and wound rotor. Wind turbines and low head hydro plants use induction generators.

2) Synchronous Generator

Like the induction generator, synchronous generators are rotating machines. A prime mover turns the rotor that induces a voltage on the stator winding. A magnetic field is produced in the rotor by either a dc field current or by a permanent magnet. The electrical frequency of the induced voltage depends on the speed of rotation of the generator. When connected to an electric power system, the synchronous generator must run at a constant speed called 'synchronous speed' and generate voltages corresponding to the supply frequency. High power turbines and reciprocating engines use synchronous generators.

3) Power Electronic Devices

Any type of DER can be connected to the electric power system using power electronic interface. Microturbines, fuel cells, PV systems, energy storage systems and some wind turbines use PE based inverters.

C. Power Electronic Interfaces

Usefulness of DER's can be increased with the use of power electronic PE interfaces to integrate DER's to the grid.
The advancement in technological innovations for semiconductor materials, and microprocessor (or digital-based) control systems work are a big advantage, wherein devices are being made to enhance generation and delivery systems. These low-cost devices combined with their versatility and reliability is fast replacing the traditional electromagnetic and electromechanical systems. Solid state based packages can now convert any form of energy into a

useable form. This is the reason why PE based systems are ideal for distributed energy systems.
In addition to this is the advantage of fast response time making its applicability high for advanced applications.

1) Properties and Attributes of PE Interface

PE interfaces have several characteristics. Circuitry is used to convert power from one form to another. Inverters and rectifiers are used. The PE interface also contains protective functions for both the distributed energy system and the local electric power system that allow paralleling and disconnection from the electric power system. Functions should meet the IEEE Standard 1547 interconnection requirements [7], but can be set more sensitive depending on the situation and utility interconnection requirements. Metering and control functions are also met with by the PE interface.

2) Components of PE

Essentially PE devices have four basic categories of components: 1) semiconductor switches; 2) switch gating and controls systems; 3) inductive components; and 4) capacitive components. Inductive and capacitive components are used to dynamically store energy for circuit power flow dampening, filtering, and transformation. Switch gating and controls turn the semiconductor devices ON and OFF so that the circuit provides the desired power conversions, ancillary services, and protective functions in an efficient and stable manner. Innovations and improvements in semiconductor switch designs have been the driving force for the advancements and implementation of PE interfaces. Operations are analogous to that of a switch, which essentially "opens" or "closes". [11] talks about the various types of PE devices. They are roughly characterized as:
a) Diode: The diode is a two terminal PE device that can conduct current only in one direction and block voltage in the reverse direction. A typical use of a diode is in circuits, where unidirectional current flow is required and reverse voltage levels must be blocked. Diodes exhibit a negative temperature coefficient and are especially efficient when higher current levels are required.
b) Thyristor: The thyristor family of semiconductor switches include a host of similar devices with slightly different operational capabilities. They wield the highest power handling capabilities of all the semiconductor devices and are found being applied in circuits handling thousands of amperes at almost any voltage level, including high-voltage transmission levels.
c) MOSFET: The MOSFET is a gate voltage controllable switch. They are used in low-voltage (<500 V) and low power systems and are capable of the highest switching frequencies—a desirable feature while minimizing magnetic materials in a circuit. Unlike thyristors, MOSFETs can quickly start and stop forward conduction even with a constant forward voltage applied making them useful in switch-mode power supply applications, where dc is being converted to another magnitude or to ac. By their nature, MOSFETs have large conduction losses at high voltages making them uncompetitive with other types of devices. An added advantage by virtue of their construction, MOSFETs allow uncontrolled (and inefficient) reverse current to flow when a reverse potential is applied.
d) Insulated Gate Bipolar Transistor: Switching of PE devices these days are done mostly by the insulated gate bipolar transistor (IGBT). Like the MOSFET, the IGBT controls power flow in the switch by the gate voltage and can switch at relatively high frequencies. IGBT's are available with ratings up to 1700 V and 1200 A and are used on DE systems 10 kW and higher. The available switching frequencies for IGBTs are lower than MOSFETS, but still orders of magnitude faster than thyristors.

3) PE Topologies

a) ac to dc controlled and uncontrolled rectifiers;
b) dc to ac inverters;
c) dc to dc switchmode converters;
d) inline solid-state breakers; and
e) ac to ac cycloconverters.

Four other categories occur frequently in DE applications and are discussed as follows:
i) AC to DC Rectifier: Rectifier circuits are generally used to generate a controlled dc voltage from either an uncontrolled ac source (microturbine and small PMG wind turbine) or the utility supply. When converting from a utility supply, a rectifier's application is usually for dc linking of systems or providing dc voltage for specific-load applications, such as battery regulators and variable frequency drive (VFD) inputs.
ii) DC to DC Converter: Converter circuits most usually found in circuits that are used for renewable energy to battery charging applications. They take an uncontrolled, unregulated input dc voltage and change it depending on the specific load application. They are commonly found in PV battery charging systems. PV converter circuits are usually specialized units designed to extract the maximum power output of the PV array.
iii) DC to AC Inverter: Inverter circuits generate a regulated ac supply from a dc input. They are commonly found in systems providing stand-alone ac power, utility connected DE systems, and on the motor side of a VFD.
iv) Solid-State Breaker: As the penetration of DE technologies in power systems increase, the negative effects on protection schemes, coordination, and available fault current become more acute. Solid-state breaker technologies hold the potential to standardize and greatly simplify the installation of grid-connected DE technologies, while also minimizing their negative impacts.
The time is nigh for break through innovations in the field of solid-state breakers as they could hold the key for real-grid modernization. The simplicity in the concept of solid-state breakers: replacing traditional interrupting medium (vacuum, SF6, air, oil, etc.) in circuit breakers (or switchers) with a semiconductor switch. The speed of even the slowest semiconductor switch is scales of magnitude faster than traditional technologies.
Faster switching speeds coupled with advanced sensing and controls can be used to eliminate fault current contributions, thus making impacts of DE on coordination negligible.

The general topologies described earlier are commonly combined in single use packages. For example, an inverter used on a PV system will obviously contain a dc to ac inverter, but will also usually contain a dc to dc converter to regulate and optimize the inverter input and PV array output. [15] gives an overview of various topologies used for renewable energy applications.

D. Islanding and Islanding Detection methods

An essential requirement of the grid interconnected DG system is the capability of islanding detection [17]-[19]. Islanding occurs when a part of the distribution system is electrically isolated from the main source of supply while still being energized by the distributed generator. An islanding situation is a potential hazard to the line maintenance personnel and also a risk of the DG being damaged due to the out-of-phase reconnection to the grid.

Islanding can be either intentional or unintentional and this influences the behavior of the system. Intentional islanding is done preferably with a minimal load flow to or from the main grid otherwise it causes an unbalance in production and load. If there is a surplus of active power in the island, energy is stored in the rotating masses [20]. An effect of large power unbalance in a newly formed island can be serious; such an island may not survive very long. On the other hand, an island with perfect production balance can survive for a long time, even if there are no voltage or frequency regulators. IEEE Std. 1547 stipulates a maximum delay of 2 seconds for detection of an islanding situation

The three categories of islanding detection methods include:

a)Active method

In this case the islanding situation is detected by directly interacting with the system under consideration. This method introduces deliberate changes or disturbances to the network and the corresponding responses are monitored to determine the islanding condition.

b) Passive method

In this method the decision for an islanded or non-islanded condition is based on measuring a certain system parameter and comparing it with a pre-determined threshold.

c) Communication based method

These methods use communication structures to detect islanding. High expense and low power quality of these methods make them unattractive

d) Hybrid method

These methods are a combination of active and passive methods. They are complex and expensive [20], [21].

An important measure for the effectiveness of any islanding detection method is the Non-detection zone. Non-detection zone NDZ is the operating region where islanding conditions cannot be detected in a timely manner. [24] Smaller NDZ is observed in active methods but there is degradation in the power quality of the system [23].

Passive methods are easy to implement but suffer from large NDZ. Relying on monitoring THD and voltage imbalances for setting suitable thresholds has complexities as the parameters are entirely system dependent.

Communication methods though expensive, have the advantage of negligible NDZ.

E. Control Methods

The performance of microgrids is affected as the operating conditions can suffer due to abrupt mode changes and variations in bus voltages and system frequency. Inverter interfaced DG's can be used in power systems to improve the power quality and reliability. [24] discusses the features that bring substantial flexibility but pose complex control problems.

During an islanded situation, it is important for the micro grid to continue to provide adequate power to the main grid. [25] describes a control strategy used to implement grid connected and intentional islanding operations of distributed power generation and [26] presents a minimum output current tracking control method for interface converters to improve power sharing issues in a low voltage microgrid system.

III. IMPACT OF INTERCONNECTION

In the smart grid environment, the DG units which are considered should be included in the operational control framework so that they can be used to improve the system reliability as well as provide ancillary services like voltage support and reactive power control.

Renewable power sources can be described by three major characteristics a) variability i.e. variation of output power with respect to time b) nondispatchable i.e. limited control of renewable generation outputs and c) energy source i.e. contribution to power requirements. While the utility grid is able to manage variability of load, at high penetration levels, this variability of load has a serious impact on the utility reserve. [27] presents an analysis of the interaction between the variability characteristics of the utility load, wind, solar and ocean wave power generation, concluding that a diversified variable renewable energy mix can reduce the utility reserve requirement and help reduce the effects of variability.

Implementation of smart grids fundamentally changes the approach of assessing and mitigating system voltage deficiencies on the distribution system. If there is a lack of monitoring at the distribution level, many voltage events that occur on the distribution feeders or on the secondary side of the transformer goes unnoticed. The monitoring capabilities of a smart grid allow utilities to be proactive in identifying events that exceed the voltage threshold limitations set by ANSI Std. C84.1 before they affect the end-users. Monitoring of attributes such as voltage, current, kWh and kVA at substation transformers, distribution transformers, smart meters, distribution switching devices and installed power quality monitors permits personnel to perform remote voltage investigations as soon as events occur and before customers are affected. [28] investigates how a smart grid monitoring system can be used to improve the voltage quality of customers.

As the smooth functioning of a microgrid is affected by several factors it is necessary to ensure that the microgrid can operate efficiently in both the grid-connected mode as well as the intentional islanding mode. To facilitate the smooth operation mode transitions, voltage control for the DG

interfacing converters in both grid connected as well as islanding modes is a good option.

Challenging demands are put on the system protection with large scale implementation of distributed interconnections to the distribution feeders. Addition of a generating source to a system increases the fault duty at any point. Fault control problems are further increased with the expansion of existing buses, incorporation of large transformers and request for parallel services.

Some of the main protection issues which arise as a result of DG interconnections include:

a) nuisance tripping
b) Unintentional islanding
c) out of synchronism of automatic reclosures
d) relay de-desensitization
e) ferroresonance

The important aspect is that the DG should be able to adapt to the manner in which the utility system works. The protection relaying however is affected by the DG. [29] and [32] discuss the concerns and challenges faced for the protection of distribution feeders. Few improved methods to solve power control issues have been given in [30] and [31].

The integration of protection devices, control commands and power flow regulation in the network, along with real-time measurements should be done in a manner that maintains a good level of quality and reliability. [4] and [5] give the description of the interconnection criteria for system protection and reliability as per the IEEE 1547, CPUC Rule 21.

Considering the impacts of DER's interconnection to the system, several steps should be taken to ensure that the system remains secure and reliable while giving the desired efficiency and power quality.

a) Interconnection planning (feeder reconfiguration and voltage control) can be carried out to optimize the use of existing distribution network and reduce the cost of interconnection facility.

b) DER's have variability of load which on a small scale can be accommodated by the grid. In cases of high penetration levels there is an impact on the reserve. Finding a solution to the right mix of renewable energy resources can alleviate this problem.

c) As the microgrids need to operate in the grid connected as well as in the islanded mode, abrupt mode changes and variations in the bus voltages and system frequency occur. Enhancing power quality and reliability can be done with the efficient coordination of multiple inverter interfaced DG units in the system.

The impact of interconnection has many issues. If these are addressed and correct/remedial steps are taken then the smart grid can be enhanced in terms of its efficiency reliability and security.

IV. CONCLUSION

In this paper, aspects and impacts of interconnection have been discussed. The aspects covered are types of DER's, interconnection interfaces, PE interfaces, Islanding and Islanding Detection methods and Control methods. These components are discussed at length and an attempt has been made to highlight their important features. The aspects are followed by the impact made on the utility grid by the interconnection of DER's. The overall implication is on the protection and reliability of the system. Based on the standards for interconnection, research has to be done keeping in mind the overall outcome of any system which incorporates DER's. Creating a balance is a challenging task but required if we are to prepare the electric power system for smart grid load management and DR interconnection with good system protection, reliability and power quality.

REFERENCES

[1] S.D. Gamini Jayasinghe, D. Mahinda Vilathgamuwa and Udaya Madawala, "Direct Integration of Battery Energy Storage Systems in Distributed Power Generation", *IEEE Transaction on Energy Conv*. vol.26, no.2, pp.677-685, June 2011.

[2] X. Liu and B. Su, "Microgrids— An integration of renewable energy technologies," in *Proc. IEEE China Int. Conf. Electricity Distribution.*, 10–13, Dec., 2008, pp. 1–7.

[3] Melike Erol-Kantarci,Burak Kantarci and Hussein T. Mouftah, "Reliable Overlay Topology Design for the Smart Microgrid Network" 0890-8044/11/$25.00© 2011 IEEE.

[4] M.Vaziri, S.Vadhva, T.Oneal and M.Johnson, "Smart Grid, Distribution Generation and Standards", 978-1-4577-1002-5/11$26.00©2011 IEEE.

[5] M.Vaziri, S.Vadhva,T.Oneal and M.Johnson "Distribution Generation Issues and Standards", 978-1-4577-0966-1/11$26.00©2011 IEEE.

[6] Sheng-Yi Su, Chan-Nan Lu, Rung Fang Chang and Guillermo Gutierrez-Alcaraz, "Distributed Generation Interconnection Planning: A Wind Power Case Study", *IEEE Transactions on Smart Grid*, vol.2.no.1, pp.181-189, March 2011.

[7] IEEE Standard for Interconnecting Distributed Resources with Electric Power Systems, IEEE Std. 1547-2003, Jul. 2003.

[8] L. Goldstein,B. Hedman, D. Knowles, S. Freedman, R. Woods, and T. Schweizer, "Gas-fired distributed energy resource technology characterizations," National Renewable Energy Laboratory, Golden, CO, Tech. Rep. NREL/TP-620–34783, Nov. 2003.

[9] F. A. Farret and M. G. Sim˜oes, Integration of Alternative Sources of Energy. New York: Wiley, 2006, ISBN 0-471-71232-9.

[10] Seventh Edition Fuel Cell Handbook, EG&G Technical Services, Inc., Albuquerque, NM, DOE/NETL-2004/1206, 2004.

[11] Benjamin Kroposki, Christopher Pink, Richard DeBlasio, Holly Thomas, Marcelo and Pankaj K. Sen, " Benefits of Power Electronic Interfaces for Distributed Energy Systems", *IEEE Transaction on Energy Conv.* vol.25,no.3,pp.901-908, September 2010.

[12] A.Akhil and S. Kraft, "Battery energy storage market feasibility study-Expanded report," Sandia National Laboratories, Albuquerque, NM, SAND97-1275/2, 1997.

[13] I. Gyuk, P. Kulkarni, J. H. Sayer, J. D. Boyes, G. P. Corey, and G. H Peek, "The United States of storage", *IEEE Power Energy Mag.*, vol. 3, no. 2,pp. 31–39, Mar./Apr. 2005.

[14] O.Samuuelsson and N. Strath, 1-4244-1298-6/07/$25.00 ©2007 IEEE.

[15] J. M. Carrasco, L. G. Franquelo, J. T. Bialasiewicz, E. Galvan, R. C. Portillo Guisado, M. A. M. Prats, J. I. Leon, and N. Moreno-Alfonso, "Power-electronic systems for the grid integration of renewable energy sources: A survey," *IEEE Trans. Ind. Electron.*, vol. 53, no. 4, pp. 1002–1016, Jun. 2006.

[16] Pukar Mahat, Zhe Chen and Birgitte Bak-Jensen, "Review of Islanding Detection Methods for Distributed Generation", DRPT2008 6-9 April 2008, Nanjing China, 978-7-900714-13-8/08/ ©2008DRPT.

[17] M A Redfern , J I Barrett and 0 Usta, " A new microprocessor based islanding protection algorithm for dispersed storage and generation units", *IEEE Trans. Power Del.*, Vol. 10, No. 3, pp.1249-1254, July 1995.

[18] M.S. Thomas and P.P.Terang, "Islanding Detection using Decision Tree Approach", 978-1-4244-7782-1/10/© 2010 IEEE

[19] S.R.Samantaray, Trupti Mayee Pujhari and B. D. Subudhi, " A new approach to Islanding detection in Distributed Generations". 978-1-4244-4331-4/09/$25.00 ©2009 IEEE

[20] P.Mahat, Z. Chen and B.Bak-Jensen, "A Hybrid Islanding Detection Technique using average rate of Voltage change and Real Power Shift", *IEEE Trans. On Power Del.* ,vol.24, no.2, pp. 764-771, April 2009.

[21] Wen-Yeau Chang, "A Hybrid Islanding Detection Method for Distributed Synchronous Generators" 978-1-4244-5393-1/10/$26.00 © 2010 IEEE

[22] H. H. Zeineldin, Ehab F. El-Saadany and M. M. A. Salama, "Impact of DG Interface Control on Islanding Detection and Nondetection Zones" *IEEE Trans. Power Delivery,* vol. 21, no. 3, pp.1515-1523, July 2006

[23] H.H.Zeineldin and James L. Kirtley, " A Simple Technique for Islanding Detection with Negligible Non-Detection Zone", *IEEE Trans. Power Del.,* vol. 24, no. 2, pp.779-785, April 2009.

[24] Il-Yop Chung, Wenxin Liu, David A. Cartes, Emmanuel G Collins Jr.and Seung-Il Moon, "Control methods of Inverter-interfaced Distributed Generators in a Microgrid System", *IEEE Transactions on Industry Applications*, vol.46, no.3, May-June 2010.

[25] Irvin J. Balaguer, Qin Lei, Shuitao Yang, Uthane Supatti and Fang Zheng Peng, "Control for Grid Connected and Intentional Islanding Operations of Distributed Power Generation", *IEEE Trans on Industrial Electronics*, vol.58, no.1, pp.147-157, Jan 2011

[26] Chia-Tse Lee, Cheng-Chieh, Chia-Chi Chu and Po-Tai Cheng, 978-1-4244-2893-9/09/$25.00© 2009 IEEE

[27] Douglas A. Halamay, Ted K A Brekken, Asher Simmons and Shaun, "Reserve requirement impacts of large scale integration of wind, Solar and Ocean Wave Power Generation", *IEEE Trans. On Sustainable Energy*, vol.2, no.3, pp. 321-328, July 2011.

[28] Keery D. McBee and Marcelo G. Simoes, "Utilizing a Smart Grid Monitoring System to improve Voltage Quality of Customers", *IEEE Transactions on Smart Grid*, vol.3, no.2, pp. 738-743, June 2012.

[29] Gurukiran Kaur and Mohammad Vaziri Y, "Effects of Distributed Generstion (DG) interconnections on protection of Distribution Feeders" 1-4244-0493-2/06/$20.00© 2006 IEEE

[30] A. Mehrizi-Sani and R. Iravani, "Potential-function based control of a microgrid in islanded and grid-connected modes," *IEEE Trans. Power Syst.*, vol. 25, no. 4, pp. 1883–1891, Nov. 2010.

[31] K. D. Brabandere, B. Bolsens, J. V. D. Keybus, A.Woyte, J. Drisen, and R. Belmans, "A voltage and frequency droop control method for parallel inverters," *IEEE Trans. Power Electron.*, vol. 22, no. 4, pp. 1107–1115,Jul. 2007.

[32] S. Agematsu, S. Imai , R. Tsukui, H. Watanabe, T. Nakamura, T. Matsushima, " Islanding protection system with active and reactive power balancing control for Tokyo metropolitan power system and actual operational experiences", Developments in Power System Protection, Conference Publication No.479 0 IEE 2001.

Mini. S. Thomas (M-88, SM-99), graduated from university of Kerala, completed her M.Tech from IIT Madras both with gold medals & Ph.D from IIT Delhi all in Electrical Engineering. Her employment experiences include Regional Engineering College Calicut, Kerela, Delhi College of Engineering, New Delhi and presently as professor in the Faculty of Engg. & Tech., Jamia Millia Islamia, New Delhi. Mini S. Thomas received the prestigious 'Career Award' for young teachers, instituted by Govt. of India for the year 1999. She has published 70 papers in International/National Journals & conferences. Her current research interests are in SCADA / EMS systems and intelligent protection of power systems.

Parveen Poon Terang, graduated from NIT Silchar, Assam. Completed her M.Tech from Jamia Millia Islamia, New Delhi in Electric Power Systems Mgmt and is currently pursuing her Ph.D from Jamia Millia Islamia, New Delhi. She is working as Asst. Prof. in JSS Academy of Technical Education, Noida, UP. Her research interests include protection and interconnection of distributed generation systems and smart grids.

Investigations of Model Order Reduction Techniques for Large Scale Linear Systems

Chandan Kumar, S.K.Jha, Prerna Gaur, *Senior Member, IEEE*
Instrumentation And control division,Netaji Subhas Institute of Technology,Delhi,India

***Abstract*—In this paper, the simple approach is proposed to determine reduced order model for different higher order complex systems. The proposed approach is based on Hsia's approach on the simplification of linear systems and comparison is made with Krishnamurthy's approach on Routh criterion on reduced order modeling. Two examples are taken to show the effectiveness of proposed approach over the later one. The results are simulated in Matlab environment.**

Keywords—Reduced order model; Higher order system; Routh criterion; DC servomotor.

I. INTRODUCTION

Model Order Reduction (MOR) is a branch of systems and control theory that studies the properties of dynamical systems in application for reducing their complexity, while preserving (to the possible extent) their input-output behavior. The exact analysis of high order systems (HOSs) is both onerous and costly as HOSs are often too complicated to be used in practical problems [1-5]. Hence simplification procedures based on physical considerations or using mathematical approaches are generally employed to realize simple models for the original HOS. The problem of reducing a high order system to its corresponding lower order form is considered important in analysis, synthesis and simulation of practical systems. The modeling of complex dynamic systems is one of the most important subjects in engineering field. A model is often too complicated to be used in real problems, so approximation procedures based on physical considerations or mathematical approaches are used to achieve simpler models than the original one. The subject of model reduction is very important to engineers and scientists working in many fields of engineering, especially, for those who work in the process control area [6-9]. In control engineering field, model reduction techniques are fundamental for the design of controllers where particular numerically heavy procedures are involved. This would provide the designer with low order controllers that have less hardware requirements. Efforts towards obtaining low-order models from high-degree systems are related to the aims of deriving stable reduced-order models from stable original ones and assuring that the reduced-order model matches some quantities of the original one [10-13].

II. MATHEMATICAL PRELIMINARIES

Here in this section the mathematical preliminaries of V. Krishnamurthy's and that of T.C.Hsia's approach are illustrated in detail.

978-1-4673-0934-9/12/$31.00 ©2012 IEEE

A. V. Krishnamurthy's Approach [3]

Let the transfer function of higher order system be

$$H(s) = \frac{b_{11}s^m + b_{21}s^{m-1} + b_{12}s^{m-2} + b_{22}s^{m-3} \ldots\ldots}{a_{11}s^n + a_{21}s^{n-1} + a_{12}s^{n-2} + a_{22}s^{n-3} \ldots\ldots} \quad (1)$$

where $m \leq n$

The Routh stability array for numerator and denominator polynomials of H(s) are shown below in tables I and II respectively.

The first row of each column contains odd coefficients and second row even coefficients.

The tables are completed in conventional way

$$c_{ij} = c_{i-2,j+1} - (c_{i-2,1} * c_{i-1,j+1})/(c_{i-1,1})$$

For $i \geq 3$ and $1 \leq j \leq [(n - i + 3)/2]$ (2)

where [.] stands for integral part and n denotes the order of polynomial.

TABLE I
NUMERATOR STABILITY ARRAY

b_{11}	b_{12}	b_{13}	b_{14} . . . . .
b_{21}	b_{22}	b_{23}	b_{24} . . . . .
b_{31}	b_{32}	b_{33}	
b_{41}	b_{42}	b_{43}	
$b_{m,1}$			
$b_{(m+1),1}$			

TABLE II
DENOMINATOR STABILITY ARRAY

a_{11}	a_{12}	a_{13}	a_{14} . . . . .
a_{21}	a_{22}	a_{23}	a_{24} . . . . .
a_{31}	a_{32}	a_{33}	
a_{41}	a_{42}	a_{43}	
$a_{n,1}$	$a_{(n+1),1}$		

The transfer function thus reconstructed with the second and third rows of each table is given by

$$H_{n-1}(s) = \frac{b_{21}s^{m-1} + b_{31}s^{m-2} + b_{22}s^{m-3} + b_{32}s^{m-4} \ldots\ldots}{a_{21}s^{n-1} + a_{31}s^{n-2} + a_{22}s^{n-3} + a_{32}s^{n-4} \ldots\ldots} \quad (3)$$

Generalizing this, the transfer function of a system with reduced order k ($\leq$ n) can easily be constructed with $(m + 2 - k)^{th}$ *and* $(m + 3 - k)^{th}$ rows of table 1 and $(n + 1 - k)^{th}$ *and* $(n + 2 - k)^{th}$ rows of table 2.

$$H_k(s) = \frac{b_{(m+2-k),1}s^{k-1} + b_{(m+3-k),1}s^{k-2} + b_{(m+2-k),2}s^{k-3}+\cdots}{a_{(n+1-k),1}s^{k} + a_{(n+2-k),1}s^{k-1} + b_{(n+1-k),2}s^{k-2}+\cdots} \quad (4)$$

B. T. C. Hsia's Approach[3]

Let the high order transfer function be represented by

$$M_H(s) = k\frac{1 + b_1 s + b_2 s^2 + b_3 s^3 + \cdots b_n s^m}{1 + a_1 s + a_2 s^2 + a_3 s^3 + \cdots a_n s^n}$$
$$where\ n \geq m \quad (5)$$

Let the approximated low order transfer function be represented by

$$M_L(s) = k\frac{1 + c_1 s + c_2 s^2 + c_3 s^3 + \cdots c_n s^q}{1 + d_1 s + d_2 s^2 + d_3 s^3 + \cdots d_n s^p}$$
$$where\ n \geq p \geq q. \quad (6)$$

Here we are keeping zero frequency gain k of the two transfer functions same to keep steady state behavior preserved even in low order approximation. Furthermore we assume that poles of both transfer functions be in left half to avoid instability.

Approximation criteria:

$$\frac{|M_H(jw)|^2}{|M_L(jw)|^2} = 1 \quad (7)$$

This implies that amplitude characteristics of the two systems in frequency domain are similar which may lead to similar time responses of two systems.

The approximation procedure involves the following two steps:

1. Choosing the appropriate orders of the numerator polynomial (q) and denominator polynomial(p) of $M_L(s)$.
2. Determining the coefficients $c_1, c_2, c_3 \ldots\ldots c_q and\ d_1, d_2, d_3 \ldots\ldots d_p$ so that approximation criterion is satisfied.

$$\frac{M_H(s)}{M_L(s)} = \frac{1 + b_1 s + b_2 s^2 + b_3 s^3 + \cdots b_n s^m}{1 + a_1 s + a_2 s^2 + a_3 s^3 + \cdots a_n s^n} \times \frac{1+d_1 s+d_2 s^2+d_3 s^3+\cdots d_p s^p}{1+c_1 s+c_2 s^2+c_3 s^3+\cdots c_q s^q} = \frac{1+m_1 s+m_2 s^2+m_3 s^3+\cdots m_u s^u}{1+l_1 s+l_2 s^2+l_3 s^3+\cdots l_v s^v} \quad (8)$$

where u= m+p and v= n+q.

We know that

$$\frac{|M_H(jw)|^2}{|M_L(jw)|^2} = \frac{M_H(s)}{M_L(s)}\frac{M_H(-s)}{M_L(-s)} \quad at\ s = jw \quad (9)$$

where $M_H(s)M_H(-s)$ And $M_H(s)M_H(-s)$ are even polynomials of s.

$$\frac{|M_H(jw)|^2}{|M_L(jw)|^2} = \frac{1+e_2 s^2+e_4 s^4+\cdots e_{2u} s^{2u}}{1+f_2 s^2+f_4 s^4+\cdots f_{2v} s^{2v}} \quad at\ s = jw \quad (10)$$

$$\frac{|M_H(jw)|^2}{|M_L(jw)|^2} = 1 + \frac{(e_2 - f_2)s^2+(e_4-f_4)s^4+\cdots}{1+f_2 s^2+f_4 s^4+\cdots f_{2v} s^{2v}} \quad at\ s = jw \quad (11)$$

If u = v the last term in numerator will be $(e_{2u} - f_{2u})s^{2u}$

Then to satisfy the approximation criteria we conclude that

$$(e_2 = f_2),\ (e_4 = f_4) \ldots\ldots\ldots (e_{2u} = f_{2u})$$

However if u < v in most practical cases then beyond the term $(e_{2u} - f_{2u})s^{2u}$ there will be

$-f_{2(u+1)}s^{2(u+1)} - f_{2(u+2)}s^{2(u+2)} - \cdots - f_{2v}s^{2v}$

Hence error generated will be

$$|e| = \frac{|M_H(jw)|^2}{|M_L(jw)|^2} - 1 = \frac{-f_{2(u+1)}s^{2(u+1)} - f_{2(u+2)}s^{2(u+2)} - \cdots - f_{2v}s^{2v}}{1 + f_2 s^2 + f_4 s^4 + \cdots f_{2v}s^{2v}} \quad at\ s = jw \quad (12)$$

The conditions $(e_2 = f_2),\ (e_4 = f_4) \ldots\ldots\ldots (e_{2u} = f_{2u})$ are used to solve for unknown coefficients in $M_L(s)$ if $M_H(s)$ is given. This is done by writing

$$\frac{M_H(s)}{M_L(s)}\frac{M_H(-s)}{M_L(-s)} = \frac{(1+m_1 s+m_2 s^2+m_3 s^3+\cdots m_u s^u)}{(1+l_1 s+l_2 s^2+l_3 s^3+\cdots l_v s^v)} \times \frac{(1-m_1 s-m_2 s^2-m_3 s^3-\cdots m_u s^u)}{(1-l_1 s-l_2 s^2-l_3 s^3-\cdots l_v s^v)} = \frac{1+e_2 s^2+e_4 s^4+\cdots e_{2u} s^{2u}}{1+f_2 s^2+f_4 s^4+\cdots f_{2v} s^{2v}}$$

By equating coefficients we get

$$(e_2 = 2m_2 - m_1^2)$$
$$(e_4 = 2m_4 - 2m_1 m_3 + m_2^2)$$
$(e_6 = 2m_6 - 2m_1 m_5 + 2m_2 m_4 - m_3^2)$ and so on.

III. NUMERICAL EXAMPLES

Here we are taking two third order open loop systems which are converted to second order reduced model form by applying V. Krishnamurthy's approach and the proposed T. C. Hsia's frequency domain approach.

A. V. Krishnamurthy's Approach[3]

1) Consider that forward transfer function of a unity feedback control system is

$$G(s) = \frac{8}{s(s^2+6s+12)}$$

So the closed loop transfer function is

$$\frac{8}{s^3+6s^2+12s+8}$$

Step 1: closed loop characteristics equation is

$C(s) = s^3 + 6s^2 + 12s + 8$

Step 2: applying routh criterion to above characteristic equation

TABLE III DENOMINATOR STABILITY ARRAY

s^3	1	12
s^2	6	8
s^1	32/3	0
s^0	8	0

Step 3: Using krishnamurthy's approach reduced order closed loop characteristics equation is C_r (s)= $6s^2 + (32/3)s + 8$

Step 4: Hence the reduced order transfer function is

G_r (s) = $\frac{8}{6s^2+(32/3)s+8}$

2) Open loop transfer function of a position control system is given as

G(s) = $\frac{\theta(s)}{E_f(s)} = \frac{K_T}{s(L_f s+R_f)(Js+B)}$

= $\frac{K_T}{L_f Js^3+(BL_f+JR_f)s^2+BR_f s}$

Step 1: closed loop characteristics equation is C(s) = $L_f Js^3 + (BL_f + JR_f)s^2 + BR_f s + K_T$

Step 2: applying routh criterion to above characteristic equation

TABLE IV DENOMINATOR STABILITY ARRAY

s^3	$L_f J$	BR_f
s^2	$(BL_f + JR_f)$	K_T
s^1	Z= $\frac{(BL_f+JR_f)BR_f-L_f JK_T}{(BL_f+JR_f)}$	0
s^0	K_T	0

Step 3: Using krishnamurthy's approach reduced order closed loop characteristics equation is

C_r (s)= $(BL_f + JR_f)s^2 + Zs + K_T$

where Z= $\frac{(BL_f+JR_f)BR_f-L_f JK_T}{(BL_f+JR_f)}$

Step 4: Hence the reduced order open loop transfer function is

G_r (s) = $\frac{K_T}{(BL_f+JR_f)s^2+Zs}$

Step 5:

Suppose, the parameters of D.C servomoter are given below

J=2.2× 10^{-3} , B=3.025× 10^{-3}, L_f=0.5× 10^{-2},

K=25× 10^{-3}, R_f=0.9

Original model

G(s) =$\frac{0.025}{1.1\times10^{-5}s^3+0.001995s^2+0.002723s}$

The reduced order model

G_r(s)= $\frac{0.025}{0.001995s^2+0.002585s}$

B. T. C. Hsia's Approach[4]

1) Consider that forward transfer function of a unity feedback control system is

G(s) = $\frac{8}{s(s^2+6s+12)}$

So the closed loop transfer function is $\frac{8}{s^3+6s^2+12s+8}$

Or Original model can be written as

$\frac{1}{1+1.5s+0.75s^2+0.125s^3}$

Then let the reduced order model is of second order

$$M_L(s) = \frac{1}{1+ d_1 s + d_2 s^2}$$

$$\frac{M_H(s)}{M_L(s)} = \frac{1 + d_1 s + d_2 s^2}{1 + 1.5s + 0.75s^2 + 0.125s^3}$$

$$= \frac{1+m_1 s+m_2 s^2}{1+ l_1 s+l_2 s^2+l_3 s^3}$$

$l_1 = 1.5 , l_2 = 0.75 , l_3 = 0.125 , m_1 = d_1 , m_2 = d_2$

Now using equation

$\frac{M_H(s)}{M_L(s)}\frac{M_H(-s)}{M_L(-s)} = \frac{1+e_2 s^2+e_4 s^4}{1+f_2 s^2+f_4 s^4+f_6 s^6}$

$e_2 = f_2 = 2m_2 - m_1^2 = 2d_2 - d_1^2$, $e_4 = f_4 = 2m_4 - 2m_1 m_3 + m_2^2 = d_2^2$

Similarly $f_2 = 2l_2 - l_1^2 = 2 \times 0.75 - 1.5^2$ = -0.75,

$f_4 = 2l_4 - 2l_1 l_3 + l_2^2$ =2×0 -2×1.5×0.125 +0.75^2 = 0.1875

Hence d_2^2 = 0.1875 so d_2 = 0.433 now solving $2d_2 - d_1^2$= -0.75 we get d_1 = 1.271

So the reduced order model is

$M_L(s) = \frac{1}{1+1.271s+0.433s^2} = \frac{2.31}{s^2+2.936s+2.31}$

2) Consider reduced order modeling of position control system Original model

$$\frac{0.025}{1.1 * 10^{-5} s^3 + 0.001995s^2 + 0.002723s + 0.025}$$

=$\frac{1}{1+0.1089s+0.0798s^2+4.4*10^{-4} s^3}$

Then let the reduced order model is of second order

$$M_L(s) = \frac{1}{1+ d_1 s + d_2 s^2}$$

$$\frac{M_H(s)}{M_L(s)} = \frac{1 + d_1 s + d_2 s^2}{1 + 0.1089s + 0.0798s^2 + 0.00044s^3}$$

$$= \frac{1+m_1 s+m_2 s^2}{1+ l_1 s+l_2 s^2+l_3 s^3}$$

$l_1 = 0.1089 , l_2 = 0.0798 , l_3 = 0.00044 , m_1 = d_1 , m_2 = d_2$

Now using equation

$\frac{M_H(s)}{M_L(s)}\frac{M_H(-s)}{M_L(-s)} = \frac{1+e_2 s^2+e_4 s^4}{1+f_2 s^2+f_4 s^4+f_6 s^6}$

$e_2 = f_2 = 2m_2 - m_1^2 = 2d_2 - d_1^2$, $e_4 = f_4 = 2m_4 - 2m_1 m_3 + m_2^2 = d_2^2$

Similarly $f_2 = 2l_2 - l_1^2 = 2 * 0.0798 - 0.1089^2$ = 0.1477, $f_4 = 2l_4 - 2l_1 l_3 + l_2^2$

=2*0 -2*0.1089*0.00044 +0.0798^2

= 0.006272

Hence d_2^2 = 0.006272 so d_2 = 0.0792 now solving $2d_2 - d_1^2$=0.1477 we get d_1 = 0.10344

So the reduced order model is

$$M_L(s) = \frac{1}{1 + 0.10344s + 0.0792s^2}$$

Fig.1 gives comparative step responses for original and reduced order models for example 1 and Fig.2 gives comparative step responses for original and reduced order models for example 2 respectively. Table 5 and table 6 give

the comparative performance indices value corresponding to these two examples.

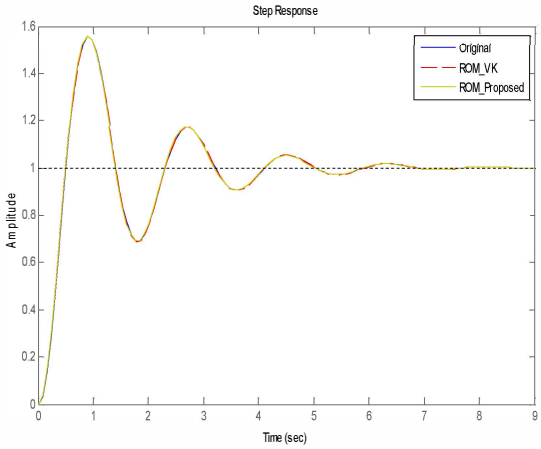

Fig.1. Comparative step responses for original and reduced order models for example 1

TABLE V

First example	Rise time (sec)	Settling time (sec)	% Over-Shoot	Peak value	Peak time (sec)
Original	2.110	3.758	0	1.0000	8.105
proposed	2.099	3.582	0.03	0.9997	6.039
VK	2.041	4.744	2.262	1.0226	4.249

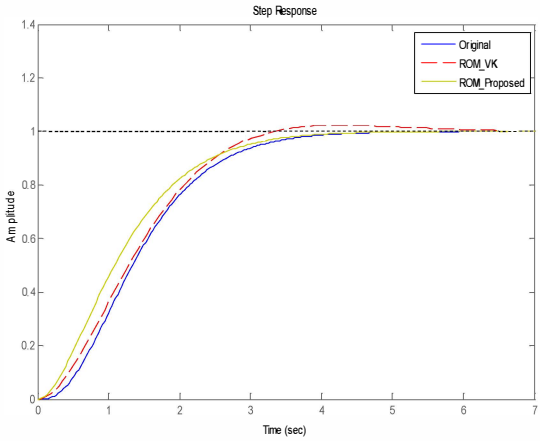

Fig.2. Comparative step responses for original and reduced order models for example 2

TABLE VI

Second Example	Rise time(sec)	Settling time(sec)	% Overshoot	Peak value	Peak time(sec)
Original	0.3394	5.6478	55.4480	1.5545	0.8846
Proposed	0.3396	5.6407	55.4909	1.5549	0.8836
VK	0.3407	5.6666	55.6687	1.5567	0.8907

IV. RESULTS AND DISCUSSION

Two unity feedback systems are studied. First one is simple third order unity feedback system and other one is third order open loop position control system i.e. DC servomotor with unity feedback. Both the third order systems are converted to its corresponding second order form by two different approaches, V.Krishnamurthy's approach on Routh criterion on reduced order modeling and proposed T.C.Hsia's approach on the simplification of linear systems. The results are simulated in MATLAB and comparative study for step responses of original system and two reduced order models obtained from both the approaches are plotted in fig. 1 and fig. 2 respectively. The step response of original third order system is compared with step responses of reduced second order models obtained from both the approaches. This comparison is done for both the systems taken under consideration in terms of their performance index (PIs). The PIs such as rise time, peak time, percentage overshoot, and settling time etc. corresponding to their transient and steady state characteristics are arranged in a tabular fashion to show the effectiveness of proposed approach over the former one. Here we observe that the PIs shown by the proposed method is in close agreement with the original one contrary to that shown by VK's. rise time, peak time, and settling time for original system of example first are 2.11, 8.105 and 3.758 respectively which is in close agreement with the proposed method for which the respective values are 2.099, 6.039 and 3.582 sec respectively whereas VK's approach displays much deviation from the original one, quite discernible from table 5. Most prominent deviation appears to be with respect to percentage overshoot which for original system, proposed, and VK's approach are 0, 0.03 and 2.262 respectively. Similarly the rise time, peak time, and settling time for original system of example second are 0.3394, 0.8846 and 5.6478 respectively which is in close agreement with the proposed method for which the respective values are 0.3396, 0.8836 and 5.6407 sec respectively whereas VK's approach displays much deviation from the original one, quite discernible from table 5. Similar deviation appears with respect to percentage overshoot which for original system, proposed, and VK's approach are 55.448, 55.4909 and 55.6687 respectively. Design aspect of higher order system entails higher order controllers which in turn requires large hardware requirement that is not economically viable. Therefore this necessitates for evolution of ROMs of original HOSs. This would provide the designer with low order controllers that have less hardware requirements and hense economically viable option

V. CONCLUSION

In this paper, the simple approach is proposed to determine reduced order model for different higher order complex systems. The proposed approach is based on Hsia's approach on the simplification of linear systems and comparison is made with Krishnamurthy's approach on Routh criterion on reduced order modeling. Two examples are taken to estimate the performances indices of transient and steady state response to show the effectiveness of proposed approach over the later one. The results are simulated in Matlab environment. Observation of results vindicates that the proposed approach gives all the performance indices which are more closer to the performance indices of original one than the other approach.

REFERENCES

[1] Y.Shamash,"stable reduced order models using pade type approximation,"IEEE Trans.,Automat. Contrl.,vol.19,pp.615-616,1974.

[2] M.F.Hutton and B.Friedland, "Routh approximation for reducing order of linear, time invariant systems,"IEEE Trans.,Automat. Contrl.,vol.20,pp.329-337,1975.

[3] V.Krishnamurthy and V. Seshdri, "Model Reduction using Routh Stability criterion," IEEE Trans.,Automat. Contrl.,vol.23,pp.729-730,1978.
[4] Automatic control systems B.C.KUO eighth edition, pp.283-288.
[5] R. Prasad ,S.P Sharma and A,K Mittal , "Linear model reduction using the advantages of Mikhailov criterion and factor divison," Journal of Institution of Engineers, vol. 84, pp. 7-10, 2003.
[6] T .N. Lucas, "Baised model reduction by factor division,"Electronics letters ,vol. 20 p.582, 1984.
[7] J.Pal, "An algorithm method for tfhe simplification of linear dynamic systems,"International Journal of control, vol. 43 ,pp 257, 1986.
[8] Y. Shamash, "Truncation method of reduction :A variable alternative," Electronics letters ,vol. 17 pp.97-99, 1981.
[9] S.Mukherjee and R.N.Mishra,"Order reduction of linear system using an error minimization technique,"J. Frank Inst.,vol. 323,pp 23-32,1987.
[10] R.Parthsarthy and S.John, "cauer continued fraction methods for model reduction ," Electronics letters ,vol. 17 no.21 pp.792-793, 1981.
[11] A.M. Davidsion, "Balanced systems and model reduction," Electronics letters ,vol. 22 no.21 pp531-532, 1986.
[12] M. Gopal, control systems (principles and design),Tata Mcgraw Hill,2008
[13] D.R. Choudhury, Modern Control Engneering, Prentice Hall India, 2005.

BIOGRAPHIES

Chandan Kumar received his B.Tech Degree in Instrumentation and control Engineering in 2010 from Netaji Subhash Institute of Technology, Dwarka (New Delhi) and presently pursuing his final year M.Tech from same college. He has been conferred with "Meritorious Student Award" for overall best performance in 10th standard by honorable chief minister of Delhi, Mrs. Sheila Dixit in 2003. He was awarded with first divison in International Mathematics Olympiad level A held in year 2003.

S. K. Jha received his B.Sc.(Engg.) degree in Electrical Engineering from Bhagalpur College of Engineering, Bhagalpur and M.E. degree in Control & Instrumentation from Delhi College of Engineering, Delhi University in 1994 and 2003 respectively. He joined the industry (U.B.Engineering Ltd) in 1995 and Netaji Subhas Institute of Technology (NSIT) as a Lecturer in 1999. Currently he is holding the post of Assistant Professor in the Instrumentation & Control engineering Department at N.S.I.T, New Delhi. His research interests include optimal control, robust control, electric drives etc. He is a Life Member of the Indian Society for Technical Education (ISTE).

Prerna Gaur received her B.Tech and M.E in 1988 and 1996 from G.B. Pant College of Technology, Uttranchal, India and Delhi College of Engineering, Delhi University, respectively. She is PhD in the field of AI based Motion Control of PMSM. She joined the industry in 1989 and Delhi College of Engineering as a Lecturer in 1994. She is an Associate Professor in the Instrument and Control Engineering Division at Netaji Subhas Institute of Technology, Delhi. She is a Life Member of the Indian Society for Technical Education (ISTE) and Senior Member of Institute of Electrical and Electronics Engineers (IEEE). Her research interests includes Power Electronics, Electric Drives, Artificial Intelligence based control etc.

Load Compensation with DSTATCOM and BESS

Alka Singh
Electrical Department
Delhi Technological University
alkasingh.dr@gmail.com

Suman Bhowmick
Electrical Department
Delhi Technological University
su.bhowmick@gmail.com

Kapil Shukla
Electrical Department
Delhi Technological University
kapilstriker@gmail.com

***Abstract*— This paper deals with modeling & control of Distribution Static Compensator (DSTATCOM) and Battery Energy Storage System (BESS) using Simulink and SimPower System in MATLAB environment. The results are presented for a test system with/without DSTATCOM for a wide variety of system disturbances. The modeled DSTATCOM is also tested for load compensation of linear and non-linear loads in both steady state and dynamic conditions. Battery Energy Storage System (BESS) is also modeled, controlled & tested for compensation of load. Simulation results justify enhanced power quality of system with DSTATCOM and BESS under different tested conditions.**

Keywords- DSTATCOM; BESS; Power Quality; SRF; PCC.

I. INTRODUCTION

Electricity supply plays an important role in the economic development and technology advancement throughout the world. The quality and reliability of power supplies relates closely to the economic growth of a country. However, power quality disturbances such as sags, swells, flicker, harmonics, voltage imbalance etc., create a lot of problems in achieving a reliable and quality power supply. To mitigate these problems, power electronics based FACTS devices [1, 2] are used in transmission systems.

The FACTS devices have been used to solve voltage stability problem and attain bulk power transfer. The FACTS based application of power electronic devices can also be effective for the power distribution systems to enhance the quality and the reliability of power delivered to the consumers. A compact solution to the present power quality problems as seen by the utilities and power distributors is offered in form of custom power technology. Custom power (CP) technology [3] utilizes switching equipment and controllers in order to enhance the reliability of electrical energy supplied to consumers. This technology is appropriately applied in modern power system, having high proliferation of power electronics based loads which cause a lot of power quality problems [4, 5] such as voltage imbalance, harmonics, transients etc into the system and corrupts the system performance.

Custom Power Devices [6-8] are used in distribution systems to mitigate power quality problems and a number of configurations are increasing in use world-wide. A custom power device could be series connected, shunt connected or both simultaneously across the system. The amount of compensation offered by the device depends on the design of VSC i.e. DC link capacitor, device rating of IGBT switches and interface inductors. Distribution Static Compensator (DSTATCOM), Dynamic Voltage Regulator (DVR), Unified Power Quality Conditioner (UPQC), BESS are some of the custom power devices used at distribution level.

Load compensation using DSTATCOM in weak ac supply systems [10, 11] has been used in distribution systems for maintaining the source currents to perfect sinusoid. Loads are connected in distribution systems through feeders, which cause voltage drop. A new switching control scheme is used which makes the source current balanced in case of unbalanced loads and makes the supply current harmonic free and of unity power factor. Battery Energy Storage System (BESS) increases the flexibility of control [12, 13] such that different aspects of a system could be controlled at the same time.

II. SYSTEM CONFIGURATION OF DSTATCOM AND BESS

The DSTATCOM configuration considered in the paper consists of a two-level VSC, a dc energy storage device and a coupling transformer connected in shunt with the ac system. Fig 1 shows the schematic representation of the DSTATCOM. The VSC converts the dc voltage across the storage device into a set of three-phase ac output voltages. These voltages are in phase and coupled with the ac system through the reactance of the coupling transformer. Suitable adjustment of the phase and magnitude of the DSTATCOM output voltages allows effective control of active and reactive power exchanges between the DSTATCOM and the ac system.

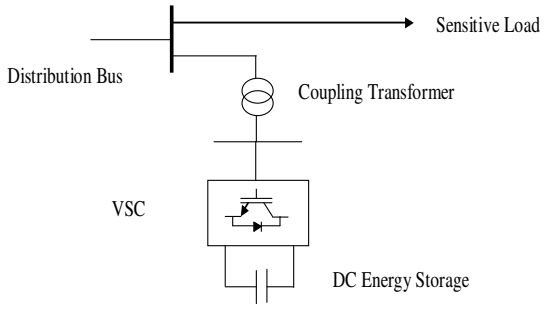

Fig.1. DSTATCOM

978-1-4673-0934-9/12/$31.00 ©2012 IEEE

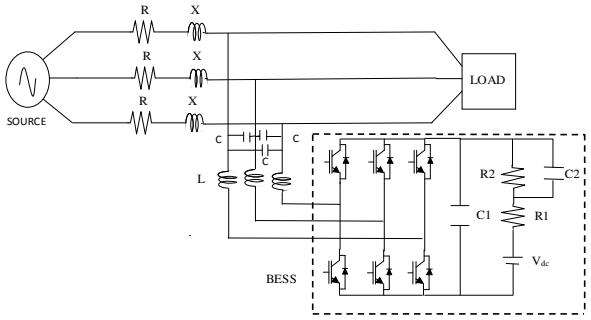

Fig.2. Schematic diagram of system with BESS connected in shunt configuration

Normally the loads are varying in power distribution systems. BESS can be used for delivering the desired amount of active and reactive power required by the load such that the source currents become sinusoidal and the Point of Common Coupling (PCC) voltage is maintained at its reference value. The configuration of BESS as shown in Fig 2 consists of a battery at the DC link; hence the DC link voltage remains constant. A DC battery (800 V) has a linked small series resistance (R1) connected in with a parallel combination of a resistor (R2) and a large capacitor (C2). A DC link capacitor (C1) is also connected as shown. The performance of BESS is tested under dynamic linear load change condition for maintaining the source currents constant and equal sharing of active power between source & BESS. The parameters values are shown in the appendix.

III. CONTROL SCHEME

Synchronous Reference Frame theory [9] is used here for controlling of DSTATCOM and BESS. The synchronous reference frame theory is based on the transformation of currents in synchronously rotating d-q frame. Basic block diagram of this control scheme is shown in Fig 3. The load currents which are in a-b-c frame are first transformed into α-β frame using Clark's transformation as shown in (1), and then these currents in α-β frame are transformed in d-q frame as shown in (2). If θ is the transformation angle, then the currents transformation from α-β to d-q is defined as:

$$\begin{bmatrix} i_\alpha \\ i_\beta \end{bmatrix} = \sqrt{\frac{2}{3}} \begin{bmatrix} 1 & -1/2 & -1/2 \\ 0 & \sqrt{3}/2 & -\sqrt{3}/2 \end{bmatrix} \begin{bmatrix} i_a \\ i_b \\ i_c \end{bmatrix} \quad (1)$$

$$\begin{bmatrix} i_d \\ i_q \end{bmatrix} = \begin{bmatrix} \cos\theta & \sin\theta \\ -\sin\theta & \cos\theta \end{bmatrix} \begin{bmatrix} i_\alpha \\ i_\beta \end{bmatrix} \quad (2)$$

This is also called as Park's transformation. The DC components are extracted from these currents by passing them through a low pass filter (LPF). The extracted DC components i_{ddc} and i_{qdc} are transformed back into α-β frame as shown in (3) using inverse Park's transformation.

$$\begin{bmatrix} i_{\alpha dc} \\ i_{\beta dc} \end{bmatrix} = \begin{bmatrix} \cos\theta & \sin\theta \\ -\sin\theta & \cos\theta \end{bmatrix} \begin{bmatrix} i_{ddc} \\ i_{qdc} \end{bmatrix} \quad (3)$$

Inverse Clark's transformation can now be made to obtain three phase reference currents in a-b-c coordinates from the iα, iβ dc components as shown in (4).The PCC voltages are passed through a PLL for finding out the values of cosθ and sinθ. These values of cosθ and sinθ are used in Park's and Inverse Park's transformation for calculating the required currents.

$$\begin{bmatrix} i^*_{sa} \\ i^*_{sb} \\ i^*_{sc} \end{bmatrix} = \sqrt{\frac{2}{3}} \begin{bmatrix} 1/\sqrt{2} & 1 & 0 \\ 1/\sqrt{2} & -1/2 & \sqrt{3}/2 \\ 1/\sqrt{2} & -1/2 & -\sqrt{3}/2 \end{bmatrix} \begin{bmatrix} i_0 \\ i_\alpha \\ i_\beta \end{bmatrix} \quad (4)$$

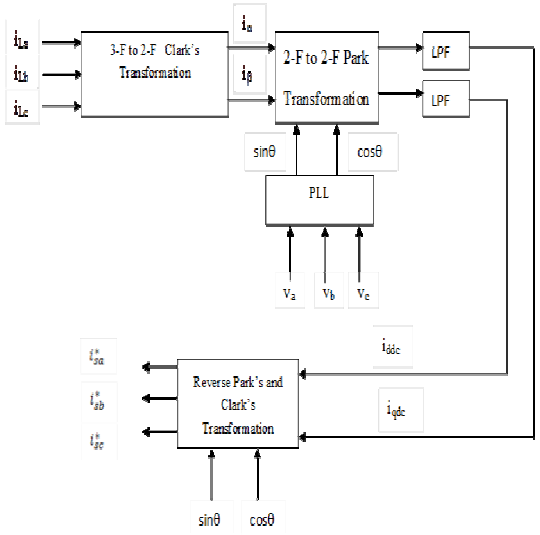

Fig.3. Block diagram of the reference current extraction through SRF theory

IV. MATLAB BASED MODELING OF SYSTEM

In this paper a test system is employed with three phase source feeding a variety of consumer loads. The source is connected to load by a feeder impedance (R, L). The DSTATCOM is connected in shunt configuration at the PCC. The modeled system is tested on different load conditions such as linear load, non linear load, unbalance loads and phase out conditions. A single line diagram of test system is shown below in Fig 4. The system parameters are listed in Table 1. The MATLAB model of test system is shown in Fig 5.

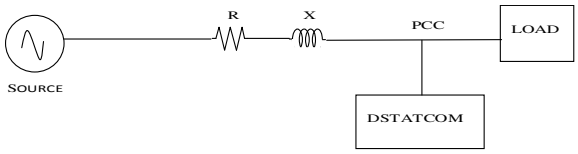

Fig.4. Single Line diagram of Test System

TABLE I. SYSTEM PARAMETERS

Parameter	Value
V_S	415 V, 50 Hz
R	0.05 Ω
L	1 mH
Load	10 kW, 10 kVAR
V_{DC} reference	800 V

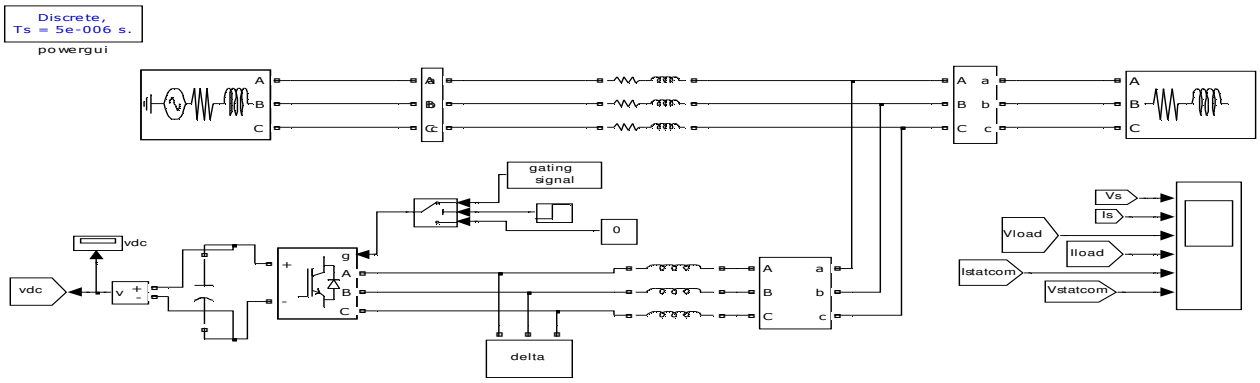

Fig.5. Simulink model of test system

V. PERFORMANCE OF DSTATCOM AND BESS

A. *Performance of DSTATCOM for Linear Load*

In this case a 3-phase series RL load drawing active power component 20kW and reactive power component 10kVAR is considered. Another linear 3-phase series RL load is switched on for a duration of 0.2 sec between 0.2 and 0.4 sec. The additional load draws active power component of 10kW and reactive power of 10kVAR. Fig 6 shows the response of system with load change introduced at t = 0.2 sec which is brought back to normal conditions at t = 0.4 sec. This figure shows the plots of supply currents (i_{source}), DSTATCOM currents ($i_{statcom}$), Load currents (i_{load}), PCC voltage (V_{PCC}) and DC link voltage (V_{DC}) w.r.t time. At t= 0.2 sec as load is increased, there is a voltage dip in PCC voltage due to the increase in load but the DSTATCOM is able to regulate PCC voltage. The PCC voltage is well regulated by the DSTATCOM during sudden increase at t = 0.2 sec and load removal at t = 0.4 sec. DC link voltage is also regulated to its reference value of 800 V.

B. *Performance of DSTATCOM for Non-Linear Load*

In this case a universal diode bridge with different combinations of resistance, inductance and capacitance connected across it is taken as non linear load.

1) *With R-L connected at end of diode rectifier*

In this case a series combination of resistance and inductance of values 100 Ω and 300 mH respectively is connected across the bridge. Fig 7 shows that the DSTATCOM has been able to regulate the PCC voltage to a reference of 339 V and the DC link voltage is also maintained at 800 V reference. THD level of supply currents is observed to be improve from 29.65% to 3.05% with the help of DSTATCOM. The plots showing the waveform & the FFT analysis of supply currents without/with DSTATCOM are shown in Fig. 8 & Fig 9.

2) *With RLC load connected at the end of diode rectifier*

Next, a capacitor of value 200 μF is coneected in parellel with the above series RL load. Fig 10 shows the plots of supply current (isource), DSTATCOM currents (istatcom) and Load currents (iload) of phase 'R', PCC voltage (VPCC) and DC link voltage (VDC) w.r.t time. The distorted source currents become sinusoidal after installation of DSTATCOM as shown in Fig 10. The DC link voltage is also maintained at its reference value of 800 V. The THD value in source current without DSTATCOM is 132.63% which reduces to 4.75% with DSTATCOM. This is also reflected in Fig. 11 & Fig 12 from the waveform and THD plots of supply currents. A comparison of the THD values of supply and load currents is presented for both types of non linear loads considered in this paper.

TABLE II. COMPARISON OF THD ANALYSIS FOR DIFFERENT NON-LINEAR LOADS

Universal diode bridge with	Currents	THD without DSTATCOM	THD with DSTATCOM
RL	i_L	29.65%	29.65%
	i_S	29.65%	3.05%
RLC	i_L	132.63%	132.63%
	i_S	132.63%	4.75%

C. *Performance of BESS*

The same control algorithm, SRF is used for controlling BESS. Two performance cases for BESS control are studied as discussed below.

1) *Equal Sharing of Active Power*

In this case a 3-phase series RL load drawing active power component 20kW and reactive power component 10kVAR is considered. Another linear 3-phase series RL load is switched on for a duration of 0.1 sec from 0.15 sec to 0.25 sec. The additional load draws active power component of 10kW and reactive power of 10kVAR. Fig 13 shows the response of system with load change. The total reactive power is delivered by the BESS and the controller is tuned to maintain the PCC voltage and DC link at their reference values of 339 V and 800 V respectively. At t= 0.15 sec, as load is increased, and the additional active power required by the load is also equally shared by the source and BESS.

2) *Constant Source Power*

The same system parameters are taken but the BESS is now controlled to deliver constant power. Fig 14 shows the response of system with load change. The amount of active power delivered by the source is maintained constant at10kW, while the additional active (10kW) and reactive power (10kVAR) is supplied by the BESS as shown in Fig 14. The PCC voltage and DC link are regulated at their reference values of 339 V and 800 V respectively. The supply currents have a peak amplitude of 45A which is maintained constant.

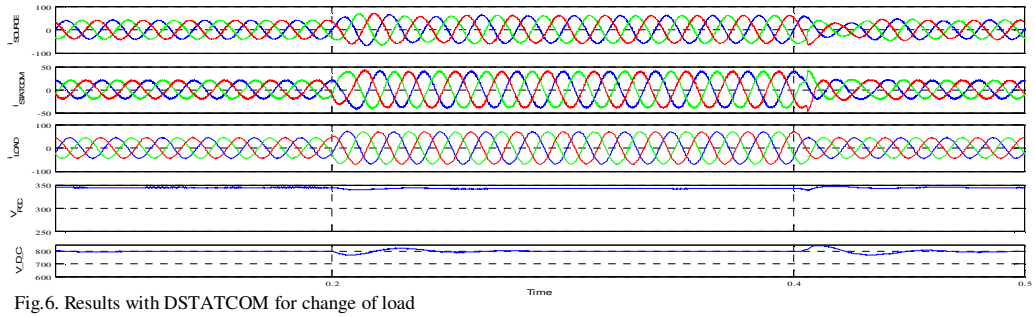

Fig.6. Results with DSTATCOM for change of load

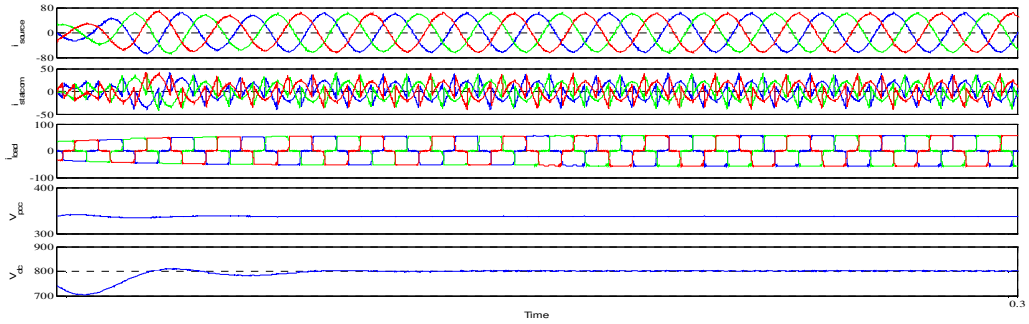

Fig. 7 Results with DSTATCOM for a universal diode bridge with RL load

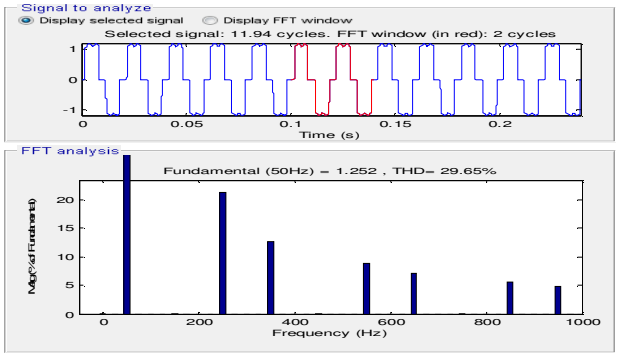

Fig. 8 Source current THD for a universal bridge without DSTATCOM for RL Load

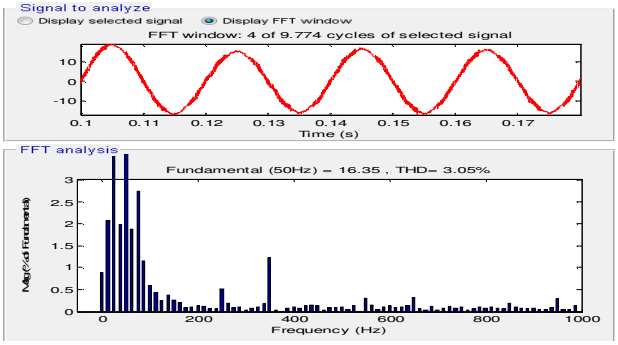

Fig.9. Source current THD for a universal bridge with DSTATCOM for RL load

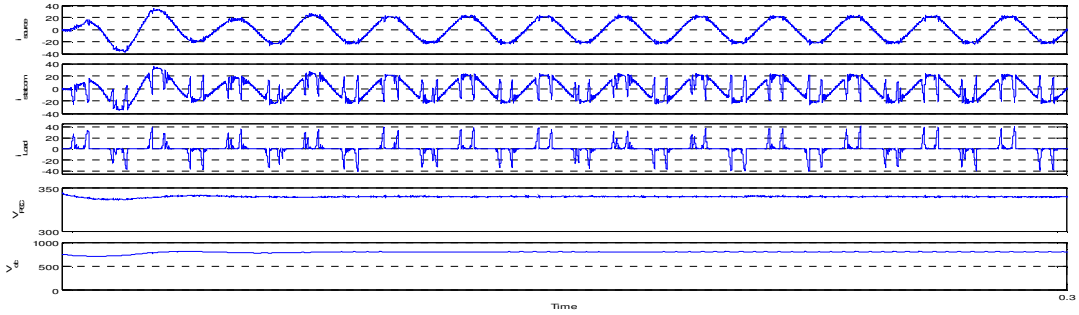

Fig. 10 Results with DSTATCOM for a universal diode bridge with RLC load

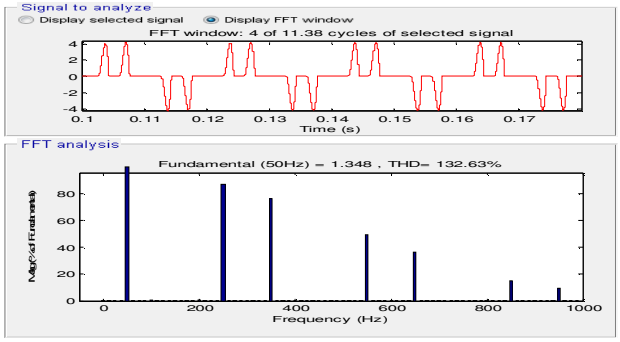

Fig.11 Source current THD for a non linear RLC load without DSTATCOM

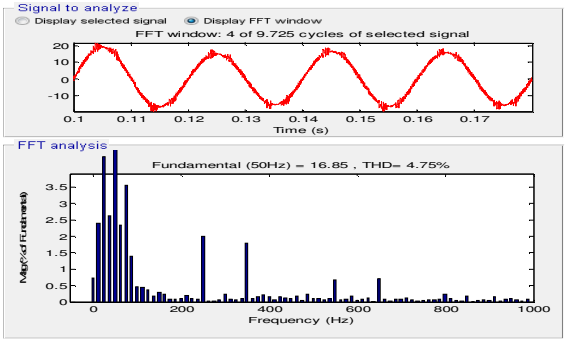

Fig.12 Source current THD for a non linear RLC load with DSTATCOM

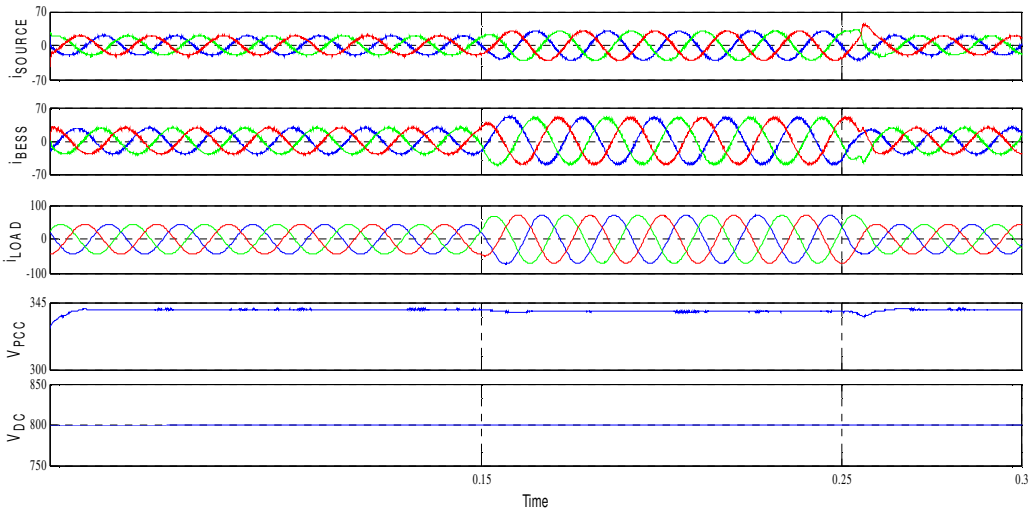

Fig. 13 BESS Equal Active Power Sharing Results

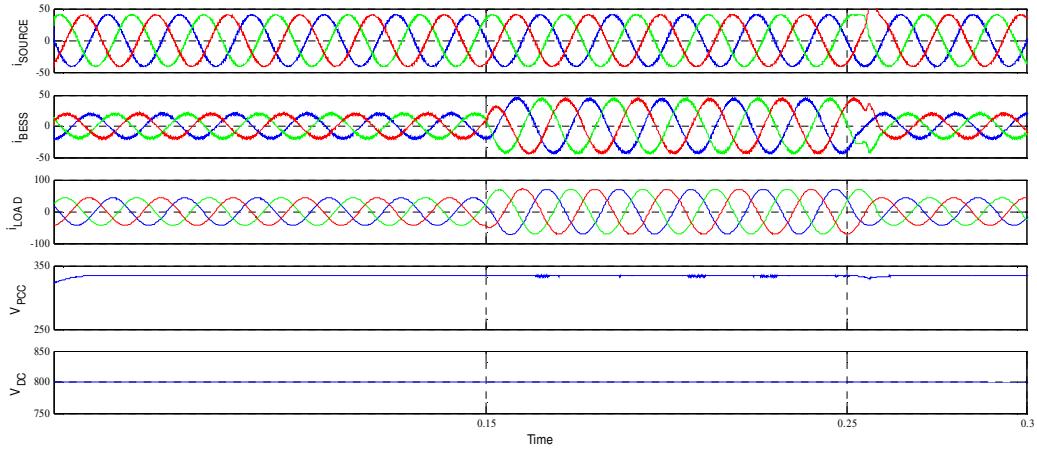

Fig 14 BESS Constant Source Current Results

VI. CONCLUSIONS

In this paper two custom power devices viz. DSTATCOM & BESS have been modeled and simulated in MATLAB environment. The same control algorithm has been applied to DSTATCOM & BESS with slight modification. The performance of DSTATCOM has been analyzed for varying linear and non-linear loads under steady state as well as dynamic conditions. DSTATCOM has been found to regulate PCC voltage under varying load condition and load unbalancing. The performance of DSTATCOM with non-linear loads is also found to be satisfactory and it is able to reduce the supply current THD to less than 5% level as per IEEE 519 standards, even though the load current THD has a high value of 132%. BESS has also been modeled, controlled and simulated for real as well as reactive load sharing. The performance results of BESS with equal load sharing and constant source current under dynamic load conditions have been found to be satisfactory. Both the devices have a huge scope in improving power quality in distribution systems.

REFERENCES

[1] Narain Hingorani & L. Gyugi, Understanding FACTS, Concepts and Technology of Flexible AC Transmission Systems, IEEE Press, 2000.

[2] K. R. Padiyar, "FACTS controllers in power transmission and distribution", New age international publishers (2007).

[3] Ghosh & Ledwich, Power Quality Enhancement using Power Custom Devices , London, Kluwer Academic Publishers,2009

[4] Roger C. Dugan, Mark F. McGranaghan, Surya Santoso & H. Wayne Beaty, Electrical Power Systems Quality, McGraw-Hill publications.

[5] R.Sastry Vedam, Mulukutla S. Sarma, Power Quality VAR Compensation in Power System, CRC Press, 2009.

[6] N. G. Hingorani, "Introducing custom power" , IEEE Spectrum, Vol. 1, No. 6, Jun 1995, pp. 41-48.

[7] Alexander Domijan Jr., Alejandro Montenegro, Albert J. F. Keri, Kenneth E. Mattern, "Custom Power Devices: An Interaction Study", IEEE Transactions on Power Systems, Vol. 20, No. 2, May 2005 pp. 1111-1118.

[8] T.Devaraju, Dr.V.C.Veera Reddy, Dr. M. Vijaya Kumar, "Role of custom power devices in Power Quality Enhancement: A Review**",** International Journal of Engineering Science and Technology Vol. 2(8), 2010, pp. 3628-3634.

[9] B. Singh and J. Solanki, "A comparative study of control algorithms for DSTATCOM for load compensation", in Proc. IEEE ICIT, Dec. 15–17, 2006, pp. 1492–1497.

[10] Rajesh Gupta, Arindam Ghosh, and Avinash Joshi, "Performance Comparison of VSC-Based Shunt and Series Compensators Used for Load Voltage Control in Distribution Systems", IEEE Transaction on Power Delivery, Vol. 26, No. 1, January 2011, pp.268-278.

[11] Arindam Ghosh and Gerard Ledwich, " Load Compensating DSTATCOM in weak ac systems", IEEE Transactions on Power Delivery, Vol. 18, No. 4, Oct 2003, pp. 1302-1309.

[12] B. Singh, Zakir Hussain, "Application of Battery Energy Storage System (BESS) in Voltage Control and Damping of Power Oscillations", Conference on Industrial and Information Systems, ICIIS 2010, July/August 2010, pp. 514-519.

[13] B.Singh, Alka Adya, A. P. Mittal and J. R. P Gupta, "Application of Battery Energy Operated System to Isolated Power Distributed Systems", IEEE Conference on PEDS, 2007, pp. 526-532.

APPENDIX

Source Voltage (rms) – 415 V L-L

Frequency – 50 Hz

Line Parameters – R = 0.05 Ω, L = 1 mH

Voltage Source Converter: DC link capacitor C_{dc} = 1500 μF

V_{dc} ref = 800 V

AC inductor = 2.2 mH

Non-Linear Load – Universal Diode Bridge with

connected load of R = 100 Ω, L= 300 mH,

C = 200 μF

PI Constants for DC controller Kp = 0.3, Ki = 8

PI Constants for AC controller Kp= 0.01, Ki = 0.1

Parameters of BESS – V_{dc} = 800 V, R_1 = 0.01 Ω, R_2 =

10000 Ω, C_1 = 1500 μF, C_2 = 300000 F,

L = 2.2 mH

Master-Slave Current Control DGs in a Microgrid for Transient Decoupling with Mains

Vishal Verma, Member, IEEE
Department of Electrical Engineering
Delhi Technological University, Delhi, INDIA
vishalverma@dce.ac.in

Girish Gowd Talapur
Department of Electrical Engineering
Delhi Technological University, Delhi, INDIA
girish223@gmail.com

Abstract— **Modern power system is envisaged to incorporate microgrids in the power grids to realize efficiently flexible and reliable flow of power by effectively utilizing renewable energy sources and storage systems. The microgrids in such cases thus operate in grid connected and islanded mode. The paper presents a control scheme that is used to implement grid connected and islanded operation of master distributed generation (DG) unit and current control of slave DGs so as to share the load as per their rating, and absorbs the transients arising from load perturbations and DG source switching. Master DG is operated in indirect current control while in grid connected operation and is operated with PWM switching to present a voltage source for slave DGs which are always operated in direct current control mode under central command generating references for different DGs based on sensed voltage and current at different nodes. Simulated results under MATLAB environment are presented to validate the effectiveness of the control scheme.**

Keywords-; microgrid; load sharing; distributed generation

I. INTRODUCTION

Renewable Energy Sources (RES) and their effective utilization as distributed generation (DG) sources is a matter of prime importance now-a-days. The DG units employs grid tied voltage source converters (VSC) used in parallel to form a microgrid which cater to the demanded load and additionally improves the quality and reliability of the supply [1][2][3]. DGs are either operated in Grid connected/Islanded mode or in Standalone mode depending on the situation. For grid connected mode, the voltage and the frequency of the DGs are governed by the utility grid, whereas in Islanded operation of the microgrid the voltage and frequency are regulated locally.

VSCs acts as grid couplers for DGs operating in voltage controlled mode with distinct droop characteristics [4]. Such operation provides flexibility to each source operating with inputs from point of common coupling (PCC). And, P/f and Q/V droop characteristics control the active power flow and reactive power flow [4][5][6][7]. And if correct control of real/reactive power is not done, huge circulating current may result, making it vulnerable as they generally are of low capacity. When the VSCs are operated as current source under grid connected mode, each DG needs to be operated under central command to decipher current references for each parallel connected DG catering to clustered area. Under such case insertion or desertion of DGs does not disturb the voltage profile of the grid, and their restricted current capacities provide auto protection. Such configuration offer good transient response compared to their connection as voltage source. Other issues remains similar to both, such as operation control, tackling faults, sag/swell mitigation, synchronization, voltage regulation and other Power Quality issues [8].

Alternators in the grid automatically share the demanded load according to their capacities through droop characteristics, which in turn alters their frequency and voltage. Since VSC is static power electronic converter and does not alter frequency with over loading/under loading naturally, thus only voltage regulation is thus marred by deficit/surplus of both real and reactive power in the microgrid [9]. Thus a demarcation in real/reactive power is needed to be done by determining the real and reactive components of current drawn from the net connected loads, and the storage system at PCC. The DGs and storage systems are intelligently operated to fulfill the transient loading conditions and voltage regulation [10].

As a current controlled source Master Slave technique is widely reported in the literature for operation of microgrid in Islanded/standalone mode with mix of voltage and current control. One DG unit acts as “Master unit with highest rating” and sets the voltage and frequency of the microgrid, while other units adopts the voltage and frequency [11][12][13]. Recent research has demonstrated the operation mode of a DG in both grid connected mode (current control) and islanded mode (voltage control) with intelligent load shedding [12]. Wherein, for a microgrid, several DGs are required to be moved in and out as a group from the main grid besides sharing of real and reactive power amongst them. An effective control is therefore required to alter the mode of operation of master DG in grid connected/off grid operation, besides fast sharing of power in current controlled DGs to absorb transients.

This paper describes the control strategy used for microgrid for operation in grid connected/Islanded mode. The generated central commands incorporates the sharing of connected load as per their capacities and keeping a drawl of constant power from the mains so as to help in estimation of load for efficient power management and make transient free operation of the mains. All the VSCs operate as current source respecting the voltage and frequency provided by the mains. In the islanded mode the load matching is done as per the capacity of available generation on the microgrid. The master is operated under its capacity, by appropriate sharing of loads by other DGs. The track on capacity limitation of master is kept by monitoring the voltage at the terminals, where power is drawn from it at unity power factor. To better support the microgrid is islanded mode third harmonic injection in PWM switching is also considered for switching of VSC in master DG.

978-1-4673-0934-9/12/$31.00 ©2012 IEEE

II. System Configuration

Fig.1 depicts the schematic diagram of considered microgrid which is connected to mains through a static transfer switch (STS). The considered micro grid comprises of three DG's (DG1, DG2 and DG3), and local RL load, connected in parallel through a single distributed line. The considered DG's are comprised of micro sources with battery support and are represented by a battery. The LCL filter at the terminals of each VSC reduces the harmonics in the line. At every node current sensing is done in micro grid for exact computation of the loads. In case the load is connected to one end and sources to the other, this configuration eases out the use of extra sensors for load estimation to generate the references, which in turn decreases the cost and complexity of the microgrid formation. The system is akin to 'Master-Slave' configuration operating but operating in current controlled mode, with the supply grid acting as the master in grid connected mode, and, DG-1 acting as master in islanded/standalone mode. The DG sources are invariably configured to work as current source adding current to the nodes. Any perturbation in load power is catered by DG sources, upto their capability. In the Islanded/standalone mode the voltage template of the erstwhile grid tied mode is freezed by the PLL which provides the reference template to the Master DG for generation of voltage by switching the mode from current control mode to PWM mode.

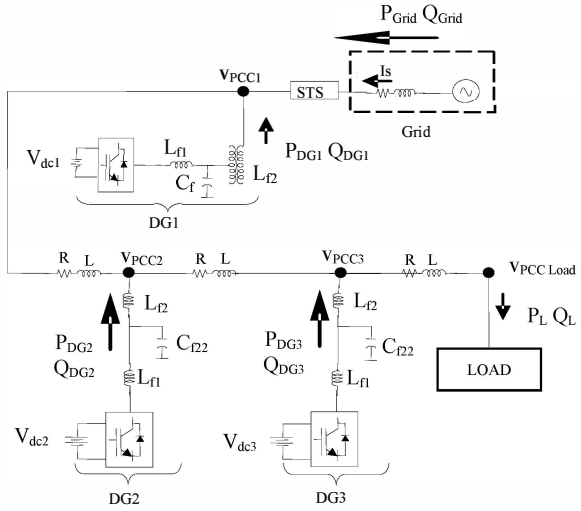

Fig.1: Microgrid in Grid connected mode.

III. Control Theory

Fig.2 depicts the block diagram of control scheme adopted for the proposed microgrid. The control scheme is based on demand and supply equilibrium.

The sensed load current is transformed from abc to dq frame by using Clarke and park transformation (1), the sin and

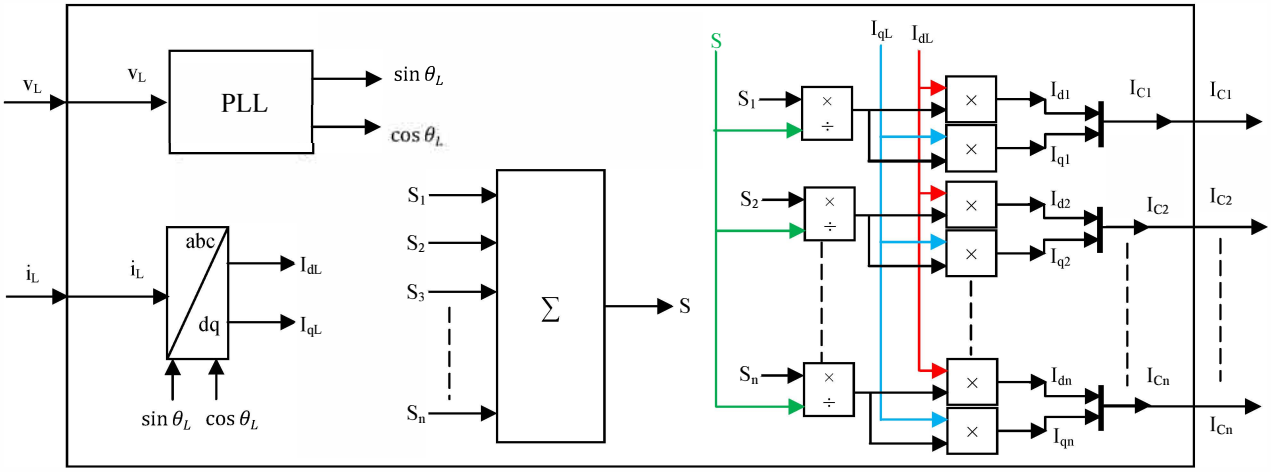

a: Centralized Control Unit

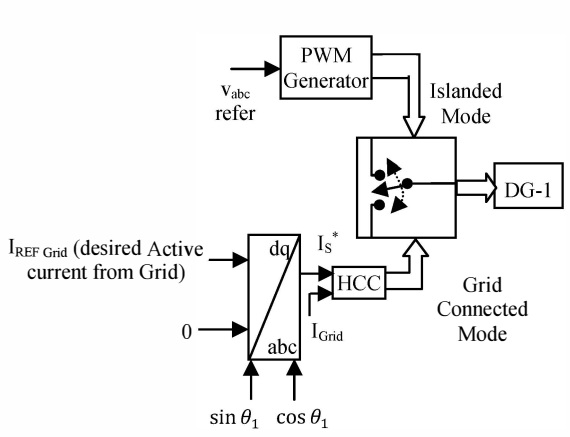

b: Control scheme for Master

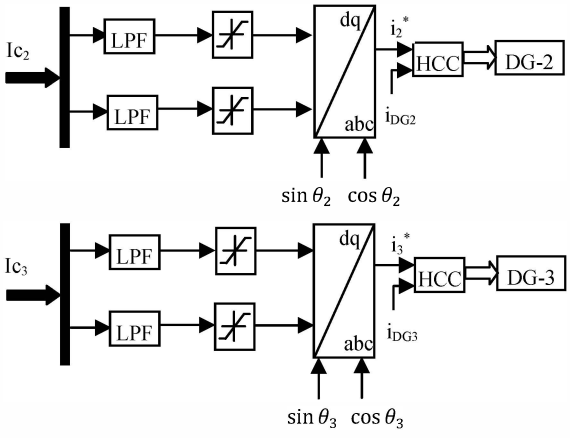

c: Control scheme for Slaves

Fig.2: Control Scheme of Microgrid

cos signals for transformation is obtained from load PCC point.

$$\begin{bmatrix} f_d \\ f_q \end{bmatrix} = M(\theta) \begin{bmatrix} f_a \\ f_b \\ f_c \end{bmatrix} \quad (1)$$

Where

$$M(\theta) = R(\theta)C = \frac{2}{3}\begin{bmatrix} \cos(\theta) & \cos\left(\theta - \frac{2\pi}{3}\right) & \cos\left(\theta - \frac{4\pi}{3}\right) \\ \sin(\theta) & \sin\left(\theta - \frac{2\pi}{3}\right) & \sin\left(\theta - \frac{4\pi}{3}\right) \end{bmatrix}$$

and

$$R(\theta) = \begin{bmatrix} \cos\theta & \sin\theta \\ -\sin\theta & \cos\theta \end{bmatrix}; C = \begin{bmatrix} 1 & -\frac{1}{2} & -\frac{1}{2} \\ 0 & \frac{\sqrt{3}}{2} & -\frac{\sqrt{3}}{2} \end{bmatrix}$$

$\theta = \omega t$ and ω is the fundamental frequency of the power system.

The centralized control unit shown in Fig.2-a generates the current commands in dq frame for all DG's to supply real and reactive power according to their ratings.
Where S1, S2, S3, S4, --------Sn is the rating of DG1, DG2, DG3, DG4, ---------- DGn, the total capacity of the Microgrid is given by:

$$S = S1 + S2 + S3 + S4 + \text{--------} + Sn \quad (2)$$

then, reference current signal for K_{th} DG_k is given by

$$I_{CK} = i_L \times \frac{S_K}{S} \text{ (where k=1,2,3,-------,n)} \quad (3)$$

where S_K is the rating of K_{th} DG and i_L is the total load current.

Fig.2-b and Fig.2-c depicts the basic control block for master and slaves respectively. It comprises of a low pass filter, saturation block, dq/abc conversion block, PWM generator and hysteresis current controller (HCC) for control of the VSC's such that commanded reference current is tightly followed. Fig.2-c depicts the command reference obtained from central controller in dq frame for slave DGs which is filtered by LPF are then inverse park and clarke transformed to three phase reference currents. The reference currents so obtained when compared with actual currents of the DG, in the HCC, provides gating signals for the corresponding VSCs.

Fig.2-b shows the control scheme of DG1. When the microgrid is operating in grid connected mode The DG1 is operated in indirect current control mode in order to keep mains appears as constant current voltage source at unity power factor.

Whenever the reference voltage and frequency at the interface of the microgrid, deviate from the standards then the microgrid is islanded from the mains. In Islanded mode, DG1 is operated in voltage control mode to maintain the micro grid voltage and frequency, to facilitate the continued operation of other slave DG's in current control mode. The control for DG1 acts similar to DG's when the microgrid is operating in grid connected mode.

IV. MATLAB SIMULATION

The Grid, Isolation transformer, DGs with input side LCL filter, STS, Control unit, distributed line impedance respected as RL line impedance, three phase RL load and passive RC filter are modeled in MATLAB using Power System Block set. Fig. 3 depicts the setup used to study the performance of the Microgrid in Grid connected mode/Islanded mode with proposed control scheme through simulation.

The Grid block consists of a three-phase voltage source "infinite bus" supplying the microgrid to gauge the performance of the Microgrid with proposed scheme under specified conditions. The considered loads to evaluate the effectiveness of the proposed scheme are star connected 100 KVA RL load at 0.8 pf depicted in Fig. 3. Out of this load 35 KVA load is considered critical, which is all the time supported. The RC high pass passive filter is used to absorb the harmonics in voltage at load terminals. The Intentional islanding has been done with the help STS to study the performance of micro grid in Islanded mode. The simulated results are studied to gauge the performance of Microgrid under grid connected/Islanded modes. Table I depicts parameters of the considered system.

TABLE I. PARAMETERS OF THE CONSIDERED SYSTEM

DG1 Power Rating	40 KVA
DG2 Power Rating	25 KVA
DG3 Power Rating	15 KVA
Isolated Transformers Power rating	100 KVA
Line Impedance	0.01334 Ω, 0.03 mH
Load	35-100 KVA at 0.8 pf
LCL filter (L_{f1}, C_f, L_{f2})	1.5 mH, 15 µF, 0.5 mH
Passive filter (RC)	1Ω, 100µF
Passive filter	1µF
DC Voltage (Each DG)	800v

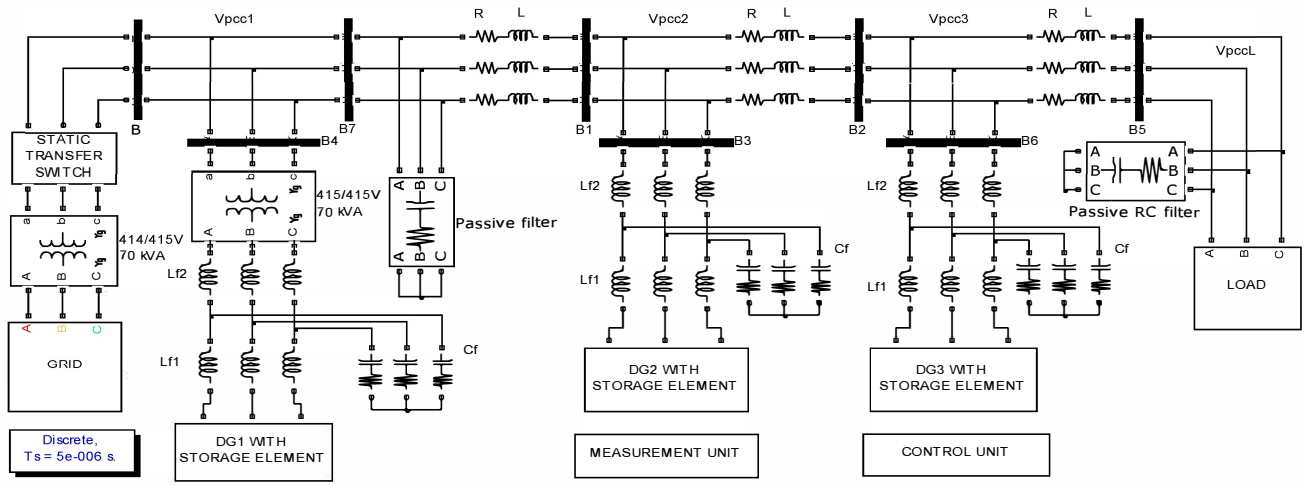

Fig. 3 Simulink model of the considered system

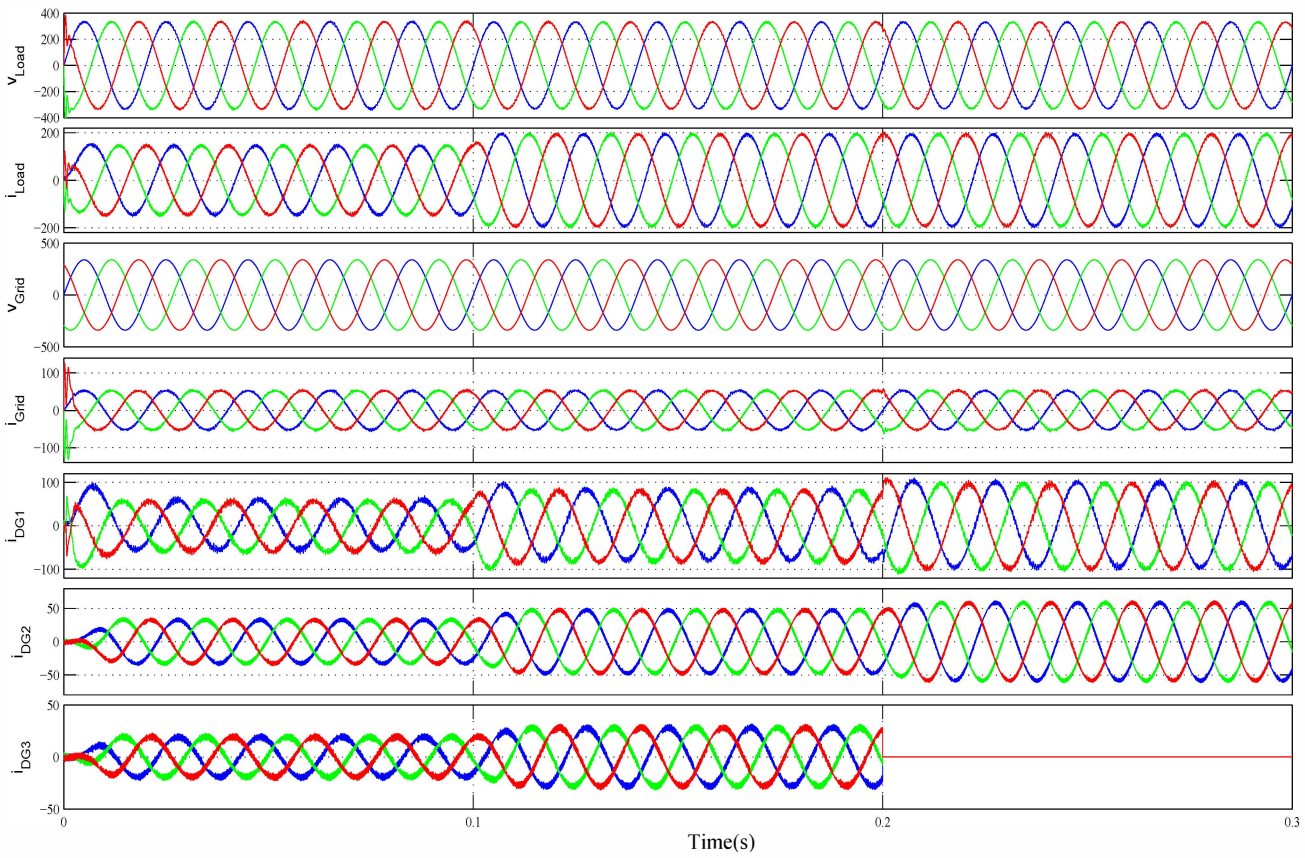

Fig.4: Current and Voltage wave forms of Microgrid under Grid connected mode

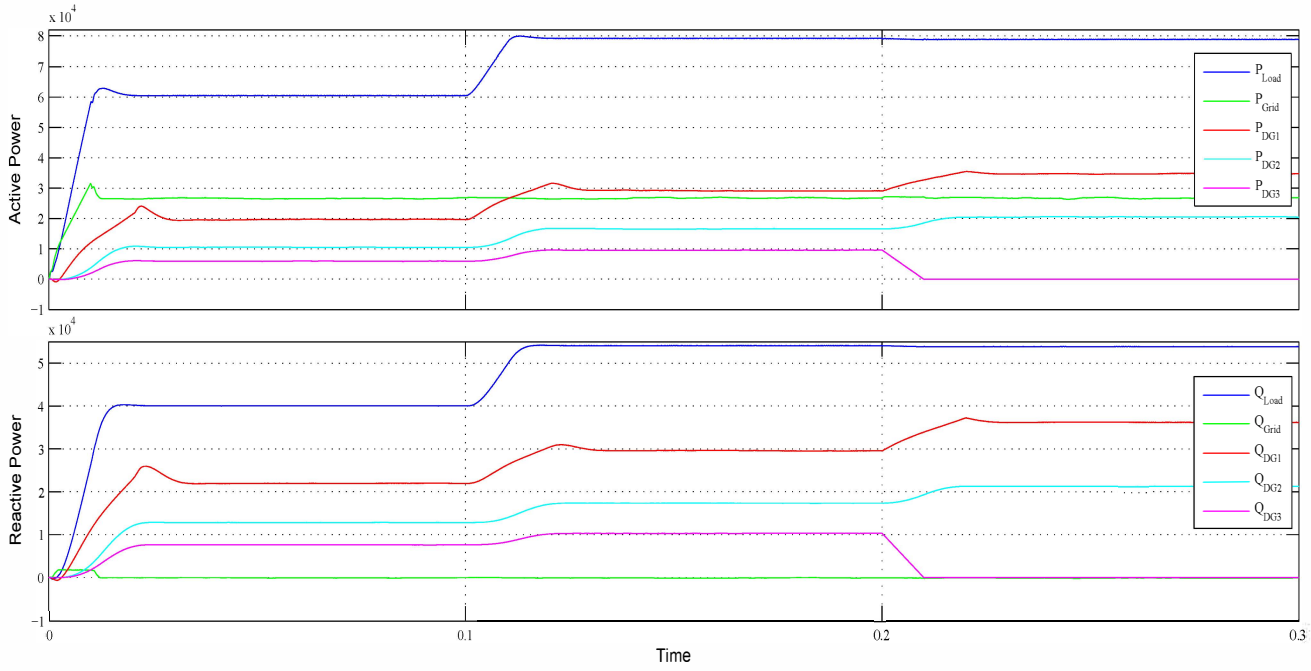

Fig.5: Active and Reactive Power wave forms of Microgrid under Grid connected mode

V. PERFORMANCE EVALUATION

The performance of the system is studied under two cases normally: Grid connected mode and Intentional Islanding mode.

A. Grid connected mode

The mains is considered supplying constant power of 26.7 KW to the microgrid, and the balance power is supplied by the active DG's in the microgrid. It may be observed from Fig(4), that initial load demand of 72.67 KVA at 0.8 pf is catered by mains which contributes 27.5KW, and the remaining 34 KW

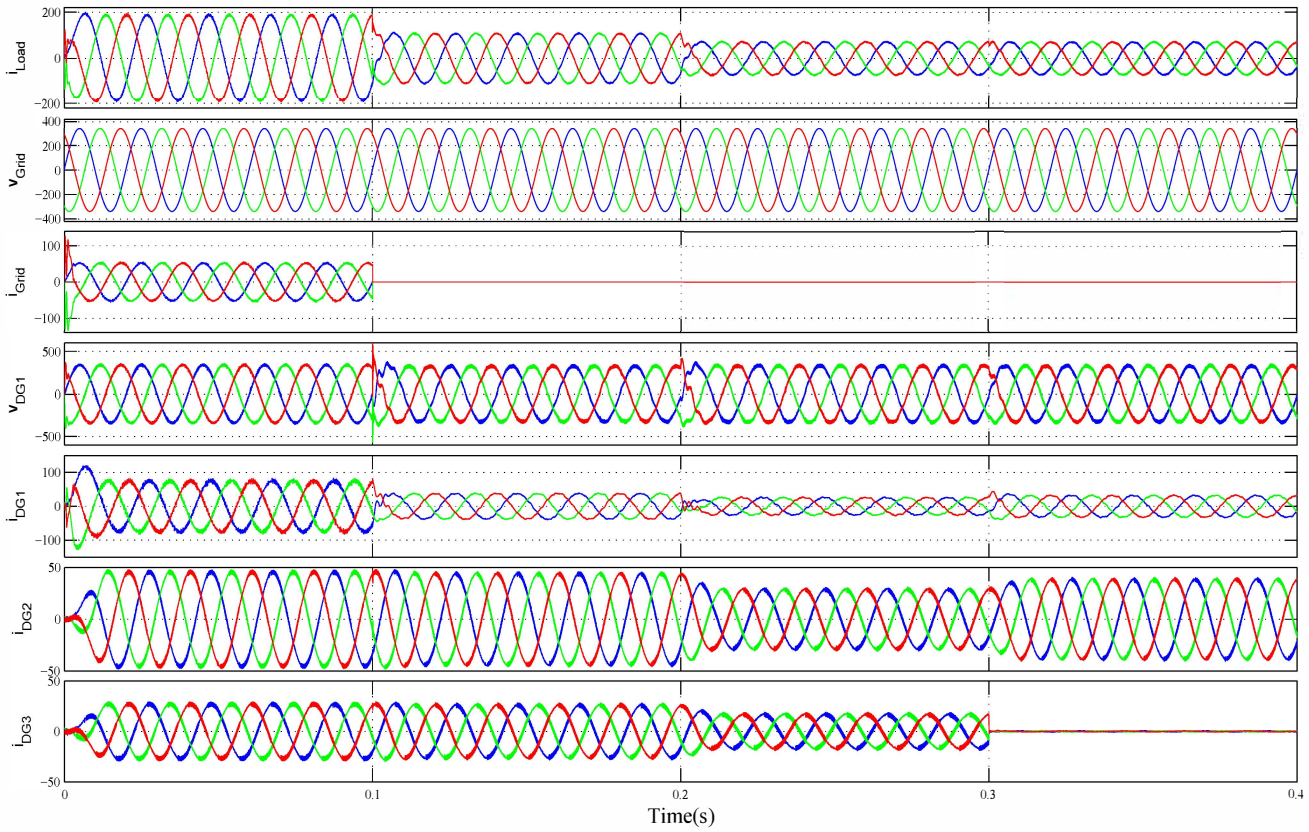

Fig.6: Current and Voltage wave forms of Microgrid under Islanded mode

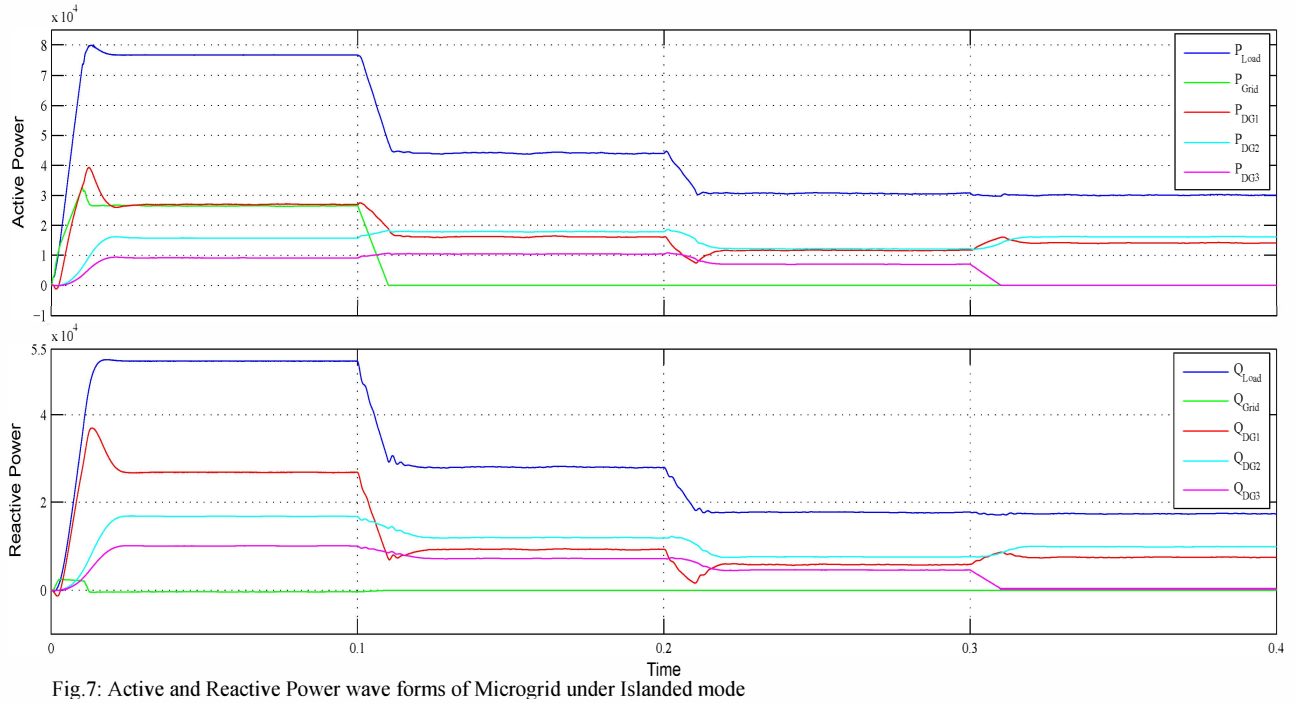

Fig.7: Active and Reactive Power wave forms of Microgrid under Islanded mode

and 40 KVAR demand is contributed by DG's depending upon their ratings as 19.7 KW and 21.98 KVAR, 10.54 KW and 12.8 KVAR and 5.91 KW and 7.63 KVAR respectively from DG1, DG2 and DG3 (including microgrid losses). It may also observe that current drawl from the mains is at unity power factor where current is shown to be in phase with the voltage.

From Fig.5 it may be observed that, the transients due to disturbances like load perturbations, DG failures ect. is taken care by the DG1. Starting at t=0, during the transient period the active and reactive power contribution by DG1 is increased from 0 KW to 24.1 KW and 0 KVAR to 26 KVAR, and after the transient period the active and reactive power contribution

of DG1 is settled to 19.7 KW and 21.98 KVAR. When at t=0.1s the load is increased to 95.87 KVA at 0.825 pf, the increased demand is supplied by the active DG's in the system where as the main's contribution remains constant. During transient period the active and reactive power contribution of DG1 is increased from 19.7 KW to 31.5 KW and 21.98 KVAR to 31 KVAR, and after the transient period the active and reactive power contribution by DG1 is settled to 29.2 KW and 29.61 KVAR. At t=0.2 sec, DG3 fails, ultimately making the current IDG-3 =0, its share of power is then contributed by other DG's which are active. The transient here also are contributed by DG1 and the same may observed in Fig.4.

B. Islanded mode

Control of DGs become critical while its operation in islanded mode amidst their limited capacities. It is therefore load corresponding to sum of capacities of slave DGs and 50% capacity of master DG is kept in the Islanded microgrid and remaining non critical load is shedded. The shedding of the non-critical load is done in a chunk as soon as islanded condition is detected. Fig.6 depicts the microgrid response to load perturbations and failure of DG3 from the microgrid. From t=0s to t=0.1s the grid connected operation is considered, accordingly connected load of 93 KVA at 0.82 pf is supported. The contribution of mains remains of 26.7 KW and remaining power of 50.15 KW and 52.22 KVAR is shared by DG's as per their ratings as 27 KW and 26.82 KVAR, 15.7 KW and 12.8 KVAR and 5.91 KW and 7.63 KVAR respectively from DG1, DG2 and DG3 (including microgrid losses). At t=0.1s it may be observed that microgrid is islanded from mains and connected load is reduced to 52 KVA at 0.84 pf. It may further be observed that distortion due to switching is now present due to DG1 taking over as a voltage source. It may also be clear that transition of DG1 from current source to voltage source is made with in half cycle and voltage is restored almost instantly with freezed synchronizing template such that operation of DGs are not distributed, and they share the load as per their rating as 18.45 KVA at 0.86 pf, 21.3 KVA at 0.83 pf and 12.6 KVA at 0.82 pf from DG1, DG2 and DG3 respectively, maintaining sinusoidal current wave shape (refer Fig.6). At t=0.2s load is decreased to 35 KVA at 0.85. pf to match the local generation by DGs. The power is accordingly shared as 13 KVA at 0.9 pf, 14 KVA at 0.85 pf and 8.32 KW at 0.85 pf between DG1, DG2 and DG3. As explained before in grid connected mode, here also the transient was taken care by DG1, its contribution is decreased from 16 KW to 7.419 KW and 9.2 KVAR to 1.5 KVAR. After the transient period its contribution is settled to11.6 KW and 5.7 KVAR. It may be observed that the capacity of DG1 is not breached even if it is acting as a voltage source. When at t=0.3s DG3 fails, its capacity is shared between DG1 and DG2 as 15.9 KVA at 0.88 pf and 18.84 KVA at 0.85 pf respectively by ensuring that capacity of DG1 is never breached. In Fig.7 it may be observed that DG2 has shared the load greater than the corresponding ratio.

VI. CONCLUSION

The new control scheme for distributed generation sources in the microgrid using indirect current control approach has been successfully demonstrated through simulation results. The scheme has been shown working satisfactorily with faster dynamics for sharing of loads during load perturbations and failure of DG sources in both grid connected and Islanded conditions. The transients arising from switching of loads or DG sources are mitigated locally in the microgrid and are not passed to the grid. The indirect current control in islanded mode always ensure that capacity of master is never breached, which acts as voltage source, while all other DGs are in current control mode. The scheme is simple, fast sassily implementable for operation in both modes of operation and switching between them. The scheme inherently is capable of improving the power quality both in grid connected and Islanded mode of operation. The scheme also power the way for easy integration of DGs without any amendment in the hardware.

REFERENCES

[1] G. Joos, B.T. Ooi, D. McGillis, F.D. Galiana, R. Marceau, "The potential of distributed generation to provide ancillary services", Proc. IEEE PES'00 Conf., 2004, pp. 1762-1767, vol.3.

[2] W. Xiongfei, J.M. Guerrero, C. Zhe, "Distributed energy resources in grid interactive AC microgrids", in Proc. IEEE PEDG'10 Conf.,16-18 June, 2010, pp. 806-812.

[3] P.Chiradeja and R. Ramakumar, "An approach to quantify the technical benefits of distributed generation", IEEE Trans. Energy Conversion, vol. 19, no.4,pp. 764-773, Dec. 2004.

[4] D. M. Divan , M.C. Chandorkar and R. Adapa, "Control of parallel connected inverters in standalone ac supply systems", IEEE Trans. Industry App., vol. 29, no.1, pp.136-143, Jan 1993.

[5] J.M.Guerrero, J. Matas, J.Miret ,L. G. Vicuna and M. Castilla, "Wireless-control strategy for parallel operation of distributed-generation inverters", IEEE Trans. Industrial Electronic, vol.53, pp.1461-1470, Oct 2006.

[6] A. Woyte, B. Bolsens, J. Driesen, J. Keybus, K. Brabandere and R. Belmans, "A voltage and frequency droop control method for parallel inverters", IEEE Trans. Power Electronics, vol. 22, no.4, pp. 1107-1115, July 2007.

[7] A. Engler and N. Soultanis, "Droop Control in LV-grids", in Proc. IEEE Future Power Systems Conf., 18 Nov 2005, pp. 6.

[8] A.Ghosh, F.Zare, G. Ledwich and R. Majumder "Load sharing and power quality enhanced operation of a distributed micro grid", Renewable Power Generation IET, vol.3, pp. 109-119, 2008.

[9] U.Borup, F. Blaabjerg, P.N. Enjeti," Sharing of nonlinear load in parallel-connected three-phase converters", IEEE Trans. Industry Applications, vol.37, no.6, pp. 1817-1823,Dec 2001.

[10] J.M. Guerrero, J. Uceda and Lijun Hnag, "Control of distributed uninterruptible power supply systems", IEEE Trans. Industrial Electronics, vol.55, no. 8, pp. 2845-2858, Aug 2008.

[11] K. Siri, C.Q. Lee, T.F. Wu, "Current Distribution Control For Paralle1 Connected Converters: Part I", IEEE Trans. Aerospace and Electronic Systems, vol.28, no.3, pp. 829-840,Jul 1992.

[12] I.J. Balaguer, F. Z. Peng, S. Yang, Q. Lei, and U. Supatti, " Control for grid-connected and intentional islanding operations of distributed power generation", IEEE Trans. Ind. Electronics, vol. 58, no.1, pp. 147-157, Jan 2011.

[13] C.L. Woo, K.L. Taeck, H.L. Sang, H.K .Kyung, S.H. Dong, Y.S. In, "A master and slave control strategy for parallel operation of three-phase UPS systems with different ratings", Proc. IEEE APEC'04 Conf.,2004, pp. 456-462, vol.1.

IOSR Journal of Electronics and Communication Engineering (IOSR-JECE)
e-ISSN: 2278-2834, p- ISSN: 2278-8735. Volume 4, Issue 5 (Jan. - Feb. 2013), PP 56-59
www.iosrjournals.org

Microstrip Antenna for WLAN Application Using Probe Feed

Amit Kumar[1], Prof.P.R.Chadha[2]
[1](Electronics & Communication Engneering, Delhi Technological University, Delhi,India)
[2](Electronics & Communication Engneering, Delhi Technological University, Delhi,India)

Abstract : *Microstrip patch antennas have been widely used in a various useful applications, due to their low weight and low profile, conformability, easy and cheap realization. A low profile patch antenna for WLAN application is proposed in this paper. This proposed antenna is made by using the probe feeding and aperture coupled feeding methods. This antenna is designed in order to improve the impedance bandwidth and obtain the circular polarization without using truncated corners in patch. The impedance bandwidth will be increased by making slots onto the patch. This unequal parallel slots patch antenna is the modified structure of E patch antenna and U slot Patch antenna. This patch antenna provides a bandwidth of around 16.4% with 1.5 VSWR. The simulation process has been done through high frequency structure simulator (HFSS). The properties of antenna such as bandwidth , S parameter, VSWR have been investigated. This paper also aims at comparing between different feeding methods.*

Keywords *– Aperture coupling, HFSS,Microstrip patch antenna, Probe feed, Return Loss, VSWR (Voltage Standing Wave Ratio).*

I. INTRODUCTION

A microstrip antenna consists of a very thin metallic patch placed on conducting ground plane, separated by a dielectric substrate . A microstrip patch consists of a radiating patch of any planar geometry (e.g. Circle, square, Ellipse, ring and rectangle) on one side of a dielectric material substrate and a ground plane on the other side. Microstrip antennas have numerous advantages such as lightweight, low profile, easy fabrication and simple modeling. They can be designed to operate over a large range of frequencies (1- 40 GHz) and easily combine to form linear or planar arrays. It can generate linear, dual, and circular polarizations. The microstrip antenna has different feeding techniques like probe fed, aperture coupled, proximity and insert feed. The substrate dielectric constant used for microstrip antenna generally low (typically ~ 2.5) to reduced fringing field but for less critical applications . The proposed antenna is designed for 2.45 GHz frequency with E shaped patch and U slot patch . The proposed antenna is made by using probe fed and aperture coupled fed and simulated by HFSS'11. A typical patch antenna is Shown in Figure 1.1

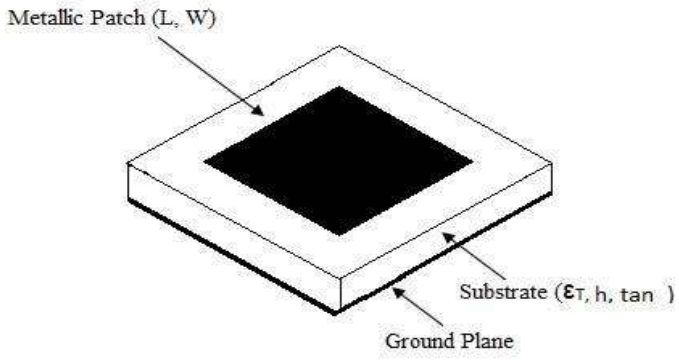

Fig No-1.1 **Microstrip Antenna**

II. TYPES OF FEED

2.1 Coaxial Probe Feed

Coaxial feed is the simplest feed for microstrip antennas. In this, an inner conductor of coaxial line is attached to the radiating patch while outer conductor is connected to ground plane. The structure of coaxial probe feed is display in figure 2.1. It has spurious radiation because the radiating and feeding systems are disposed on two sides of ground plane and shielded from each other. The proposed antenna is designed for 2.45 GHz frequency for WLAN application. This antenna has patch size (L X W) mm with $_r$ = 2.2 dielectric substrate. The serious limitation of microstrip antenna is narrow bandwidth, which is usually few percent (<1%).

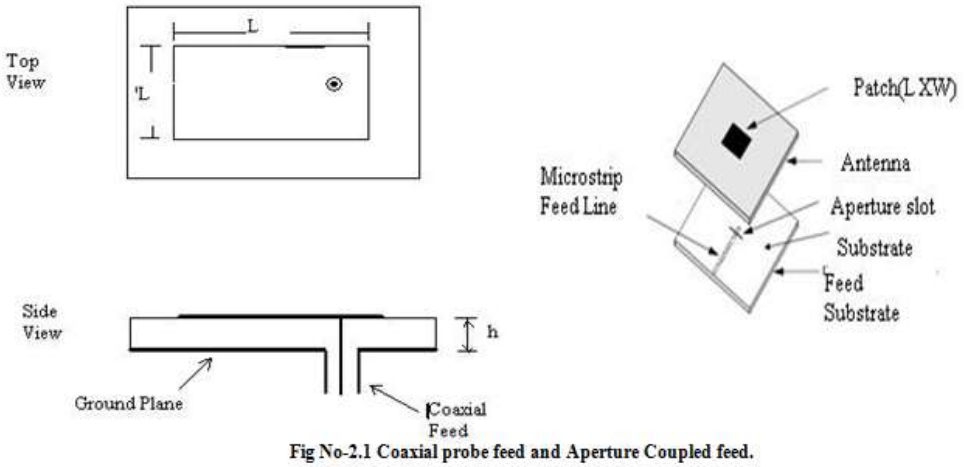

Fig No-2.1 Coaxial probe feed and Aperture Coupled feed.

2.2 Aperture Coupled Feed

In this the radiating patch is etched on the top of the antenna substrate and feed line is etched on the bottom of substrate. The thickness and dielectric constants of these two substrates may thus be chosen independently to optimize the distinct electrical functions of radiation and circuitry. The basic structure of aperture coupled microstrip antenna is shown in figure 2.1.

III. ANTENNA GEOMETRY FOR PROBE FEED

In this paper, We used various patch shapes like U slot, E Shaped and some another unequal shapes slots in rectangular patch with different dielectric constants. But the best result is provided by unequal E shaped slot with rectangular patch.

3.1 E Shaped Rectangular Patch Antenna

In this paper, the well known technique of an E shaped patch used for a wide band width. An E-shaped patch antenna is easily formed by cutting two slots from a rectangular patch [4]. By cutting the slots from a patch, gain and bandwidth of microstrip antenna can be enhanced. For this proposed antenna, size of ground plane is (L X W) 76 X 88 mm and thickness of dielectric substrate is 6.7 mm with r = 2.2.The geometry of E shaped patch antenna is shown in table 1. 1

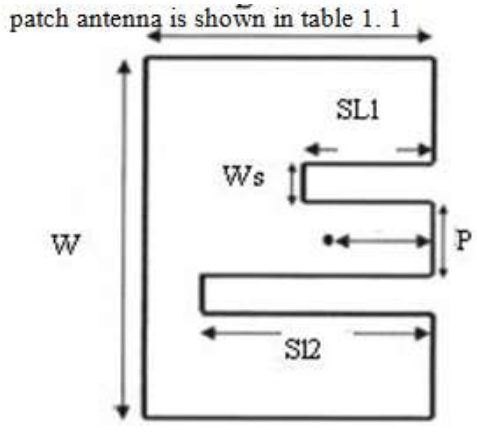

W	L	Ws	SL1	SL2	P	F	H	£r
48	36	6.3	30	30	11.4	9	6.7	2.2

TABLE 1. The Dimensions of Patch In MM

Figure 3.1 Geometry of Unequal E Shaped Patch Antenna

This E shaped patch antenna provides a 7.8 % (2.34 - 2.53 GHz) impedance bandwidth with 5.8 dB gain. The figure 3.2 (a) and 3.3 (a) is shown the return loss in dB and smith chat for equal size of slots in patch. The E shaped patch antenna is designed here, has -33 dB return loss. The gain curve is shown in figure 3.4 (a). This antenna provides good VSWR (~1.02).

When the slot S_{L1} gets shorter, it forms the unequal slots E shaped patch antenna as shown in fig 3.1 [5]. This unequal E shapedpatch antenna provides circular polarization. This antenna provides 16.4 % (2.15 GHz -

2.53 GHz) impedance bandwidth at -10 dB return loss and 6dB gain.

IV. Antenna Design Results

The figures 4.1 , 4.2 and 4.3 are showing the return loss in dB and smith chat for unequal length of slots in patch. The E shaped patch antenna designed here has near about (-32) dB return loss. The gain curve is shown in figure 4.4 , this antenna provides good VSWR (~1.5) . Table 2 shows simulated results.

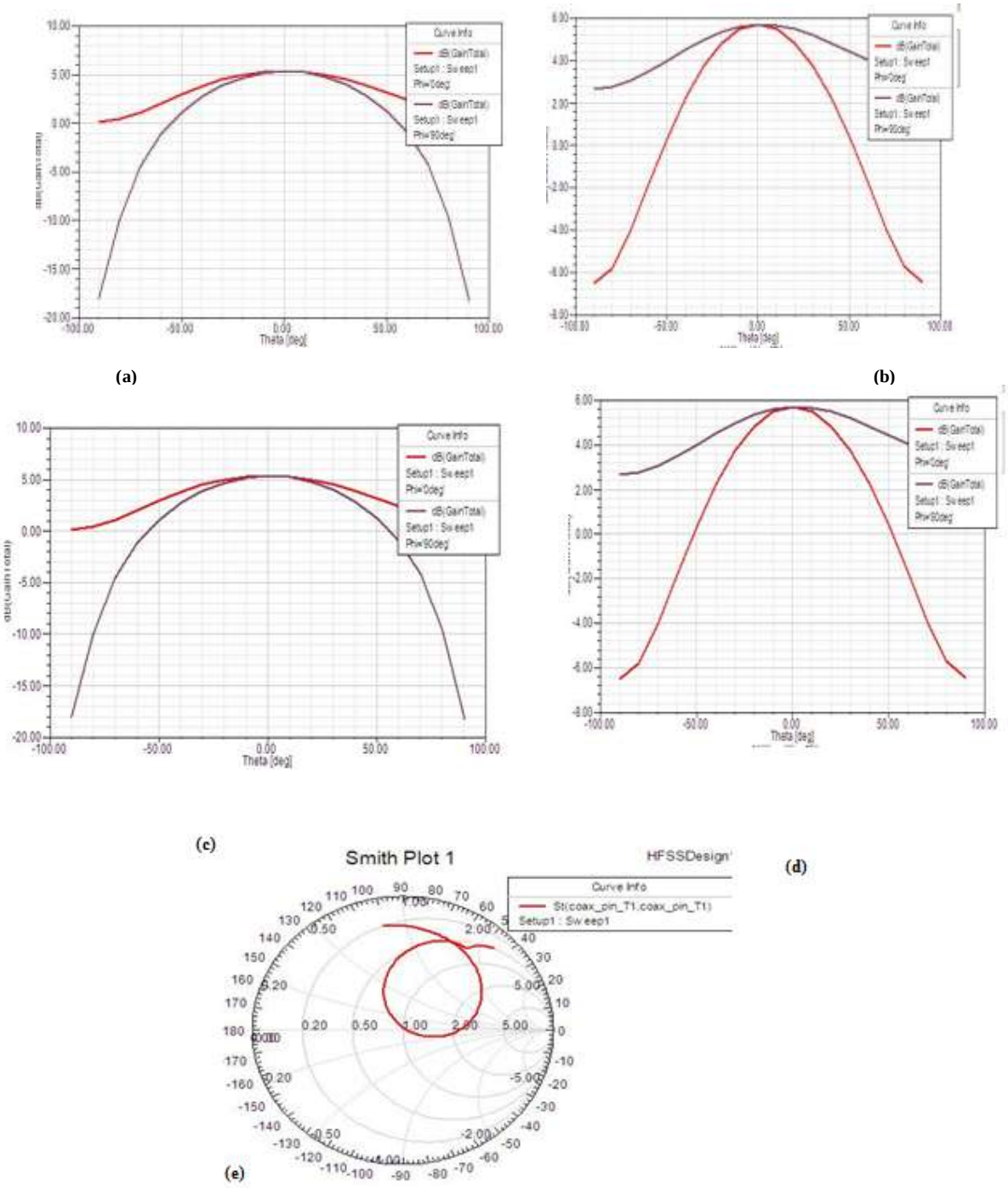

Fig No-4.1a, b, c, d, e, Antenna Design Results.

Patch Shape	Frequency	Gain	Return Loss	Bandwidth
E Shaped Patch	2.45 GHz	5.6 dB	-33 dB	7.8 %
Unequal arms E Shaped Patch	2.43 GHz	6 dB	-31.2 dB	16.4 %

TABLE 2. Simulated Results For Probe Feed Patch Antenna

V. Conclusion

An E shaped microstrip patch antenna is designed and by observing the simulated results we can say that antenna is resonating at 2.45 GHz .which is most suited for WLAN application .From the above obtained results we can say antenna is resonating at 2.45GHz ,and antenna will be used in WLAN application. The design is simulated in HFSS.

A small-size Microstrip antenna for WLAN Application using probe feed and aperture feed is proposed and successfully implemented. From the comparative study of different configurations of feeding techniques, it is concluded that unequal slot in patch provides a bandwidth of 16.4 % with 6 dB gain and near about 1.06 VSWR and an aperture coupled feed microstrip antenna provides a bandwidth of around 24% with 1.04 VSWR. This proposed microstrip antenna enhanced the impedance bandwidth and provides good matching. This antenna is simulated by HFSS'11

REFERENCES

Journal Papers:

[1] K. F. LEE1, K. M. LU, K. M. MA, AND S. L. S. YANG1, "ON THE USE OF U-SLOTS IN THE DESIGN OF DUAL-AND TRIPLE-BAND PATCH ANTENNAS" IEEE ANTENNAS AND PROPAGATION MAGAZINE, VOL. 53, NO.3, JUNE 2011.

[2]. Qinjiang Rao, Tayeb A. Denidni, "A New Aperture Coupled Microstrip Slot Antenna" IEEE Transactions on Antennas and Propagation, Vol.53, No. 9, September 2005.

[3]. .Subodh Kumar Tripathi1, Vinay Kumar2, "E-Shaped Slotted Microstrip Antenna with Enhanced Gain for Wireless communication" International Journal of Engineering Trends and Technology- July to Aug Issue 2011.

[4] D. M. Pozar, "Microstrip antenna aperture-coupled to a microstripline," Electron. Lett**.,** vol. 21, no. 2, pp. 49-50, Jan. 1985.

[5]. Antenna Theory, C.Balanis, Wiley, 2nd edition (1997), Chapter 14. ISBN 0-471-59268-4.

[6]. Ahmed Khidre, Kai Fang Lee, Fan Yang, and Ate' Eisherbeni "Wideband Circularly Polarized E-Shaped Patch Antenna for Wireless Applications" IEEE Antennas and Propagation Magazine, Vol. 52, No.5, October 2010.

[7]. Hall, P. S. Wood, C and Garrett, C, _"Wide bandwidth microstripcantennas for circuit integratio", Electron. Lett. , 15, pp. 458-460, 1979.

[8]. Pues H. F. and Van De Capelle A. R. _"Impedance-matching of microstrip resonator antennas", Proceedings of the North American Radio Science Meeting, Quebec, p. 189, 1980.

[9]. Ravi Kant and D.C.Dhubkarya, _"Design & Analysis of H-Shape Microstrip Patch Antenna", publication in the _Global Journal of Research in Engineering, Vol. 10 Issue 6 (Ver. 1.0), pp. 26-29, Nov. 2010.

[10]. Punit.S.Nakar, "Design of a Compact microstrip Patch Antenna for use in Wireless /Cellular Devices. Florida University,2004..

Mitigation of Induction Generator Effect Due to SSR with STATCOM in Synchronous Generator

S.T.Nagarajan
Electrical Engineering Department,
Delhi Technological University, Delhi, India.
email:selukka@yahoo.com

Narendra Kumar
Electrical Engineering Department,
Delhi Technological University, Delhi, India.
email:dnk_1963@yahoo.com

Abstract— **Torsional oscillations of the shaft in steam turbine driven synchronous generator is form of Subsynchronous resonance (SSR) in power system. But SSR can also be revealed in the form of induction generator effect (IGE) in power system. This paper analyses the possibility of the IGE effect of SSR in synchronous generators and proposes its mitigation technique. Flexible AC Transmission System (FACTS) devices can be used to enhance the performance of the transmission line. STACOM a FACTS device suitable for enhancing power transfer capability and dynamic VAR support in power system is proposed for the mitigation of SSR due to IGE. The performance of the proposed device has been tested on the IEEE First bench mark model for SSR studies, to mitigate the IGE due to SSR. Time domain simulations have been carried out with DIGSILENT Power Factory for conformation.**

Keywords—Subsynchronous Resonance; Induction generator effect; STATCOM; Series compensation

I. INTRODUCTION

Subsynchronous resonance (SSR) in series compensated line is a well documented phenomenon. Failure of the shaft in steam turbine generator due to SSR was first reported at Mohave Generating station in Southern Nevada [1]. But the SSR phenomenon was first predicted long before this first incidence [2] in the form of overvoltage. Steam turbine generators are more prone to torsional interaction [TI] effect of SSR than the hydro generators. To prevent steam turbine generator shaft from damages caused by SSR various devices and techniques have been proposed in literature [3]. However SSR may reveal itself in the form of overvoltage as induction generator effect (IGE) in series compensated system [4]. So there is always a possibility of SSR due to IGE of SSR even in hydro generators.

From the literature it was found that the TI effect of SSR has been analyzed and well understood compared to the IGE effect of SSR. Also mitigation techniques available in literature correspond mainly to TI effect of steam turbine generators. Most of the mitigation techniques proposed was tested at a compensation level where the TI effect is at its maximum value [3]. Even though IGE effect is possible due to SSR, scant information is available for the mitigation of IGE which can occur in steam turbine generator and even in hydro generators connected to series compensated system.

The analysis of SSR in literature has been mainly performed by eigenvalue method, frequency response or damping torque analysis and time domain analysis. Each method has its own merits and limitations. Eigenvalue analysis is accurate and best suited for small systems. Frequency response or Damping torque analysis can be performed for approximate results. Time domain analysis is the best but limited by the computation time requirements and hence not suitable for very long duration of simulations [4]. Also two benchmark models are available for the analysis of SSR and comparisons of results [5-6]. The First benchmark model for the study of SSR [5] has been considered in this study for analysis.

Flexible AC transmission systems (FACTS) have been employed in modern power system due to its capability to work as VAR generation and absorption systems. STATCOM a FACTS device belongs to second generation Static VAR Compensator (SVC) based on voltage sourced inverter and has better reactive power support even at low voltages [7]. STATCOM can be placed at the centre of the transmission line or at the Generator terminal for reactive power support. For this work STATCOM was considered to be placed at the generator terminal for reactive power support and investigated for its applicability to damp IGE effect of SSR in series compensated line. STATCOM uses a self commutating device like GTOs and can be designed as two level six-pulse bridge, three level twelve-pulse bridge, and forty eight pulse converter. The forty eight pulse converter has superior performance as the output current of the converter almost nears the sinusoidal form and the harmonic distortion is minimum compared to others [8]. The STATCOM considered in the study is a three level six pulse bridge converter with PWM technique.

O.Saito *et al* [9] has proposed suppression of self-excited oscillations by excitation control. A.Ajami et al [10] discusses a hybrid Fuzzy/LQR method for damping torsional oscillations using STATCOM.

In this work a study has been performed on the IEEE first bench mark model for SSR studies to analyse the conditions under which IGE effect was revealed. Also a mitigation technique with a STATCOM is proposed. Nonlinear time

978-1-4673-0934-9/12/$31.00 ©2012 IEEE

domain simulations are carried out using DIgSILENT Power factory [11] to verify STATCOM performance to damp out the IGE.

The rest of the paper is organized as follows: Section II briefs the SSR phenomenon. Section III describes the study system, the model of series compensated network. Section IV presents a case study with and time domain results. Section V concludes the paper.

II. SUBSYNCHRONOUS RESONANCE

The phenomenon of SSR can be explained as follows [1]: When a line is series compensated it results in excitation of SSR currents at electrical frequency

$$f_n = f_s\sqrt{\frac{X_C}{X_L}} \quad (1)$$

Where X_c= reactance of the series capacitor; X_L= reactance of the line including generator and transformer; and f_s= the nominal frequency of the power system. These currents result in rotor torques and currents at the complementary frequency:

$$f_e = f_S \pm f_n \quad (2)$$

These currents results in subsynchronous armature voltage components which may enhance subsynchronous armature currents to produce SSR.

SSR manifests in three forms [4]
(1)Torsional interaction: Torsional interaction (TI) involves both electrical and mechanical dynamics. This may occur when the electrical resonant frequency is near the complement of a torsional resonant frequency of the turbine generator (TG) shaft system.

(2)Torsional amplification: This is generally referred to as transient torque on (TG) shaft resulting from the SSR currents in the network caused by faults or switching operations.

(3) Induction generator effect (IGE) or self excitation: Self excitation of the electrical system alone is caused by induction generator effect
In this work only IGE effect is considered. The IGE can be explained from the following equations. For the nominal system frequency f_s and rotor frequency fm the rotor operates at a slip

$$s_s = \frac{f_s - f_m}{f_s} \quad (3)$$

One of the complementary frequencies of (2) is above the synchronous speed hence called super synchronous frequency and the other is below the synchronous speed hence called subsynchronous frequency. At this subsynchronous frequency, the slip s_{SSR} is given by

$$s_{SSR} = \frac{f_e - f_m}{f_e} \quad (4)$$

Since f_e is normally less than f_m, slip $s_{SSR} < 0$ for SCIG. Hence from the steady state equivalent circuit of IG shown in Fig.1 the equivalent rotor resistance R'_r/s at subsynchronous frequency is negative. If the magnitude of this resistance exceeds the resistance of the armature and network sum, the system has a negative resistance at this subsynchronous frequency. This can result in self-excitation leading to sustained oscillatory growing armature currents known as IGE effect.

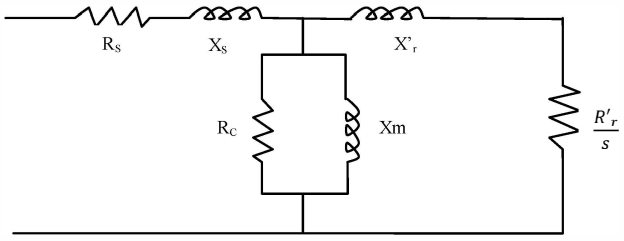

Fig. 1. Equivalent circuit of induction generator.

III. STUDY SYSTEM

The entire power system components represented with their non linear equations/models for the IEEE first benchmark power system model for SSR studies shown in Fig.2 has been simulated on DIgSILENT Power factory. The system parameters for generator and transmission line has been taken form ref [5] given in Appendix.

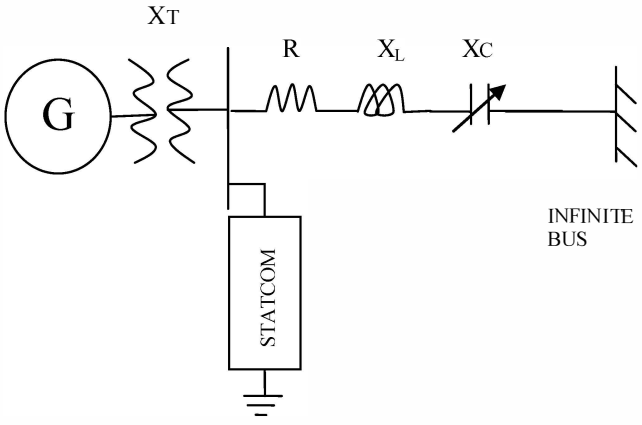

Fig. 2. System Model

As only the IGE effect of the SSR has been analysed, the turbine shaft parameters were not taken into account and generator rotor is represented with a single lumped mass as shown in Fig.3. It has been assumed that the turbine generator shaft is very rigid and is considered to rotate in unison. Also the friction and self damping of the generator was neglected so that the simulation reflects the worst self damping.

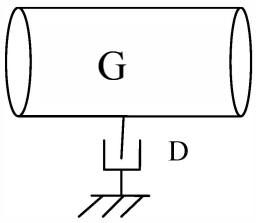

Fig. 3. Lumped model of the generator

From the discussion in the Section II it can be stated that the IGE effect can be revealed only when

i. The magnitude of the equivalent rotor resistance viewed from stator side of the generator is greater than the summation of the resistance of transformer and transmission line.
   Or
ii. The summation of the resistance of transformer and transmission line is less than the equivalent rotor resistance viewed from the stator side of the generator.

In practical condition both these are possible but needs to be taken care to avoid the IGE during planning a new generating station with existing transmission line or new transmission line with existing generating station. In this study the transmission line parameters has been varied with the data of generator given in ref [5] to find the compensation level at which IGE is revealed.

The IGE effect was analysed for the condition at which IGE effect was revealed in the study system and STATCOM was connected to the generator bus and tested for the mitigation of IGE. The STACOM considered in the study is two level converter with PWM technique. The control structure of the STATCOM is a simple Proportional Integral (PI) controller for both quadrature currents. The detailed operation of STATCOM is given in ref [8]. The schematic representation of the controller for the STATCOM is shown in Fig.4. It has two control loops. The outer voltage control loop and the inner current control loop

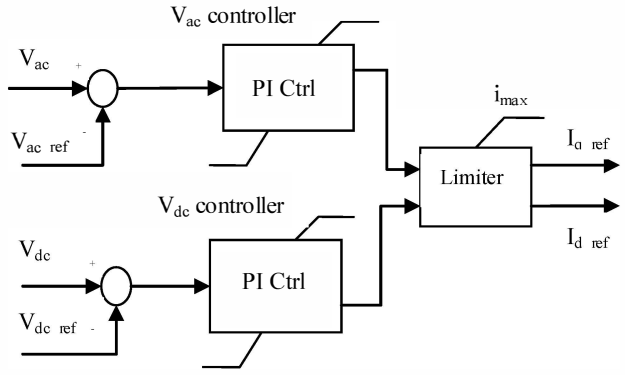

Fig. 4a. Structure of STATCOM outer voltage control loop

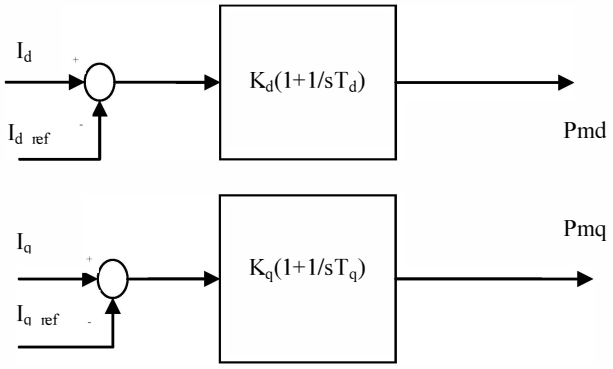

Fig. 4b. Structure of STATCOM inner current control loop

The following section deals with the simulation study results.

IV. SIMULATION STUDY

The system considered is a modified IEEE FBM [5] as shown in Fig.2 with STATCOM of rating 100MVA at the generator bus on high voltage side of transformer for reactive power support, simulated on DIGSILENT Power factory. Load flow study was performed to keep the synchronous generator at full load, 0.9 pf at rated terminal voltage of 1.0pu and all the system variables were initialized.

The study has been performed for two cases:

A. With out STATCOM for transmission line resistance 5.603ohms and transmission line resistance 2.603 ohms
B. With STATCOM connected for transmission line resistance as 2.603 ohms

The system has been observed for oscillations due to IGE with respect to

i. Electric torque and
ii. Generator terminal voltage
iii. STATCOM reactive power and active power

A. Analysis of study system without STATCOM

Case a: with transmission line resistance R=5.603 ohms

The study was performed for a compensation of 50%, 70% and 90%. A three phase fault is applied on the generator bus after reaching steady state at time t=0 s and removed after a duration of 0.075s As the turbine generator is modeled into a single mass representation in the study, no torsional interaction is observed and it is seen from Fig. (5-7) that the rotor speed and generator voltage oscillations are damped due to the damping in the system and the SSR due to induction generator is not revealed with even 90%compensation.

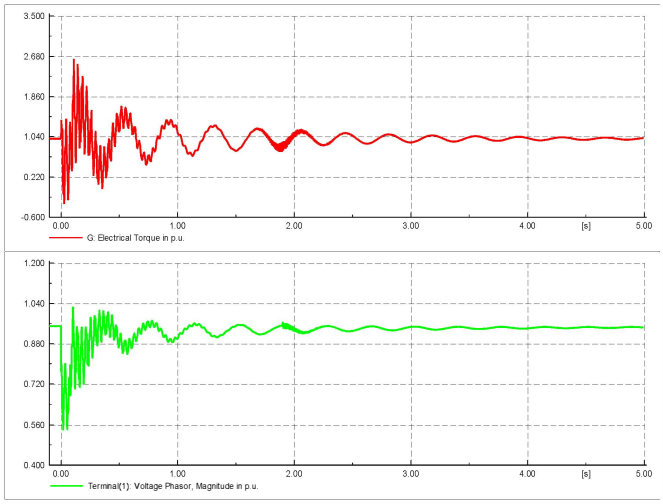

Fig. 5. Electric torque and Terminal voltage of generator for 50% compensation

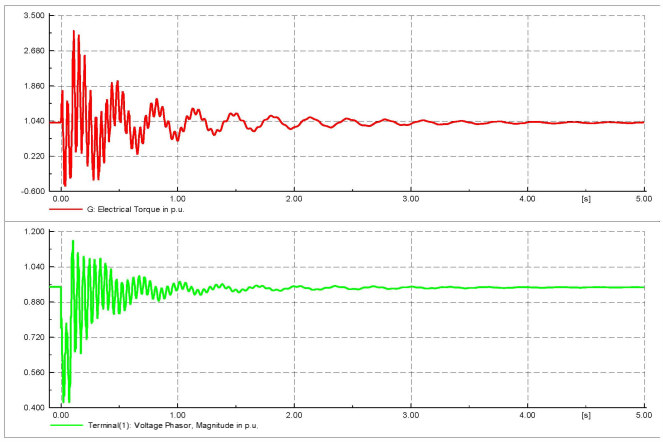

Fig. 6. Electric torque and Terminal voltage of generator for 70% compensation

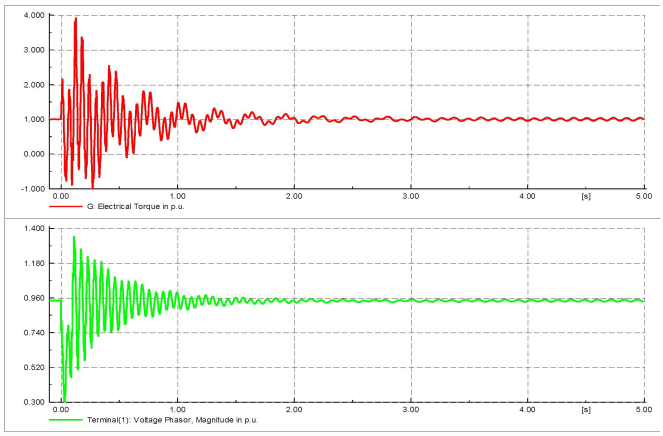

Fig. 7. Electric torque and Terminal voltage of generator for 90% compensation

Case b: with transmission line resistance R=2.603 ohms

The simulation was repeated as in Case a, but with lower resistance of the transmission line with 2.603ohms. From Fig. (8-10) it can be seen that the rotor speed and generator voltage oscillations are damped due to the damping in the system till 70% and the SSR due to induction generator is not revealed, but with 90%compensation IGE is revealed and the system becomes eventually unstable.

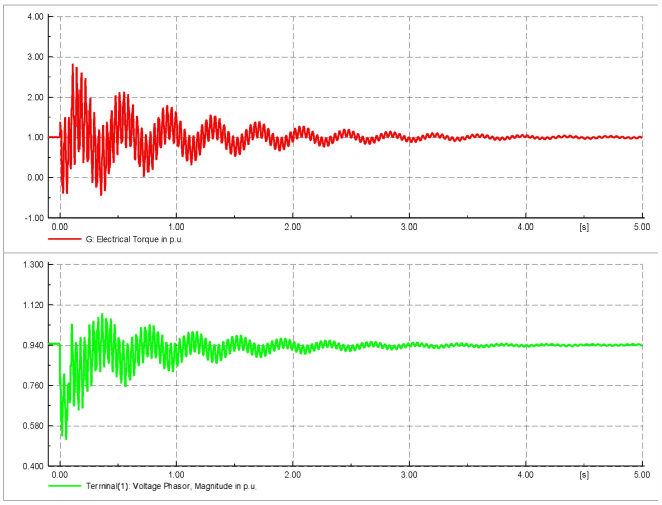

Fig. 8. Electric torque and Terminal voltage of generator for 50% compensation

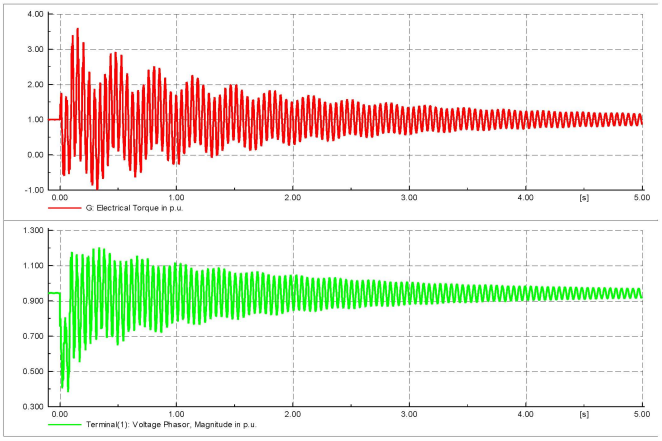

Fig. 9. Electric torque and Terminal voltage of generator for 70% compensation

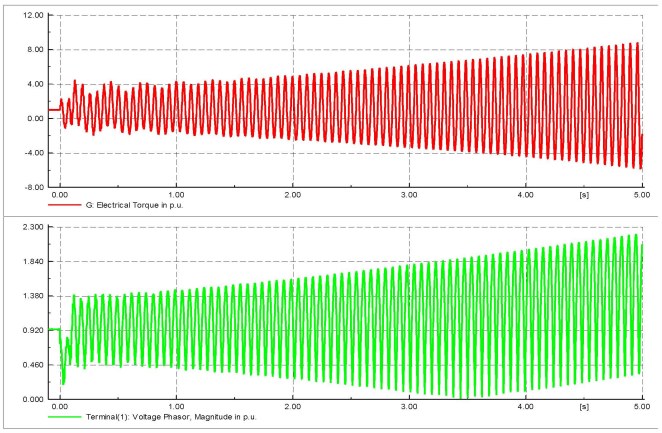

Fig. 10. Electric torque and Terminal voltage of generator for 90% compensation

B. Analysis of the study system with STATCOM

The simulation was repeated as above in Case B with STATCOM connected at the generator terminals with 90% compensation of the line. From the Fig.11 it can be seen that the IGE effect is suppressed and the system is stable.

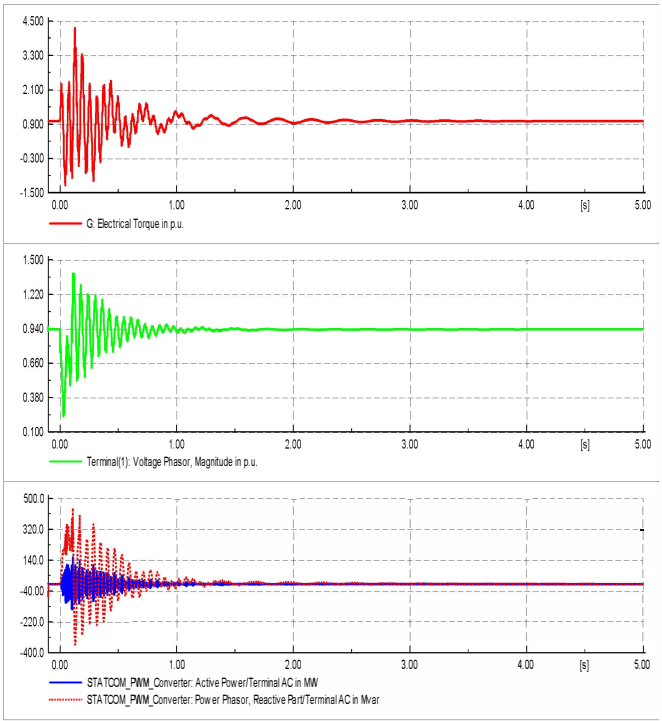

Fig. 11. Electric torque and Terminal voltage of generator, STATCOM Reactive and Active power for 90% compensation.

Discussion

From the above cases it can be seen that IGE is not revealed when the total resistance of the transmission line and transformer is higher than the generator rotor resistance viewed from rotor side at complement of SSR frequency. But when it is lesser the IGE effect is revealed with overvoltage and growing oscillations of the rotor leading to instability. Also it is to be noted that the compensation at which this occur is extremely and higher compared to the compensation at which TI effect is maximum as available in literature. Hence suitable countermeasure is needed in case of series compensated line even in non steam turbine generators where there is a possibility of SSR due to IGE.

A STATCOM is proposed for the mitigation of IGE. From Fig.11 it can be seen that the reactive power supplied by the STATCOM is high during the fault and then it reaches the steady state near 20MVAR. Since the STATCOM has to take active power losses from the terminals during its operation, it can be seen that the active power drawn from the terminals is high during fault and then reaches the steady state to a negligible value.

V. CONCLUSION

A study of possible induction generator effect due to Subsynchronous resonance has been carried out on First IEEE bench mark system for the study of Subsynchronous resonance in synchronous generator. The study shows that the induction generator effect is not revealed under normal conditions and the self excitation phenomenon is damped out naturally. But when the transmission system resistance is lowered the SSR due to induction generator may be revealed which leads to instability. Hence suitable countermeasures need to be taken to prevent this SSR. STATCOM a FACTS device which is normally used for the dynamic VAR support is proposed to mitigate IGE effect of SSR. With the proposed STATCOM it has been shown through time domain simulation on DIgSILENT Power Factory the IGE effect due to SSR can be damped successfully.

APPENDIX

Generator data:

892.4MVA, 60Hz, 26 kV

X_d=1.79 pu, X_d'=0.169 pu, X_d''=0.135pu,

X_L=0.13 pu, X_q=1.71 pu, X_q'=0.228 pu, X_q''=0.2 pu

T_{do}'=4.3 s, T_{do}''=0.032 s, T_{qo}'=0.85 s, T_{qo}''= 0.05 s, R_1=0.0

Transmission line data

500KV, R_1=.02 pu, X_1=0.56pu, X_0=1.62pu

Transformer data

X_1=0.14 pu

STATCOM data:

100 MVA, (100MVA Reactive TO 100 MVAR Capacitive)

PI AC Voltage Regulator: K=10, T_p=0.002s

PI DC Voltage Regulator: K=4, T_v =0.002s

PI d-axis Current Regulator: K=0.6, T_d=0.002s

PI q-axis Current Regulator: K=0.6, T_d=0.07s

i_max= 3.67A, i_min= -3.67A

REFERENCES

[1] P.M.Anderson, B.L.Agrewal and J.E Van Ness, *Subsysnchronous Resonance in Power System,* IEEE Press, New York, 1990.

[2] J.W.Butler and C. Concordia, "Analysis of Series Capacitor Application Problems", *AIEE Trans*., vol.56, August 1937, pp.975-988. Discussions, vol.57, February 1938, pp. 110-111.

[3] IEEE Working Committee Report, "Fourth Supplement to a Bibliography for the Study of Subsynchronous Resonance between Rotating Machines and Power Systems", *IEEE Trans. On Power Systems*, vol.12, no.3, 1997, pp.1276-1282.

[4] IEEE Committee Report, "Reader's Guide to Subsynchronous Resonance", *IEEE Transactions on Power Systems,* vol. 7, no.1, 1992, pp. 152-157.

[5] IEEE SSR Task Force, "First benchmark model for computer simulation of subsynchronous resonance", *IEEE Trans. On PAS,* vol. PAS-96, Sept.-Oct. 1977, pp. 1565-1572.

[6] IEEE SSR Working Group, "Second benchmark model for simulation of subsynchronous resonance", *IEEE Trans. On PAS*, vol. 104, no.5, 1985, pp. 1057-1066.

[7] K.R.Padiyar and Nagesh Prabhu, "Design and Performance Evaluation of Subsynchronous Damping Controller with STATCOM", *IEEE Trans on Power Delivery*, vol.21, no.3, 2006, pp.1398-1405.

[8] N.G. Hingorani and L. Gyugyi, *Understanding FACTS,* IEEE Press, 1996.

[9] O.Saito, H.Mukae, K.Murotani, "Suppresion of Self Excited Oscillations in Series compensated Transmission Lines by Excitation Control of Synchronous Machines", *IEEE Trans .On Power Apparatus and Systems*, PAS-94, Sep/Oct 1975, pp. 1777-1788.

[10] A.Ajami and N.Teheri, "A Hybrid Fuzzy/LQR Based Oscillation Damping Controller Using 3-level STATCOM", Proceedings of Second International Conference on Computer and Electrical Engineering, ICCEE, vol. 1, 2009, pp 348-352.

[11] Power Factory user manual, DIgSILENT GmbH, Heinrich-Hertz-Strasse9, D-72810 Gomaringen, Germany. (http//www.digsilent.de)

Performance Evaluation of BLDC Motor with Conventional PI and Fuzzy Speed Controller

Madhusudan Singh
Electrical Engineering Department
Delhi Technological University
madhusudan@dce.ac.in

Archna Garg
Electrical Engineering Department
Delhi Technological University
garg.anu16@gmail.com

***Abstract*— Performance evaluation of a brushless DC (BLDC) motor with conventional PI and Fuzzy Logic based speed controller is presented in this paper. The BLDC motor with non-sinusoidal (trapezoidal) back-electromotive force has been analyzed with both the speed and current controllers. It is the always preferred to have a drive with faster and smoother speed response and reduced ripples in current and torque. The controlling schemes for BLDCM using its Back EMF have been conventionally used into many applications. In this paper, a simple control scheme has been implemented which does not need to know the back emf or shape function and even no complicated calculations. In order to solve the problems associated with conventional PI speed controller, Fuzzy logic speed controller is proposed to reduce starting current, eliminate overshoot in the torque and fast speed response. It is simple in design and eliminates the complex mathematical computation. The effectiveness of proposed system has been validated by simulation results and improved performance of controlling BLDCM. The proposed algorithm gives robust control. The robustness of the proposed algorithm is demonstrated through the MATLAB simulation.**

Keywords-Brushless dc (BLDC) motor; PI control; Fuzzy Logic Control (FLC).

I. INTRODUCTION

The Permanent Magnet Brushless DC (BLDC) motor is the ideal choice for applications that require high power-to-volume ratio, high reliability, and high efficiency. BLDC motor is considered to be a high performance motor and is capable of providing large amounts of torque over a vast speed range. BLDC motors are a derivative of the most commonly used DC motor and they share the same torque and speed performance curve characteristics. The only major difference between the two is the use of brushes. BLDC motors do not have brushes so named "brushless DC" but the DC motors used to have brushes [1]. BLDC motor uses the electronic commutation for the process of changing the motor phase currents at the appropriate times of instants to produce rotational unidirectional torque. In a brush DC motor, the motor assembly contains a mechanical commutator which is moved by means of actual brushes in order to move the rotor. A BLDC motor has high reliability since it does not have any brushes to wear out and replace the mechanical brushes. Instead of mechanical commutation with brushes, electronic commutation is performed. This reduces the friction and thus, increases reliability. The tradeoff is more complex and much expensive controllers. However, the economies of scale of electrical components are much different from those of the motors themselves, and thus a system-wide cost performance evaluation favors brushless motors in many applications. [2] So when operated, the life expectancy is over 12,000 hours. DC motors costs the time and money, perhaps a great deal depending on how long it takes to replace the worn out part and get the operation started again. Although a BLDC motor may cost more than a brushless DC motor, it will often more than pay for itself in the amount of work time saved.

To alternate the role of brushes and commutator, the PMBLDC motor is provided with an inverter and a speed sensor that detects rotor speed.

Scheme using the electrical and mechanical equations of the motor to control the commutation of BLDC is modeled and simulated in MATLAB in [3, 4]. Schemes using the trapezoidal characteristics of the back-emf to estimate the speed by the zero crossing detection have been implemented in [5]. Another scheme estimated the back-emf from the line voltage differences [6] and speed computed using the zero crossing detection algorithms but it was a tedious task to know the ZCP after every 60 degree. 180 degree commutation scheme checking the polarity of back-emf [7] was developed. The schemes using the trapezoidal back-emf waveform of BLDC to estimate the rotor position failed as the magnitude of back-emf being low at the start of motor which is too small to detect to be used for commutation purpose. The property of the variation of inductance also been calculated [8] to know the rotor position but the computation is difficult. A lot many schemes using controllers like FPGA based control of BLDC [9] and DSPIC based [10] control of BLDC has been described. Fuzzy logic controller provides feasibility and ease in accessing the controllers in terms of linguistic variables. Schemes based Adaptive Neuro-Fuzzy Controller Based on Emotional Learning Algorithm [11, 12] meant for speed control of brushless direct current (BLDC) drives have been implemented. Digital implementation of FLC for wide range speed control [13] and smooth speed reversal using fuzzy controller [14] has already been implemented. In this paper, a simple scheme with the speed and current controller is implemented. The performance is observed with PI Speed controller and Fuzzy logic speed controller and comparison is done to know which gives the better results. The drive system is dependent on the position and current sensors for control.

978-1-4673-0934-9/12/$31.00 ©2012 IEEE

II. SYSTEM DESCRIPTION

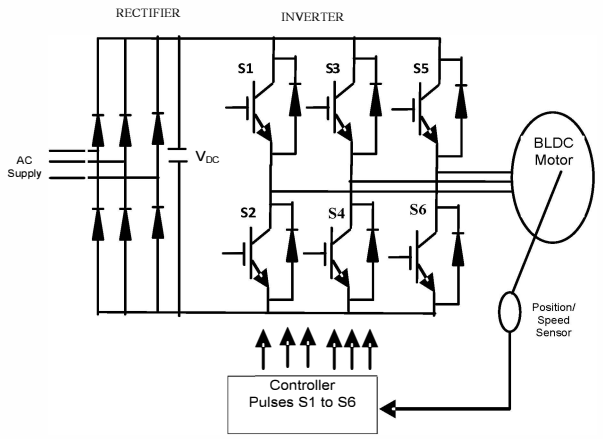

Fig.1. PMBLDC Motor Drive

Fig.1 shows the PMBLDC drive with its power circuit and controller. The AC supply is rectified using the uncontrolled bridge rectifier and filtered. This DC voltage is then fed to the 3-phase inverter to get variable AC supply. This variable AC supply is then fed into the BLDC motor stator. The status of the BLDC motor parameters is given to the controller which compares it with the set point value and accordingly performs the switching of the inverter. Fig.2 explains the control scheme for the controller. The BLDC drive here is operated in speed and current control mode. The actual speed of the motor is measured which is then compared with the reference speed and this speed error decides the magnitude of the current in the each phase.

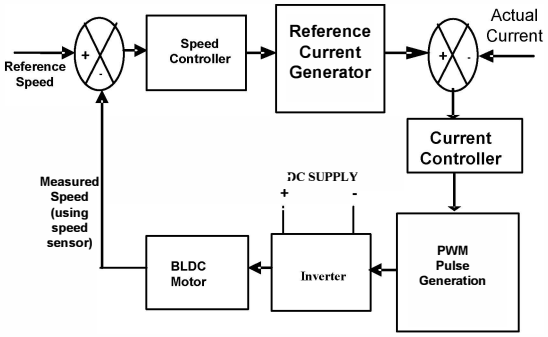

Fig.2. Control Scheme

This reference current is compared with the actual current in each phase winding and the error is processed by a current controller which generates the pulses for the proper switching of the inverter so that error could be minimized.

III. CONTROLLER DESCRIPTION

A. Speed Controller

The speed Controller used here is the PI controller and Fuzzy logic Controller and the difference in the performance of the PMBLDC drive is presented in section IV.

1) PI Speed Controller: The actual speed of BLDC motor is obtained using the speed/position encoder and is compared with the set value and the error is processed by the PI speed controller as shown in Fig.3 to get the reference torque.

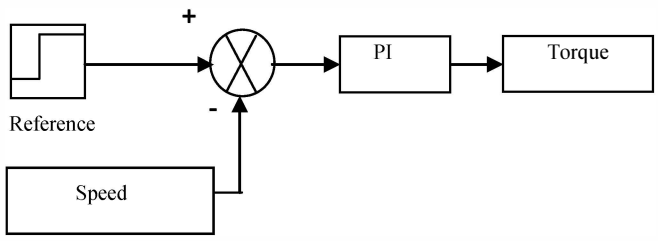

Fig.3. PI Speed controller implementation

2) Fuzzy Logic Speed Controller: Fig.4 shows the block diagram of the fuzzy logic controller (FLC). The FLC does not require a mathematical model of the system and it works on a structure prepared from the knowledge base. The description of FLC block is as follows:

a) Fuzzification: The first block inside the controller is Fuzzification, which is a look-up in the membership function to derive the membership grade. The membership function (also known as degree of belonging) is in the range of 0 to 1.

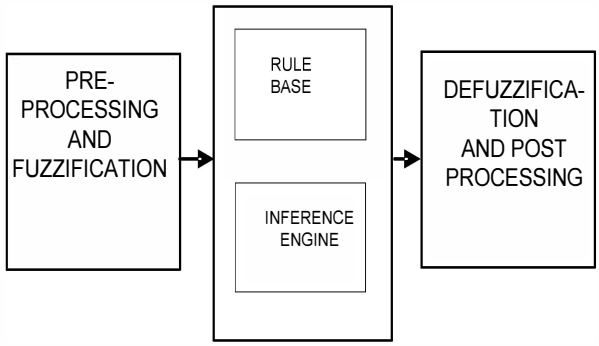

Fig.4. Fuzzy Logic Controller

b) Rules base: A rule-base allows for several variables both in the premise and the conclusion. A linguistic controller used here contains rules in the "if-then" format. These rules are imprecise and expressed in terms of linguistic variable. The Rule Base used for the Fuzzy Logic Speed controller used is shown in Table I. The fuzzy members chosen are: Zero: ZO, Positive Big: PB, Positive Small: PS, Negative Big: NB, Negative Small: NS.

In Fuzzy Logic Speed controller the inputs used are the speed error and rate of change of speed error The fuzzy logic control output i.e. the torque is a function of $\Delta\omega$ (speed error) and $\Delta\omega'$ (change of speed error) and is expressed as $T = FLC(\Delta\omega', \Delta\omega)$.

The triangular shaped membership function has been chosen due to the resulting best control performance and simplicity. The height of the membership functions in this case is one for all. Some degree of overlap is provided for neighboring fuzzy subsets.

TABLE I. RULE BASE FOR THE FUZZY LOGIC SPEED CONTROLLER

$\Delta\omega$ \ $\Delta\omega'$	NB	NS	ZO	PS	PB
NB	NB	NB	NB	NS	ZO
NS	NB	NS	NS	ZO	PS
ZO	NB	NS	ZO	PS	PB
PS	NS	ZO	PS	PS	PB
PB	ZO	PS	PB	PB	PB

c) Defuzzification: The reverse of Fuzzification is called Defuzzification. The rules of FLC produce required output in a linguistic variable. Linguistic variables have to be transformed to crisp output. By using the center of gravity "centroid" defuzzification method, crisp output is obtained. The output of the Fuzzy Logic speed controller is torque.

B. Reference Current Generator

The reference current $(I^*)$is determined form the reference torque (T^*) by the following expression:

$$T^* = I^* K_T \tag{1}$$

where K_T is the torque constant of motor.

C. Position Estimation

Electrical position of rotor can be calculated from the mechanical angular speed by the expression given in (2).

$$\theta_e = \int (p * \omega)\, dt \tag{2}$$

where p is number of pole pairs, θ_e is the electrical rotor position and ω is the mechanical speed of the motor.

D. Three phase Reference Current

This reference current magnitude calculated from (1) is then used to calculate three phase reference current which depends upon the value of electrical position of rotor given by (2). The three phase reference currents can be computed as per Table II.

TABLE II. THREE PHASE REFERENCE CURRENT GENERATOR

Rotor Elect. Position	i_a^*	i_b^*	i_c^*
0-60	I^*	$-I^*$	0
60-120	I^*	0	$-I^*$
120-180	0	I^*	$-I^*$
180-240	$-I^*$	I^*	0
240-300	$-I^*$	0	I^*
300-360	0	$-I^*$	I^*

E. Hysteresis Current Controller

The error of three phase reference currents and actual value of the three phase currents is given to the hysteresis comparator as shown in Fig.5 to generate necessary PWM signals for the inverter.

If $(i_a^* > i_a)$ S1 ON and S2 OFF
If $(i_a^* < i_a)$ S1 OFF and S2 ON
If $(i_b^* > i_b)$ S3 ON and S4 OFF
If $(i_b^* < i_b)$ S3 OFF and S4 ON
If $(i_c^* > i_c)$ S5 ON and S6 OFF
If $(i_c^* < i_c)$ S5 OFF and S6 ON

The Hysteresis band taken here is 0.01A

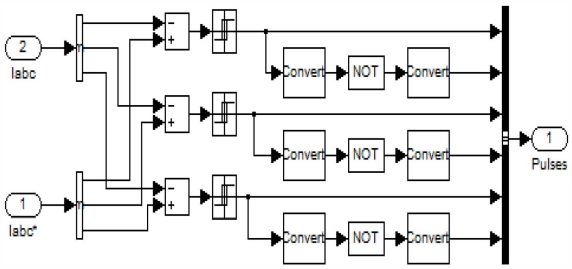

Fig.5. Hysteresis Current Controller

IV. SIMULATION RESULTS

Modeling and simulation of a 3 phase, 4 poles, and 3.2 Nm PMBLDC motor is carried out using MATLAB/ SIMULINK. The performance characteristics are presented. Complete specifications of the PMBLDC motor are given in APPENDIX. The purpose of the simulation is to evaluate the performance of the PMBLDC drive system when PI speed controller is used and comparing its performance when Fuzzy Logic speed controller is used.

A. Starting and load perturbation performance

Fig.6 shows the performance of the BLDC motor during starting and load perturbation with PI speed controller and hysteresis current control loop. The motor is set for a reference speed of 700 rpm up to 0.2 seconds which is then changed to 900 rpm. At the instant 0.1 seconds a sudden load of 0.1 Nm is applied. From the speed response it is observed that the motor takes approx. 0.06455 seconds to reach the initial reference speed of 700 Rpm. Also the sudden application of the load of 0.1Nm at 0.1 seconds on the motor did not result in a dip in motor speed. From the torque response, it is observed at instant 0.2sec., when there is change in reference speed; the electromagnetic torque rises to a value about 2.934 Nm. Also here the starting torque produced is approx. 1.511 Nm. From

the torque response it is observed that the torque produced by the motor contains high ripples. From the current response, it is observed that when the reference speed is changed then there is a quick change in the value of current drawn by the motor from about 2.806 A to 3.829 A . Also the starting current drawn by the motor is very large approx 4A. But here the current behavior is much deviated from the desirable rectangular one and is peaky also.

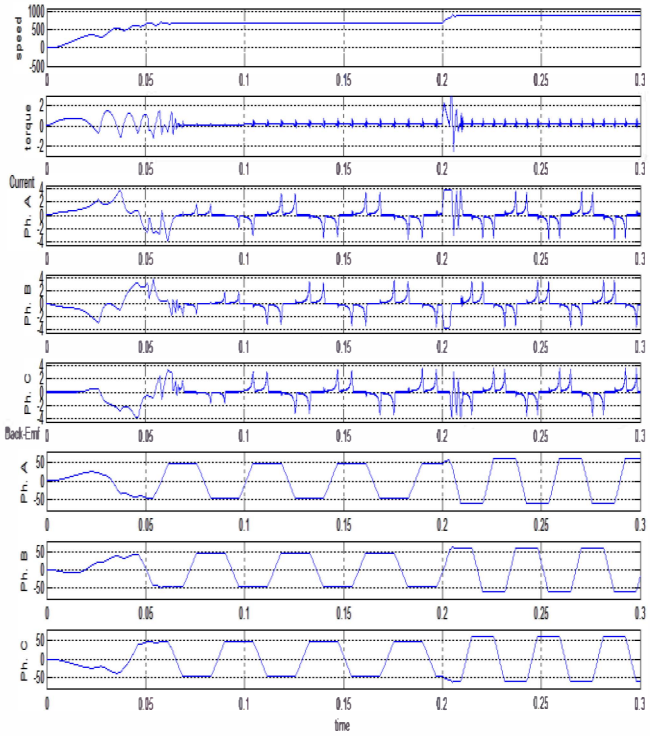

Fig.6. Performance of the PMBLDC motor during Starting and Load Perturbation using PI speed controller

Fig.7. shows the performance of the BLDC motor during starting and load perturbation with Fuzzy Logic speed controller and hysteresis current control loop. From the speed response shown in Fig.7, it is observed that the motor takes approx. 0.05972 seconds to reach the initial reference speed of 700 rpm. The sudden application of the load of 0.1Nm at 0.1 sec. on the motor results in a small dip in motor speed. From the torque response it is observed that the torque produced by the motor contains ripples but comparatively much less than the torque ripples with PI speed controller. It is also observed that the torque ripples is confined within 1Nm. Also here the starting torque produced is approx. 0.9781 Nm. Also, when the reference speed is changed then there is a less change in the current values which otherwise could be harmful to the windings. It changes very slightly from about 0.2712 A to about 0.909 A Here the current behavior is much similar to the rectangular one which otherwise is very much deviated from this behavior in case of PI speed controller. The back-emf of all three phases is also shown in Fig.7.

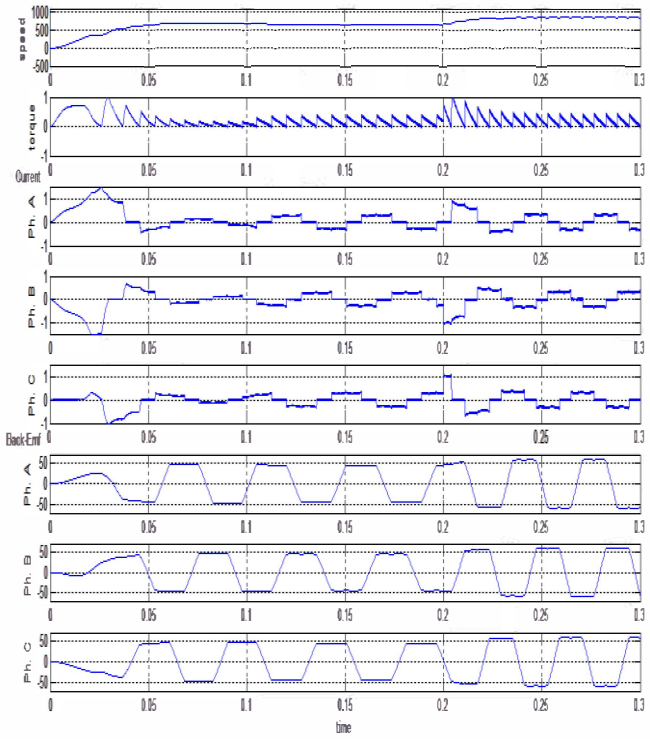

Fig.7. Performance of the PMBLDC motor during Starting and Load Perturbation using Fuzzy Logic speed controller

B. Speed reversal performance

Here the motor is running at the reference speed of 700 rpm up to 0.25 sec. At 0.25 sec. the reference speed is suddenly reversed.

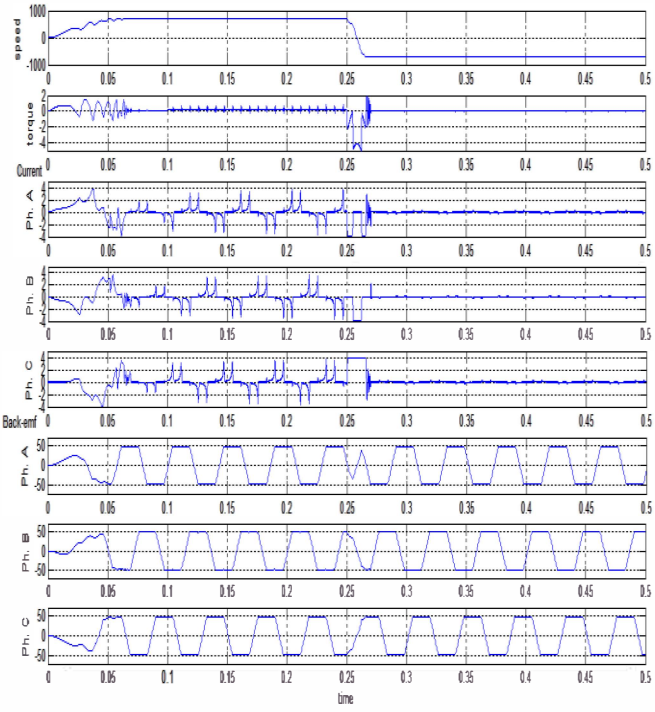

Fig.8. Performance of PMBLDCM during speed reversal using PI speed controller

From the speed response shown in Fig.8, it is observed that the motor takes approx. 0.06503 seconds to reach the initial reference speed of 700 rpm. At the instant 0.25 seconds, when there is a sudden speed reversal then the drive simulated with PI speed controller reaches zero speed at 0.2593 seconds time and reaches the reference speed of 700 rpm in reverse direction at 0.2667 seconds time. Thus the BLDC motor tracks the reference speed effectively.

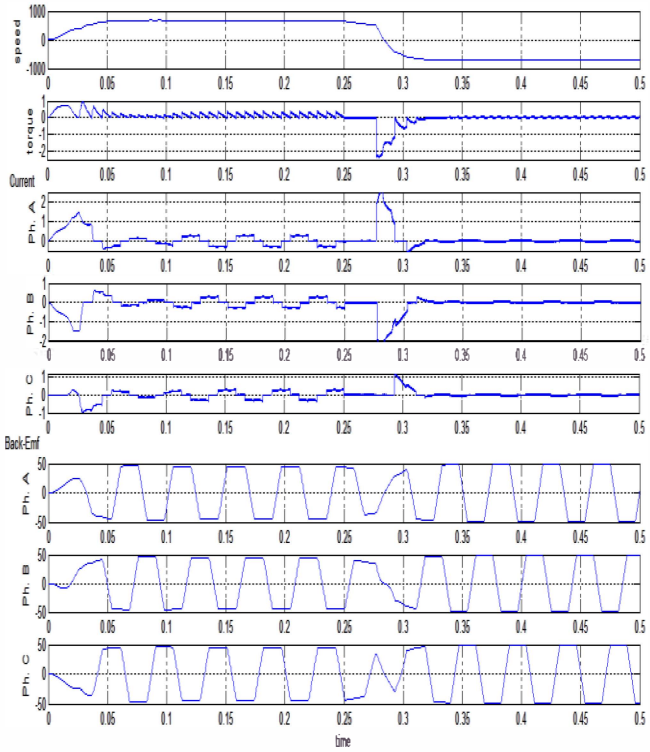

Fig.9. Performance of PMBLDCM during speed reversal using Fuzzy Logic speed controller

The sudden application of the load of 0.1Nm at 0.1 seconds on the motor did not result in a small dip in motor speed as observed. From the torque response it is observed that the torque produced by the motor with PI speed controller contains many ripples and are confined within 6Nm. When the reference speed is changed then there is a quick large change in the current values. The motor draws a current about 4 A at the start and about 4.074 A at the instant the speed reverses. But here the current behavior is much deviated from the desirable rectangular one and is peaky also.

Fig.9 shows the performance of the BLDC motor during speed reversal with Fuzzy Logic speed controller and hysteresis current control loop. From the speed response shown in Fig.9, it is observed that the motor takes approx. 0.05921 sec. to reach the initial reference speed of 700 rpm. At the instant 0.25 sec., when there is a sudden speed reversal then the drive simulated with Fuzzy Logic speed controller reaches zero speed at 0.284 sec. time and reaches the reference speed of 700 rpm in reverse direction at 0.3198 sec. time. The sudden application of the load of 0.1Nm at 0.1 sec. on the motor results in a small dip in motor speed as observed. Though here the dynamic performance of the motor is slow but from the torque response it is observed that the torque produced by the motor with fuzzy speed controller contains ripples but comparatively much less than the torque ripples with PI speed controller. The torque ripples is confined within 0.8Nm. Also, here the starting torque produced is approx. 0.9632 Nm. When the reference speed is changed then there is a not a quick large change in the current values. The motor draws a current about 1.514 A at the start and about 2.918 A at the instant the speed reverses. Here the current behavior is much similar to the rectangular one which otherwise is very much deviated from this behavior in case of PI speed controller during speed reversal.

V. CONCLUSION

Performance of BLDC motor drive with conventional PI controller and FLC has been simulated and discussed. In this paper, use of a fuzzy control on speed error and computation of the reference current from speed error is also demonstrated. A comparison of the performance of the PMBLDCM drive with PI and Fuzzy Logic Speed Controller is carried out. It has been observed that the FLC produces good results in terms of torque ripples and current control limits for the windings. Low starting current is achieved if FLC is used which leads to low cost inverter switch. Although starting torque is reduced compared with using PI controller but it does not lead to starting problems. Thus, this method can be easily applied to industrial applications which require the low-cost and reliable drive operation of BLDC motor. The technical validity of the proposed algorithm has been shown through computer simulation using the MATLAB.

APPENDIX

PMBLDC Motor Parameters

HP	1.35 Hp
Rated speed	3000 rpm
Rated current	8.6 A
Number of Poles	4
Resistance/Phase(ohm)	10.91
Inductance/Phase(H)	30.01e-3
Moment of inertia(kg/m^2)	2.9e-4
Voltage constant(V_peak L-L/kRpm)	136.1357
Torque constant(Nm/A)	1.3

REFERENCES

[1] Pragasan Pillay and R. Krishnan,"Modeling Simulation and Analysis of Permanent Magnet Motor Drives, Part II: The Brushless DC Motor Drives", in *IEEE Trans. on Industrial Applications*, vol. 25, no. 2, pp. 274-279, March/April 1989.

[2] Pragasan Pillay and R. Krishnan,"Modeling of Permanent Magnet Motor Drives", in *IEEE Trans. on Industrial Electronics*, vol. 35, no. 4, pp. 537-541, November 1988.

[3] Balogh Tibor,Viliam Fedák, František Ďurovský, "Modeling and Simulation of the BLDC Motor in MATLAB GUI," International Symposium on Industrial Electronics (ISIE), pp. 1403-1407,2011.

[4] Ji Hua, Zibo, Li Zhiyong, "Simulation of Sensorless Permanent Magnetic Brushless DC Motor Control System" *Proceedings of the International Conference on Automation and Logistics Qingdao*, pp. 2847-2851, 2008.

[5] E. Kaliappan, C. Chellamuthu Professor, "A Simple Sensorless Control technique for PMBLDC Motor Using Back EMF Zero Crossing,"

European Journal of Scientific Research ISSN 1450-216X vol.60 No.3 , pp.365-378.

[6] P. Damodharan and Krishna Vasudevan, Member, "Sensorless Brushless DC Motor Drive Based on the Zero-Crossing Detection of Back Electromotive Force (EMF) From the Line Voltage Difference" *IEEE Trans. on Energy Conversion*, vol. 25, no. 3, pp. 661-668, 2010.

[7] Boyang–Hu and Swamidoss Sathia Kumar, "Sensorless drive of Permanent Magnet Brushless DC motors with 180 degree commutation," vol. 1, pp. 467-472, 2010.

[8] Nicola Bianchi, Silverio Bolognani, Ji-Hoon Jang, and Seung-Ki Sul, "Comparison of PM Motor Structures and Sensorless Control Techniques for Zero-Speed Rotor Position Detection," *IEEE TRANS. on Power Electronics*, vol. 22, no. 6, pp. 2466-2475, 2007.

[9] A. Albert Rajan, R. Daniel Raj Dr. S. Vasantharathna "Fuzzy Based Reconfigurable Controller for BLDC Motor" *Second International conference on Computing, Communication and Networking Technologies (ICCCNT),* pp.-1-7, 2010.

[10] K. S. Rama Rao, "Sensorless Control of a BLDC Motor with Back EMF Detection Method using DSPIC" at *2nd IEEE International Conference on Power and Energy (PECon 08),* pp. 243-248, 2008.

[11] A. Halvaei Niasar, A. Vahedi, H. Moghbelli "Speed Control of a Brushless DC Motor Drive via Adaptive Neuro-Fuzzy Controller Based on Emotional Learning Algorithm," *International Conference on Electrical Machines and Systems (ICEMS),* vol. 3, pp 230-234, 2005.

[12] Chung-Jin Kwon, Woo-Yong Han, Sung-Joong Kim and Chang-Goo Lee "Speed Controller with Adaptive Fuzzy Tuning For BLDC Motor Drive Under Load Variations" at *SICE Annual Conference in Fukui,* pp 3118-3121, *2003.*

[13] R.Shanmugasundram, K.Muhammed Zakariah, and N.Yadaiah," Digital Implementation of Fuzzy Logic Controller for Wide Range Speed Control of Brushless DC Motor," *International Conference on Vehicular Electronics and Safety* (*ICVES)* pp. 119-124, 2009.

[14] Ajay Kumar Bansal, R. A. Gupta, , and Rajesh Kumar," Fuzzy estimator for Sensorless PMBLDC Motor Drive under Speed Reversal," *India International Conference on Power Electronics (IICPE)*, pp.1-7, 2011.

Study of Potential Energy Term in VMINS model

Pallavi Bhatt[1], Hardik P. Trivedi[1], Lalit K. Gupta[2], Anil Kumar[3*]
Than Singh Saini[4], Krishna Chandra[5] and Jai Prakash Gupta[6]

[1]Department of Physics, Mewar University, Chittorgarh (Rajasthan) INDIA,
[2]Department of Physics, Krishna Engineering College, Ghaziabad, INDIA
[3]Department of Physics, Vivekanand College of Tech. & Magt. Aligarh (UP) INDIA
[4]Department of Physics, Delhi Technological University, Delhi-42 INDIA
[5]Department of Physics, Goldfield institute of Technology & Management, Faridabad-, INDIA
[6]Department of Physics, D. S. College, Aligarh (UP), INDIA
[*]anil_kgupta@rediffmail.com

1. Introduction

Now, it has been experimentally [1] suggested that the ground state bands for even-even nuclei away from closed shells can be expected throughout the Periodic Table. Theoretically, a number of models [2-7] have been proposed to correlate such a data. In this attempt, the variable moment of inertia (VMI) model proposed by Mariscotti *et al*; [2] is one of the earliest and very popular among the nuclear science community. In this model, the excitation energy of the state J is defined as the sum of the rigid rotational energy (with moment of inertia 'θ' varying with angular momentum 'J') and a potential energy term (harmonic in angular momentum dependent moment of inertia θ_J about its mean ground state value θ_0. Latter this VMI model extended by Klein and his associates [5, 6] on the basis of the predictions of the interacting boson model [IBM-1] in to two generalizations of VMI model, namely, the Variable A harmonic Vibrator Model (VAVM) and the Generalized VMI (GVMI) model. Batra *et al*; [7-9] extended VMI model by taking in to account the concept of nuclear softness. This extended version of VMI generally called VMINS model. In this present work we studied the importance of potential energy term in VMINS model.

2. The Model

In the original variable moment of inertia (VMI) [2] model, the excitation energy of the member of the ground-state band with angular momentum J is given by

$$E(J) = \frac{\hbar^2}{2I} J(J+1) + \frac{c}{2}(I - I_0)^2 \qquad \text{(i)}$$

Here the potential term is added to the usual rotational term. The coefficients c and I_0 are parameters, characteristic for each nucleus. Where I_0 is called the ground state moment of inertia and c is denoted as stiffness parameter.

Gupta *et al*; [7, 8] expressed the variable moment of inertia (VMI) model for the ground state band in even-even nuclei in terms of his nuclear softness (NS) model [3]. In NS model the variation of moment of inertia θ with J is given by

$$\theta = \theta_0(1 + \sigma J) \qquad \text{(ii)}$$

Where θ_0 is the ground state moment of inertia and σ is the softness parameter.
After putting the value of Moment of Inertia (I) in terms of Nuclear Softness Parameter (σ) in equation (i) we get the following expression-

$$E(J) = \frac{\hbar^2 J(J+1)}{2\theta_0(1+\sigma J)} + \frac{C}{2}\sigma^2\theta_0^2 J^2 \qquad \text{(iii)}$$

Equation (iii) has three parameters
(a) Ground State Moment of Inertia (θ_0)
(b) Softness Parameter (σ)
(c) Stiffness Constant (C)

Two of the parameters Ground State Moment of Inertia (θ_0) and Stiffness Parameter (C) are same as 'I_0' and 'c' in original VMI model, while the Softness Parameter (σ) is different parameter which represents the softness of a particular nucleus. The first term in right hand side of equation (iii) has two parameters (i.e. θ_0 & σ), while the second term has three parameters (i.e. C, θ_0 & σ). The parameters θ_0 and σ are calculated by following the conditions given in reference [9].

In the present work we study the second term of equation (iii) (i.e. Potential Energy Term, $E_{pot.}$) with spin 'J' of the nucleons and with ground state of moment of inertia and with nuclear softness parameters of different nuclei of quadrant-I.

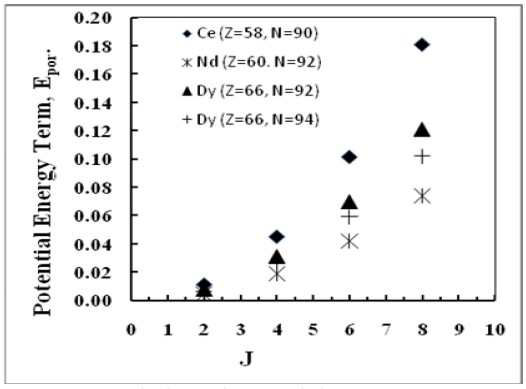

Fig- (1): Variation of Potential Energy Term ($E_{pot.}$) with Spin (J).

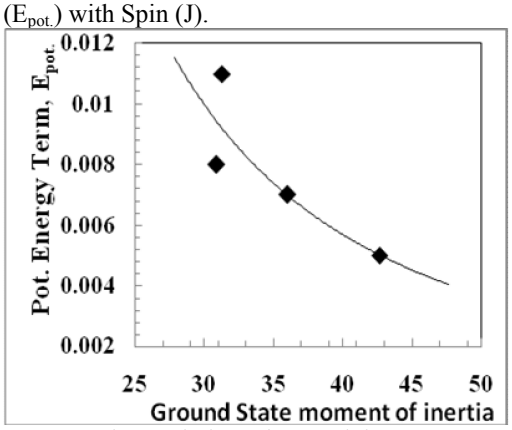

Fig-(2): The Variation of Potential Energy Term ($E_{pot.}$) with Ground State Moment of Inertia.

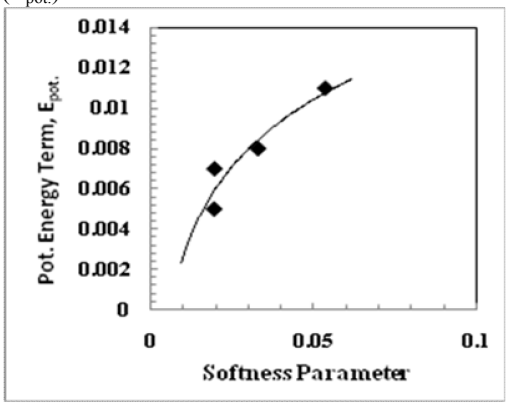

Fig-(3): The Variation of Potential Energy Term ($E_{pot.}$) with Nuclear Softness Parameter.

3. Result and Discussion

3.1: Dependence of E_{pot} on Spin J

The variation of potential energy term for the different even-even nuclei in the region of I-quadrant based on the valence particle and hole pairs consideration [8]{Ce(N=90), Nd (N=92), Dy (N=92) & Dy (N-94)} with spin (J) has been shown in fig. (1). It is clear from fig. (1), that the value of potential energy term is increasing almost linear with increasing spin (J) for all the nuclei. In case of Dy (D=92) the potential energy term is less than that of Dy (N=94) for a particular value of spin (J).

3.2: Dependence of E_{pot} on Ground State Moment of Inertia

In figure (2) the variation of potential energy, $E_{pot,}$ with ground state moment of inertia is shown. It is apparent from this figure that the potential energy term is decreases almost exponentially with ground state moment of inertia.

3.3: Dependence of E_{pot} on Nuclear Softness Parameter

In figure (3) the variation of potential energy, $E_{pot,}$ with nuclear softness parameter has shown. The nuclear softness parameter of nuclei is increases with nuclear softness parameter in the same way as that of decreases with ground state moment of inertia.

Acknowledgement

Pallavi Bhatt and T. S. Saini are very grateful to the Professor J. B. Gupta and Associate Prof. Anil Kumar for fruitful discussion.

References

[1] M. Sakai: Quasi-Bands (Institute for Nuclear Study, University of Tokyo, Tokyo, 1982)
[2] M. A. J. Mariscotti, G. Scharff-Foldhaber and B. Buck: Phys. Rev. 178, 1864 (1969)
[3] R. K. Gupta: Phys. Lett. 36B, 173 (1971)
[4] M. Satpathy and L. Satpathy: Phys. Lett. 34B 377 (1971)
[5] D. Bonatsos and A. Klein, Phys. Rev. C29, 1879 (1984), Atomic data and Nuclear Data Tables 30, 27 (1984)
[6] A. Klein, Nucl. Phys. A 347, 3(1980)
[7] R. K. Gupta, *et al*; Nucl. Data for Sci. & Tech. (Mito, Japan), 729 (1988)
[8] J. S. Batra, *et al*; Phys. Rev. C43, 1725(1991)
[9] J. B. Gupta, *et al*; Phys. Rev. C56, 6, 3417 (1997)

Temperature Dependent Analysis of Thermoelectric Module using Matlab/SIMULINK

Aarti Kane *, Vishal Verma **, Bhim Singh***
* College of Engineering, Bharati Vidyapeeth, Delhi, India
** Delhi Technological University, Delhi, India
*** IIT, Delhi
sanikakane@rediffmail.com, vishalverma@dce.ac.in, bsingh@ee.iitd.ac.in

Abstract— **This paper is an attempt of detail the comparative study of the analysis of thermoelectric module (TEM) for static and dynamic modeling with temperature dependent parametric variations. This study provides an insight on computation of various parameters of TEM used for modeling power generators. Initially a brief analysis is carried out for estimation of efficiency, power, voltage and current assuming a static model. Later dynamic model has been developed under MATLAB/Simulink environment with a consideration of its dependence with temperature and results of simulation are compared. Such comparative study not only validates the efficacy of the developed model with dynamic operating conditions but also pave the way for designing the balance of system more accurately. This paper presents a near accurate model of thermoelectric generator (TEG) with realistic conditions with a user-friendly approach. The inputs of the considered model are temperature dependent parameters, temperature of hot source and ambient temperature to which cold junction is exposed. The results are computed to evaluate the performance of TEM for generated voltage, power and efficiency.**

Keywords: ***Seebeck and Peltier effect, clean technology, Mathematical Modelling Thermoelectric module, Thermoelectric generator, temperature dependence of thermoelectric module.***

I. INTRODUCTION

Thermoelectric technology provides an alternative to traditional methods of solar power generation, generation from waste heat, heating and cooling. Thermoelectric module can convert heat energy to electrical power directly. Compared with other methods TEM possesses the salient features of being compact, light-weighted, noiseless in operation, highly reliable, maintenance free, and involving no moving or complex parts. It is environment friendly operation, free of carbon dioxide emission and radioactive substances and does not contribute to the depletion of natural resources.

Thermoelectric phenomenon was observed in 1821 by Seebeck. Extension to Seebeck research, in 1834, Peltier discovered that the passage of an electric current through a junction between two dissimilar conductors in a certain direction produces a cooling effect. A correlation between the Seebeck and Peltier coefficients was experimentally proven by Thomson which is known as Thomson effect. This effect co-relates the heating or cooling in a single element when current passes through it in the presence of a temperature gradient.

A small amount of electrical power can be generated by a TEM if a temperature difference is maintained between two terminals, or can operate vice-a-versa as a heat pump based on Seebeck and Peltier effects[1-5]. Typical TEM is composed of two ceramic substrates that serves as a foundation and electrical insulation for P-type and N-type thermo elements, which are connected electrically in series and thermally in parallel between the ceramic plates as shown in Fig 1.

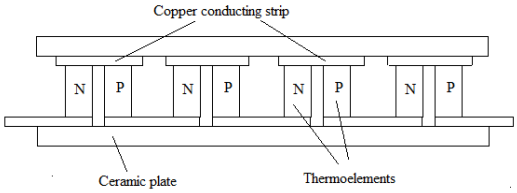

Fig. 1. Basic thermoelectric module.

According to working modes of TEM these can be classified into three modes- a) Coolers (or heaters) b) Power generators c) Thermal energy sensors.

Materials can be classified based on application as a generator or heater/cooler. For refrigeration application the most suitable material available is Bismuth Telluride (Bi2Te3), a semiconductor alloy that has highest figure of merit and have operating temperature of around 450 K. For generation purpose alloys based on lead telluride and silicon germanium alloy are popularly used. Lead telluride has the next highest figures-of-merit whereas silicon germanium alloys has the lowest. The operating temperatures hovers around 1000K and 1300K, respectively [3, 6-7]. Maximizing figure of merit is the major objective in optimized selection of thermoelectric materials.

To develop the efficient and cost effective thermoelectric system suitable for various applications especially waste heat recovery in active heat sinks for electronic systems, air conditioning and vehicle exhaust systems an accurate model of TEM needs to be developed, so as to design the balance of systems around it for energy conversion to meet the demand of particular application.

This paper presents a Simulink based dynamic module for TEM for applications to TEG accommodating parameters dynamically changing with temperatures. The developed module provides dynamic simulation by computations both in space and time domain through

embedding s-functions. Such flexibility of model provides wider scope for including parametric variation in each step of computation, thus yielding more realistic model of TEG. The developed model may be used to design the balance of system around the TEM and the MPPT scheme for implementation of TEM in generation system. Both static module without dependence of temperature and the proposed Simulink model with temperature dependent parameters are compared to estimate the improvement and evaluate relative merit.

II. THERMOELECTRIC ENERGY CONVERSION

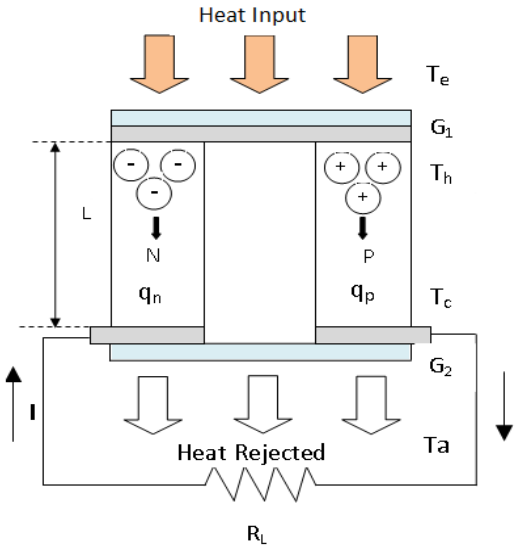

Fig. 2. Schematic representation of the single couple TEM with a thermal load and heat sink.

The fundamental unit of a TEG is a single couple composed of an n-type and a p-type semiconductor leg, both with length L. In this model, the hot side of the device is attached to a hot source whose temperature is T_e, while the cold side is open to an idealized cold source (ambient) with a constant temperature T_a. The temperatures of the hot and cold junctions of the TEG are represented by T_h and T_c, respectively.

i) The electrical resistance $R(\Omega)$ of a couple of pellets is

$$R = \rho_p \frac{L}{A} + \rho_n \frac{L}{A} \tag{1}$$

Where ρ_p and ρ_n is electrical resistivity of p and n type of material given in (Ω-m). If N no of couples are connected in TEM, then total internal resistance R_m of TEM is given as

$$R_m = R.N \tag{2}$$

ii)Joule heating is the physical process representing heat dissipation in the resistive elements**.** The Joule heating q_j (w) is assumed to be uniformly generated throughout the volume of the TEM and is given by

$$q_j = I^2 R_m \tag{3}$$

iii) Peltier cooling/heating is the phenomenon of the absorption (or dissipation) of heat by a junction between two dissimilar materials when electrical current flows through the junction. Peltier cooling/heating q_{pa}, q_{pe} occurs at the junctions and is assumed to be concentrated at the interfaces. The heat q absorbed/emitted by the TEM is

$$q_{pa/pe} = \alpha_m T_{h/c} I \tag{4}$$

The Peltier cooling/heating is sensitive to current direction; thus, half of the TEM's junctions that conduct the current in one direction absorb the heat whereas the other half, where current flows in opposite direction, releases the heat.

iv) Thermal conductance *G(w/k)* of a couple of pellets is given by

$$G = k_p \frac{A}{L} + k_n \frac{A}{L} \tag{5}$$

Where k_p and k_n is thermal conductivity (W/mK) of p and n type of material

Then total thermal conductance of the *N* couples of a module, which are connected thermally in parallel, will be

$$Gm = N.G \tag{6}$$

v) Seebeck coefficient (V/K) corresponding to a specific pair of materials is given as

$$\alpha = \alpha_p - \alpha_n \tag{7}$$

For N couples in a TEM Seebeck coefficient will be calculated as

$$\alpha_m = \alpha.N \tag{8}$$

The electromotive force (EMF) of the TEM is given by:

$$V = \alpha_m (T_h - T_c) \tag{9}$$

Thompson effect described by Thompson coefficient $\tau = dV/dt$ (volt per square Kelvin) is generally very small and therefore is neglected in the modeling.

III. TEMPERATURE DEPENDANCE ANALYSIS

As shown in Fig. 2, L is the length of thermoelectric module which is divided into equal parts. Let 'dx' is the small section of L, Heat flow in p and n type of materials can be given as[8]

$$dQ_{p,n} = Q_{p,n}(x+dx) - Q_{p,n}(x) \tag{10}$$

The Fourier's heat conduction law depicting relation between heat flow and temperature gradient is represented as:

$$q = -GA\, dT/dx \tag{11}$$

Using temperature boundary conditions $T_{p,n}(0) = T_h$ and $T_{p,n}(L) = T_c$ we find the heat conduction rate at the hot and cold junctions of each leg can be estimated as[10]:

$$q_{p,n}(0) = G_{p,n}(T_h - T_c) - I^2 \frac{R_{p,n}}{2} \tag{12}$$

$$q_{p,n}(L) = G_{p,n}(T_h - T_c) + I^2 \frac{R_{p,n}}{2} \tag{13}$$

Where q_p and q_n are the conduction heat flow in p-type or n-type leg and '*A*' is the uniform cross sectional area of the p- or n-type leg. By applying energy balance

equations for steady state conditions and introducing Peltier terms αIT_h and αIT_c at the two boundary points, the rate of heat transfer from the heat source to the single-couple TEG and from the device to the heat sink can be obtained as

$$q_h = q_p(0) + q_n(0) + \alpha_m I T_h = \alpha_m I T_h + G_m(T_h - T_c) - I^2 R/2 \quad (14)$$

$$q_c = q_p(L) + q_n(L) + \alpha_m I T_c = \alpha_m I T_c + G_m(T_h - T_c) - I^2 R/2 \quad (15)$$

If the two externally irreversible heat transfer processes are considered, we can get:

$$q_h = G_1(T_e - T_h) \quad (16)$$

$$q_c = G_2(T_c - T_a) \quad (17)$$

where G_1 and G_2 are the interface thermal conductance between the generator and the heat source and sink in the hot and cold sides, respectively. Equations (13) - (16) constitute the basic heat flow balance equation set of the TEG. Total thermal conductance, electrical resistance and Seebeck coefficient of TEG therefore can be calculated from TEG design parameters (length (L), area (A), Thermal conductivity, electrical resistivity and Seebeck coefficient of p and n type materials etc.). Thermal system parameters G_1, G_2, T_e, and T_a are thermal boundary conditions which are known. The expression of current in the generator supplied by the built-in Seebeck voltage is given as:

$$I = \frac{\alpha_m (T_h - T_c)}{R_m + R_L} \quad (18)$$

The load resistance R_L is known for the considered electrical circuit. By using equations (13)-(17) five unknowns q_h, q_c, T_h, T_c, and I can be computed. The voltage V of the electrical port of TEM is function of Seebeck voltage and internal resistance of the TEM which is described as:

$$V = IR_m + \alpha_m (T_h - T_c) \quad (19)$$

The efficiency can thus be calculated as:

$$\eta(m) = \frac{I^2 R_m}{q_h} \quad (20)$$

And the power can be calculated as:

$$P = Q_h - Q_c \quad (21)$$

The maximum generated power is estimated by computing first partial derivative of P with respect to I and setting it to zero which gives:

$$I_m = \frac{\alpha_m (T_h - T_c)}{2R} \quad (22)$$

This expression of maximum current when used for calculation of maximum heat at hot and cold junctions, it is given by:

$$(T_h)_m = [U_h A_h T_e - 2RI_m K/\alpha_m + .5(I_m)^2 R]/(\alpha_m I_m + U_h A_h) \quad (23)$$

$$(T_C)_m = [U_L A_L T_C - 2RI_m K/\alpha_m + .5(I_m)^2 R]/(U_L A_L - \alpha_m I_m) \quad (24)$$

By solving heat balance equation all five unknown variables q_h, q_c, T_h ,T_c and I respectively may be computed.

Maximum power can then be calculated using equation (25) as:

$$P_m = \alpha_m [(T_h)_m - (T_c)_m] I_m - (I_m)^2 R \quad (25)$$

The next section deals with the development of mathematical model in Matlab-simulink for characterization of TEM with temperature dependent parameters.

IV. Model Development

Mathematical models reported so far[9-15] considered constat temperature across TEM thus parameters remain more of less temperature invarient. Developed mathematical model is an attempt to consider effects ignored by the temperature-independent assumptions and analyse the performance of TEM.

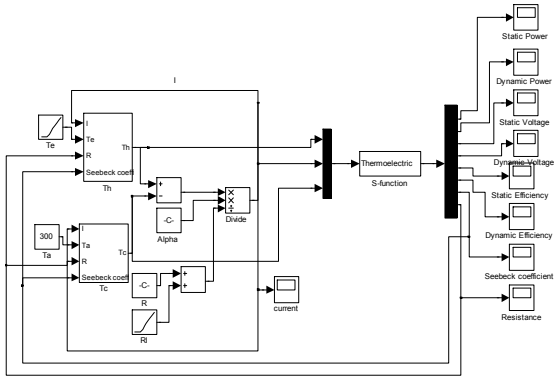

Fig. 3. Mathematical model developed in Matlab for characterizing thermoelectric module.

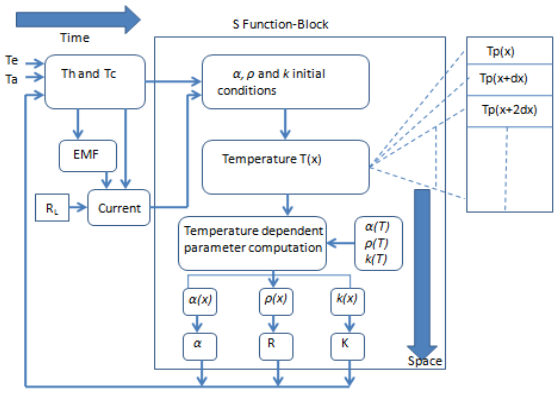

Fig. 4. Flow chart for model development in time and space domain

There are two stages of functioning of the model: i) in Time and ii) in Space domain as shown in Fig 4. These two stages are not only complementing each other but also happening simelteniously and therefore dynamically affect electrical parameters of TEM.

A) Time domain - In this stage varying temperature of hot source is considered accordingly hot junction temperature of TEM is also varying. As shown in Fig 3. SIMULINK model depicts that heat at hot junction, T_h and heat at cold junction, T_c is calculated using the equations 12-17. Two subsystems T_h and T_c are created in Simulink using these equations. Output Current of TEM is calculated by equation 17 and used again for calculation of thermal parameters.

B) Space domain- This model is computed in space for a time step for calculating temperature dependent parameters along the length of TEM. MATLAB SIMULINK offer the advantage of writing programs in user defined S-function. In this paper 'Dynamic' S-Function is developed which can compute a set of program and interface it with simulink model to enable dynamic changes through passing of parameters. The inputs to this function are T_h, T_c, and I respectively. Initial values indicated in table 1 has been used for starting the simulation. Output of this function is the feed back again for next time step. We have assumed that TEM can be broken up into many segemts according to its length and each segment will have its own parameters. TEM is considered divided into equal sized segments and Temperatue T_{dx} at every small length 'dx' of TEM is calculated. This temperature distribution along the length of TEM and equations for α, k and ρ in terms of temperature are used to update all temperatue dependent parameters for length dx of different segments of TEM. Thus every segment has its own, individual set of thermoelectric parameters defined by its temperature. Based on above individual parameters final calculation for full length of TEM is obtained. Same process is repeated for changing values of hot source temperatures and results are updated .

Table 1 The parameters of TEM

Sr.no	Parameter	Assumed Value
1	Seebeck coefficient (V/K)	$\alpha_p = 230*10^{-6}$ $\alpha_n = 195*10^{-6}$
2	Thermoelectric (W/cmK)	K_p= 0.014, K_n = 0.012
3	Electrical Resistivity (Ohm-cm)	$\rho_p = 1.75*10^{-3}$ $\rho_n = 1.35*10^{-3}$
4	Interface thermal conductance (W/cm^2K)	G_1=0.7 W/cm^2K G_2=0.7 W/cm^2K
5	Length of cell (cm)	L_p=1cm, L_n=1cm
6	Area of cell (cm^2/couple)	A_p=1cm^2/couple A_n=1.14cm^2/couple
7	Area of interface heat exchanges (cm)	A_h=0.104cm^2 A_l=0.104cm^2

V. RESULTS

To validate the efficacy of the developed model, commercially available Be_2Te_3 semiconductor thermoelectric module has been selected. Simulation has been carried out using material parameters shown in Table 1 for p-type semiconductor (25%Bi_2 Te_3 and 75% Sb_2 Te_3) and n-type semiconductor material (75%Bi_2 Te_3 and 25% Bi_2 Se_3). [11] Dimensions of TEM are selected based on available thermocouple size mentioned above. The load resistance is selected equal to the effective internal resistance of the TEM to get maximum output power at rated conditions. The temperature dependent mathematical model of TEM is simulated in Matlab-simulink environment and simulation results for electrical and thermal performance of the module at different hot source temperatures are depicted in Fig. 5-11. Results are compared appropriately for both static and dynamic models with varying temperature conditions.

Fig.5-11 shows simulated results for hot source temperature range of 310K to 400K with cold junction temperature assumed constant at T_c=300K.

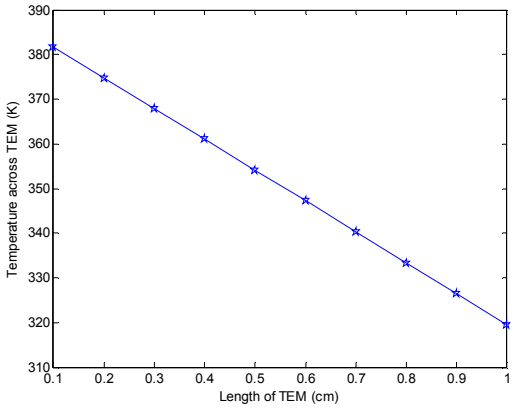

Fig. 5. Temperature profile of single couple of TEM operated at maximum hot source temperature 400K

Fig.5 shows temperature variation over the length of single couple of TEM. From the graph it is observed that variation in temperature is almost linear which, is different from logarithmic variation occurs in heat transfer process. Seebeck effect converts some amount of heat energy flowing from high temperature side to low temperature side into electricity, and therefore the heat flow from high temperature side is not equal to heat flow to the low temperature side which leads to the linear variation in the temperature of TEM.

Fig. 6-9 depicts the comparison made between static and dynamic modeling of TEM for efficiency, voltage, current and power output as a function of hot source temperature. For dynamic modeling temperature dependence of TEM is taken into consideration whereas, in static modeling the parameters are considered as constants i.e. invariable with temperature change.

Output Voltage is a function of temperature difference (ΔT) and Seebeck Coefficient which is also a temperature dependent parameter. In reported literature of static modeling, seebeck coefficient has been considered as

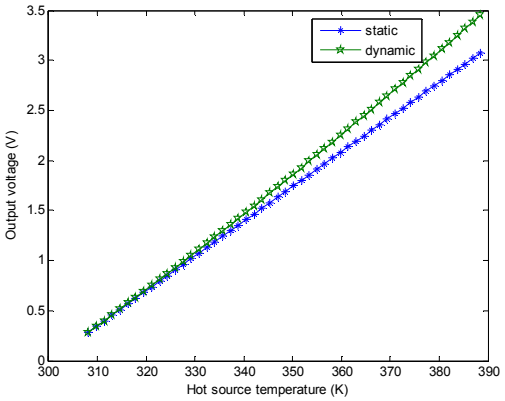

Fig. 6. Voltage generated across TEM

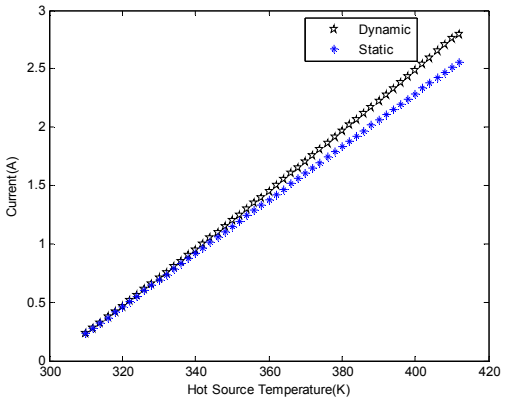

Fig. 8. Current output of TEM

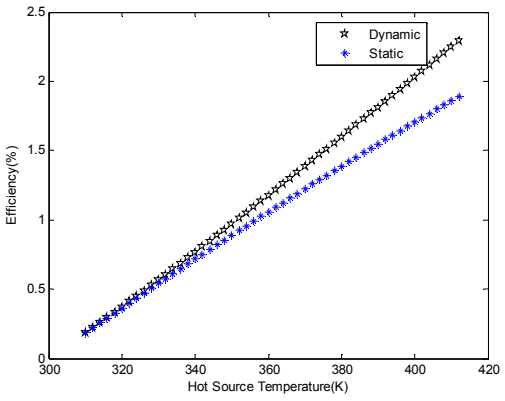

Fig.7 Efficiency of TEM

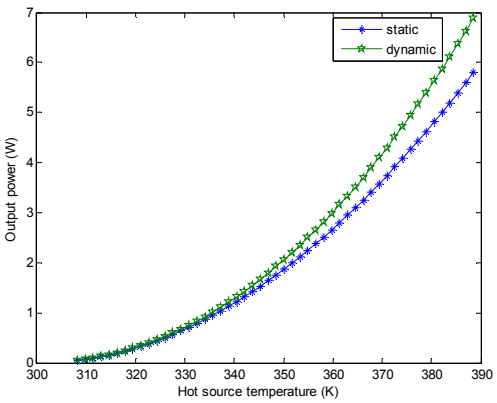

Fig. 9. Power output of TEM with internal resistance equal to load resistance.

constant and output voltage is changing with respect to change in temperature. The developed dynamic model reflects higher voltage generated for same temperature difference as is evident in comparative study shown in Fig.6. The higher voltage is the effect of increase in the value of Seebeck coefficient with increase in temperature, which remained unnoticed in static model.

The output current and efficiency also follow the same rising trend due to increase in Seebeck coefficient with respect to temperature and depicted in Fig.7 and Fig.8.

Fig. 9. shows variation of the power output with the hot source where temperature is changed from 300K to 400 K keeping cold junction temperature constant at 300 K. Power varies quadratically with temperature difference between hot and cold junctions of TEM. It can be seen that the maximum power output increases parabolically with an increase in hot source temperature. An increase in hot source temperature results in increase of temperature difference through the modules and leads to increased power output. It is worthwhile to mention that difference in output power from static and dynamic model will be quiet large and cannot be neglected when temperature difference across the TEM is substantial. Such unfair estimation may yield development of unsuitable balance of system for the TEG.

The relative study for static and proposed dynamic model with temperature dependent parameters reveals drastic changes in the output and thus affect the controllers and balance of system attached for energy harvesting. It can also be seen that a significant increase in power output i.e. about 20% is observed for the temperature gradient of 90K. Fig. 10-11. illustrates the variance of Seebeck coefficient and resistance of thermoelectric material with temperature.

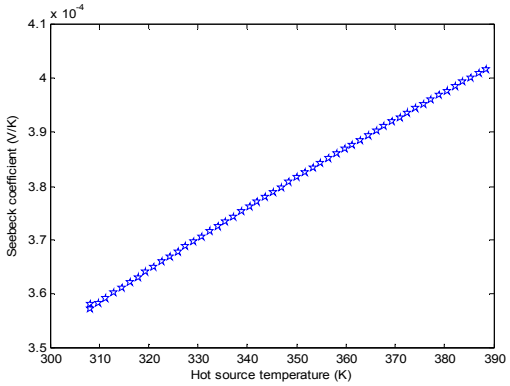

Fig. 10. Seebeck coefficient with changing hot source temperature

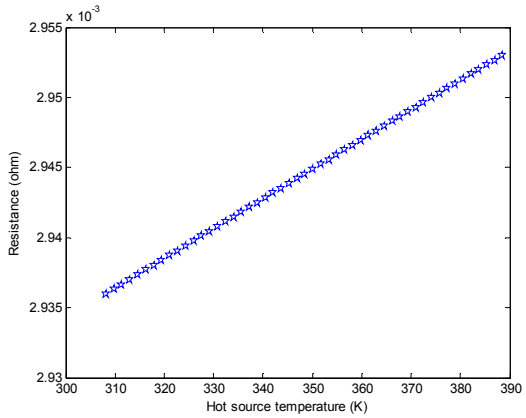

Fig.11 Resistance of single couple of TEM with changing hot source temperature

Simulation results depicted in Fig.6-9 shows same characteristic as those obtained by Min Chen [8] as the characteristic curves are of same nature but results are different due to different model selected for simulation. Output power and efficiency of dynamic curve is more than static curve as temperature dependent parameters are varying with temperature unlike in static case. As resistance and seebeck coefficient increases output power and efficiency also increases as shown in Fig.7 and Fig.9.

VI. CONCLUSION

A dynamic model of Thermoelectric Generator has been successfully developed Simulink MATLAB considering temperature dependence of various parameters like electrical resistance, seebeck coefficient of TEM and its effect on output. The model covers processing of data both in time and space to accommodate simultaneously the electrical and thermal systems. The demonstrated results clearly conform to exactness of the developed model, and thus may help the design and development of its Balance of System correctly. The results show increased generated energy with higher efficiency when compared with model with constant resistance and seebeck coefficient of the TEM cell. The developed model is capable of taking up dynamic changes in operating conditions and computing the transient solutions.

REFERENCES

[1] Rowe D.W., et al. CRC Handbook of Thermoelectrics. Boca Raton, FL: CRC Press.

[2] Rowe, D.M.; Min, G.;" Design theory of thermoelectric modules for electrical power generation", Science, Measurement and Technology, IEE Proceedings - Volume: 143 , Issue: 6, 1996 , pp.351 – 356

[3] R.E. Simons; R. C. Chu; "Application of Thermoelectric Cooling to Electronic Equipment:A Review and Analysis, 3rd ed., vol. 2. Oxford: Clarendon, 1892, pp.68–73.

[4] Tsuyoshi, A.; Kagawa, S.; Sakamoto, M.; Matsuura, K.; "A study of commercial thermoelectric generation in a processing plant of combustible solid waste", Thermoelectrics, 1997. Proceedings ICT '97. XVI International Conference on 1997, pp.555-558

[5] C.A. Gould; N.Y.A. Shammas; S. Grainger;I. Taylor, "Comprehensive Review of Thermoelectric Technology, Micro-electrical and Power Generation Properties," Phil. Trans. Roy. Soc. London, vol. A247, April 1955, pp. 529–551.

[6] H. J. Goldsmid; "Increasing the Thermoelectric Figure of Merit for Bismuth and Bismuth-Antimony", International Conference on Thermoelectrics, 2006, pp. 357–360.

[7] Thierry Caillat; Jean-Pierre Fleurial; Jeff Snyder; and Alexander Borshchevsky; "Development of High Efficiency Thermoelectric Materials and Unicouples for Power Generation Applications", 4th Pacific Rim International Conference on Advanced Materials and Processing Honolulu, Hawaii, USA, Dec. 2001.

[8] Min Chen; Lasse A. Rosendahl; Thomas J. Condra, John K. Pedersen.; "Numerical Modeling of Thermoelectric Generators With Varying material Properties in a Circuit Simulator", IEEE Transactions on Energy Conversion, vol. 24, no. 1, March 2009,pp. 112-124.

[9] Lineykin S.; Ben-Yaakov,S; "Modeling and Analysis of Thermoelectric Modules", Industry Applications, IEEE Transactions on Volume 43, Issue 2, March-april 2007 pp.505 – 512

[10] Emil Sandoz-Rosado; Robert J. Stevens "Experimental characterization of Thermoelectric Modules and Comparison with Theoretical Models for Power Generation", Journal of Electronic Materials, vol. 38, no. 7, 2009, pp.1239-1244.

[11] Chih Wu;"Analysis of waste-heat thermoelectric power generators," Applied Thermal Engineering vol. 16, No. 1, pp. 63-69

[12] J. Yu and H. Zhao, "A numerical model for thermoelectric generator with the parallel plate heat exchanger", Journal of Power Sources, Vol. 172, 428–434, July 2007.

[13] D.M. Rowe and G. Min, "Evaluation of thermoelectric modules for power generation", Journal of Power Sources, Vol. 73, pages 193–198, 1998.

[14] J. Chen, B. Lin, H. Wang, and G. Lin, "Optimal design of a multi-couple thermoelectric generator", Semiconductor Science Technology, Vol. 15, pages 184–188, 2000.

[15] R.O. Suzuki and D. Tanaka, "Mathematical simulation of thermoelectric power generation with the multi-panels", Journal of Power Sources, Vol. 122, 201–209, February 2003.